Suction bucket jackets for offshore wind:

a reliability based analysis of geotechnical installation design.

MSc Thesis by:
J.A. Remmers

ŤUDelft

Supervisors:
prof. dr. K. Gavin
dr. F. Pisano
dr. C. Reale

DEME

Supervisors:
B. Nekeman
S. Raymackers

October 9, 2018

Preface

Dear Reader,

In front of you lies the final result of a research performed to obtain a MSc degree in Hydraulic Engineering as well as Offshore & Dredging Engineering at Delft University of Technology. This research has been performed in close cooperation with GeoSea (DEME Group).

Over the past months I lived in Antwerp and was allowed to taste the atmosphere at a major offshore contractor while combining this with an academic research. Combining the experience, mindset and data available in practice with a scientific background results in insights which otherwise could not have been obtained. Therefore my gratitude goes out Bas, Sylvie and the entire geotechnical group at GeoSea. I would like to thank Cormac, Federico and Ken as well. Although I resided in a different country they managed to stay involved and gave me good academic guidance. During my final project I noticed that I implemented lessons learned from my former colleagues at Witteveen+Bos Indonesia, Deltares and Delft University as well. They deserve an equal amount of gratitude.

This project marks the end of my study and therefore my life as a student. Many people helped me throughout the years in a way with which no university or company can compete. I would like to thank all my former roommates, project teammates, cooking clubs and friends from all over the world for providing me with endless drinks, dinners and interesting conversation. I feel blessed that I was able to live in so many countries and work with so many amazing people over the past six years.

I sincerely hope I can make a contribution to these kind of innovative topics in the future and that the lessons learned during this project will not be the last ones. Enjoy reading.
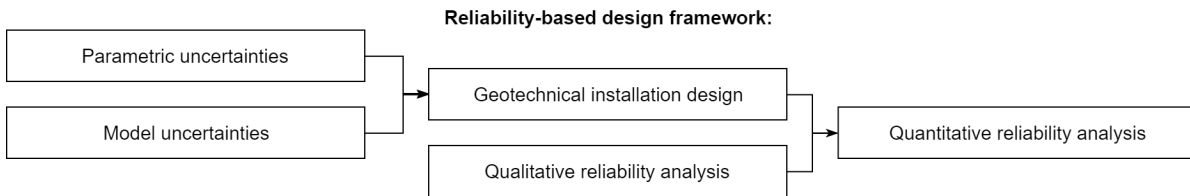
Joost Remmers
Delft, October 2018

Summary

Suction bucket jackets are an alternative foundation type for offshore wind turbines in deeper water which can be silently installed. Geotechnical installation design is key for the feasibility of this concept. Risks during geotechnical installation should be well understood before parties are willing to invest in the installation of suction bucket jackets for offshore wind. This leads to the following research question:

What is the impact of geotechnical uncertainties on installation design of suction bucket jacket foundations for offshore wind turbines?

Reliability-based design methods can be used to quantify the variability of geotechnical design parameters and their impact on the installation design results. Previous studies and applications of reliability-based design were used to set up a framework for the analysis performed in this research:

Reliability-based design framework:

Parametric uncertainties

Model uncertainties

Geotechnical installation design

Qualitative reliability analysis

Quantitative reliability analysis

Penetration of suction bucket jackets is possible due to the reduction in soil resistance by the underpressure applied inside the buckets. The difference between limit and required suction determines installation feasibility. Two methods, based on the principles of open-ended pile design, exist for computation of the required suction: the Houlsby & Byrne and the CPT-based method. The Houlsby & Byrne method uses (un)drained soil parameters while the CPT-based method correlates penetration resistance with the cone resistance obtained in a cone penetration test. The original methods are only valid for application in homogenous subsoils.

Subsoils of uniform permeability seldom occur in practice. Therefore an axisymmetric finite element seepage model was integrated in both design methods. This model computes non-linear underpressure development in layered subsoils. Additionally the fixed values available for the empirical end-bearing factor in CPT-based design (k_p) are replaced by a method in which it is estimated based on site specific information. A formulation relating estimated in-situ relative density to the end-bearing coefficient in dense sands was developed based on the self-weight penetration data of large diameter monopiles.

The variability of design soil parameters in a case study wind farm was determined. First proper identification of the soil layers at each installation location is required. Four techniques were used: geological history and soil type, Robertson classification, the statistical moving window method and Bartlett profiling. Probability density functions, describing the likelihood of a certain value of a soil parameter, were used to quantify the variability of the soil unit weight (γ_s), the angle of internal friction (ϕ) and the permeability (k) per soil type. Goodness of fit tests were used to assess the fit of the functions. Random field modelling was used to simulate probable variation of the filtered cone resistance value along a vertical trendline.

The parametric uncertainties were implemented in the design methods during the quantitative reliability analysis. This allows for assessment of their impact, feasibility of installation as well as the accuracy of the models applied. Regular Monte Carlo simulation (MCS) was applied first. Afterwards attempts were made to improve the speed by implementing a Markov Chain Monte Carlo method (MCMC). Self-weight and suction-assisted penetration was examined in combination with possible contingency measures like ballasting and backfilling with grout. Not all physical phenomena which can occur during suction bucket (jacket) installation can be accurately described by existing design methods. Contingencies like jetting and two-way cycling or failure mechanisms like excessive loosening and soil plug heave are difficult to quantify. Large model uncertainty therefore hinders the computation of an exact and accurate failure probability.

Results of the direct reliability analysis show underperformance of the Houlsby & Byrne method. This can be attributed to several causes. Estimation of the parameters is often more difficult since less (test) data is available. Often the data is not retrieved from the exact installation locations as well. However, the main reason for the underperformance is the sensitivity to the ratio of horizontal over vertical stresses (K). Estimating the stress ratio in non-cohesive soils is infeasible. Additionally high stress ratio estimates can have unrealistic design outputs due to inaccurate stress enhancement estimates as a consequence.

Integration of the seepage analysis made the CPT-based method feasible for application in subsoils with varying permeability. Correlation of the empirical factors with site specific data resulted in improved design results. It is recommended to extend and examine this formulation for all soil types. The CPT-based design approach is recommended if a cone penetration test is performed at the installation location.

Working with a realistic survey dataset gave more insight in the practical application of reliability-based design methods. No flawless layer identification method was found. Methods which use statistics of a moving window require adaptation of the window width per location to identify thinner layers. Geophysical survey data, borehole logs and Robertson classification are essential for successful profiling too. A combination of methods is advised.

Vertical random field modelling of the cone resistance is feasible based on several closely spaced cone penetration tests provided that extensive matching criteria are applied. Applying horizontal random field modelling to the cone resistance is infeasible based on data from geotechnical surveys of offshore wind farms. As a consequence installation design needs to be performed for each individual bucket. A system reliability approach on feasibility of installation of the entire jacket configuration is not possible due to the continuous process of installation.

A full reliability analysis might not be feasible or required each individual time a foundation is installed. However, using elements of the analysis performed in this research can already increase understanding of the impact of uncertainties, both in practice and in research.

Contents

<div align="right">1</div>

Research introduction

The main objective of this research is quantifying uncertainties in geotechnical installation design of suction bucket jackets for offshore wind. First some background information regarding developments leading to this research is presented. Afterwards the research topic, structure and limitations are described.

1.1. Background

Offshore wind farms are moving to deeper water, suction foundation technology is getting more mature and reliability-based design is expected to become more important for geotechnical engineers. These three developments lead to the research topic described in Section 1.2.

1. Offshore wind farms moving to deeper water

In recent years more commitment is shown to the development of renewable energy alternatives (UNFCC, 2015; European Commision, 2014). Offshore wind has become a realistic renewable energy source and the industry grows rapidly (Rodrigues et al., 2015). Nowadays wind farms are built in ever increasing water depths. These locations have larger and more constant wind speeds and are often positioned further offshore. Therefore they cause less visual pollution as well (Bilgili et al., 2011). Constructing wind farms in deeper water provides challenges considering support structure design (Breton and Moe, 2009). Formerly used monopiles are not feasible support structures for most deep water sites (Lozano-Minguez et al., 2011). Industry and research have developed many different concepts to deal with these increased water depths. In general four options are considered feasible for deep water sites: XL monopiles, floating foundations, lattice structures (e.g. jackets and tripods) and gravity based structures (Leanwind, 2017). These support structures transfer loads to a foundation consisting of either driven piles, a gravity based interface or suction installed skirted foundations (Randolph et al., 2005).
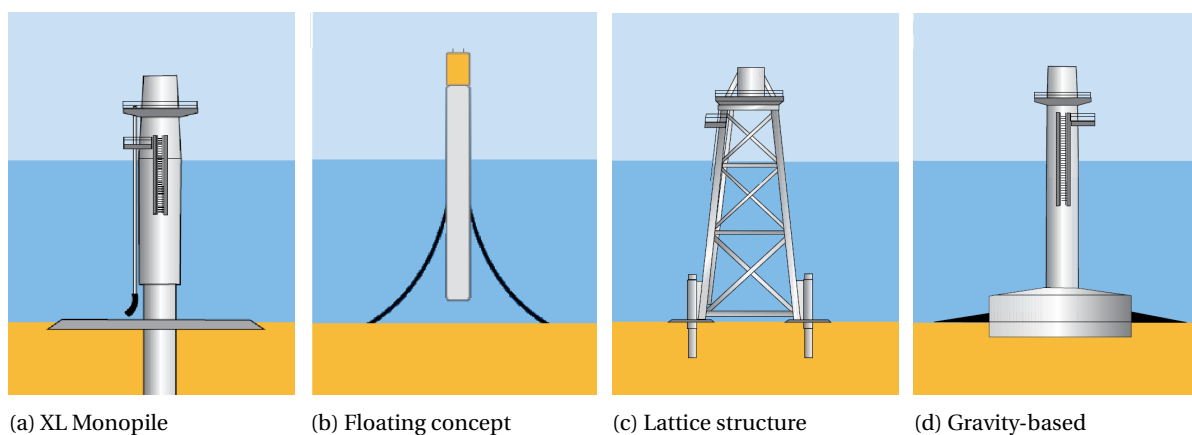

(a) XL Monopile   (b) Floating concept   (c) Lattice structure   (d) Gravity-based

Figure 1.1: Foundation concepts for offshore windmills in deeper water (based on: European Wind Energy Association, 2013)

<div align="center">1</div>

2. Suction foundation technology

Suction foundation technology provides a silent and easy alternative for driven piles and has the potential for easy decommissioning (Wang et al., 2018; Topham and McMillan, 2017). A typical foundation represents an upside down bucket which is penetrated into the seabed by applying underpressure in the enclosed area under the lid (Foglia and Ibsen, 2014). Soil conditions are of critical importance for the design and installation of this type of foundation (Zaaijer, 2003).

Many suction founded structures for oil and gas purposes were installed in the past (Tjelta, 2015). However, both experience and guidelines on the application in offshore wind is scarce (Tjelta, 2014). While fabrication of suction bucket jackets is more comprehensive, gains can be achieved during installation. This is expected to be faster and require less resources with respect to other foundation types. The combination of a lattice structure and suction foundation technology has been applied for several meteorological masts and as a demonstrator project in the wind farm Borkum Riffgrund I (Tjelta, 2014). In 2018 installation of suction bucket jackets started at the farm locations Aberdeen Bay and Borkum Riffgrund II. Noise regulations become stricter due to the known impact offshore pile installation on marine life (Bailey et al., 2010). Considering this development suction bucket (jacket) based solutions could provide a silent alternative in the future.

(a) Monopod at HornsRev [110]   (b) Suction bucket jacket at Borkum Riffgrund I [118]

Figure 1.2: Suction founded concepts installed for offshore wind purposes

3. Reliability-based design in geotechnical engineering

Geotechnical engineers typically design on the bases of in-situ and laboratory tests in combination with analytic and numerical models (Lacasse and Nadim, 2007). Geotechnical engineers can use four strategies for dealing with uncertainties. One can choose to ignore it, be conservative or use observations and correct afterwards. The final strategy is quantifying the uncertainty using reliability-based design methods (Christian, 2004). While the first three methods give an impression of certainty, they do not provide explicit uncertainties (Lacasse and Nadim, 2007). Reliability-based design methods are typical for modelling low probability and/or high risk scenarios (e.g. nuclear power plants). Over the years reliability-based design methods have been applied in many engineering fields (Vrijling, 2001).

Reliability-based design is still relatively uncommon in geotechnical engineering. The main reason for this is that application requires realistic estimates of the variability of soil parameters (Phoon, 2008). Unfortunately soil parameters have large inherent uncertainties and available data is always limited. Nevertheless, reliability-based design has been applied in levee design, seismic hazard assessments and lately even in offshore pile capacity computations (Phoon and Kulhawy, 2005). Design codes have been made for general reliability principles and certifiers start incorporating criteria for reliability-based design in their foundation specific codes (DNVGL, 2017b; ISO, 2015). Reliability-based design quantifies uncertainty and therefore allows for optimization. Using it can lead to more cost efficient design and operations (Fenton, 1999).

1.2. Topic

The three background topics described in Section 1.1 form the backbone of the motivation and research question of this research. This Section describes both and concludes with the restrictions of this research.

1. Motivation

Aberdeen Bay and Borkum Riffgrund II are the first projects in which multiple suction bucket jackets are installed. At this moment no similar projects are planned in the nearby future. However, noise regulations in Western Europe become stricter and offshore wind is moving to ever deeper water. This could result in consideration of suction bucket jackets as an alternative for future projects. Installing a foundation and support structure for an offshore wind turbine is still a costly undertaking. It is also an exhaustive offshore operation. All parties involved want to have as good an insight as possible in the risks during installation before they will invest in the application of suction bucket jackets. Installation is critical for design and therefore feasibility of suction bucket jackets. Soil conditions are the main cause of problems during installation and therefore an obvious starting point for technically reducing the risks. Reliability-based design can be used for quantifying geotechnical uncertainties and therefore contribute to a better understanding of the installation risks. Concluding one can say that this research can cut both ways. Firstly it aims to increase understanding of suction bucket jacket installation design and the feasibility of the concept. Secondly it can contribute to the application of reliability-based design for offshore geotechnical engineering purposes.

2. Research questions

The main research question summarizes all of the above. It is formulated as follows:

> *What is the impact of geotechnical uncertainties on installation design of suction*
> *bucket jacket foundations for offshore wind turbines?*

Six objectives need to be achieved to find an answer to the research question. These objectives roughly correspond to the elements of the reliability-based framework. This framework is described in Section 1.3.

1. Development of an overview of methods for geotechnical installation design of suction bucket (jackets).

2. Insight in the possible events and failure mechanisms which can occur during geotechnical installation.

3. Quantification of the variability of geotechnical parameters required for installation design.

4. Reduction and quantification of the model uncertainty of the geotechnical installation design methods.

5. Integration of the quantified parametric variability and/or model uncertainty into the geotechnical installation methods to perform direct reliability analyses.

6. Assessment of the impact of uncertainties on the outcomes of geotechnical installation design.

3. Restrictions

Installation design of suction foundations is a multidisciplinary task which requires knowledge of both structural as well as geotechnical design. Failure of installation can be caused by three types of limitations: the pumping system (e.g. cavitation), structural capacity (e.g. buckling) and the soil (e.g. piping) (Lesny and Richwien, 2011). Setting suction limits is a research on its own. Therefore only a brief analysis on soil suction limits is included in this research.

Installation design of suction foundations is an extensive procedure. Complex finite element (FE) studies and lab tests are performed during detailed design. Only analytic and empirical models are used in this research. This is a more logical approach for initial feasibility assessment. Furthermore the incorporation of complex FE models in a direct reliability analyses requires too much computational resources.

Reliability based design requires realistic estimates of the variability of soil parameters (Phoon and Kulhawy, 1999). This requires sufficient geophysical and geotechnical survey data. In several ways this study is limited to the data available. A case study dataset based on an actual offshore wind farm survey campaign is used in this analysis. In Appendix A more information regarding the background of this data is presented.

1.3. Structure

A reliability-based design framework is used to structure both the research as well as this report.

1. The reliability-based design framework

A proper framework is required to make a comprehensive reliability-based analysis which incorporates as much uncertainties as possible. The assessment of reliability of flood defences in the Netherlands is used as a basis for the framework (Jonkman et al., 2017; Vrijling, 2001). This method is used because it provides an excellent example of the thorough application of a reliability-based design approach. Starting point of this assessment is a collection of the design methods available. Afterwards a qualitative reliability analysis is performed. In this step the system is analyzed for possible events and failure mechanisms which could occur. In an ideal scenario the design methods available describe all possible events and failure mechanisms. The third step is the quantification of variability due to uncertainties within both parameter estimates as well as the design models. This variability is integrated in the design methods to perform a quantitative reliability analysis. In this final step the effect of uncertainties on design and on the probability of occurrence of events and failure mechanisms is examined.

The assessment of geotechnical uncertainties which is described by several leading authors regarding soil variability is integrated into this research (Lacasse and Nadim, 2007; Uzielli et al., 2006; Christian, 2004; Phoon and Kulhawy, 1999). Geotechnical uncertainties can originate from both parameter estimation as well as model imperfections. Both of these have an effect on installation design and are considered separately in this research. The used reliability-based design framework is presented in Figure 1.3.
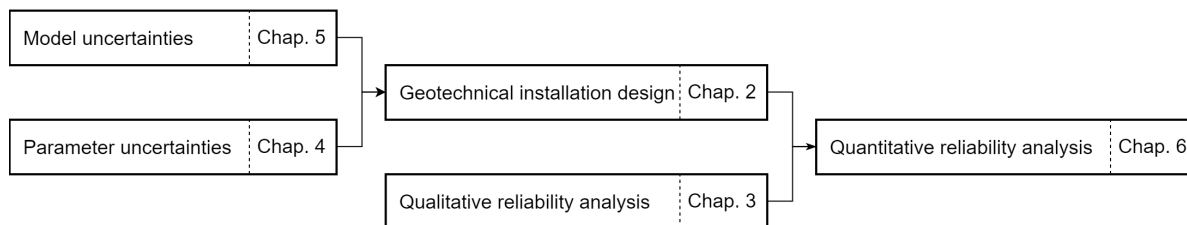

Figure 1.3: Reliability-based design framework and corresponding research and report structure

2. Report outline

The report outline follows a similar structure as the framework presented in Figure 1.3. Each of the steps in the framework corresponds to a different Chapter in the main body of the report. First elaboration is given on the current geotechnical installation design methods used for penetration studies (Chapter 2). Then the event- and fault trees are developed in the qualitative reliability analysis (Chapter 3). Parametric and model uncertainties are quantified (Chapters 4 and 5). Finally all preceding steps will be used to perform a quantitative reliability analysis in Chapter 6.

Each Chapter contains an introduction which introduces the step in the reliability-based design framework and provides more context to the methods used. Likewise all Chapters leading to the quantitative reliability analysis end with an evaluation of the methods applied and notes on their integration in the total framework.

In Chapter 7 the findings, discussion and recommendations are presented. Since the research cuts two ways a subdivision is made between findings on suction bucket installation design methods and findings regarding the application of reliability-based design in offshore geotechnical engineering. Recommendations for future research as well as application in practice are discussed in this Chapter too.

Two Appendices are attached to this report. Appendix A provides background information on the case study wind farm dataset used. Appendix B elaborates on the smaller modelling decisions and background of methods applied throughout the research.

2

Geotechnical installation design

Determining the installation feasibility requires a set of solid design methods. In this Chapter the methods which can be used for geotechnical installation design will be determined and evaluated.

2.1. Overview

The scope of this research is a small part of the overall suction bucket jacket design. In this Section the design and installation processes are described after which the available design methods are discussed.

1. Suction bucket jacket design

Geotechnical installation design is only a small part of a larger design process for suction bucket jackets. Design of suction based foundations for offshore wind turbines is a three phase process (Ibsen et al., 2005). First a design basis is made in which the wind turbine structure, environmental loads, design standards and geotechnical conditions are evaluated. Afterwards a conceptual design is made in which simple analytic models are used to evaluate bucket dimensions. In this phase feasibility of installation of the buckets (from a structural and geotechnical perspective) is checked as well. The final phase consists of detailed design studies in which finite element models and dynamic analyses are used for optimization of design. Geotechnical installation design is part of the conceptual design phase (Figure 2.1).

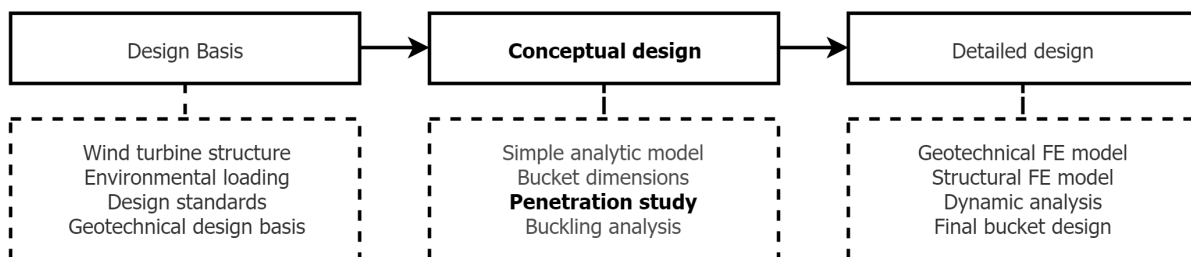| Design Basis	→	**Conceptual design**	→	Detailed design
Wind turbine structure Environmental loading Design standards Geotechnical design basis		Simple analytic model Bucket dimensions **Penetration study** Buckling analysis		Geotechnical FE model Structural FE model Dynamic analysis Final bucket design

Figure 2.1: (Considered) design phases for suction founded support structures (based on: Ibsen et al., 2005)

2. Geotechnical installation process

The penetration process of suction bucket foundations consists of two phases: self-weight and suction-assisted penetration (Randolph and Gourvenec, 2011; Lesny and Richwien, 2011). During the phase of self-weight penetration the bucket skirts penetrate into the soil with the buoyant weight of the structure as sole driving force. The suction-assisted penetration phase is the penetration of the bucket skirts into the soil with both buoyant weight and differential pressure as driving forces.
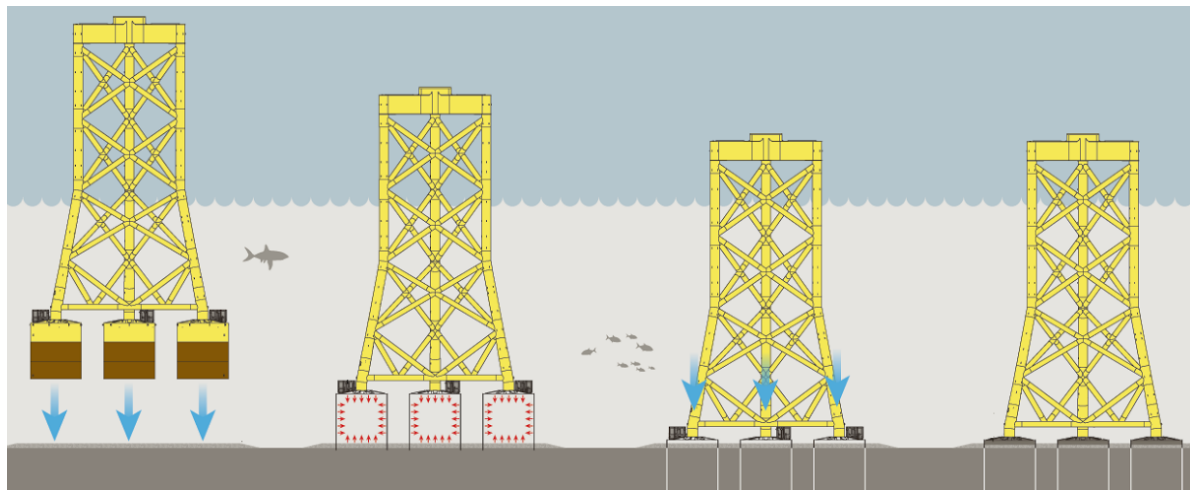

Figure 2.2: Installation procedure of a suction bucket jacket (Wittrup, 2016)

2.1 Self-weight penetration

The goal of this installation phase is to form a sufficient seal which allows for suction-assisted penetration (Houlsby and Byrne, 2005b). If this is not the case, channels can be formed due to the high hydraulic gradient caused by the suction process. This could cause premature refusal (Lesny and Richwien, 2011). Suction buckets penetrate to shallower depths compared to piles. Therefore scour is unnacceptable and a large risk (Byrne and Houlsby, 2003). Scour protection is applied to mitigate this risk. The filter layer of the scour protection is installed before geotechnical installation starts. Therefore the first part of self-weight penetration goes through the filter layer (Asgarpour, 2016). After penetration of the filter layer the buckets should penetrate into the subsoil under the buoyant weight of the jacket. The amount of self-weight penetration can be increased when ballast weight is applied (Randolph and Gourvenec, 2011). This installation phase is completed when it is possible to generate stable underpressure and penetration of the bucket(s) can be achieved.

2.2 Suction-assisted penetration

In this installation phase underpressure is applied inside the bucket by pumping out water of the enclosed area between the lid and subsoil (Foglia and Ibsen, 2014). Applying suction creates differential pressures and seepage flow (Lesny and Richwien, 2011). While both induce further penetration, the dominant process differs between soil types. Suction creates a seepage flow through the soil plug in non-cohesive soils (Houlsby and Byrne, 2005b). Seepage flow reduces effective stresses and therefore the soil resistance. This allows for further penetration (Tjelta, 1994). In pure cohesive soils seepage flow can be ignored due to the absence of sufficient permeability. Suction-assisted penetration in cohesive soils is mainly induced by the differential pressure acting on the soil plug (Foglia and Ibsen, 2014; Houlsby and Byrne, 2005a). This increases the driving force and therefore induces further penetration. In layered soils the dominant process can differ over penetration depth. Therefore installation is more challenging in these conditions (Panayides et al., 2017). The suction-assisted penetration phase is completed when all buckets have penetrated until target penetration depth. If there is any empty space between the bucket lid and the seabed grout can be used to assure structural integrity of the system.

3. Design methods

There are no design codes which cover the full installation design process of suction bucket jackets to an extent which is required for this thesis (Tjelta, 2015). Several design codes provide guidelines on offshore soil mechanics, geotechnical engineering and the application of suction anchors in clay (DNVGL, 2017a; 2017b). Specific design frameworks for the installation of individual suction buckets are available (Malhotra, 2011; Ibsen et al., 2005). All design frameworks are based on the installation of one suction bucket. Multiple buckets on one jacket are not expected to be behave independently. Figure 2.3 gives an overview of the design framework for one bucket.
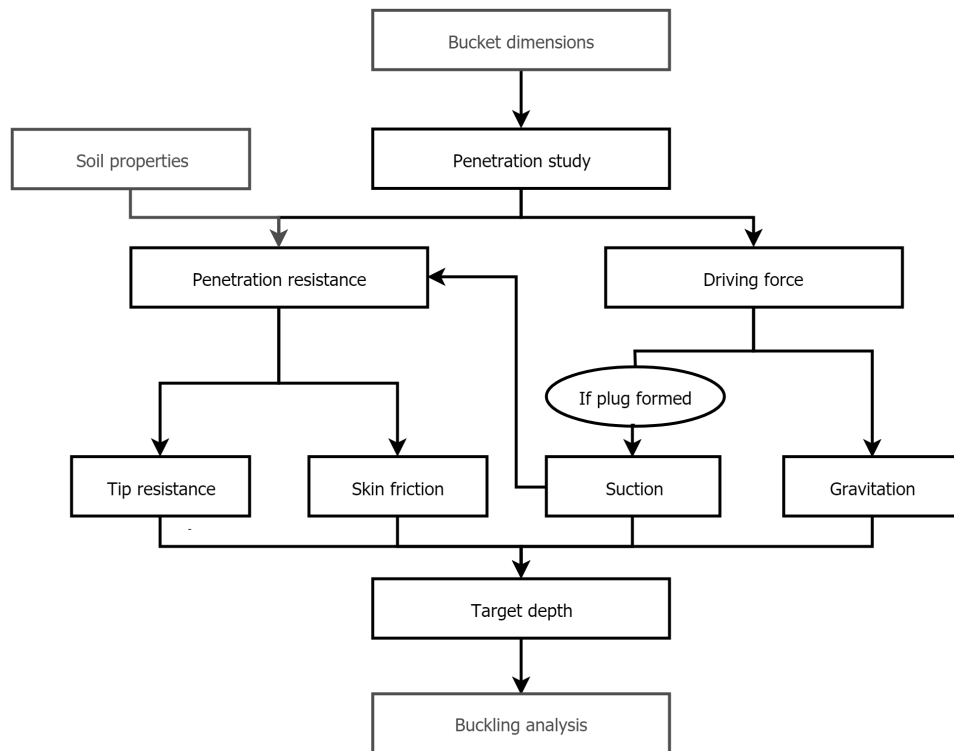

Figure 2.3: A flowchart for the penetration study of one suction bucket (based on: Malhotra, 2011 and Ibsen et al., 2005)

At this moment two design formulations are available to perform a suction bucket penetration study. The first is an analytical formulation based on principles borrowed from pile design and bearing capacity of shallow foundations (Houlsby and Byrne, 2005b; 2005a). The second is a CPT-based empirical formulation which is used to perform a penetration study on the bases of direct correlation with the results of a Cone Penetration Test (CPT) (Senders and Randolph, 2009; Andersen et al., 2008). Both methods make a distinction between the self-weight and suction-assisted penetration phase. The outputs of the design methods are an expected self-weight penetration depth and a profile of the required suction over depth.

The resulting parameters from both design methods do not provide any explicit information regarding installation feasibility. Several bounds on installation are imposed by the site conditions. Suction limits need to be determined to assure that the applied suction does not induce any mechanism leading to installation failure (Senders and Randolph, 2009). In addition to this it is required to check whether the planned suction during installation does not exceed the feasible limits of pumping imposed by cavitation and buckling (Lesny and Richwien, 2011). Finally the soil profile composition (in layered soils) creates bounds to the applicable suction. A seepage analysis needs to be performed to check the influence of the soil profile on the achievable suction.

The design methods described in the previous paragraphs do not cover all geotechnical aspects of suction bucket jacket installation. However, at the time of writing these are the two most prominent and usable methods available. After performing the qualitative reliability analysis (in Chapter 3) the applicability of the design methods within the reliability-based design framework is discussed.

2.2. Houlsby & Byrne method

The Houlsby & Byrne method is a design method with simplified equations which borrows techniques from pile design (Houlsby and Byrne, 2005b). It is a reasonable approximation for individual suction bucket installation in relatively homogeneous deposits of sand or clay (Houlsby and Byrne, 2005b; 2005a). The approach was developed by Houlsby and Byrne in 2005 and was verified with field data and lab tests. The method distinguishes between the self-weight and suction-assisted penetration phase and computes the soil resistance as the sum of inner- and outer shaft friction combined with the end-bearing of the skirt (Figure 2.4a).

1. Self-weight penetration

Self-weight penetration is possible when the acting buoyant weight on the bucket is larger than the soil resistance. The computation differs between cohesive and non-cohesive soils.

1.1 Non-cohesive soils

The effective stresses over depth need to be determined in order to estimate the shaft friction and end-bearing capacity. First the in-situ vertical effective stress is determined using the volumetric weight of the soil (Verruijt, 2012). During installation in non-cohesive soils the vertical stress adjacent to the skirt of the bucket is enhanced by frictional forces further up the skirt. This effect cannot be ignored because it would provide a non-conservative estimate (Houlsby and Byrne, 2005b). Determining the enhanced stresses requires a numerical solution to the differential equation following from stress equilibrium in a small slice of the soil plug (Figure 2.4b). Equation 2.1 shows the calculation procedure for the outer enhanced stress. The parameter f_0 refers to the load distribution of the friction and is often assumed to be equal to one. Reference is made to Houlsby and Byrne (2005b) for a full overview of equations.

$$\frac{d\sigma_v'}{dz} - \frac{\sigma_v'}{Z_o} = \gamma' \quad , \quad Z_o = \frac{D_o\left\{\left[1+\left(\frac{2f_0 z}{D_o}\right)^2\right]-1\right\}}{4(K\tan\delta)} \tag{2.1}$$

(a) Outline of a suction bucket   (b) Equilibrium of horizontal slice soil plug
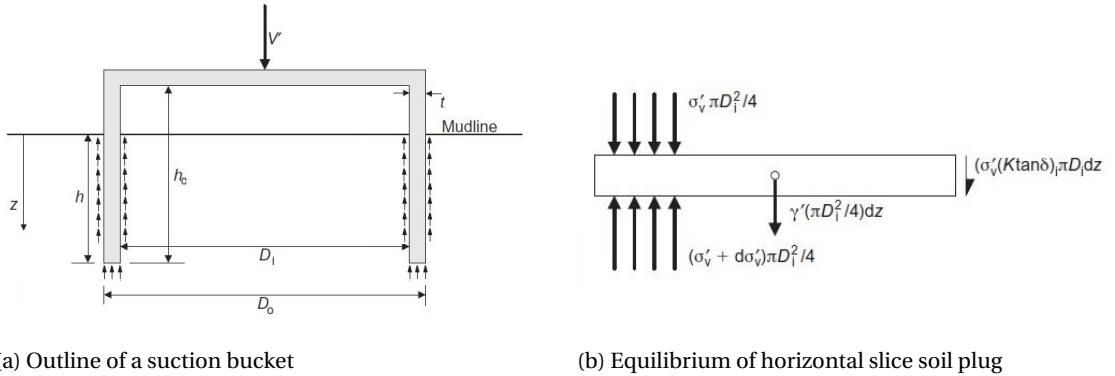
Figure 2.4: Schematization of the models applied to determine self-weight penetration with the Houlsby & Byrne method (adapted of Houlsby and Byrne, 2005b)

When the outer and inner enhanced vertical effective stresses are determined the shaft and end-bearing resistance can be computed. The shaft friction is determined by multiplying the horizontal effective stresses with the tangent of the interface friction angle (δ). To do this the stress ratio (K) between horizontal (σ_h) and vertical effective stresses (σ_v) is required. After the friction has been determined the shaft resistance can be found by integrating the friction over the penetration depth and the circumference of the bucket. The tip resistance is found using conventional practice. Bearing capacity factors (N_q and N_γ) are used to estimate the bearing capacity of the subsoil after which this is multiplied with the steel tip area (Equation 2.2).

$$V = \int_o^h \left(\sigma_{vo}(K\tan\delta)_o + \sigma_{vi}(K\tan\delta)_i\right)dz + (\sigma_v N_q + \gamma'\frac{t}{2}N_\gamma)(\pi D t) \tag{2.2}$$

1.2 Cohesive soils

The undrained shear strength of the soil over depth is required to estimate the soil resistance in non-cohesive soils. Adhesion forces inside and outside the skirt can be determined by multiplying the undrained shear strength with an adhesion factor (Houlsby and Byrne, 2005a). Methods to determine the adhesion factor can be retrieved from conventional undrained pile design methods (Doherty and Gavin, 2011). Again the shaft resistance is found by integrating adhesion forces over the penetration depth. The end-bearing resistance is found by combining bearing capacity factors (N_c and N_q) with both the undrained shear strength, soil unit weight and the steel tip area of the bucket.

$$V = \int_0^h \Big(\alpha_o s_{u1}(\pi D_o) + \alpha_i s_{u1}(\pi D_i) \Big) dz + (\gamma' N_q + s_{u2} N_c)(\pi D t) \tag{2.3}$$

1.3 Layered soils

The Houlsby & Byrne method can be used to compute self-weight penetration in layered soils quite easily. In profiles in which the layers are both cohesive as well as non-cohesive the design method is a linear combination of both formulations.

Stress enhancement is not a relevant phenomenon for cohesive subsoils due to the absence of frictional effects along the skirt. However, continuity of vertical stresses still applies. This requires a changing boundary condition for the differential equation describing stress enhancement over depth. This can be implemented in the design method in a relatively straightforward manner.

The end-bearing capacity estimation of the Houlsby & Byrne method in layered soils does not reflect the real soil behavior. This is because the original coefficients of end-bearing are based on homogeneous soils in which the capacity is coupled to the assumption of an influence zone. In layered soils the conventional way of determining these coefficients does not fully apply because the soil in the influence zone could be non-homogeneous (Verruijt, 2012). Finite element models can be used for better estimates of the end-bearing but fall outside the scope of this research.

2. Suction-assisted penetration

Suction-assisted penetration occurs when the driving force (buoyant weight and differential pressure) is larger than the soil resistance affected by the suction effects. The effect of differential pressure is simply computed by multiplying the plug area with the suction pressure applied. The resistance is again computed as the sum of shaft and tip resistances. Computation differs for cohesive and non-cohesive soils.

2.1 Non-cohesive soils

Again the vertical effective stresses are required for the computation of resistance. However, when suction is applied the effective stresses reduce. Houlsby and Byrne (2005b) propose the suction decreases linearly with depth to a value of $a \cdot s$ at the skirt tip. The coefficient a represents the reduction of suction at the caisson tip for different penetration depths. This coefficient can be determined using a formula derived from the results of FE models from existing studies. It only holds for homogeneous sands. Therefore it is not generally applicable. In layered sands with different permeabilities the stress reduction is not linear over depth. Elaboration on the effects of a non-linear reduction in suction pressure is given in Section 2.4.

(a) Tip resistance ($\sigma_i = \sigma_o$)   (b) Tip resistance ($\sigma_i \neq \sigma_o$)
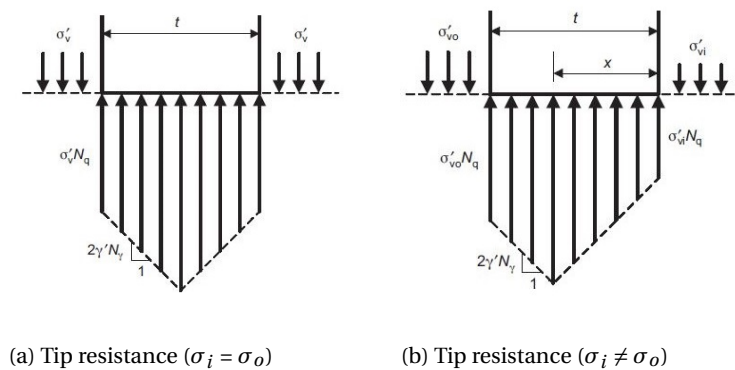
Figure 2.5: Effect of suction-assisted penetration on the stress profile at the tip (Houlsby and Byrne, 2005b)

Applying suction decreases the soil resistance. Shaft resistances are computed similarly as in the self-weight penetration phase but with an effective stress reduction taken into account. The computation of tip resistances changes due to the fact that the suction pressure can affect the stress distribution at the tip of the skirt (Figure 2.5a and 2.5b). Three scenarios are defined: inward-, outward- and intermediate flow of soil. Because the inner effective stress is reduced significantly more than the outer effective stress outward flow and intermediate conditions are only expected to occur at the start of suction-assisted penetration. Besides the changing stress distribution at the skirt tip, the change in effective stresses affects the tip resistance as well. Equation 2.4 shows the final vertical equilibrium for inward flow. Reference is made to Houlsby and Byrne, 2005b for the entire set of equations.

$$V + s\left(\frac{\pi D_i^2}{4}\right) = \int_o^h \Big((\sigma_{vo} - as)(K\tan\delta)_o + (\sigma_{vi} - (1-a)s)(K\tan\delta)_i\Big)dz + (\sigma_v - (1-a)s)N_q + \gamma' t N_\gamma)(\pi D t) \quad (2.4)$$

2.2 Cohesive soils

The suction-assisted penetration design procedure for the Houlsby & Byrne method is more straightforward for sole cohesive subsoils. The shaft resistance computation does not change with respect to the self-weight penetration phase. The tip resistance is only affected by a reduction of the overburden term due to the applied suction pressure (Equation 2.5). This reduction is based on the assumption of pure inward flow (Houlsby and Byrne, 2005a).

$$V + s\left(\frac{\pi D_i^2}{4}\right) = \int_0^h \Big(\alpha_o s_{u1}(\pi D_o) + \alpha_i s_{u1}(\pi D_i)\Big)dz + (\gamma' N_q + s_{u2}N_c - s)(\pi D t) \quad (2.5)$$

2.3 Layered soils

Based on the previous paragraphs one can state that the effect of suction on the effective stress distribution over depth is the governing mechanism for non-cohesive soils while the differential pressure is the governing mechanism for cohesive soils. However, when the soil consists of layers with varying permeability the dominant mechanism can vary. In these cases significant adjustments to the design method are required.

When non-permeable (cohesive) layers are present in the profile the suction effects over depth can change significantly. In general one distinguishes sand over clay an clay over sand scenarios. During penetration in a sand over clay subsoil the design method does not change for the top sand layer. However, when the skirt penetrates into the cohesive soil, the suction below the top of the clay layer diminishes. From that moment onwards the principles of installation in clay should be used with a slight correction for the shaft friction in the non-cohesive top layer. If clay is positioned over sand it is hard to establish seepage flow during penetration. Therefore the resistance of the subsoil increases significantly. Installation in these conditions has been completed in the past (Panayides et al., 2017; Saue et al., 2017). It is expected that phenomena like cracking of the clay plug occurs in some situations which allows seepage flow to develop through a clay layer (Senders, 2008). However, current design methods lack approaches to take this into account.

Soil layering can have a large effect on the seepage profile and therefore on the accuracy of the Houlsby & Byrne design method. Especially when permeabilities differ, the effect of suction over depth can have non-linear behaviour. The Houlsby & Byrne method for non-cohesive soils requires knowledge of the suction profile over depth. The simplifying assumptions of Houlsby and Byrne (2005b) using coefficient *a* do not hold in these cases. Another method should be used. Estimates of underpressure development over depth can be determined using a seepage analysis. Because the seepage analysis is not part of the original design method it is discussed separately in Section 2.4.

2.3. CPT-based method

The CPT-based method is an empirical design formulation which correlates the cone resistance found in a Cone Penetration Test (CPT) directly with the penetration resistance of the suction bucket (Senders and Randolph, 2009; Andersen et al., 2008). Identically to the Houlsby & Byrne method the penetration resistance in CPT-based design is determined as the sum of shaft resistances and the end-bearing capacity.

1. Self-weight penetration

The estimated self-weight penetration is found by comparing the resistance of the soil with the buoyant weight on the bucket. The end-bearing capacity is correlated with the cone resistance data from a CPT-test (Senders and Randolph, 2009; Andersen et al., 2008). Although sleeve friction measurements are available the frictional forces on the skirt are correlated with the cone resistance from the CPT-test as well (Andersen et al., 2008). This is due to the large variability possible in sleeve friction measurements (Lunne et al., 1997). Empirical coefficients (k_p, k_f) are used to correlate the measured cone resistance with end-bearing and shaft friction or adhesion on the bucket. These coefficients differ for cohesive and non-cohesive soils.

$$V = \pi D_i k_f \int_0^h q_c(z)\,dz + \pi D_o k_f \int_0^h q_c(z)\,dz + (\pi D t) k_p q_c(h) \tag{2.6}$$

1.1 Non-cohesive soils

Several studies advise values for the empirical coefficients for estimating end-bearing capacity (k_p) and shaft friction (k_f) in non-cohesive soils. In 1992 DNV suggested most probable values of 0.001 for k_f and 0.3 for k_p and highest expected values of 0.003 for k_f and 0.6 for k_p. In 2008, Andersen et al. suggested a range of 0.01-0.55 for k_p if k_f is equal to 0.0015 and a range of 0.03-0.60 for k_p if k_f is equal to 0.001. The ranges determined by Andersen et al. are based on prototypes and model tests in dense sands. It is expected that these coefficients are not generally applicable. Senders (2008) used an empirical formulation for k_f borrowed from open-ended pile design Lehane et al. (2005). The resulting values are consistent with the DNV range and overestimate the k_f values of Andersen only slightly. All these studies apply to North Sea sand conditions.

1.2 Cohesive and layered soils

There are few studies on the coefficients k_f and k_p in cohesive soils. DNVGL (2017b) suggests most probable values of 0.03 for k_f and 0.4 for k_p and highest expected values of 0.05 for k_f and 0.6 for k_p. Resistance in layered soils can be obtained using a linear combination of the empirical coefficients (k_f and k_p).

2. Suction-assisted penetration

Estimating the influence of suction on penetration resistance can be challenging (Tran et al., 2007). In the empirical CPT-based design method several deliberate simplifications have been applied.

$$V + s\left(\frac{\pi D_i^2}{4}\right) = \pi D_o k_f \int_0^h q_c(z)\,dz + \left(\pi D_i k_f \int_0^h q_c(z)\,dz + (\pi D t) k_p q_c(h)\right)\left(1 - \frac{s}{s_c}\right) \tag{2.7}$$

2.1 Non-cohesive soils

Two conditions of suction-assisted penetration are taken into account: application of suction below and at the critical limit. When suction below the critical limit is applied the driving force balances the soil resistance affected by the underpressure. At critical suction the soil resistance almost diminishes because the hydraulic gradient has become too large. It is assumed that the internal shaft friction and the end-bearing capacity linearly reduce between the self-weight penetration resistance (at zero suction) and zero (at critical suction). In the CPT-based design method the outer shaft friction is assumed to be unaffected by the underpressure applied (Equation 2.7). An estimate of critical suction is required for application of this method (Section 2.5).

2.2 Cohesive and layered soils

Penetration resistance can be obtained using a linear combination of the empirical coefficients (k_f and k_p). Similar principles as in the Houlsby & Byrne method are applicable to suction-assisted penetration. In sand over clay scenarios the design method does not change for the non-cohesive layer while suction diminishes when penetration into the cohesive layer occurs. In clay (over sand) only the driving force increases due to the effect of differential pressure. However, the linear reduction based on critical suction can result in errors. This is because proper methods for the computation of soil suction limits in layered soils have not yet been developed (Panayides et al., 2017).

2.4. Seepage analysis

Reduction of effective stress is the governing phenomenon for suction bucket installation in non-cohesive soils (Tjelta, 1994). Therefore knowledge of the development of suction pressures over depth is essential. A seepage analysis provides valuable information on whether underpressure development (and therefore a reduction of effective stress) is feasible in layered soils (Tjelta, 2015).

1. Theoretical background

Hydrostatic water pressure no longer applies when pore water flow is generated by suction under the lid of the bucket. Darcy's law is most commonly applied to describe steady state water flow in soils. It is a product of the permeability and the hydraulic gradient in multiple directions (Verruijt, 2012). When Darcy's law is integrated into the continuity equation one finds a form of the Laplace equation (expressed in cylindrical coordinates in Equation 2.8). This is a partial differential equation which can be solved if all boundary conditions, around the domain considered, are defined (Biot, 1962). Solving this problem over the domain results in the variation of pore pressure (u) over depth.

$$\bigtriangledown^2 u = \frac{1}{r}\frac{\delta u}{\delta r} + \frac{\delta^2 u}{\delta r^2} + \frac{\delta^2 u}{\delta z^2} + \frac{1}{r^2}\frac{\delta^2 u}{\delta \phi^2} \tag{2.8}$$

2. Axisymmetric finite element model of normalized underpressure

Old analytic methods for solving 2D seepage problems (e.g. a flow-net) are not easy to implement in a direct reliability analysis and lack accuracy (Verruijt, 2012). Therefore a 2D finite element analysis program was developed. The geometry is modelled as an axisymmetric element around the vertical centerline of the bucket. Neumann (impermeable) boundaries are applied at all but the top boundaries of the domain. A constant non-zero head (suction) is applied as a boundary condition inside the bucket while outside zero head is applied (Ibsen and Thilsted, 2010). When one applies axisymmetry it is assumed that the suction behavior of each bucket is independent of other buckets. This can be different for suction bucket jackets because multiple buckets are positioned close to each other. However, integration of a 3D coupled analysis in a direct reliability analysis will prove to be computationally infeasible. This model is therefore a practical solution.

After solving the steady-state analysis the variation of underpressure along the skirt wall can be determined (Ibsen and Thilsted, 2010). The suction is normalized with respect to the boundary condition inside the bucket. The problem only has to be solved only once per penetration depth because of the linear behaviour of permeability in Darcy's law. When the normalized underpressures over depth are known they can be applied for different levels of applied suction using this linear relation (Figure 2.6a). The outcomes of the seepage model were verified with earlier studies (Figure 2.6b). The possibility to vary the permeability of the soil plug has been added based on recommendations in literature (Harireche et al., 2014 & Section 5.3).
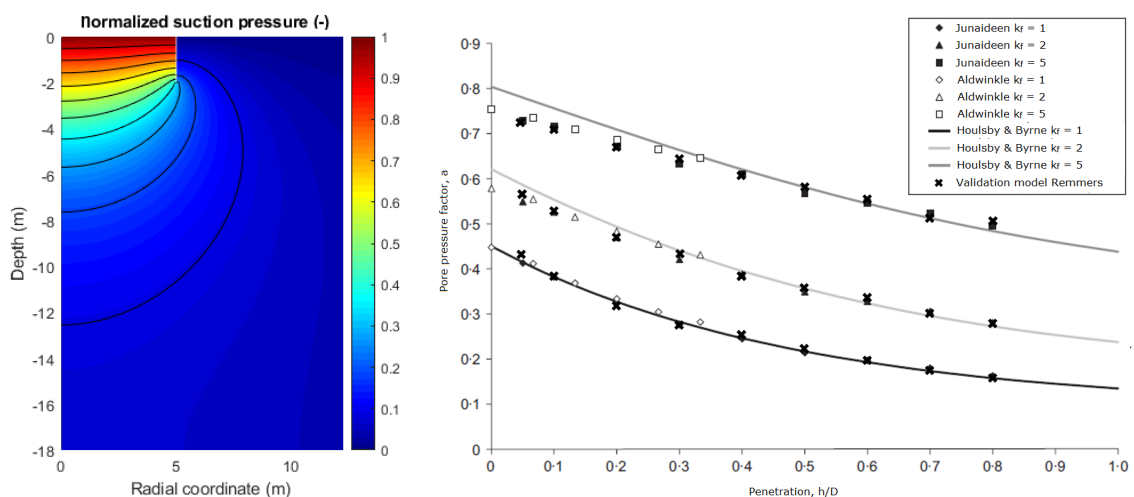
(a) Normalized underpressure plot   (b) Validation developed seepage model with Houlsby and Byrne (2005b)

Figure 2.6: Results and validation of seepage analysis required of variation underpressure over depth

2.5. Critical suction

The Houlsby & Byrne and CPT-based design method are used to compute the required suction for penetration. The methods in this Section can be used to determine the maximum underpressure allowed.

1. Definition

Critical suction is defined as the maximum value of suction which can be applied inside the caisson at which penetration can still be achieved. Suction levels exceeding critical suction can cause installation failure. Critical suction is governed by cavitation, structural (e.g. buckling) or soil limitations. In permeable soils high suction levels can cause formation of piping channels which breaks the soil plug and can cause excessive soil heave (Ibsen and Thilsted, 2010). In impermeable soils critical suction is often considered to be the suction level at which the soil plug becomes unstable (Randolph and Gourvenec, 2011).

2. Cavitation limits

Cavitation occurs when the underpressure is equal to the atmospheric pressure (p_a) added to the hydrostatic water pressure minus the pressure at which cavitation occurs (p_c) (Equation 2.9). The cavitation pressure is set equal to zero in this research (Senders, 2008). Suction bucket jackets for offshore wind are often located in relatively shallow water (h < 30 m). This imposes relatively strict cavitation limits (Ibsen and Thilsted, 2010).

$$s_c = p_a + \gamma_w h - p_c \quad \text{with:} \quad p_a = 100\,\text{kPa} \quad \text{and} \quad p_c = 0\,\text{kPa} \tag{2.9}$$

3. Soil limits

While it is straight forward to estimate cavitation limits the critical suction levels causing failure mechanisms in the subsoil are harder to estimate. They also differ for non-cohesive and cohesive soils.

3.1 Non-cohesive soils

The soil suction limit in permeable soils is defined as the suction which causes a critical hydraulic gradient to occur adjacent to the lower part of the inner skirt wall. Feld (2001) used FE models (SEEP) to estimate the effect of seepage on the effective stress reduction and proposed an empirical formula based on the ratio of penetration depth over diameter and the effective soil unit weight. Houlsby and Byrne (2005b) incorporated the influential parameter of soil permeability ratio ($k_f = k_i/k_o$) and developed an empirical formula based on earlier FE studies. Senders and Randolph (2009) did several numerical simulations and established an empirical relation based on exit seepage length. Finally Ibsen and Thilsted (2010) used a finite difference code (FLAC) to estimate soil suction limits in sands. Equation 2.10 presents the result of Ibsen and Thilsted (2010) which shows similarities with the formulations in other studies.

$$\frac{s_c}{\gamma' D} = \left(\frac{H}{D}\right)\left(\pi - \arctan\left[5\left(\frac{H}{D}\right)^{0.85}\right]\left(2 - \frac{2}{\pi}\right)\right) \tag{2.10}$$

Research showed that critical gradients higher than predicted by these models could be applied in some cases. Empirical formulas appear to be too conservative. Especially when soil arching, a pressure reduction due to shear stresses of yielding soils, occurs these equations do not hold (Panagoulias et al., 2017). These mechanisms are not considered in this research because there are no solid design methods available to describe them. In Section 5.3 the used computation of the soil suction limit is developed.

3.2 Cohesive soils

Critical suction in purely cohesive and impermeable soils is governed by the phenomenon of soil heave. This occurs when the underpressure multiplied with the soil plug area (A_p) becomes equal to the inner skirt resistance (R_i) and the buoyant soil weight (W') (Randolph and Gourvenec, 2011; Randolph et al., 1998). Solving this vertical equilibrium leads to the soil suction limit for these situations (Equation 2.11).

$$s_c = \frac{R_i + W'}{A_p} \tag{2.11}$$

3.3 Layered soils

The empirical formulas for soil suction limits do not apply for layered soils with different permeabilities. Ibsen and Thilsted (2010) determined soil suction limits for a layered profile on the basis of a similar seepage study described in Section 2.4. However, this did not result in an applicable design method in general.

2.6. Evaluation

Proper design methods are a requirement for a reliability analysis. This Chapter elaborated on the methods which are most dominant in current research and practice. In this Section these methods will be evaluated and the consequences of using these methods within the reliability-based design framework will be discussed.

1. Discussion on design methods
Several elements of the current design methods can be questioned on the basis of previous Sections and discussion and recommendations in existing literature. Before the specific shortcomings are discussed it should be noted that existing methods only apply for individual suction bucket installation. Installing multiple suction buckets at the base of a jacket simultaneously is expected to cause slight differences. The difference in seabed level as well as the variation in soil profiles between buckets become important. It is also plausible that the seepage patterns of individual buckets could influence each other.

Both design methods (CPT-based and Houlsby & Byrne) have shortcomings when applied to layered soils of varying permeability. First of all the seepage assumptions in both methods are developed for uniform sands or impermeable clays. The results of the seepage analysis should be reflected in the penetration studies to give more realistic predictions. The CPT-based method is only valid in dense sands according to Andersen et al. (2008). Relatively little background is given regarding the estimation of the empirical parameters (k_f & k_p) based on site specific data. The original method of Houlsby & Byrne does not show how to compute stress enhancement for layered soils (Houlsby and Byrne, 2005b; 2005a). This problem can easily be solved by numerically solving the equations and checking on vertical stress continuity. Finally the accuracy of the soil suction limit estimation methods can be questioned. All empirical correlations are only valid for uniform sands while this is a situation which is rare in practice. Although soil suction limits for pure cohesive and uniform sandy soils can be estimated, methods are absent for subsoils with varying permeability which are often encountered in practice. Finally it is expected that that cavitation or buckling could impose even stricter limits in shallow waters (Ibsen and Thilsted, 2010).

2. Integration in the reliability-based design framework
Two types of uncertainties are present when performing the installation design computations for suction bucket jackets. The model uncertainties caused by empiricism or model shortcomings are discussed in Chapter 5. Parametric uncertainties can cause significant variation in the model outcomes as well. Several parameters are required as input for the installation design computation. In this research it is assumed that the geometric characteristics of a suction-bucket jacket are constant, while soil parameters are expected to vary. Table 2.1 presents all parameters required as input for the installation design computation. The estimation method and variability of these parameters will be discussed in Chapter 4.

Table 2.1: Environmental parameters required for design methods on suction bucket installation design

Parameter	Sign	Unit	Required for:
Level mudline	h	m	CPT-based- and Houlsby & Byrne method
Soil unit weight	γ	kN/m^3	Houlsby & Byrne method, critical suction
Stress-ratio	K	-	Houlsby & Byrne method (and critical suction)
Internal friction angle	ϕ	^{o}	Houlsby & Byrne method (and critical suction)
Interface friction angle	δ	^{o}	Houlsby & Byrne method (and critcial suction)
Undrained shear strength	s_u	kN/m^2	Houlsby & Byrne method
Adhesion factor	α	-	Houlsby & Byrne method
Permeability	k	m/s	Critical suction (e.g. seepage analysis)
Cone resistance	$q_{c,t}$	kPa	CPT-based method

The results of the design methods presented in this Chapter do not give explicit information regarding the feasibility of design. The outcomes of the design methods will be split up in a feasible and infeasible domain later in this research (Chapter 6). The boundary between these domains is called a limit state. Limit states define the scenarios for which installation failure occurs. Based on the failure mechanisms described in Chapter 3 these limit states will be formulated at the start of the direct reliability analysis in Chapter 6.

3

Qualitative reliability analysis

Proper understanding of possible events and failure mechanisms which could occur during installation is required for a good feasibility assessment. In this Chapter these elements are investigated after which they are integrated into the reliability-based design framework.

3.1. Overview

The qualitative reliability analysis is an essential part within the reliability-based design framework. This Section describes the function of this analysis and also elaborates on the four system elements which are relevant for geotechnical installation of suction bucket jackets.

1. Introduction

Geotechnical installation design computations reflect a complex process of soil structure interaction while installation in practice often consists of a set of simple actions. To make a proper reliability-based analysis of the feasibility of installation it is required that there is good insight in both of these aspects (and their interaction). It is therefore beneficial to create a fixed structure in which all scenarios are orderly presented.

Contractors which perform offshore installation often work with a base case scenario and possible contingencies. The feasibility of installation is assessed based on the base case scenario while preparations are made for the application of contingency measures. Flowcharts and decision trees are used to assess the need for application of contingency measures during installation (Section 3.2). These flowcharts give a good overview of installation sequences and provide a step by step analysis. However, they are not ideal to assess installation feasibility within the reliability-based design framework.

It was decided to perform the qualitative reliability analysis of this research with two tools: event trees and fault trees. Event trees represent the base case and contingencies available. They systematically evaluate the possible (practical) scenarios possible during installation (Jonkman et al., 2017). Fault trees represent the processes which underlie these events and could cause installation failure.
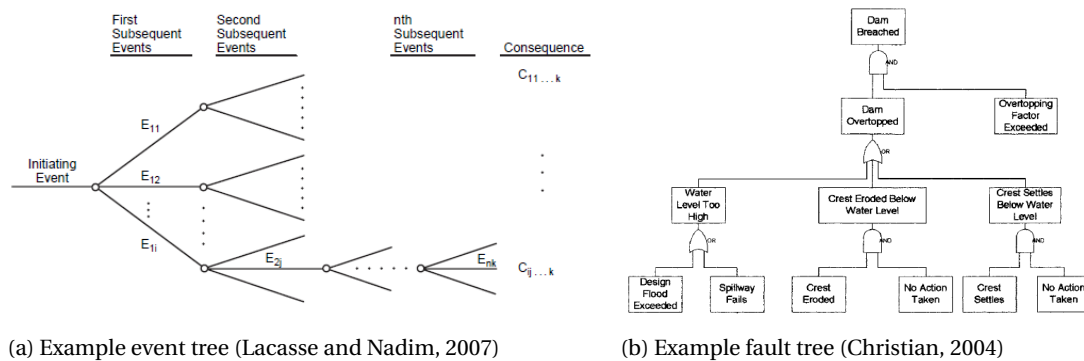

(a) Example event tree (Lacasse and Nadim, 2007)   (b) Example fault tree (Christian, 2004)

Figure 3.1: Examples of qualitative reliability analysis tools used in this research

2. System analysis

Four elements form the total system during geotechnical installation: the suction bucket jacket, the filter layer of the scour protection, the seabed and the subsoil (Lesny and Richwien, 2011).

2.1 Suction bucket jacket

This component consists of either a three or four legged lattice structure and a suction bucket positioned at the base of each leg. The suction buckets are rigidly connected to the jacket leg. The buckets have no difference in vertical position. Each bucket consists of a cylindrical steel element (skirt) and a lid closing of the top (Foglia and Ibsen, 2014). All buckets beneath the jacket have similar dimensions and are equipped with a venting and pumping system.

During installation several parameters in and around the bucket are monitored. The governing parameters for installation success are clearance to the seabed, penetration depth and tilt of the jacket. However, process parameters like differential pressures, pump flow and static pressures are monitored for installation purposes as well.

2.2 Filter layer of the scour protection

A fully installed scour protection consists of multiple layers of coarse material (e.g. rocks). A filter layer is installed on the seabed to prevent winnowing out of sand through the scour protection (Whitehouse et al., 2011). Scour protection is often required because suction buckets rely heavily on soil close by (Zaaijer, 2003). The filter layer is placed before geotechnical installation due to increased accessibility as well as for the prevention of scour during installation. The filter layer of the scour protection is placed directly on the seabed, consists of smaller rocks with specific grading and is often a few decimeters thick. During the entire geotechnical installation the suction buckets interact with the filter layer. The filter layer is governing installation resistance when the skirts need to penetrate through this layer (Asgarpour, 2016).

2.3 Seabed level

The seabed forms the interface between the filter layer and the subsoil. Contrary to single suction anchors the seabed is an important element for suction bucket jacket design. This is the case because seabed elevation can differ per individual bucket of a jacket. The seabed level can differ due to sloping or seabed features like ripples. Geohazards like seabed scour, man-made hazards and boulders could be encountered at the seabed. These hazards can negatively interact with the foundation during installation. During geophysical surveys the seabed is mapped and potential geohazards can be identified.

2.4 Subsoil

Together with the suction bucket jacket the subsoil is the most important element under consideration. It consists of all the soil layers and other objects below the seabed. Often the subsoil consists of multiple layers of soil which show different behavior. These layers are often inhomogeneous, can be inclined and can contain lenses (Sturm, 2017). Circumstances can differ per suction bucket of one jacket due to the large heterogeneity of the subsoil. The subsoil can contain geohazards like boulders and shallow gas deposits. These can negatively interact with the foundation during installation (Houlsby and Byrne, 2005a). The elements and characteristics of the subsoil are identified during geophysical and geotechnical surveys.

(a) Jacket [28]   (b) Filter layer   (c) Seabed   (d) Subsoil [100]
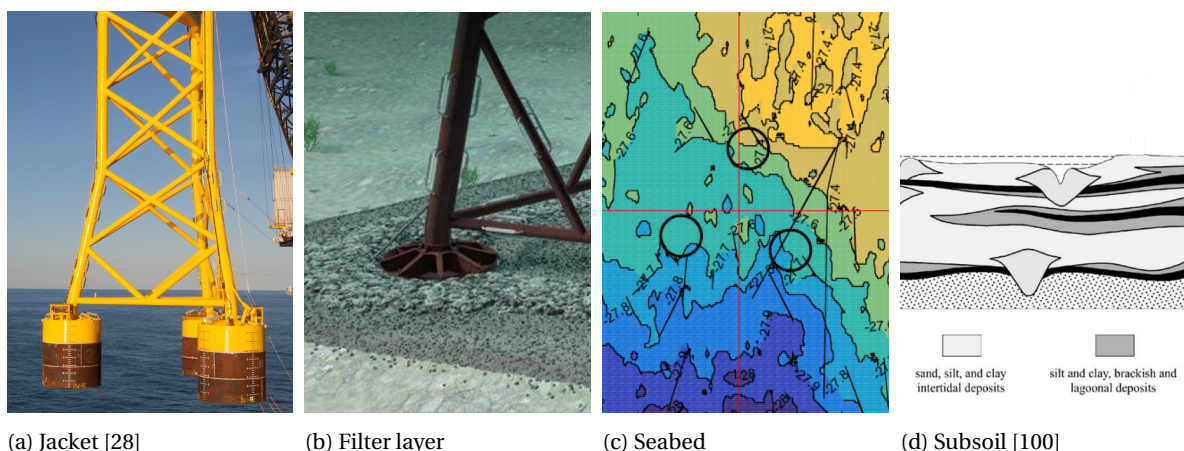
Figure 3.2: Main elements in the process of geotechnical installation of suction bucket jackets

3.2. Installation events

The installation procedure is a process of actions, events and contingency measures. In this Section the current way of dealing with events during installation is described after which an event tree is made for geotechnical installation of suction bucket jackets.

1. Current practice

At the moment of writing decision trees are used to deal with possible events during installation. These trees consist of tasks, assessment steps and contingency measures to apply. A decision tree for both the self-weight as well as the suction-assisted penetration phase is used in design practice. Part of these decision trees are displayed in Figure 3.3.

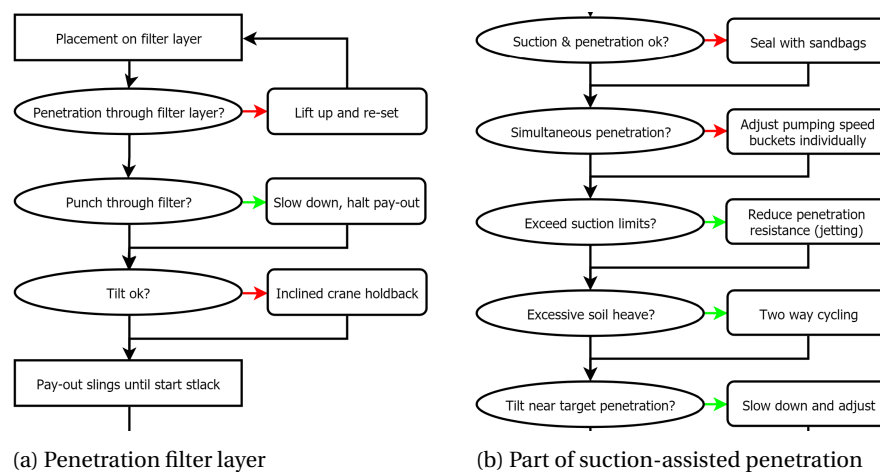(a) Penetration filter layer   (b) Part of suction-assisted penetration

Figure 3.3: Part of the decision trees used in practice during installation of suction bucket jackets

It can be identified that geotechnical installation of suction bucket jackets is a series system. When one installation phase fails the entire installation procedure fails. Four phases are identified:

1.1 Penetration of the filter layer

The first phase is penetration through the filter layer. It starts after horizontal placement of the suction buckets on top of the filter layer and ends when the skirts of all buckets have penetrated the entire layer. Risks during this installation phase are refusal, punch-through of bucket(s) and excessive tilt. Ballast cannot be applied in this phase due to the high end-bearing capacity of the filter layer and the corresponding risk of buckling. The suction bucket jacket is still attached to the crane in this phase. This allows for corrections.

1.2 Self-weight penetration

The second phase is self-weight penetration into the subsoil. It starts when the skirts reach the seabed and ends if the jacket tilt is stable when or after the required self-weight penetration has been reached. Ballast can be applied when the buckets do not penetrate until the required self-weight penetration depth. This increases the buoyant weight and therefore induces further penetration (Randolph and Gourvenec, 2011).

1.3 Start of suction-assisted penetration

The third phase is the start of suction-assisted penetration. It starts at the end of self-weight penetration and ends when stable underpressure and penetration are achieved. When the suction bucket jacket is tilted at the start of suction-assisted penetration, suction is applied first on the least penetrated bucket. If the underpresssure is unstable or no penetration is achieved a survey has to be executed to check for the occurrence of piping. If this is not the case pumping speed could be increased. Ballast should be applied to increase the seal if piping does occur (Tjelta, 1994). As a last resort sandbags can be used to seal potential piping channels.

1.4 Suction-assisted penetration until target depth

The fourth and final phase of installation is the suction-assisted penetration until target depth. It starts when underpressure and penetration is achieved at all buckets and ends at target depth. If even penetration cannot be achieved the pumping speeds of buckets must be adjusted individually. This prevents excessive tilt. Jetting or two way cycling of the seepage flow can be used to decrease soil resistance when premature refusal occurs (Senpere and Auvergne, 1982). Often backfilling the empty spaces with grout occurs as a final step.

2. Event tree definition

Event trees are an optimum way to quantify hazards and risks within the reliability-based design framework (Lacasse and Nadim, 2007). Contrary to the decision trees used during installation, event trees are used to describe risks at an early stage in design. They also allow for integration of possible results of direct reliability analyses within reliability-based design framework (Jonkman et al., 2017). Each event tree starts with an initiating event which can lead to a set of consequences. In this case the two possible consequences are successful installation or failure. A sequence of sub-events takes place between the initiating event and each possible outcome. The probability of each outcome is the product of the conditional probabilities of all sub-events (Lacasse and Nadim, 2007; Christian, 2004).

To assure optimal functioning of the event tree several requirements need to be met. Firstly the events incorporated in the event tree should be exhaustive. Secondly all known possible outcomes of the initiating event should be included (Lacasse and Nadim, 2007). This assures that the sum of probabilities at each node in the event tree is equal to one. Thirdly the subsequent events should be mutually exclusive, which means they cannot occur at the same time (Jonkman et al., 2017). Fourthly the probabilities incorporated in the event tree should be conditional. This implies that the probability of an event in the tree is not affected by preceding events. The final requirement of the event tree is that they should lead to an outcome which describes either success or failure (Christian, 2004).

Conditions that could lead to potential installation failure are often quite plentiful (Sturm, 2017). Initiating events with many possible consequences could lead to large and cluttered event trees. Several requirements regarding application of the event tree are set for this analysis. Failure is indicated in the bottom branches of the event tree. No excessive details are included to avoid a too large event tree. Finally sub-trees are used to include all mechanisms within subsequent steps of suction bucket installation (Jonkman et al., 2017). The next subsection describes the total event tree used in this research.

3. Event tree application

To avoid a complex and cluttered event tree a general event tree is used (Figure 3.4). The initiating event of the event tree is the horizontal placement of the suction bucket jacket on the filter layer. All four installation phases are implemented as branches in the tree. When all installation phases are completed successfully the suction bucket jacket is properly installed. However, when one of the four phases cannot be completed the installation fails.
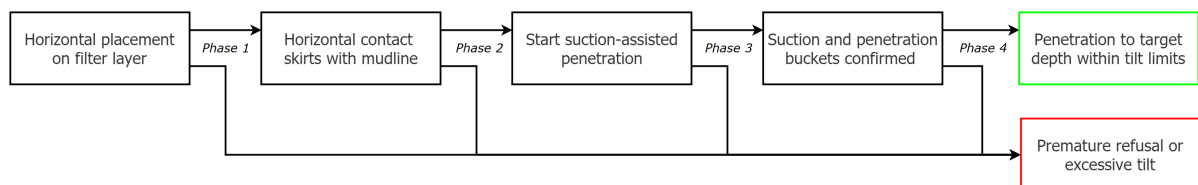

Figure 3.4: General event tree for geotechnical installation suction bucket jackets

3.1 Sub-event tree 1: Penetration of the filter layer

Penetration through the filter layer is the first phase of geotechnical installation of suction bucket jackets. The sub-event tree for this phase is presented in Figure 3.5. Ideally the skirts of the buckets penetrate through the filter layer and touch the seabed without any tilt. However, refusal can occur due to the high bearing capacity of the filter layer. Installation fails if all buckets refuse to penetrate through the filter layer. Ballast cannot be applied at this stage due to the risk of buckling. An attempt can be made to reposition the suction bucket jacket on a different location or at higher speed. Since this requires a new attempt of installation it is considered as installation failure in this research. If only one or two buckets are refused by the filter layer it can be tried to apply a moment on the crane (to which the suction bucket jacket is still attached). If the top layers of the subsoil are relatively weak a risk of punch-through exists. When punch-through occurs the consequences can be mitigated by holding back the crane. The consequences of all these sub-events are either installation failure or crane intervention. Because crane intervention lies outside the scope of this research further details will not be discussed.
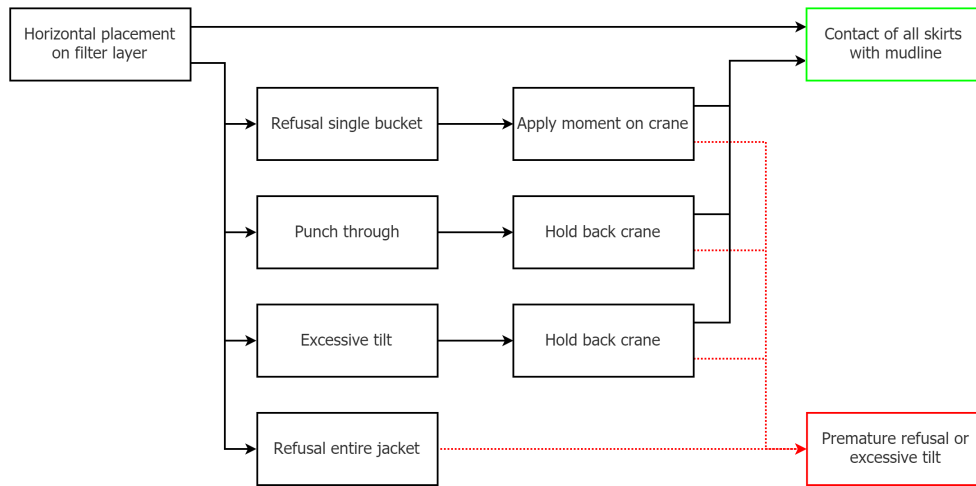
Figure 3.5: Sub-event tree of the penetration of a suction bucket jacket through a filter layer

3.2 Sub-event tree 2: Self-weight penetration

Self-weight penetration is the second phase of suction bucket jacket installation. The sub-event tree corresponding to this phase is displayed in Figure 3.6. Ideally the skirts of the buckets penetrate the subsoil layers in a stable manner until or below the required self-weight penetration depth. If excessive tilt or instability occurs the venting gaps of (individual) buckets can be closed. This creates overpressure inside bucket(s) and therefore hinders further penetration. This mitigation measure could potentially improve the verticality and stability of the structure. Ballast can be applied if the self-weight penetration is below the set criteria. This enlarges the buoyant weight on the buckets and therefore increases self-weight penetration (Randolph and Gourvenec, 2011). Finally excessive scour can occur adjacent to the suction buckets during self-weight penetration. This could decrease the seepage length drastically and contribute to installation failure (Sturm, 2017). In this research it is expected that the filter layer will prevent excessive scour.
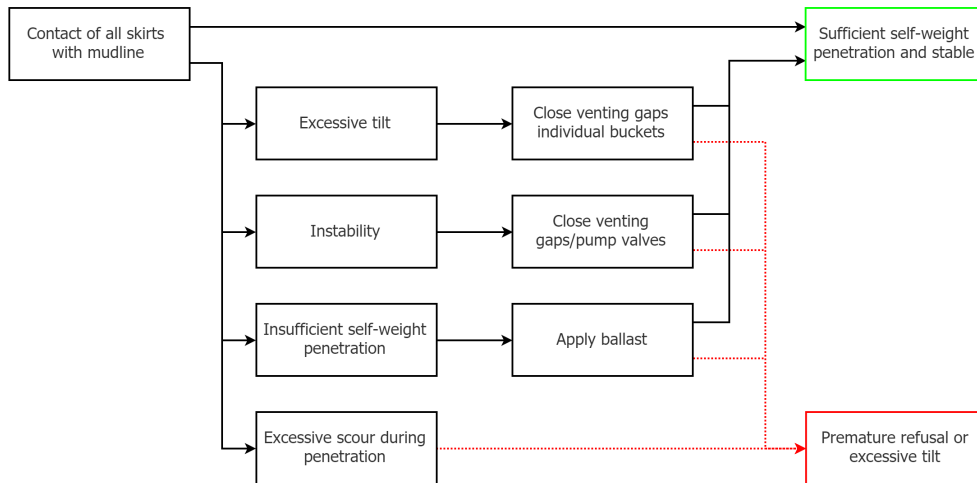

Figure 3.6: Sub-event tree of the self-weight penetration of a suction bucket jacket in the subsoil

3.3 Sub-event tree 3: Start of suction-assisted penetration
This phase is the most critical and complex of all phases of suction bucket jacket installation. The sub-event tree corresponding to the start of suction-assisted penetration is displayed in Figure 3.7. If the suction bucket is tilted at the end of self-weight penetration the suction should be applied on the least penetrated bucket first. This phase is successfully completed when the underpressure is stable for all buckets and penetration of the skirts is achieved. If excessive leakage occurs one can attempt pumping at a higher speed (Sturm, 2017). This is only allowed when there are no signs of piping. If there are signs of piping the seal can be improved by applying more ballast. If piping still occurs after the application of ballast a last attempt can be made to start suction-assisted penetration by sealing the piping channels with sand bags. If this does not stop piping the bucket(s) will refuse further penetration and installation fails.
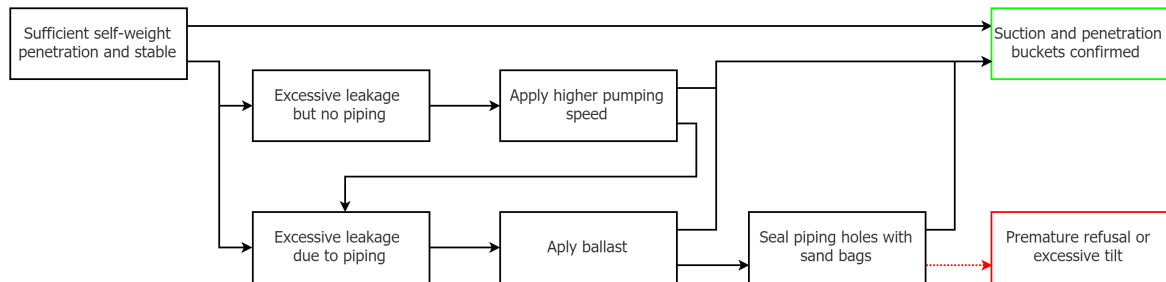

Figure 3.7: Sub-event tree for the start of suction-assisted penetration of a suction bucket jacket

3.4 Sub-event tree 4: Suction-assisted penetration until target depth
The fourth and final phase is the penetration until target depth while applying underpressure under the lid of the bucket. The sub-event tree corresponding to this phase is displayed in Figure 3.8. This phase is successful when penetration of all skirts reaches target depth and the structure stays within tilt limits. When excessive tilt occurs during penetration the underpressure can be varied per bucket to level penetration speeds and therefore improve verticality. Jetting or cyclic pumping can be applied when the suction limit of the pumps or critical suction levels in the soil are reached (Senpere and Auvergne, 1982). Bucket penetration could be prevented by excessive soil heave inside the plug. In this case two way cycling can be used to mitigate the heave and induce further penetration. Finally it can occur that the bucket is penetrated until target depth but the tilt requirements are not met. In this phase it can be attempted to jack up bucket(s) by applying overpressure and so adjust the verticality of the jacket.
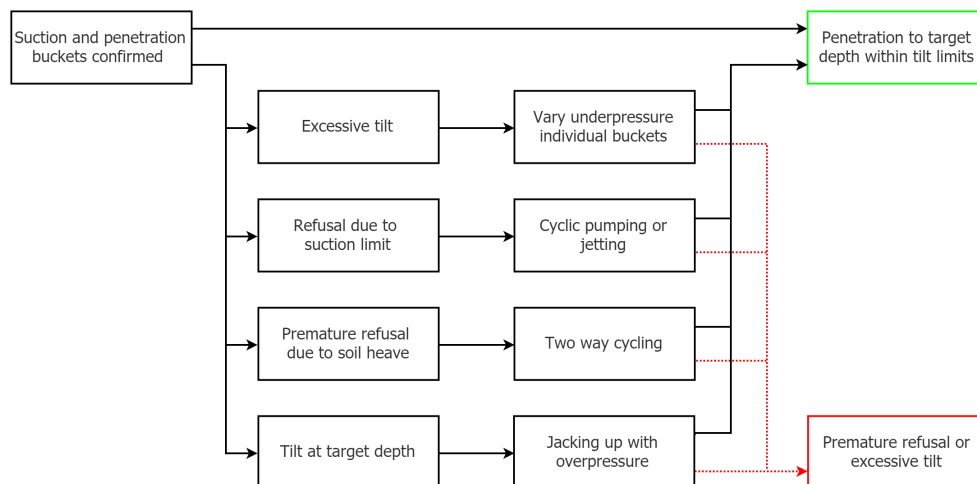

Figure 3.8: Sub-event tree for suction-assisted penetration of a suction bucket jacket until target depth

It is common in practice that free space is left between the lid of the buckets and the seabed after successful installation. This can have two causes. Firstly it could be that seabed level differences cause free spaces in individual buckets. Secondly it is possible that the target depth required by the client is lower than the bucket skirt length. At this moment it is common in practice to fill any free space with grout.

3.3. Installation failure

Failure occurs when the result of installation does not meet the requirements set in advance. Failure can be caused by multiple mechanisms which are integrated into a fault tree in this Section.

1. Definition

Successful installation is achieved by reaching target penetration depth with all buckets while staying within the tilt limits of the jacket. Installation failure is therefore caused by two mechanisms: premature refusal and excessive tilt (Lesny and Richwien, 2011). Premature refusal of one or multiple buckets is defined as prevention of further penetration before target depth is reached. Premature refusal is problematic because insufficient penetration depth affects the structural integrity of the support structure over its lifetime. Excessive tilt is defined as too much vertical offset during penetration or at target depth. During installation it can cause peak stresses in the bucket skirts (Lesny and Richwien, 2011). If excessive tilt is present at target depth the support structure does not satisfy the requirements for proper functioning of the wind turbine which will be placed on top of the jacket (Ibsen et al., 2005).

2. Failure mechanisms

Installation failure can be caused by many different conditions and mechanisms. Over the years many have been described in literature for individual suction buckets (Sturm, 2017; Foglia and Ibsen, 2014). The overview presented in this research differs in two ways: it takes failure mechanisms considered in practice as well as the jacket configuration into account.

2.1 Uneven seabed (Figure 3.9a):

The seabed can be sloping or uneven (Section 3.1). These level differences can contribute to failure in several ways. It can prevent buckets from reaching target penetration depth. It can prevent sufficient self-weight penetration of individual buckets. Finally it can contribute to excessive tilt during penetration of the filter layer, self-weight penetration and close to target depth.

2.2 Boulder encounter (Figure 3.9b):

Boulders can be present depending on the geological history of the area where the wind farm is planned (Leblanc, 2009). They can be positioned at the seabed as well as in the subsoil. Similar to pile installation the encounter of a boulder by the skirt tip during installation could have refusal or structural failure as a consequence (Stuyts et al., 2017). Boulders can also contribute to piping in individual buckets due the disturbance of the soil close to the skirt during installation (Sturm, 2017).

2.3 Refusal by filter layer (Figure 3.9c):

The filter layer is present during installation. It can contribute in multiple ways to installation failure. It can cause refusal due to its large bearing resistance. This can happen for individual buckets and the total jacket configuration. There is a risk of the filter layer stones contributing to piping effects during suction-assisted penetration as well. They could disturb the soil in a similar way as boulders.
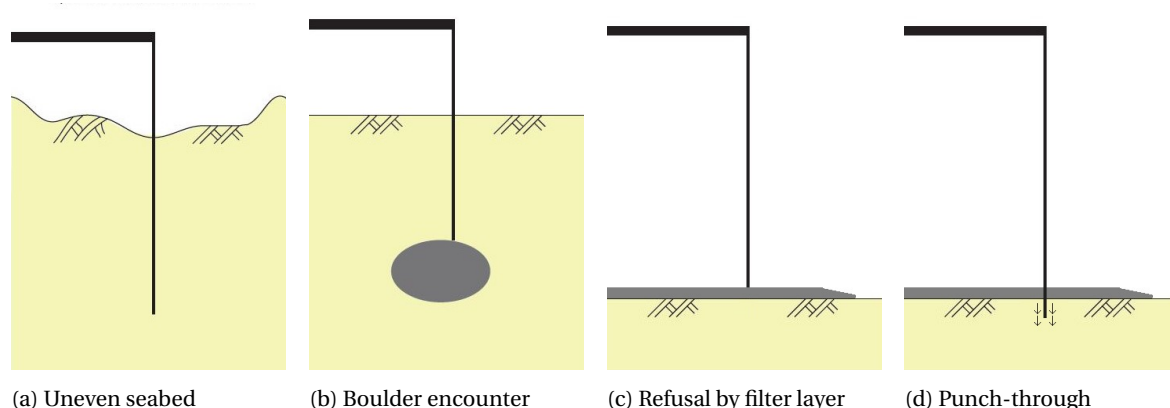

(a) Uneven seabed   (b) Boulder encounter   (c) Refusal by filter layer   (d) Punch-through

Figure 3.9: Failure mechanisms of geotechnical installation of suction buckets (1/4) (based on: Sturm, 2017)

2.4 Punch-through the filter layer (Figure 3.9d):
Punch-through can occur when a skirt reaches the bottom of the filter layer. This is especially relevant when the top layer of the subsoil is very weak. This could cause structural damage as well as excessive tilt if it occurs at individual buckets.

2.5 Insufficient self-weight penetration (Figure 3.10a):
When the top soil layer(s) provides high penetration resistance the self-weight penetration could stay below the required depth. Sufficient self-weight penetration is required for the formation of a seal which allows the start of starting suction-assisted penetration. Insufficient self-weight penetration could cause piping during the start of suction-assisted penetration and could therefore contribute to premature refusal (Sturm, 2017).

2.6 Piping (Figure 3.10b):
High seepage gradients can cause inner erosion to continuously increase. This could causes channels to be formed and the flow of excessive volumes of water through the soil plug (Tran et al., 2007). Piping channels cause a large seepage flow and this makes further penetration impossible (Sturm, 2017).

2.7 Inner erosion (Figure 3.10c):
When the grading of the subsoil is wide (e.g. a gap in the particle size distribution curve), the smaller soil particles could flow out of it when high suction pressures are applied. This could cause excessive leakage and therefore hinder suction-assisted penetration (Sturm, 2017).

2.8 Excessive loosening (Figure 3.10d):
When the effective stress in coarse subsoils is reduced the soil can loosen and dilate. This could cause filling of the inner part of the bucket which could cause premature refusal. Loosening could also stop installation due to the fact that it contributes to excessive leakage (Sturm, 2017).
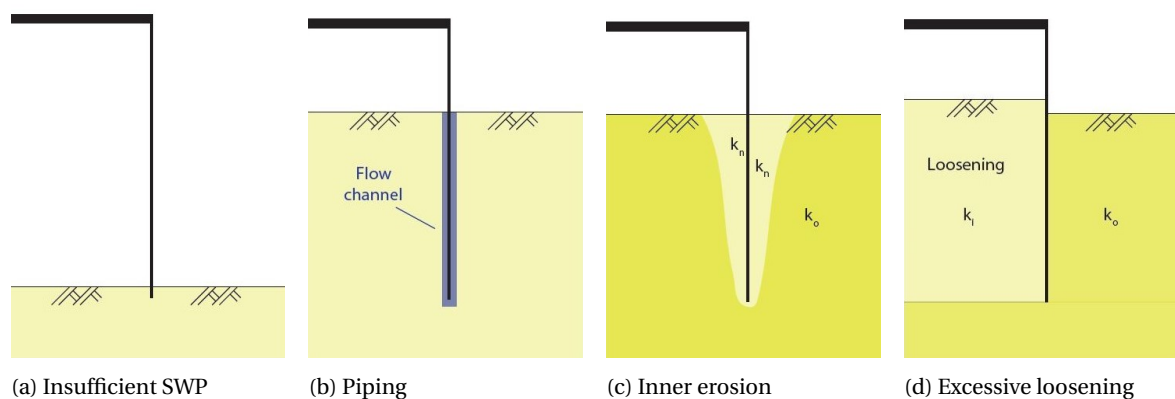

(a) Insufficient SWP   (b) Piping   (c) Inner erosion   (d) Excessive loosening

Figure 3.10: Failure mechanisms of geotechnical installation of suction buckets (2/4) (based on: Sturm, 2017)

2.9 Seabed scour (Figure 3.11a):
Scour during installation could cause problems at the start of suction-assisted penetration. It is more difficult to form a stable seal due to a decreased seepage length. This could cause premature refusal (Sturm, 2017).

2.10 Preferential flow (Figure 3.11b):
Preferential flow can occur when either high or low permeable lenses are present in part of the cross section of the soil plug. Flow can be concentrated to part of the cross section due to the horizontal variability in permeability. This could cause highly reduced effective stresses in this part which could lead to local failure and can have premature refusal as a consequence.

2.11 Stucking in high permeable soils (Figure 3.11c):
Stucking can occur when insufficient underpressure is generated in permeable layers during penetration. The drainage capacity is large due to the high permeability. This prevents achieving the required underpressure and as a consequence the reduction of inner vertical effective stress (Houlsby and Byrne, 2005a). This could cause premature refusal (Sturm, 2017).
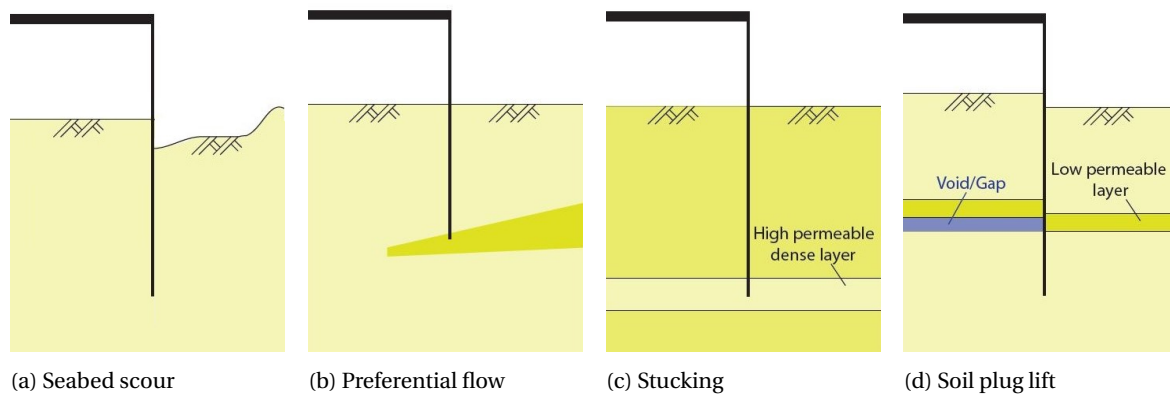
(a) Seabed scour   (b) Preferential flow   (c) Stucking   (d) Soil plug lift

Figure 3.11: Failure mechanisms of geotechnical installation of suction buckets (3/4) (based on: Sturm, 2017)

2.12 Soil plug lift (Figure 3.11d):
Soil plug lift can occur when impermeable layers are present within the soil plug. The applied underpressure could cause part of the soil plug to lift and allow for an empty space filled with water. This prevents further penetration and weakens the in place resistance after installation (Sturm, 2017).

2.13 Seepage blocking (Figure 3.12a):
The seepage in a sand layer can be blocked due to the presence of a clay layer on top of it. Therefore an effective stress reduction in the sand layer underneath the clay layer is impossible. This could cause refusal due to a too high soil resistance (Sturm, 2017; Houlsby and Byrne, 2005a).

2.14 Soil plug heave & reverse end-bearing (Figure 3.12b):
Soil plug heave is caused by displacement of the soil by the caisson and excessive underpressure which causes inward flow (Rusaas et al., 1995). In this research soil plug heave is considered together with the failure mechanism of reverse-end bearing (Houlsby and Byrne, 2005a). This is inward flow of soil due to the reduced bearing capacity of the soil plug. The increased soil level inside the bucket can cause refusal or tilt.

2.15 Soil profile differences (Figure 3.12c):
Suction bucket jackets have buckets placed at different locations and therefore in different soil conditions (Negro et al., 2014). During simultaneous penetration of the buckets local soil profile differences or circumstances could cause a difference in penetration speed. This can result in peak stresses due to tilt when penetration speeds differ or failure of the entire installation due to refusal of an individual bucket.

2.16 Sliding (Figure 3.12d):
Sliding could occur when the suction bucket jacket reaches the seabed and is still attached to the lifting crane. Due to movements of the crane the jacket could disturb the top soil layer. This could cause problems at the start of suction-assisted penetration due to a disturbed or reduced soil plug (Sturm, 2017).
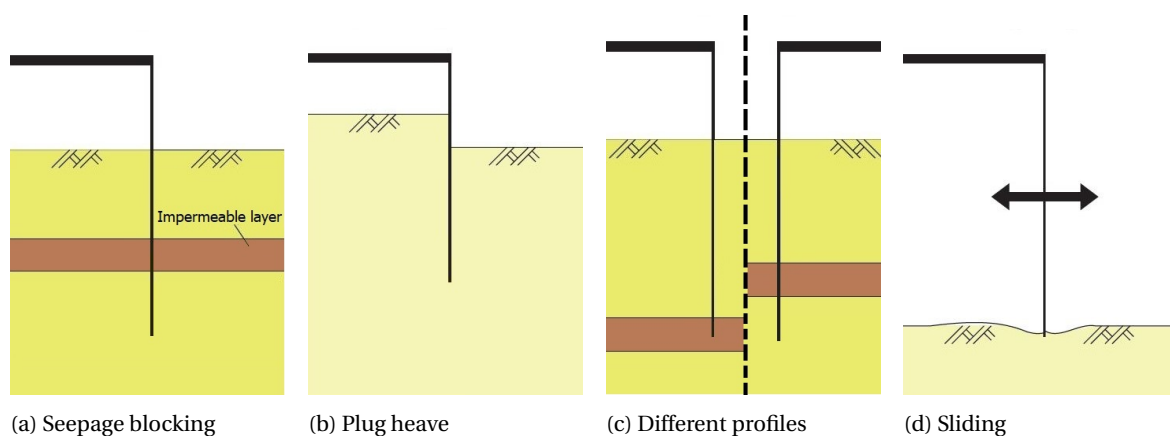

(a) Seepage blocking   (b) Plug heave   (c) Different profiles   (d) Sliding

Figure 3.12: Failure mechanisms of geotechnical installation of suction buckets (4/4) (based on: Sturm, 2017)

3. Fault tree definition

The fault tree is an ideal method to map possible problems during installation. Contrary to event trees fault trees show the conditions which should be met before installation failure can occur (Christian, 2004). The tree is developed top down by moving from condition to condition. Again several requirements are set regarding the setup of the logic tree. Firstly all the conditions at each stage must be independent. Occurrence of one condition should not affect the occurrence of the others. Secondly specific failure mechanisms require one (series system) or more (parallel system) conditions to occur. This needs to be integrated by using gates which describe the character of the failure mechanism and its conditions. The probability of installation failure is computed bottom upwards by progressively taking into account all failure mechanisms (Jonkman et al., 2017). The top of the fault tree is in this case defined as 'geotechnical installation failure'.

4. Fault tree application

Integrating all failure mechanisms in one fault tree can be a cumbersome job. A few practical decisions have been made regarding the fault tree which was developed for this research. In the fault tree no distinction is made in the manner of failure (e.g. excessive tilt or premature refusal). This is done because several failure mechanisms can be responsible for both conditions of failure. This would create dependencies if they were integrated separately. Two types of conditions were identified as the main cause of failure: obstacle encounter and soil conditions. Only parallel failure mechanisms are present in the top layers of the fault tree. This means that every failure mechanism is equal to the largest probability of its individual sub-mechanisms. Figure 3.13 presents the fault tree system.
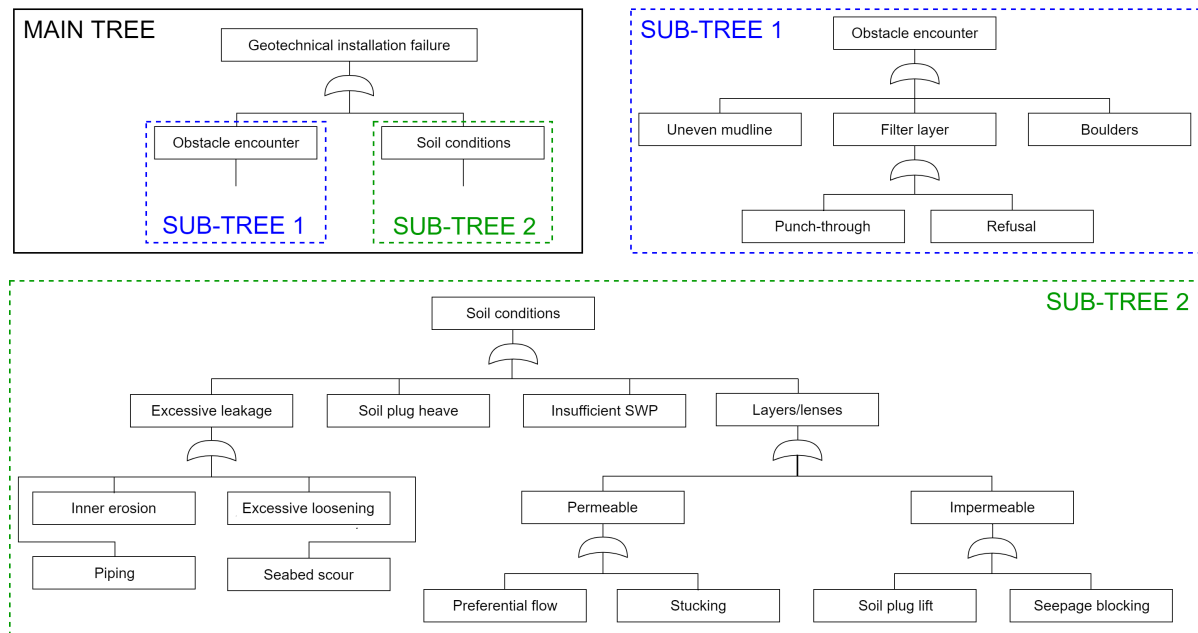

Figure 3.13: Fault tree describing failure of geotechnical installation of suction bucket jackets

It can be noted that several failure mechanisms have been removed from the fault tree. Sliding has been removed due to the fact that it falls outside the geotechnical installation scope. Seabed scour is deemed irrelevant for this research due to the application of a filter layer. The design of the scour protection is also not considered to be part of geotechnical installation design. Several failure mechanisms have been integrated into larger subsections. One can see that inner erosion, excessive loosening and piping are all attributed to the global failure mechanism excessive leakage. Reason for this is the fact that current methods describing soil limits contain all of these phenomena. In Section 3.4 more elaboration is given on the trade-offs and design decisions made during the process of developing the fault tree. Finally buckling and cavitation are structural and pumping failure so not incorporated in this fault tree.

3.4. Evaluation

The qualitative reliability analysis and geotechnical installation design form the foundation of the reliability-based design framework. The qualitative reliability analysis was performed with this in mind. This Section evaluates the integration of the qualitative reliability analysis in the reliability-based design framework.

1. Trade-offs in logic trees

There does not exist a single way of making both logic trees. In this research the event tree is based on installation decisions which should be made. The occurrence of all failure mechanisms is not specifically included. Because the event tree is more directed towards installation decisions it contains events which are hard to quantify. Effects of the application of crane actions, jetting, cyclic pumping and the interaction of the buckets with the filter layer are not possible to quantify within the scope of this research and with the available design methods. However, important contingencies like the application of ballast for increased self-weight penetration, application of grout and accounting for differences in soil conditions between buckets will be assessed.

The fault tree is ideal for examining whether a site is feasible for suction bucket jacket installation. Several trade-offs were made which allow for integration of the geotechnical installation design methods. First of all some of the failure mechanism consider a single suction bucket (e.g. excessive leakage, layers and lenses, soil plug heave). This research considers jackets with multiple buckets. It is assumed that the occurrence of a failure mechanism for a single bucket has failure of the entire installation as a consequence. Several individual failure mechanisms are positioned as subsets for larger mechanisms like 'excessive leakage' and 'layers and lenses'. This has been done deliberately in prospect of integration of the design methods into the fault tree. This is described in the next paragraph.

2. Integration in the reliability-based design framework

Design methods are required to examine the probability of occurrence of elements in the fault and event tree. Table 3.1 presents an overview of the applicability of design methods to the different mechanisms within the fault tree. A direct reliability analysis can be performed if specific design methods which describe the phenomena behind failure mechanisms or events are available. This allows for integration of quantified uncertainties and making an estimate of the probability of occurrence. When no design methods are available but the conditions in which failure mechanisms can be identified a probability analysis can be performed. In the case of some mechanisms design methods are unavailable and a probability analysis is of no use. Therefore it will be impossible to further investigate these phenomena in this research (e.g. filter layer interactions).

Table 3.1: Failure mechanisms and their integration within the reliability-based design framework

Failure mechanism	Direct reliability analysis	Probability analysis	Not quantifiable
Uneven seabed	H&B and CPT-based method		
Filter layer refusal			No methods
Punch-through filt. layer			No methods
Boulder encounter		Survey data analysis	
Excessive leakage	Soil suction limit		
Soil plug heave	Pure cohesive soils		Non-cohesive soils
Insufficient SWP	H&B and CPT-based method		
Preferential flow			Only 3D analyses
Stucking	Seepage analysis + H&B and CPT		
Soil plug lift			No methods
Seepage blocking	Seepage analysis + H&B and CPT		

Parametric uncertainties

Quantified variation of design parameters is required to determine the probability of failure mechanisms (Chapter 3) with the available geotechnical design methods (Chapter 2). This Chapter starts with a discussion on determining the required soil parameters. Afterwards their variability is quantified.

4.1. Overview

Uncertainty of a parameter estimate can have many origins. After discussing parametric uncertainty in general a short elaboration on site investigations for offshore wind farms will be given.

1. Uncertainty in soil parameters

Uncertainty in geotechnical properties can originate from two main sources: random errors (data-scatter) and systematic errors (Uzielli et al., 2006). Data-scatter is often caused by random testing errors and spatial variation of the soil parameters. Systematic errors can be caused by statistical errors in assumed trends or biases in measurement procedures (Christian, 2004). Examples of random testing errors are spikes of the cone resistance profile due to hitting small cobbles or disturbances of borehole samples during extraction. Systematic errors could arise when wrongly calibrated or inconsistent measurement devices are used (Figure 4.1b) or incorrect sampling rates are applied (Christian et al., 1994).

(a) Conceptual framework of uncertainties in soil property estimates (Christian et al., 1994)

(b) Example of systematic uncertainty due to the use of two different CPT techniques (Randolph et al., 2005)
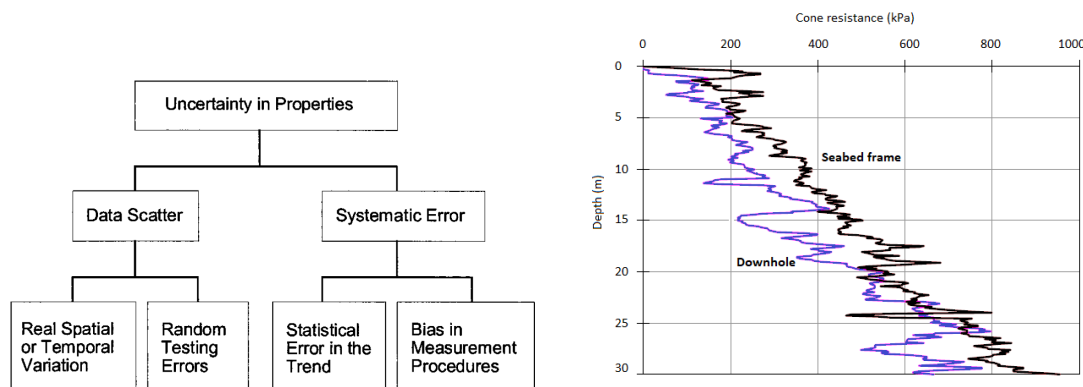
Figure 4.1: Visualizations of uncertainties in parameter estimates

Another distinction which can be made is between variation which can and cannot be reduced. Variation which can be reduced is named epistemic uncertainty. Examples of this are measurement, statistical and model uncertainty. This uncertainty can be reduced by collecting more data. Variation which cannot be reduced is named aleatoric uncertainty. An obvious example is layering of soils (Nadim, 2015).

2. Data available

Data required for soil parameter estimation is obtained during offshore site investigation campaigns. Such a campaign is often a combination of field tests and testing borehole samples in a laboratory (Randolph et al., 2005). This Section discusses the most relevant parts for suction bucket jacket installation.

2.1 Geophysical survey

Geophysical investigation is performed to gain information on bathymetric conditions, the stratigraphy of the subsoil, geological information of the soil used for foundation of the support structures and detect possible geohazards like shipwrecks, cables or boulders.

The main goal of the bathymetric survey is the mapping of the seabed level at the wind turbine foundation locations. The seabed often shows dynamic behavior in the form of sand ripples or even small or large sand waves. Indicates of the location and size of these waves can be obtained by examining the geophysical survey data as well. Magnetic and side scan sonar data can be used to identify cables, shipwrecks or other possible obstructions during installation.

Besides mapping the seabed the subsurface layer boundaries require identification as well. Seismic surveys are used to identify the layering below the seafloor. The soil units for the turbine locations can be determined when one combines this data with geotechnical surveys and the geological history. Soil units are often characterized by a geological age as well as the type of deposit. This phase results in a total overview of the subsurface of the wind farm (e.g. Figure 4.2).
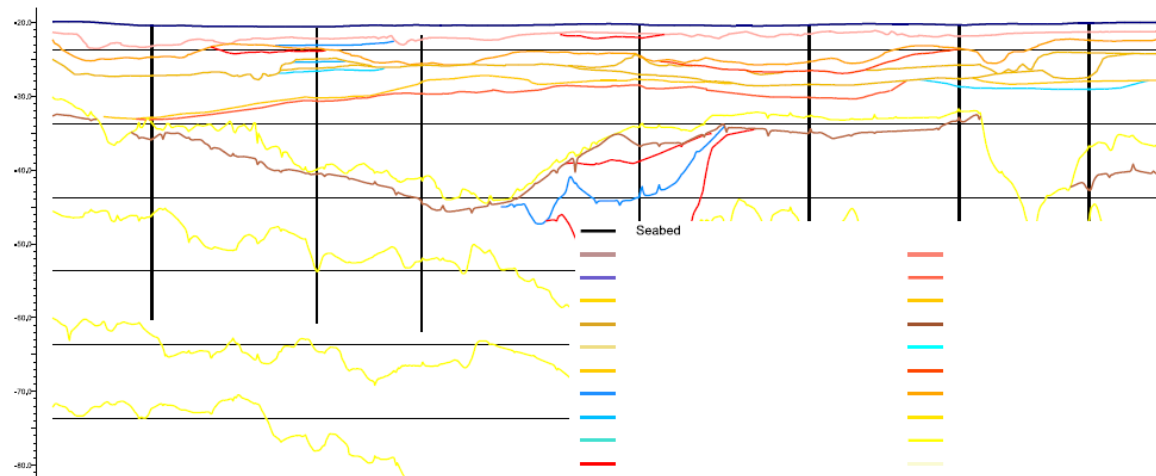

Figure 4.2: Example of mapped subsurface in geological units and soil types during a geophysical survey

2.2 Geotechnical survey

A geotechnical survey aims to determine the soil strength parameters which can be used for (installation) design of the wind turbine foundation. In general three different categories can be identified:

1. Cone penetration test (CPT):
   A cone at the end of rods is pushed into the ground during a Cone Penetration Test (CPT). During this process the resistance on the cone tip and sleeve is measured (Lunne et al., 1997). Pore pressure measurements are made if a piezocone-CPTu is performed (Firouzianbandpey et al., 2014). These measurements are taken by sensors just behind the cone and have to be corrected for depth (Figure 4.3a). The main advantages of a CPT are the ability to do fast and continuous profiling as well as generating reliable and reproducible data. They also provide a strong theoretical basis for design and interpretation. The main disadvantage is the inability to obtain soil samples (Robertson and Cabal, 2015). In a typical offshore windfarm project a cone penetration test is performed at least at each turbine location. Since suction bucket jackets are a relatively new concept a cone penetration tests at each bucket location is currently common in practice.

2. Borehole sampling:
Boreholes are drilled holes from which samples are retrieved to classify the soil types in the field. A borehole log is used to document the findings. It consists of the geology over depth which is based on observations of the samples. Soil types, color and grain size characteristics are noted and the soil layers are attributed to a certain geological deposit (Look, 2007). Classification and other types of laboratory tests can be performed on borehole samples. In some instances boreholes are made in combination with a cone penetration test.

3. Laboratory tests:
Laboratory testing is an important method for both classification as well as the estimation of soil parameters. Two important classification tools are the particle size distribution (for coarse-grained soils) and the Atterberg limits (for fine-grained soils). Important tests for determining soil parameters are the triaxial test (e.g. for estimating the internal friction angle of sands), the oedometer tests (e.g. for estimating the pre-consolidation pressure of clays) and direct shear tests (e.g. for estimating the undrained shear strength of clays).
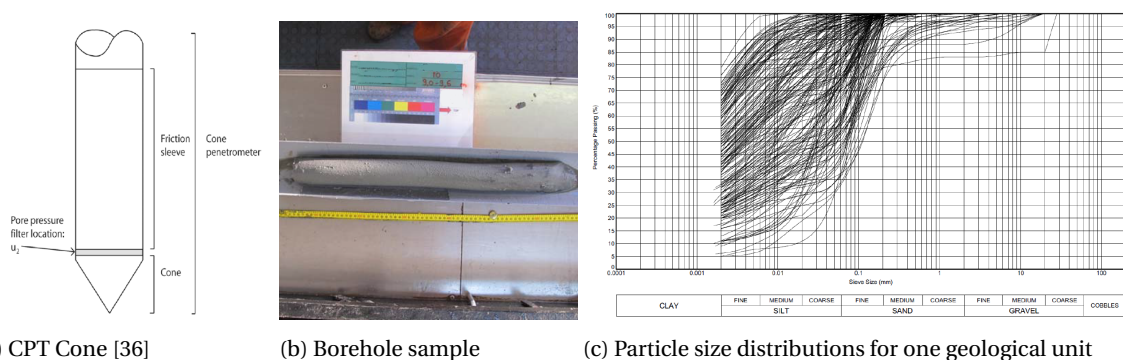

(a) CPT Cone [36]   (b) Borehole sample   (c) Particle size distributions for one geological unit

Figure 4.3: Typical data sources used during design of an offshore wind farm and in this research

3. Representation of uncertainty

The goal of this Chapter is to determine the variability of the soil parameter estimates used in installation design. The accuracy of the variability description depends mostly on the amount of data which is gathered. Unfortunately it is not as straightforward to determine a soil parameter as other environmental parameters like wind speeds and wave heights.

The methods used for quantifying variability are all mentioned in design codes on reliability-based design (ISO, 2015). Random field modelling will be used to model the spatial variability of the cone resistance (q_c, q_t) used in CPT-based design (Section 4.4). The variability of the seabed level (h) will be assessed individually based on the bathymetric survey data. Variability of all other parameters (e.g. γ_s, ϕ, k) will be quantified by using continuous probability density functions fitted to measured or estimated data series (Section 4.5).

Besides applying the correct methodology for quantifying soil variability it is even more important that the soil variability is quantified for comparable data series. If two soil units are not comparable, using both their parameters will not give an accurate description of variability. This is a classical debate between designers, geologists and geotechnical engineers. In this research it is aimed to prevent problems like this as much as possible. Therefore extensive methods of soil unit identification are implemented in the approach (Section 4.3). This will aid the application of both random field modelling as well as the use of continuous probability density functions.

Before any variability assessment can be performed the soil parameters need to be determined. Section 4.2 provides an overview of the methods used and the data series obtained. Geotechnical and geophysical surveys from a case study wind farm are used in this analysis. Appendix A provides additional background information to the data obtained.

4.2. Parameter estimation

Nine soil parameters are required before the design methods can be applied. Field-, classification and laboratory tests will be used to determine these parameters. Correlations with other parameters will be applied if insufficient direct measurements are available. All parameters will be determined using data from the site investigation reports of an example offshore wind farm site (Appendix A).

1. Cone resistance (q_c, q_t)

In the case study wind farm over 200 CPTu's were executed. Maximum penetration depths range between 10 and 40 meters. Since only the top layers are relevant for installation of suction bucket jackets all can be used for installation design. The cone resistance profile (q_c) is the main result of a cone penetration test. The measured cone resistance is corrected for pore water pressures acting on the cone. This is essential for softer clays, silts and in over water work (Robertson, 2010). Correction occurs with a coefficient (a) which represents the net area ratio. This is obtained by laboratory calibration (a $\approx$ 0.8). The corrected cone resistance is obtained by Equation 4.1. The sleeve friction is corrected as well. To simplify interpretation the cone resistance and sleeve friction are often corrected for (effective) stresses (Q_t, F_r).

$$q_t = q_c + u_2(1-a) \quad , \quad Q_t = \frac{q_t - \sigma_{v0}}{\sigma'_{v0}} \quad , \quad F_r = \frac{f_s}{q_t - \sigma_{v0}} \tag{4.1}$$

The Robertson graph presented in Figure 4.4 is the most common soil type assessment in geotechnical engineering. The dotted black line indicates a normally consolidated region while further up right the soil tends to be more overconsolidated. The patches in the Robertson graph indicate the classified soil type. A soil behavior type index (I_c) can be computed with the normalized cone resistance (Q_t) and friction ratio (F_r) (Equation 4.2). Subdivisions can be made between different sands, silts and clays based on the value of this index (Robertson, 2016).

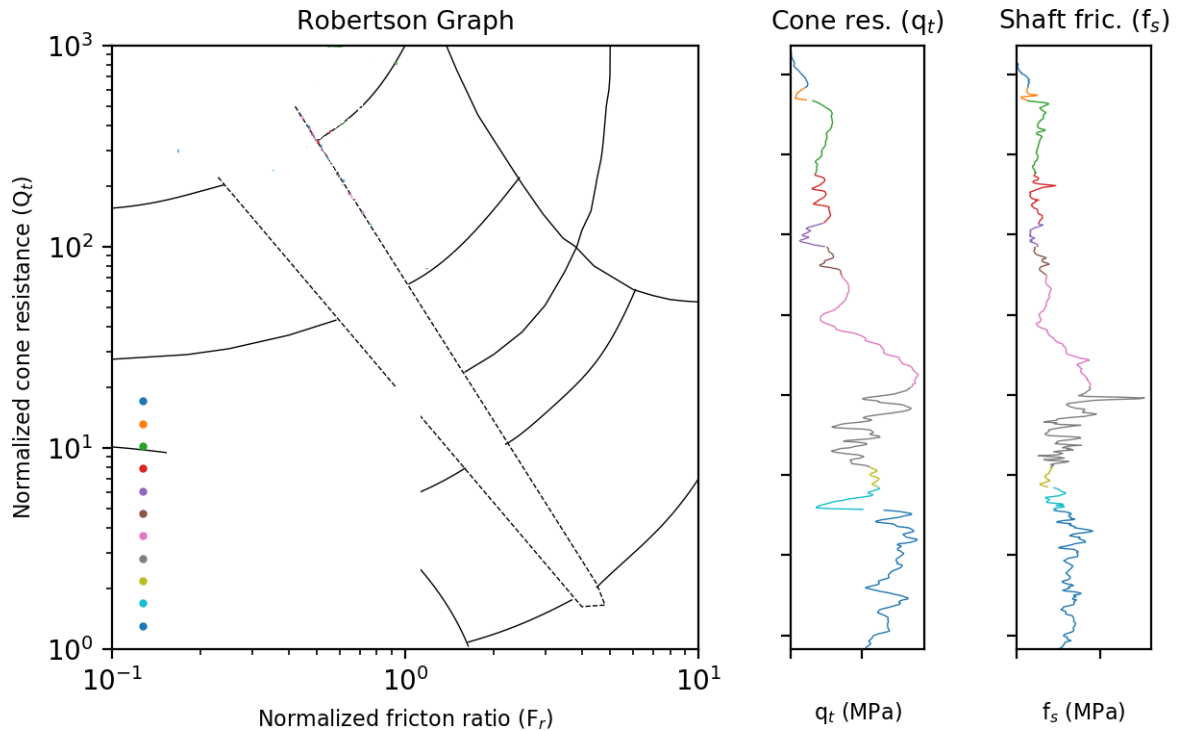$$I_c = \left[(3.47 - \log Q_t)^2 + (\log F_r + 1.22)^2 \right]^{0.5} \tag{4.2}$$

Figure 4.4: Robertson graph with scatter plots of Q_t and F_r for each identified soil layer

2. Soil unit weight (γ_s)

In the case study wind farm soil unit weights were determined onshore as part of advanced tests on the borehole samples. The saturated soil unit weight is determined based on measurements of volume and mass of the sample. Although measurements are available for the most significant soil types one parameter estimation method was examined for possible expansion of the data series.

Verruijt (2012) indicates a correlation of soil unit weight with the void ratio (e_0), specific gravity of the soil grains (d_s) and the unit weight of water (γ_w) (Equation 4.3). Since the unit weight of water (zero variation) and the specific gravity (coefficient of variation below 0.01) are approximately constant only a void ratio estimate is required for this method. During laboratory testing the void ratios were determined using dry unit weights (γ_d) and specific gravity of solid grains ($d_s = 2.67$) for 129 samples. Water content measurements of borehole samples (determined off- and onshore) can be used to estimate the void ratio as well (Equation 4.3). This relation can be used due to the fact that the soil is fully saturated (Verruijt, 2012). Figure 4.5a shows that the correlation coefficient between measured and estimated void ratio is 0.99. This correlation is deemed sufficient for use in this research.

$$\gamma_s = \gamma_w \frac{e_0 + d_s}{1 + e_0} \quad \text{with:} \quad e_0 = d_s \frac{w_d}{100} \tag{4.3}$$
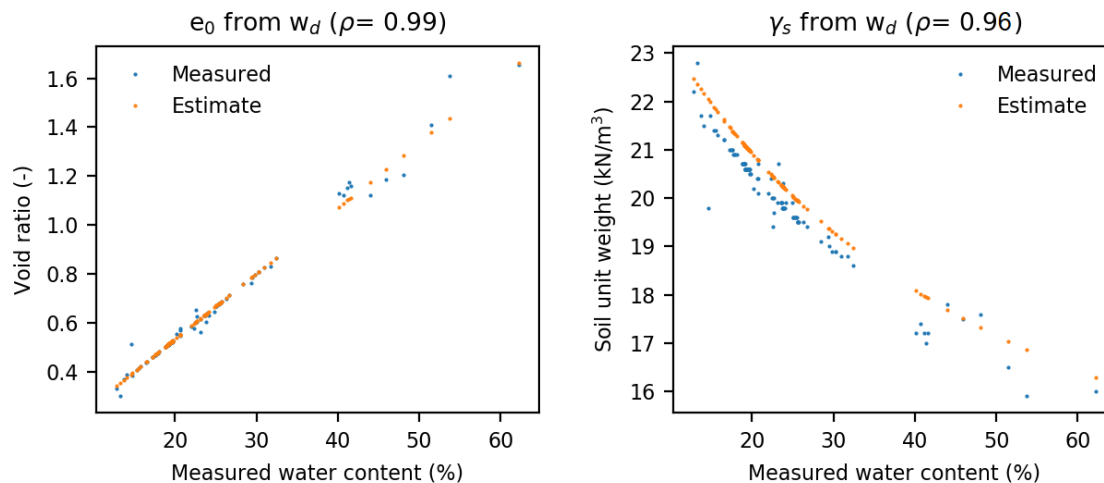
(a) Water content to void ratio   (b) Water content to soil unit weight

Figure 4.5: Correlations water content, void ratio and soil unit weight

The saturated soil unit weight (γ_s) can then be estimated based on the void ratio (e_0) and specific particle density (d_s). The correlation coefficient between the estimated soil unit weight and corresponding lab test measurements is 0.96 (Figure 4.5b). Full correlation has therefore not been achieved. When a direct correlation between water content and soil unit weight is attempted the accuracy of the estimation does not increase (Figure 4.5b). The correlation between void ratio (via water content) and soil unit weight is deemed insufficient for use in this research. This is because the variability in soil unit weight is already expected to be low and an additional error in the estimate could result in less accuracy in the variability estimate. Only direct measurements will be used to quantify the variation of this parameter. Representative deterministic estimates will be used for soil types with little data available.

3. Stress ratio (K)

The stress-ratio is hard to determine from laboratory tests. In practice values of 1 and 2 are used for displacement piles (Gavin, 2018). Ranges of 0.8-1.85 were used in previous research by Andersen et al. (2008). Equation 4.4 can be used to estimate the ratio of horizontal over vertical stresses at rest with the angle of internal friction and the overconsolidation ratio (Mayne and Kulhawy, 1982). If the overconsolidation ratio is approximately equal to one the formulation reduces to the formulation proposed by Jaky in 1944.

$$K0 = (1 - \sin\phi')OCR^{\sin\phi'} \tag{4.4}$$

In the site investigation report the clay is assumed to be normally to overconsolidated. This corresponds to an overconsolidation ratio of approximately one to four (Look, 2007). However, little tests were performed on few clay samples. The locations of these tests are also positioned very close to each other. Estimating the OCR based on site data in sand is very difficult (Lunne et al., 1997). Therefore it is advised to estimate the pre-consolidation pressure (P_c') based on the net cone resistance data from neighboring clay layers (Look, 2007). Using the pre-consolidation pressure (P_c') and in-situ stress (σ_{v0}') the OCR can be determined according to Equation 4.5. Figure 4.6 shows the estimates for all clay layers in the wind farm. Large transformation uncertainty occurs between measured and estimated values. It is expected that this originates from the fact that borehole sampling and CPT testing was not performed at similar locations.

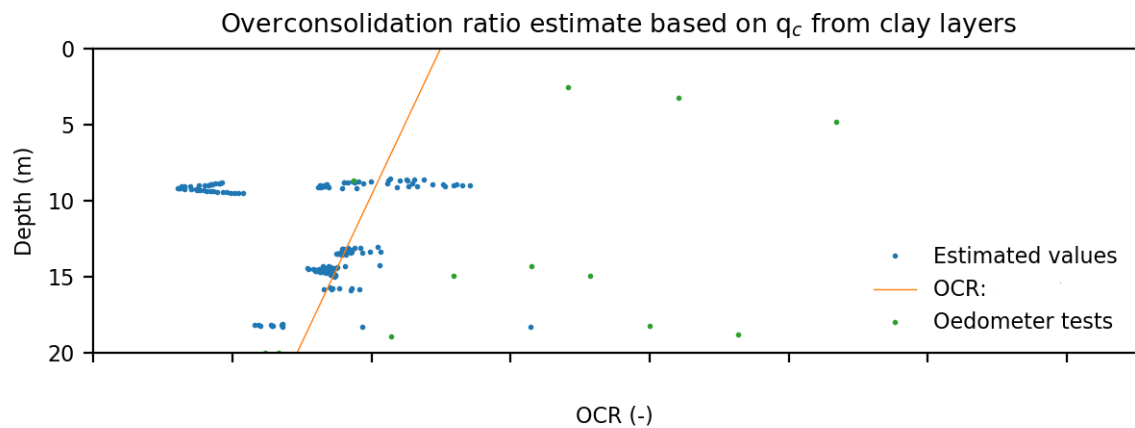$$\text{OCR} = \frac{P_c'}{\sigma_{v0}'} \tag{4.5}$$

Figure 4.6: Overconsolidation ratio estimate based on q_c values from clay layers

It was decided to use common values applied in practice of displacement piles between one and two. There are several reasons for not using the correlation presented in Equations 4.4 or 4.5. Firstly there is the inability of estimating a reliable overconsolidation ratio in sand. Secondly there is the uncertainty attributed to the estimate of the internal friction angle as well as the state of the soil. Combining both in Equation 4.4 could lead to an accumulation of variability which can lead to unrealistic estimates.

4. Internal friction angle (ϕ)
The internal friction angle can be determined using the Mohr-Coulomb failure criterion and the results of triaxial tests. In total over sixty triaxial tests on sandy specimens have been performed in the case study wind farm. Determined peak internal friction angles were generally very high, ranging between 30 and 53°. Parameter estimates are required due to the fact that little tests per soil type are available and the direct measurements show a large variation.

Installation design often makes use of the peak internal friction angle (ϕ_p). This is the highest friction angle possible to occur in sandy soils. At the peak of the stress-strain curve the peak internal friction angle (ϕ_p) acts on the grains (Figure 4.7a). Afterwards the soil starts to dilate and the friction angle decreases to a final value of the constant volume friction angle (ϕ_{cv}) (Figure 4.7b). The peak friction angle increases with relative density and decreases for higher effective consolidation stresses. It is expected that the internal friction angle differs along the skirt wall during penetration. However, the peak internal friction angle will be used according to design practice.

A relationship between relative density (R_D) and the peak internal friction angle exists (Andersen and Schjetne, 2013). However, insufficient relative density measurements are available. It is common to estimate the relative density on the bases of cone resistance data (Jamiolkowski et al. 2003; Baldi, 1986) or void ratio data (Lunne et al., 1997). The formulations presented by Bolton (1986) and expanded by Andersen and Schjetne (2013) can be used to estimate the drained peak internal friction angle (ϕ_p) with the determined relative density (R_D).

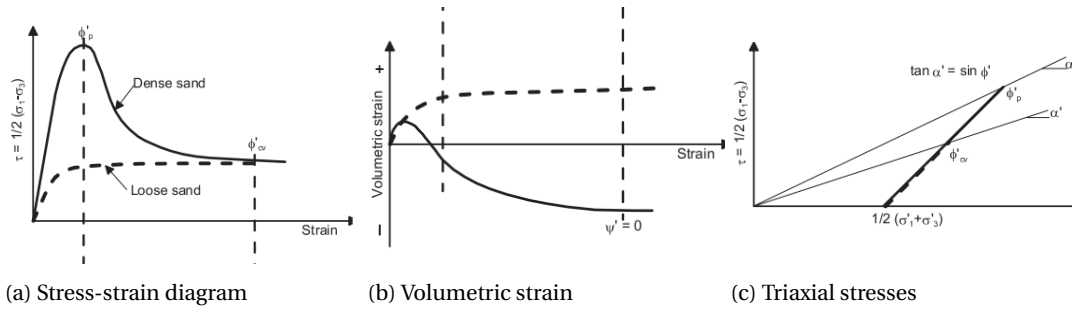(a) Stress-strain diagram   (b) Volumetric strain   (c) Triaxial stresses

Figure 4.7: Behaviour and visualization of internal friction angle development in a drained triaxial test (Andersen and Schjetne, 2013)

The void ratio (e_0) can be used to estimate the relative density (R_D) with Equation 4.6 (Lunne et al., 1997). Normally tests should be performed to obtain the minimum and maximum void ratio. However in this case they are not available. The minimum and maximum void ratios measured in the laboratory tests were approximately 0.4 and 0.8. These void ratio limits are typical values for (very) uniform (UC = D_{60}/D_{10} = 1-2) and rounded sands present in the dataset. Using the void ratio estimates the relative density was determined at the same location as where direct measurements were performed. The relative density outcomes where deemed unrealistic compared to measured data. Therefore this method is not used in this research.

$$e_0 = \frac{e_0 - e_{min}}{e_{max} - e_{min}} \tag{4.6}$$

The relative density can be estimated based on field test data using Equation 4.8 (Jamiolkowski et al., 2003) and Equation 4.9 (Baldi, 1986). Cone resistance (q_t) and mean triaxial effective stresses (p') are used to estimate the relative density (R_D). Since these relations overestimate the relative density for over-consolidated sands (present in the wind farm) the cone resistance is corrected by multiplication with a factor of $\frac{2}{3}$. The horizontal effective stress (σ'_h) is required to determine the mean triaxial effective stress (p'). A stress ratio of soil at rest (K0) of one is used in Equation 4.7. One can see several wrong estimates above one in the lower right part of Figure 4.8. These are occurring in locations with a low effective stress and high cone resistance. The correction factor of $\frac{2}{3}$ for aged and over-consolidated sands of the cone resistance does not prevent this.

$$p' = \frac{1}{3}\sigma'_v + \frac{2}{3}\sigma'_h \quad , \quad p' = \sigma'_v\left(\frac{1}{3} + \frac{2}{3}K0\right) \tag{4.7}$$

$$R_D = \frac{1}{2.93}\ln\left(\frac{q_c}{205p'^{0.5}}\right) \quad \text{(Jamiolkowski)} \tag{4.8}$$

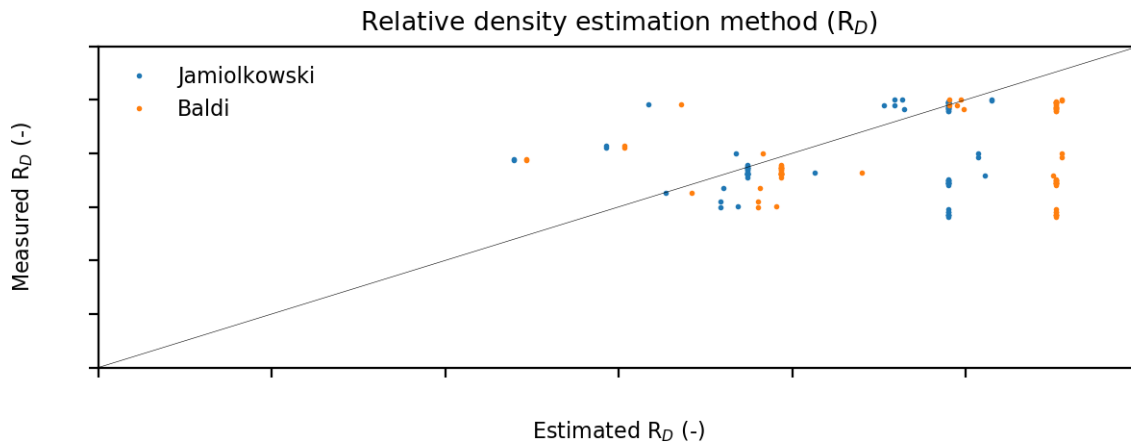$$R_D = \frac{1}{2.61}\ln\left(\frac{q_c}{181p'^{0.55}}\right) \quad \text{(Baldi)} \tag{4.9}$$

Figure 4.8: Accuracy of relative density estimate based on cone resistance data

When the relative density is obtained an estimate of the peak internal friction angle can be made using a correlation proposed by Bolton (1986). First one computes the density index (I_r) based on the relative density (R_D) and mean triaxial stress (p') after which the drained peak internal friction angle (ϕ'_p) is obtained using the density index (I_r) and the angle of repose of the soil (ϕ_{cv}) (Equation 4.10). The angle of repose of the soil is assumed to be equal to 33° (corresponding to round well graded sands) (Mayne, 2014).

$$\phi'_p = \phi'_{cv} + 3I_r \quad \text{with:} \quad I_r = R_D(10 - \ln p') - 1 \tag{4.10}$$

One can see significant scatter between the estimated and measured peak friction angles (Figure 4.9). Reason for this could be the horizontal distance between the cone penetration test and the boreholes from which the test samples were extracted. The range of estimated values represents the range of measured friction angles. Since large variation is observed in measured friction angles this method is deemed sufficient. Equation 4.8 and 4.10 will be used to determine the friction angles for each soil unit.
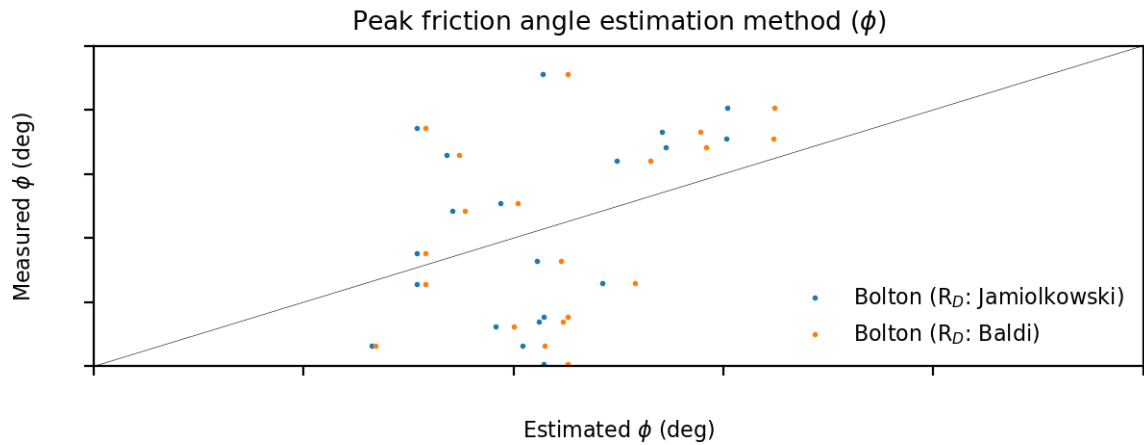

Figure 4.9: Accuracy of peak friction angle estimate based on relative density and cone resistance

5. Interface friction angle (δ)

The interface friction angle (δ) is used with the vertical stress (σ'_v) and the stress ratio (K) to determine the skirt friction in sand. It can be measured with a ring shear test. Only three of these tests were performed. The interface friction angle resulting from these tests is approximately thirty degrees. Since no further data is present the interface friction angle is determined as the peak internal friction angle minus five degrees (Equation 4.11) (Lehane et al., 1993). Another option would be to make use of the rule of thumb that the interface friction angle is equal to 90 percent of the peak friction angle (Andersen et al., 2008). Individual variability assessment is skipped since a direct correlation with the internal friction angle is used.

$$\delta = \phi' - 5 \tag{4.11}$$

6. Permeability (k)

Permeability is a notoriously hard parameter to estimate. Besides that it is not measured specifically during a site investigation campaign. Robertson (2010) proposed a relation with CPT results but this only can be used as an initial estimate. Permeability has a relationship with the grain characteristics of the subsoil (Chapuis, 2004). Because many classification tests were performed the particle size distribution and fine content are known for many samples. The Hazen formula is the most common formulation to estimate permeability (at locations with a fine content below 20%). However, research suggests the Kozeny-Carman formulation provides better estimates (Odong, 2007; Carrier III, 2003). This is mainly due to the absence of the widely varying empirical coefficient present in the Hazen formulation (C_H in Equation 4.12).

$$k = C_H D_{10}^2 \quad \text{(Hazen)} \tag{4.12}$$

$$k = 1.5 D_{10}^2 e_0^3 \frac{1 + e_{max}}{e_{max}(1 + e_0)} \quad \text{(Kozeny-Carman)} \tag{4.13}$$
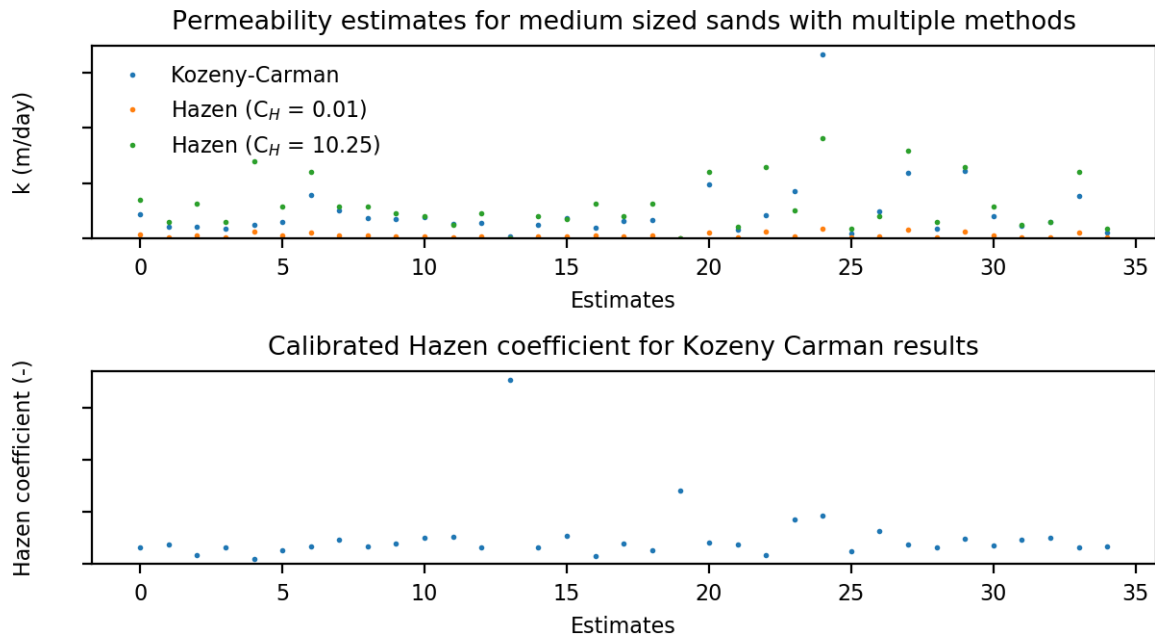
Figure 4.10: Permeability estimates by Kozeny-Carman

When both formulations are applied on the site data it can be seen that the empirical coefficient in the Hazen formulation should be manually calibrated (significantly) per location to get anywhere near the Kozeny-Carman estimates (Figure 4.10). Research suggests the Kozeny-Carman formulation is more appropriate (Carrier III, 2003). The maximum void ratio is determined based on typical values corresponding to the coefficient of uniformity of the soil (UC = D_{60}/D_{10}). Values of maximum void ratios (e_{max}) corresponding to rounded to well-rounded sands are used. The variability of permeability per soil type is relatively large (Figure 4.11). This is deemed acceptable when one considers the large variation of permeability expected in general (Robertson, 2010).
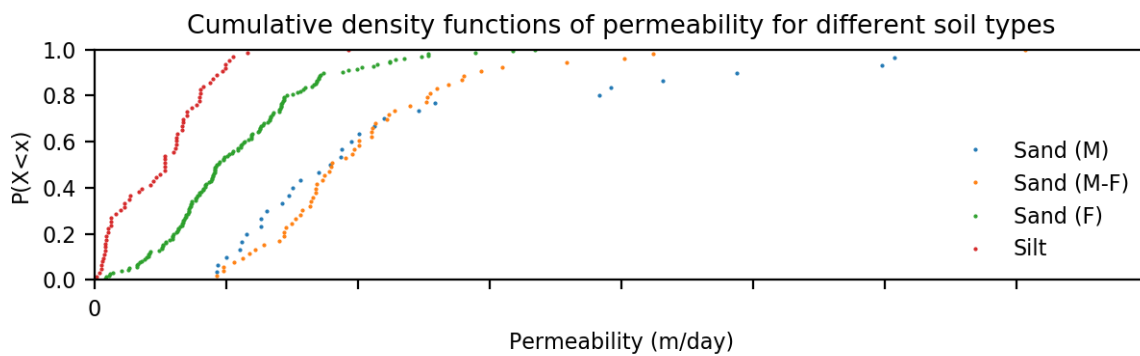

Figure 4.11: Cumulative density function of permeability estimates per soil type

Several notes regarding the permeability estimate have to be made. In sand the permeability is assumed to be isotropic. This means that the horizontal permeability (k_h) is equal to the vertical permeability (k_v) implemented in the seepage analysis. Little clay and gravel layers are present in the case study site. Seepage or blocking by layers of these soil types can have significant impact on feasibility. Therefore it was decided to select conservative (deterministic) values for both. Clay will have a permeability of $1 \cdot 10^{-9}$ m/s while gravel will have a permeability of $1 \cdot 10^{-2}$ m/s (Robertson, 2009). The permeability of gravel will be isotropic while the permeability of clay will be 10 times larger in horizontal direction ($k_h = 10 \, k_v$).

7. Undrained shear strength (s_u)
Since little clay layers are present in the area, little measurements of the undrained shear strength are available. It was measured with less than twenty consolidated triaxial undrained tests at only two locations. Measurements range between 59 and 220 kPa. Empirical correlations used for determining the undrained shear strength can be divided into three categories: cone resistance, effective cone resistance and excess pore pressure (Lunne et al., 1997). Neither of these methods give proper results for the measured undrained shear strengths. Equation 4.14 is used in combination with a cone factor (N_k) of 12.3 which is representative for normally to lightly overconsolidated offshore clays (Mayne and Peuchen, 2018).

$$s_u = \frac{q_c - \sigma_{v0}}{N_k} \quad \text{with:} \quad N_k = 12.3 \tag{4.14}$$

8. Adhesion factor (α)
Due to the limited amount of clay data available the adhesion factor will be difficult to estimate. The formulation by Randolph and Murphy (1985) will be used to estimate the adhesion factor based on effective vertical stresses and the undrained shear strength (Equation 4.15 & 4.16). Other formulations for determining the shaft resistance for undrained pile design are available (Doherty and Gavin, 2011). However, they are mostly unsuitable for application in this research due to a lack of data or inability of incorporation in the Houlsby and Byrne method (2005b).

$$\alpha = 0.5\left(\frac{s_u}{\sigma'_{v0}}\right)^{-0.5} \quad \text{for} \quad \left(\frac{s_u}{\sigma'_{v0}}\right) \leq 1 \tag{4.15}$$

$$\alpha = 0.5\left(\frac{s_u}{\sigma'_{v0}}\right)^{-0.25} \quad \text{for} \quad \left(\frac{s_u}{\sigma'_{v0}}\right) > 1 \tag{4.16}$$

9. Seabed level (h)
The final parameter considered is the level of the seabed. As stated in Chapter 3 seabed level differences can cause problems during installation if they differ over the extent of one foundation. The seabed at the case study wind farm is relatively smooth. There are ripples with sizes between 0.01 and 0.1 meter. Smaller sand waves are present with an amplitude below 0.5 meter and a wave length of approximately 100 m. Larger sand waves have an amplitude of below one meter but wave lengths of 500 m. It is therefore expected that the sand waves do not negatively influence suction bucket jacket installation. During bathymetric surveys the seabed was mapped. Where necessary different levels for the buckets will be incorporated in design.

4.3. Statistical identification of soil layers

Layer identification of the subsoil at a turbine location is essential information for geotechnical installation design. Three operations will be performed before parameter variability is quantified. First measurement errors are removed from the cone penetration test data. After this several (statistical) identification methods are used to identify comparable layers.

1. Filtering cone penetration test data

Random measurement errors need to be removed from CPT results to assure the implemented data reflects the soil profile encountered in reality (Harder and von Bloh, 1988). Often significant data scatter can be observed in CPT results. These are often spikes in the CPT profile which indicate that the cone hit a small hard object. There are not many statistical methods which have been specifically examined for filtering of CPT outliers. The median bandwidth method proposed by Wickremesinghe (1989) is applied in this research because it is considered to be the most reliable. It subdivides the CPT in segments for which the median and standard deviation is computed. Using the standard deviations of neighboring segments a representative standard deviation (σ_r) is computed with Equation 4.17.

$$\sigma_r(n) = \min\left(\sqrt{\sigma^2(n-1) + \sigma^2(n)} \quad , \quad \sqrt{\sigma^2(n) + \sigma^2(n+1)} \right) \tag{4.17}$$
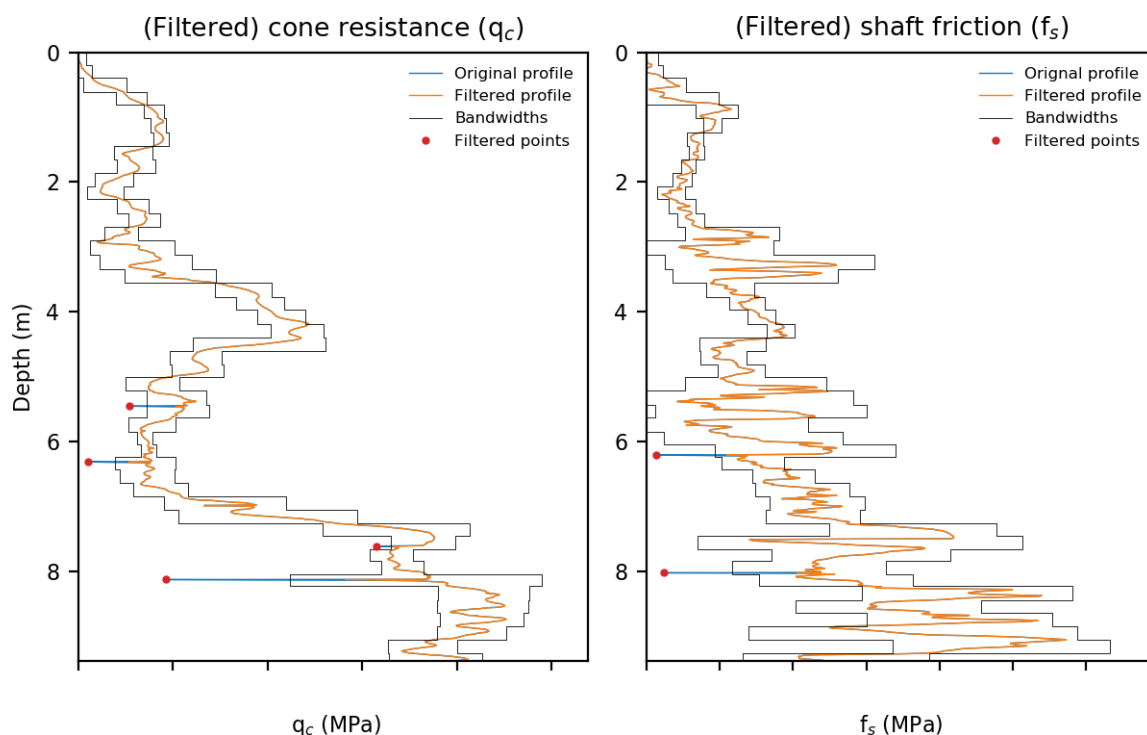

Figure 4.12: Median bandwidth filtering of one cone penetration test in the case study wind farm

A bandwidth of two times the representative standard deviation is applied around each median value (Wong, 2004; Wickremesinghe, 1989). All data points outside this bandwidth are considered to be outliers by the implemented algorithm and deleted. During implementation it was noticed that this method filters out cone resistance values between segments with a large variation in median. This should not be the case and therefore an extra criterion was implemented. Only local maxima and minima are to be eliminated.

Filtering without a manual check would be unwise because errors could be left out or finite layers could be erased. Therefore each filtered profile is checked on correctness by hand. During correction of all cone penetration tests performed in the case study wind farm no significant errors were spotted. The median bandwidth algorithm successfully eliminated the outliers.

2. Identification of physical homogeneous soil units
Faulty estimates are made when a variability analysis is performed on datasets which contain soil data which cannot be properly compared. Both random field models and distribution fitting requires comparable soil data. Therefore the identification of physically homogeneous soil units is of essential importance. A physical homogeneous soil unit can be defined in a sense of composition and behavior (Uzielli et al., 2006). Both will be used in this research to assure maximum accuracy.

The identification of physically homogeneous soil units can occur on a subjective or an objective basis (Uzielli et al., 2006). Identification on a subjective basis is often sufficient if a dataset is small, measurements are closely positioned and the profiles are relatively uniform (e.g. Prendergast et al., 2018; Firouzianbandpey et al., 2014; Fenton, 1999). This is not the case for geotechnical surveys of offshore wind farms. Although many cone penetration tests are performed, the distances between them vary between close (5-10 m) and very far away (1-2 km). This requires more rigorous (statistical) procedures. Four will be used in this research:

2.1 Robertson classification
The most used method for classification of soil types is the Robertson graph. It was developed in the early nineties and since then adapted several times (Robertson, 2016; 1989). The results can be plotted on a Robertson classification chart (Figure 4.4). This chart gives insight in which soil types are expected to be present at the location of the cone penetration tests. Section 4.2 presented more information on the background of the parameters.
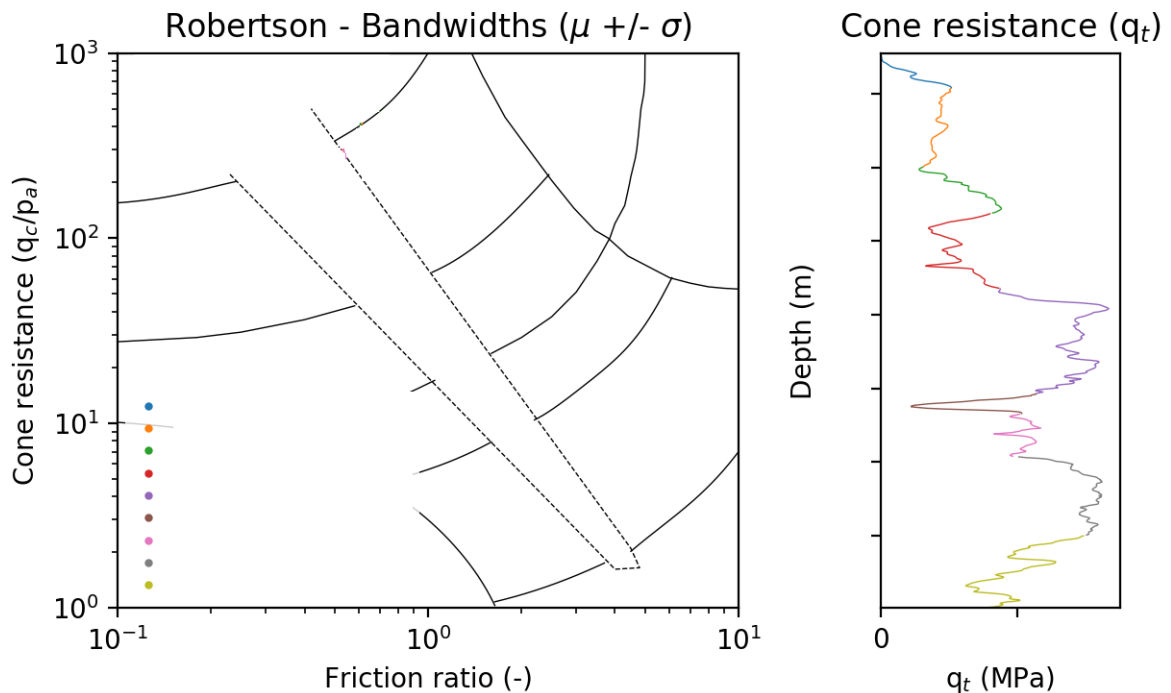

Figure 4.13: Robertson visualization of cone penetration test data for one test in the case study wind farm

In 1993 it was identified that an index parameter (I_c) can be used to represent the soil behaviour type of the Robertson graph. Based on this soil behaviour type an initial stratigraphic profile can be composed (Robertson, 2016). This stratigraphic profile will be used as a reference throughout the process of identification of physically homogeneous soil units (Figure 4.19). Another practical feature of the Robertson classification chart is that it can be used to visualize the data of identified homogeneous soil units in a second moment sense (Uzielli et al., 2005). In Figure 4.13 the mean values of each identified unit are plotted together with a bandwidth of one standard deviation. If the bandwidth deviates significantly this could indicate inconsistent behavior of the soil within the identified unit.

2.2 Geophysical survey and borehole logs

The soil profile consists of different geological layers as well as different soil types. Geophysical survey data is often used to map the geological history of the site. In the dataset of the case study wind farm it is noticeable that the top layers almost exclusively consist of marine and tidal deposits from the same age. These are followed by mixed layers which often lie outside the zone of influence for suction bucket jacket installation. At some locations small clay from till deposits were found at the seabed. Most of this characterization is based on borehole sample examination. Seismic surveys proved the absence of shallow gases and boulders in the top layers. If soil data is from different geological units caution should be exercised while comparing it.
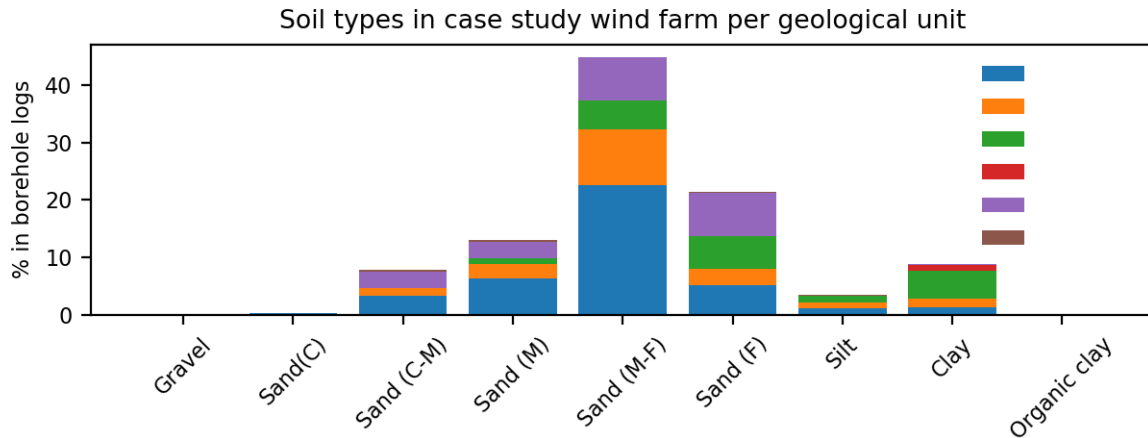

Figure 4.14: Percentage per and different soil types found in borehole logs in the case study wind farm

The samples from each borehole are visually examined and each of them is given a geologic description. A program was written in which the geological description text per sample is interpreted automatically from the borehole logs (Figure 4.15). First the geological layer is identified (e.g. Marine Postglacial). Then the soil type is identified (e.g. sand, clay, silt). Because the site considered in this research consists mostly of sandy soils the program interprets the grains size characteristics (e.g. fine, medium and coarse) as well. The output of the program is a soil type profile over depth per borehole. The closest borehole log is used as a verification tool for the identification of physically homogeneous soil units at each CPT location (Figure 4.19).
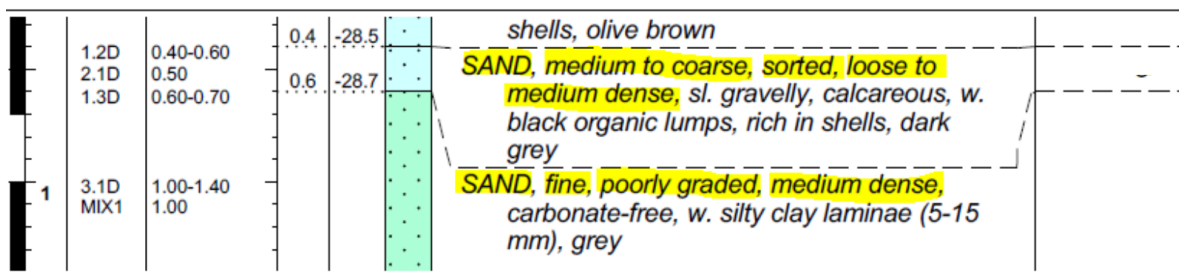

Figure 4.15: Example of borehole log and elements which are automatically identified (2 samples)

2.3 Statistical moving window method

The statistical moving window method was developed to identify layers with consistent properties using the coefficient of variation (COV). A window with a pre-defined size is moved over the cone resistance profile. For each location the coefficient of variation of the data within the window is determined. No objective method is available to determine the threshold for which a soil unit can be identified. A high coefficient of variation therefore indicates changing properties. Uzielli et al. (2006) advised a threshold of 0.1 and a window width of 1.5 m. In Figure 4.16 these test parameters do not give satisfactory results. This has to do with the large variation of the cone resistance profile (possibly due to the shallow depth).
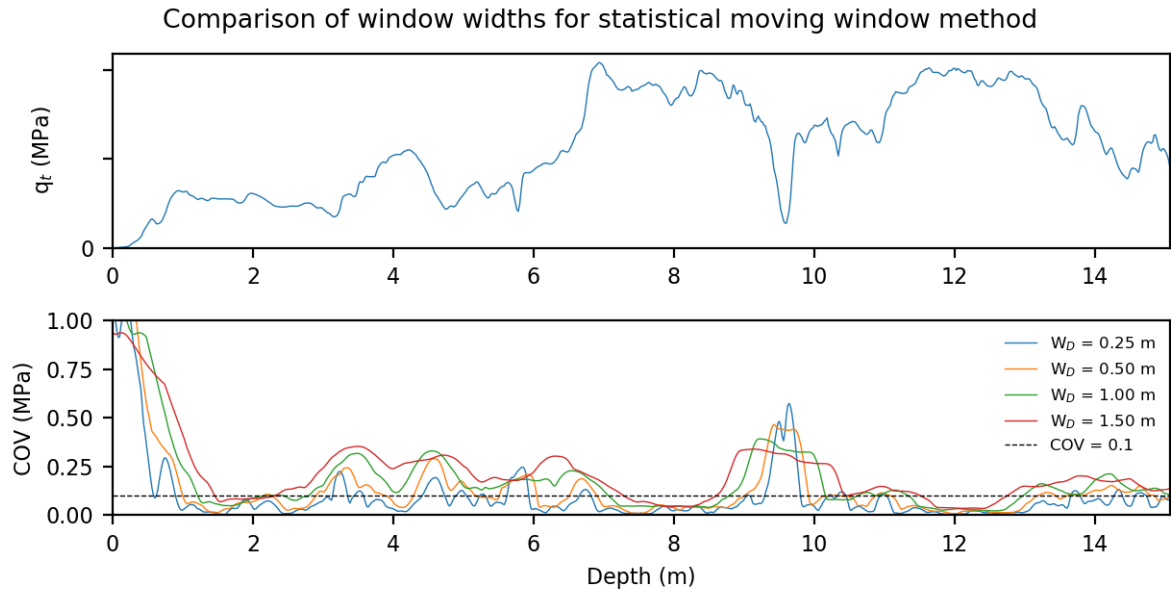
Figure 4.16: Comparison different window widths in the statistical moving window method applied on q_t with a sampling length of 0.02

During application of the statistical moving window method it was experienced that its results strongly depend on the sampling frequency/length of the cone resistance profile. Figure 4.16 shows the result for different window widths when the cone resistance value is sampled each 0.02 meters. A window width of 0.25 m ($\approx$ 12 values per window) gives the most distinct results. Please do note that this method can identify soil units but is not designed to identify layer boundaries (Uzielli et al., 2008). When the profile varies quickly the coefficient of variation shows too much variation for proper identification. This is visible at depths below 2 and between 8 and 11 meters in Figure 4.16.

2.4 Bartlett statistics
Identification using Bartlett statistics is based on the Bartlett test value which is computed for a moving window over the data series under consideration. Contrary to the statistical moving window technique the window is divided into two sections for which the standard deviations are computed (σ_{b1} & σ_{b2}). With the a amount of measurements (m_b) inside the window the Bartlett statistic is computed (Equation 4.18).
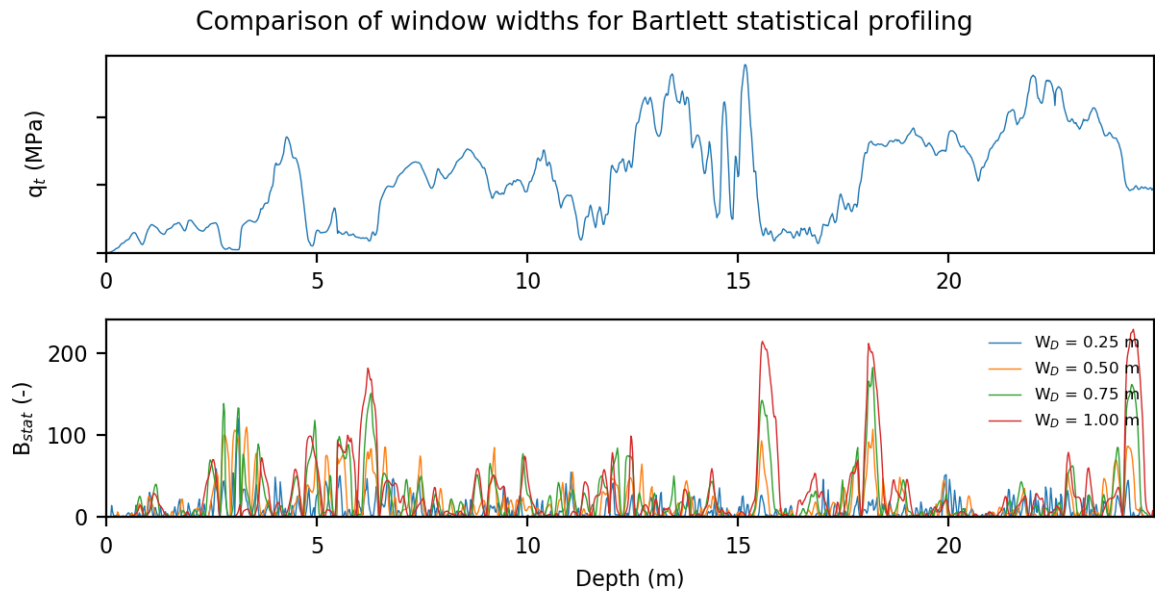

Figure 4.17: Comparison different window widths for Bartlett profiling on q_t with a sampling length of 0.02

Identically to the statistical moving window method no critical values or proposed window widths are presented in literature. Indications that a Bartlett value of 200 could be used to identify boundaries between soil units were found (Phoon et al., 2003). Again a dependence on the sampling length was found. Figure 4.17 shows the difference in results for different sampling windows using a sampling length of 0.02 cm. It is visible that the larger sampling windows result in more distinct peaks. However, smaller sampling windows can identify boundaries of thin layers (e.g. at a depth of 3.5 meter).

$$B_{stat} = \frac{2.30259(m_b - 1)}{C_b}\left[2\log\left(\frac{\sigma_{b1}^2 + \sigma_{b2}^2}{2}\right) - \left(\log(\sigma_{b1}^2) + \log(\sigma_{b2}^2)\right)\right] \quad \text{with:} \quad C_b = 1 + \frac{1}{2(m_b - 1)} \quad (4.18)$$

2.5 Results

None of the identification methods is able to automatically identify all layers required for design. As a consequence the decision was made to complete the identification process using all of the methods described above. The procedure is visible in Figure 4.19.

Discussion on each identification method is therefore possible. The borehole log could be off-set due to the distance between it and the CPT. Since the layering of the soil units is not horizontal (see Figure 4.2) the borehole log could differ from the layer profile at a CPT location. The classification index could be similar for two units with a different trend through the cone resistance profile. This could cause problems during random field modelling (Section 4.4). Bartlett profiling as well as the statistical moving window method are very sensitive to the bandwidth applied. The bandwidth size should therefore be optimized each time profiling occurs to prevent over- or undersensitive identification. Finally the soil type can be similar for layers within different identified geological units. It is possible that the parameters derived from different geological layers cannot be compared and the variation should be quantified for each geological unit.

2.6 Assessment of weak stationarity

In a strict non-stationary process two values only show a relation based on their separation distance (Rackwitz, 2000). Strict non-stationary processes are very rare in geotechnical engineering due to the strong spatial characteristic of the subsoil (Uzielli et al., 2006). Nevertheless, the data should at least be weakly stationary. When this requirement is violated a trend could be incorporated in the variation simulation and this can result in over- or underestimation of the cone resistance. An indication of weak stationarity can be found by checking whether the mean of the detrended variation is zero.
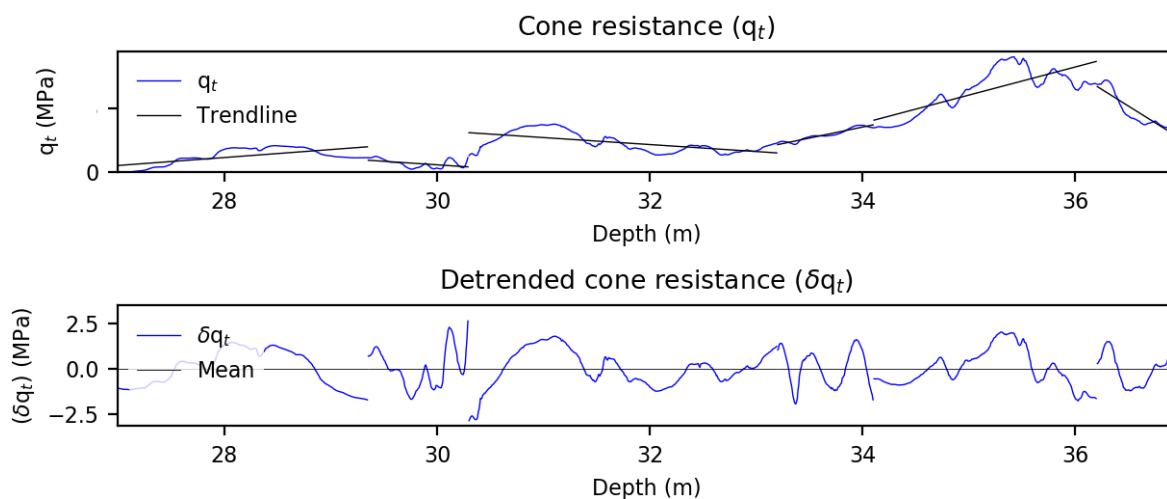

Figure 4.18: Assessment of detrended variation of cone resistance profile

The only truly objective manner of assessing whether the detrended cone resistance is weakly stationary is proposed by Phoon et al. (2004; 2003). Again Bartlett statistical profiling is used (Section 4.3). However, this time it is applied on the detrended variation profile. When the Bartlett profile of the detrended variation profile exceeds a critical (5%) reliability interval the profile of the soil unit shows too much stationarity. During application it was observed that this model is not valid in all cases and has problems with dealing with thin soil layers (Appendix B). A trade-off should be made between both prerequisites and practicality.
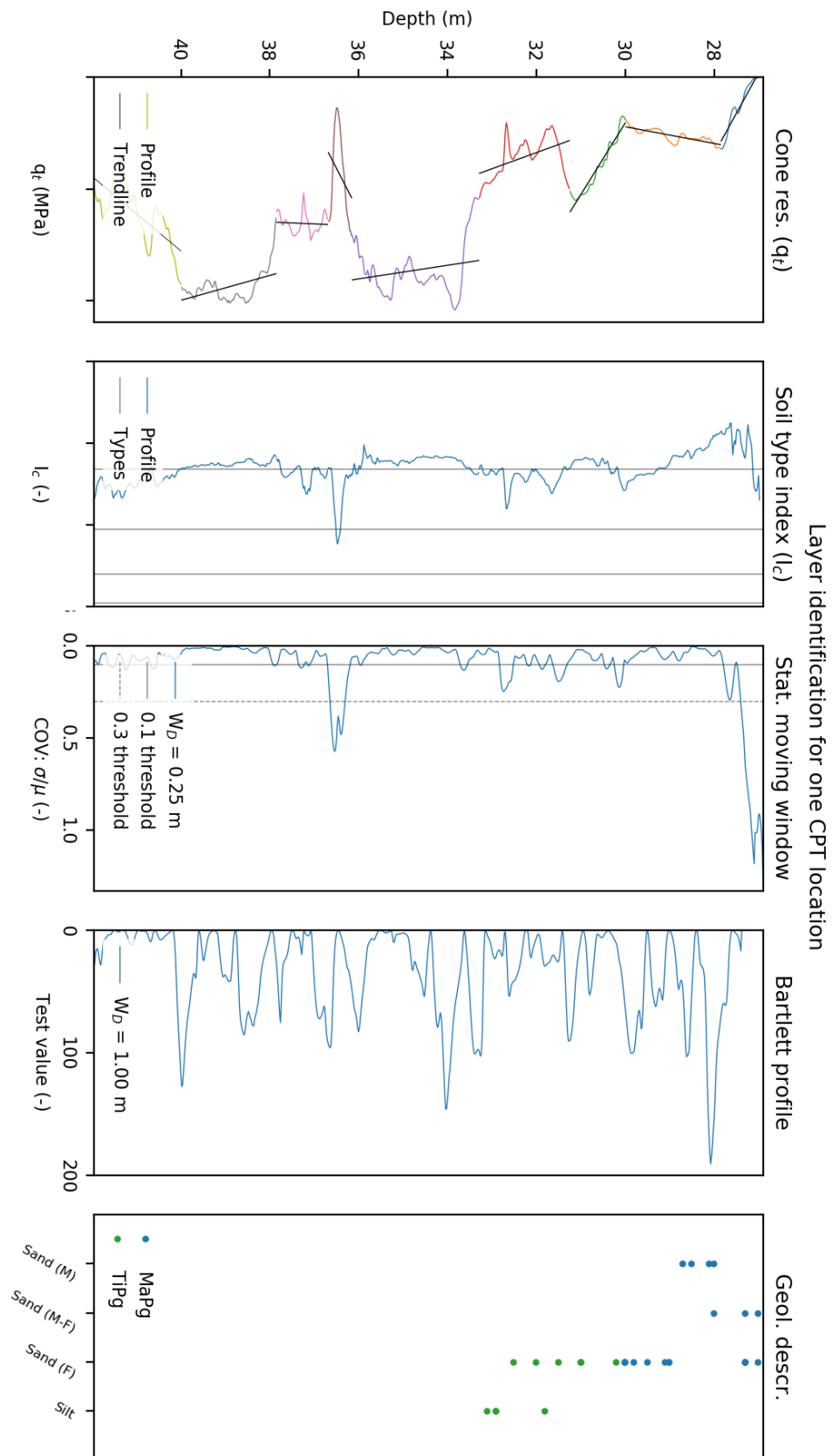
Figure 4.19: Example of application of identification methods to one cone resistance profile in the case study wind farm

4.4. Random field model of cone resistance

Cone penetration tests are point measurements. They do not reflect the variation due to the stratified and heterogeneous nature of the surrounding soil (Uzielli et al., 2006). Random field modelling is the leading technique for quantifying spatial variation in the results of cone penetration tests (Phoon, 2008).

1. Introduction

The variation of soil properties is almost never spatially independent (e.g. due to soil layering) (Fenton, 1999). A random field model can be constructed for soil properties which can be described by a (depth-dependent) trend and a random variation with zero mean (Phoon and Kulhawy, 1999). The cone resistance profile of a physically homogeneous soil unit often contains a depth-dependent trend and is therefore suitable for use in a random field model (Lunne et al., 1997). Using a random field model provides a better and stochastic approach compared to a conventional division of the CPT into classified sub-layers with characteristic values (Prendergast et al., 2018). This technique will therefore be used to simulate corrected cone resistance (q_t) profiles in the direct reliability analysis (Figure 4.20).
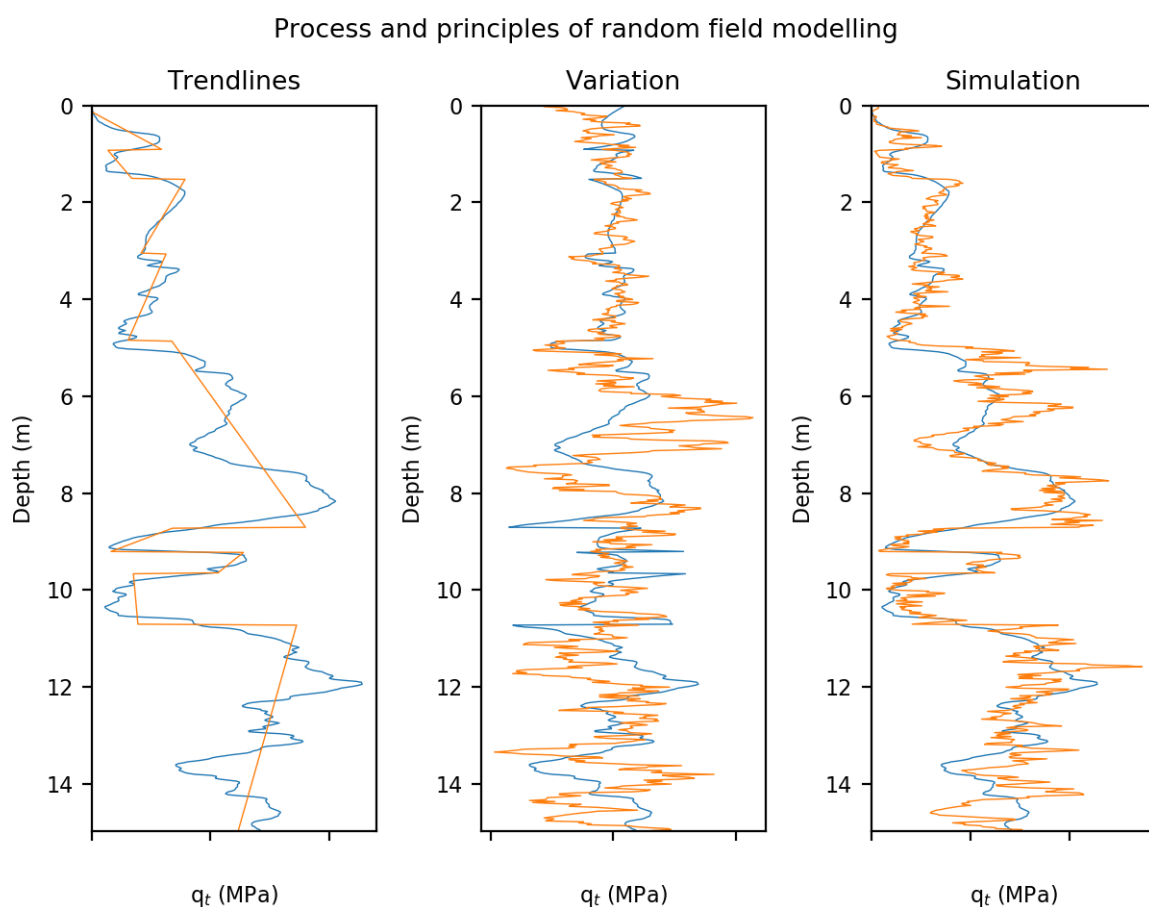

Figure 4.20: Simulating a cone resistance (q_t) profile with a random field model for the case study wind farm

Random field modelling is possible with data which satisfies two requirements: physical homogeneity and weak stationarity (Uzielli et al., 2006). Violating the requirement of physical homogeneity would result in a result based on uncomparable datasets. Weak stationarity of the variation is required to assure that the variation described by the fitted autocorrelation model only depends on separation distance (Phoon et al., 2003). In Section 4.3 these requirements were extensively checked. Since the cone resistance is a process which is highly location dependent it should be mentioned that practicing it will always be a trade-off between practicality and the prerequisites.

Furthermore, as noted in Section 4.3 it is essential that one checks whether soil units are comparable if used together in the analysis. Literature does not present any guidelines for this yet. Therefore the following three criteria are used for matching soil units in this research:

1. The difference in the mean soil behavior type index (I_c) of both units should be below 5%.

2. The vertical location of the units should overlap.

3. Both units should be part of the same geological unit.

Random field modelling is possible in both vertical and horizontal direction. In vertical direction many measurement points are available since the cone resistance profile provides a more or less continuous stream of measurements. This technique has been successfully applied in several studies over the past decades (e.g. Prendergast et al., 2018; Doherty and Gavin, 2010 Fenton, 1999). In horizontal direction random field modelling is more difficult. Due to a larger separation distance between the individual cone resistance profile it is more difficult to determine the scale of fluctuation (Lloret-Cabot et al., 2014; Firouzianbandpey et al., 2014). Nevertheless it will be attempted to determine the horizontal scale of fluctuation at the end of this Section.

2. Vertical random field modelling
A vertical random field model for a physically homogeneous soil unit consists of three components: a trend function, theoretical autocorrelation model and a value for the scale of fluctuation (Rackwitz, 2000).

2.1 Detrending and normalizing
The spatial correlation structure describes the variation of a parameter along a trendline. After the cone resistance profile of a physically homogeneous soil unit is extracted from the data a trendline is fitted through the profile (Prendergast et al., 2018). In this research a linear trendline is obtained using a least-square polynomial fit. The cone resistance profile is detrended by subtracting this trendline from the data. This should result in a variation with zero mean. The detrended signal is normalized with its variance to obtain a zero mean data series with a standard deviation of one (Fenton, 1999). Higher order detrending is mentioned in literature but reduces variation significantly (Phoon et al., 2003). A linear trendline is used to avoid underestimation of variation.
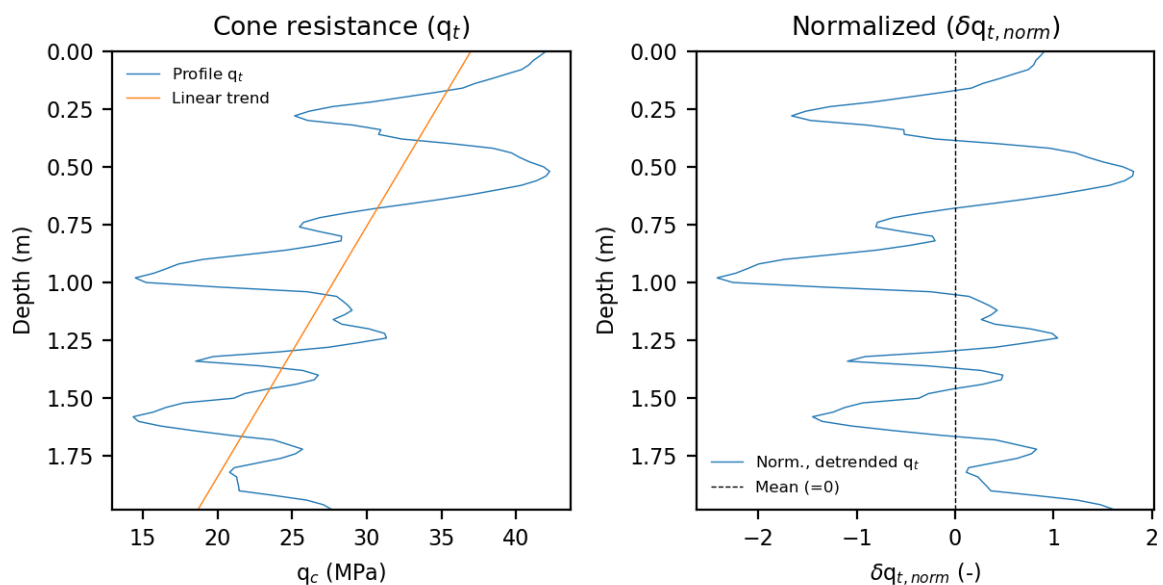

Figure 4.21: Procedure of detrending and normalizing cone resistance values for one soil unit

2.2 Autocorrelation model & vertical scale of fluctuation
The autocorrelation model and scale of fluctuation form the basis of the spatial correlation structure of the variation of corrected cone resistance. For each unit in each cone penetration test the empirical autocorrelation function is determined using Equation 4.19 (Rackwitz, 2000). The empirical autocorrelation describes the correlation of normalized variation of cone resistance values as a function of separation distance.

$$\rho(\tau_j) = \frac{1}{\sigma^2(n-j)} \sum_{i=1}^{n-j} (X_i - \mu)(X_{i+j} - \mu) \tag{4.19}$$

Table 4.1: Theoretical autocorrelation models common in geotechnical data analysis (Phoon et al., 2003)

Autocorrelation model	Equation	Scale of fluctuation
Single exponential	$R(\tau) = \exp(-\lambda\,|\tau|)$	$\delta = 2\,/\,\lambda$
Binary noise	$R(\tau) = 1 - c\,|\tau|$ (if $|\tau| = 1\,/\,c$)	$\delta = 1\,/\,c$
Cosine exponential	$R(|\tau|) = \exp(-b\,|\tau|)\cos(b\,\tau)$	$\delta = 1\,/\,b$
Second-order Markov	$R(|\tau|) = (1 + d\,|\tau|)\exp(-d\,|\tau|)$	$\delta = 4\,/\,d$
Squared exponential	$R(|\tau|) = \exp[\,-\,(\alpha\,\tau)\$^2]$	$\delta = \sqrt{\pi}\,/\,a$

An empirical autocorrelation model is not a convenient function for simulation purposes. Therefore a theoretical autocorrelation model should be selected (Rackwitz, 2000) (Table 4.1). All five models are fitted through the mean empirical autocorrelation of all matching soil units using a non-linear least square procedure (applied on the scale of fluctuation). In existing literature it is often assumed that all CPT's within one dataset show similar behavior. For a dataset from practice this might not be the case. Therefore the three matching criteria will be applied to determine whether the empirical autocorrelation models can be compared:
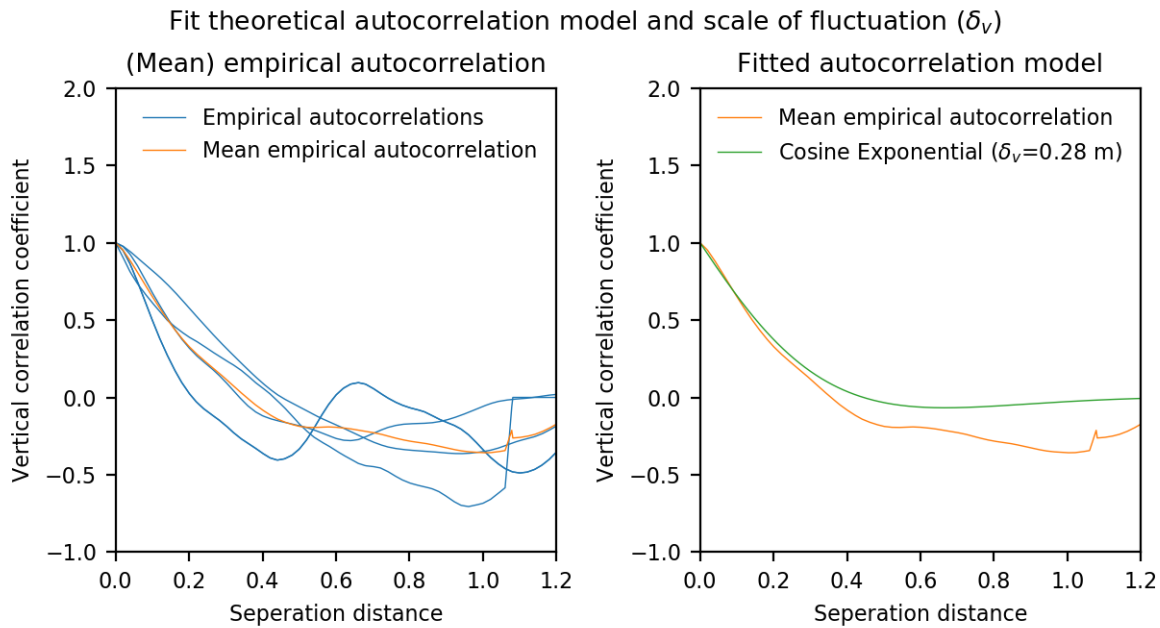

Figure 4.22: Procedure of fitting a theoretical autocorrelation model and determining scale of fluctuation (δ)

2.3 Simulation

The spatial variation can be simulated using the trendline, theoretical autocorrelation model and scale of fluctuation (δ). First the scale of fluctuation and theoretical autocorrelation model selected are used to compute a correlation matrix for the soil unit under consideration (Prendergast et al., 2018). When a cone resistance profile consists of multiple soil units these matrices should be added to form a global correlation matrix. This matrix is symmetric along its diagonal. Then the lower triangular form (using Cholesky decomposition) of this global correlation matrix (L) is multiplied with a vector of random numbers with zero mean and unit standard deviation (U). This results in a normally distributed (μ=0, $\sigma = 1$) but spatially correlated process (G) (Prendergast et al., 2018). A normally distributed random field can be added to the trendline (μ) to simulate a cone resistance profile. To do this the standard deviation of the original variation is used (Equation 4.20).

$$q_{t,n} = \mu_n + G\sigma_n \qquad \text{,with:} \qquad G = LU \tag{4.20}$$

Normally distributed variables can have tails in the negative domain. Since it is impossible to measure a negative cone resistance in the field a transformation should occur (Fenton, 1999; 2003). A bounded-normal, log-normal, or Beta distribution could be used (Prendergast et al., 2018). First the cone resistance is simulated by adding the normally distributed correlated process to the trendline. Then the profile is transformed from normally to log-normally distributed using Equation 4.21 and 4.22. If trendlines show (near) negative values they should be correct to one (Appendix B).

$$\sigma_{ln} = \sqrt{\ln\left(1 + \frac{\sigma_n^2}{\mu_n^2}\right)} \tag{4.21}$$

$$\mu_{ln} = \ln\left(\mu_n\right) - \frac{1}{2}\sigma_{ln}^2 \tag{4.22}$$

After transformation of the mean and standard deviation one can use Equation 4.23 to simulate a cone resistance with on a log-normal random field. Figure 4.20 shows the process of the simulation of one cone resistance profile simulation based on the spatial correlation structure. Figure 4.20 shows a good example of such a simulation.

$$q_{t,ln} = \exp\left(\mu_{ln} + G\sigma_{ln}\right) \tag{4.23}$$

2.4 Remarks

Even cone penetration tests closely positioned show large variation along similar trendlines. It is therefore logical that simulation (as presented in Figure 4.20) shows peaks in the cone penetration test location. In the next subsection one can see that the horizontal scale of fluctuation will be very small. This implies a large variation over short distances. Random field modelling provides an opportunity to take part of this variance into account. Furthermore it should be noted that a dataset from practice is used. The amount of cone penetration tests positioned close to each other has a large effect on the accuracy of the model.

3. Horizontal random field modelling

Creating a horizontal random field allows to simulate spatial variation of the cone resistance profile in horizontal direction (Lloret-Cabot et al., 2014). While the approach is similar there are some differences in application with respect to vertical random field modelling (Firouzianbandpey et al., 2014).

3.1 Data available

Vertical random field models are based on the spatial correlation structure derived from data with a high sample rate ($\approx$ every 0.02 m). Horizontal variation should be quantified on the basis of values further away from each other (Lloret-Cabot et al., 2014). This Section displays an attempt on horizontal random field modelling for the location presented in Figure 4.23. This location is presented because it is representative for other locations in the case study wind farm. Horizontal variation is quantified in radial direction. This means that the cone resistance values are compared based on direct horizontal separation distance.
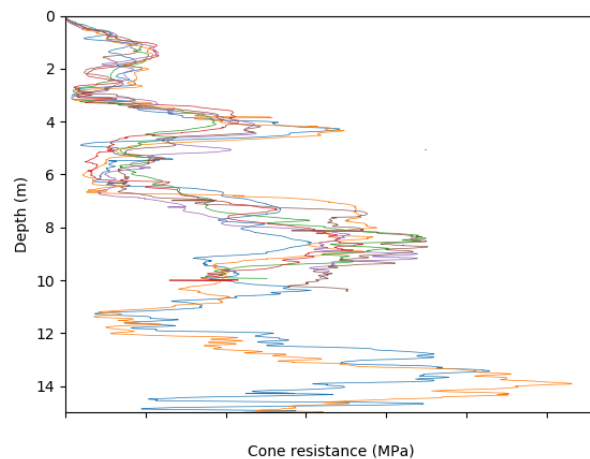
(a) Distances between cone penetration tests (b) Cone resistance profiles

Figure 4.23: Visualization of test location of horizontal random field modelling

3.2 Horizontal scale of fluctuation

All profiles are detrended along a single trendline. The detrended profiles are then subdivided into bins with an approximate width equal to the vertical scale of fluctuation ($\delta_v \approx 0.3\text{-}0.5$ m). The mean values in these bins are used to determine the empirical autocorrelation structure per bin. Figure 4.24 shows the results for all bins for one layer of one CPT. Two times the length of the horizontal scale of fluctuation should at least be larger than the separation distance for proper application. This is never the case for this dataset. In literature it can be observed that the horizontal scale of fluctuation is mostly dependent on the closest measurements (Firouzianbandpey et al., 2014; Lloret-Cabot et al., 2014). In Figure 4.24 one can see that this point has significant influence in this analysis as well.
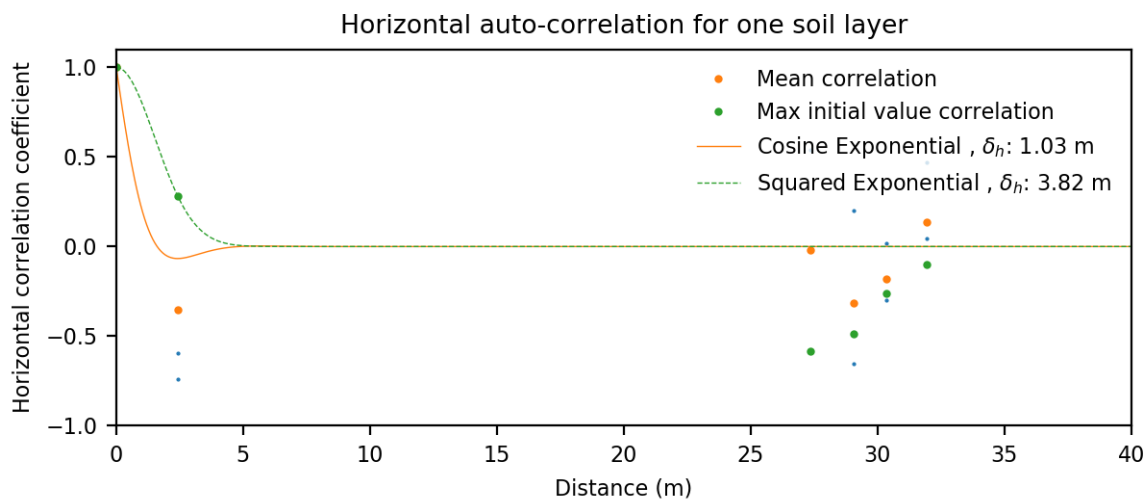

Figure 4.24: Typical results for the scale of fluctuation in horizontal direction for the case study wind farm

Attempts at other locations were not successful as well. It is believed that a definitive judgement on the horizontal scale of fluctuation is only possible when multiple cone penetration tests are performed at very close distance from each other (<5 m). Otherwise the horizontal random field model will be conditioned solely on a measurement close by which could result in physically unrealistic results. Since earlier literature also shows varying degrees of success it was decided to not investigate this topic any further throughout this research to not hamper the progress of the entire analysis.

4.5. Continuous random variables

Continuous probability density functions are used to quantify the variation of all soil parameters except the cone resistance (q_t). In this Section reasonable distributions for specific parameters are discussed and selected based on goodness of fit procedures. Attempts will be made to identify a probability density function for each individual soil type identified in the case study wind farm (Figure 4.14). If differences in geological unit are observed a distinction will be made as well.

1. Probability density functions

Random variables can take different values for which each can have a different probability. The probability of occurrence per value can be described by a continuous probability density function (Dekking et al., 2005). Several steps are performed to find the distribution best matching the data available. First the discrete sample series are displayed as a histogram. Afterwards several plausible continuous probability density functions are fitted through the empirical data series using maximum likelihood of its shape and location factors. Then the empirical and theoretical cumulative density functions are determined by integration of the histogram and continuous probability density function. The estimated continuous probability density function which scores best will be chosen as the descriptor of the parameters variability (Dekking et al., 2005).

If insufficient data is available for fitting two options remain. The first is using a deterministic and representative value. The second is examining literature for variations which already have been quantified. The latter option has two main disadvantages. First it can be the case that variations described in literature were retrieved from soil with a different geological history. Second the standard variations advised by literature are so large that implementing would not result in any valuable information.

2. Goodness of fit tests

Two goodness of tests are used to assess which of the fitted distributions is suitable for describing the variability of the soil parameter under consideration. Pearson's χ^2 test will be performed to check whether the assumption of the continuous probability density function should be rejected. The Kolmogorov-Smirnov test is applied on the cumulative density function to perform a similar check. Assumed distributions can be rejected when the test statistic corresponding to a level of significance (e.g. 1%, 5% or 10%) is exceeded. The distributions which score best are used in the quantitative reliability analysis in Chapter 6.

2.1 Pearson's χ^2 test

In Pearson's χ^2 test the observations in the histogram are sorted into bins. Afterwards the empirical probability of each bin is computed. This is then checked again the outcome of the probability density function for that bin. First the histogram is sorted into bins with at least five observations (n_i). In total all the bins add up to the total number of observations (N). The expected amount of values for each bin can be estimated by integrating the probability density function over the interval of each bin. Using the expected and observed amount of data in each bin the test statistic (D) can be determined according to Equation 4.24. The maximum value of the test statistic (D) for which the chosen distribution holds is obtained from the χ^2 distribution with a 5% reliability interval. The bin-choice can affect the outcome of the test. In this research all data series are subdivided into bins with at least five observations (Vrijling and van Gelder, 2002).

$$D = \sum_{i=1}^{k} \frac{(n_i - Np_i)}{Np_i} \quad \text{with} \quad p_i = \int_{x_i}^{x_{i+1}} f_x(x_i) \, dx \quad\quad (4.24)$$

2.2 Kolmogorov-Smirnov test

The Kolmogorov-Smirnov test rejects the assumed distribution when the largest deviation between the empirical and theoretical cumulative density functions exceeds a defined threshold (T) (Dekking et al., 2005; Massey, 1951). The closer the largest deviation between the empirical and theoretical cumulative denstiy function is to zero the better the distribution fits through the empirical data. The original Kolmogorov-Smirnov test does not apply to distributions estimated based on a data series (Vrijling and van Gelder, 2002). For these cases the threshold value should be narrower. A 5% threshold is given by Equation 4.25 (Lillifors, 1967). One can see that the threshold decreases for an increasing number of observations (N).

$$T = \frac{0.886}{\sqrt{N}} \quad \text{(Level of significance: 5\%)} \quad\quad (4.25)$$

3. Fitted continuous probability density functions

A fixed procedure is used to fit a probability density function through the data series. Several feasible distributions are selected for each of the parameters. Normally data series below a size of 30-50 points are not used for distribution fitting due to the inability to perform the χ^2 test and the uncertainty caused by the low sample size (Vrijling and van Gelder, 2002).

3.1 Soil unit weight (γ_s)

Soil unit weight is expected to be normally distributed. It cannot be negative, but bounded distributions are not required because the value of the parameter is sufficiently high and has small variation. The data shows no depth dependent trend and it is expected that variation within one soil unit does not vary significantly. Unfortunately not sufficient soil unit weight measurements are available for most soil types. This is due to the fact that during the process the correlation with the void ratio was determined as not usable. A normal distribution was fitted through the data on fine sands (Figure 4.25). This is the one of the most common soil types in the case study wind farm (Figure 4.14). Furthermore deterministic values were selected based on the mean of the measurement data available or based on standard values (Verruijt, 2012, Table 4.2).

Table 4.2: Quantified variability for soil unit weight of different soil types

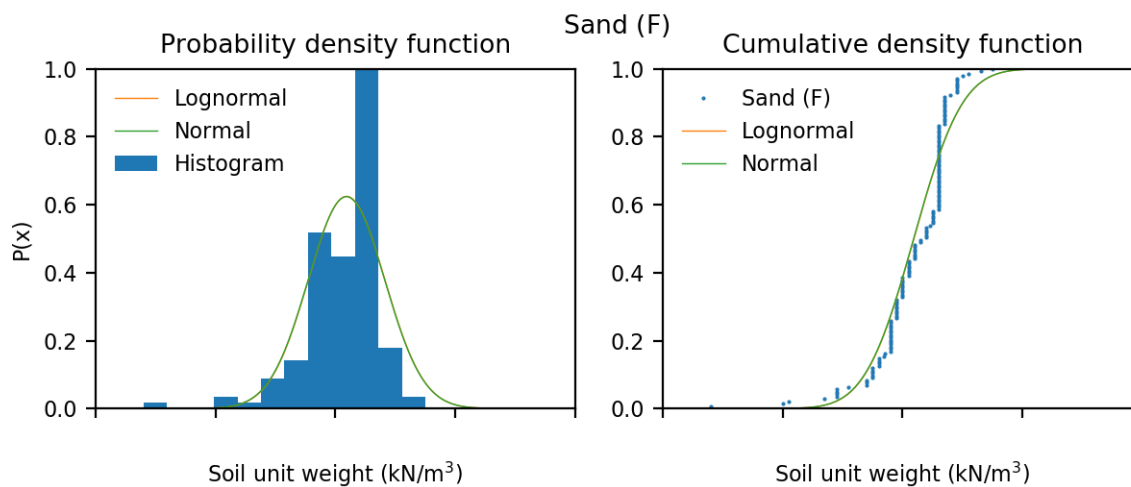| Soil type	N	Distribution	Parameters (kN/m^3)	KS	χ^2
Gravel, Sand (C, C-M)	0	Deterministic		-	-
Sand (M)	8	Deterministic		-	-
Sand (M-F)	11	Deterministic		-	-
Sand (F)	143	Normal	$\mu = ... , \sigma = ...$	0.13/0.07	37.32/171.91
Silt	19	Deterministic		-	-
(Organic) clay	4	Deterministic		-	-

Figure 4.25: Fitted distributions to permeability estimates for medium sized sand

3.2 Permeability (k)

Permeability is a parameter with large variation and therefore special caution should be exercised when estimating its variability. In Figure 4.11 the empirical cumulative density functions of permeability for each soil unit are presented. Similar behavior is observed. More information on the estimation method is given in Section 4.2. Since permeabilities cannot be lower than zero log-normal and exponential distributions were fitted. The log-normal distribution provided the best results for four of the most common soil types in the case study wind farm (Table 4.3 & Figure 4.26).

3.3 Stress ratio (K)

Common stress ratios applied in practice are between one and two. Since no parameter estimates can be done it was chosen to select a uniform distribution to model this parameter. Literature did not provide any other indications either.
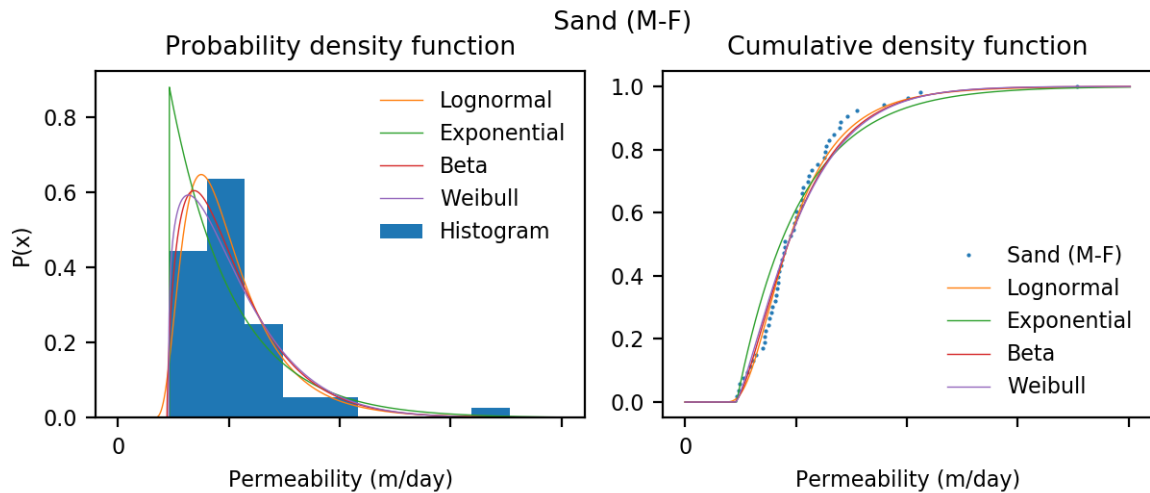
Sand (M-F)

Figure 4.26: Fitted distributions to permeability estimates for medium sized sand

Table 4.3: Quantified variability for permeability of different soil types

Soil type	N	Distribution	Parameters (m/day)	KS	χ^2
Gravel	0	Deterministic		-	-
Sand (C)	0	Deterministic		-	-
Sand (C-M)	0	Deterministic		-	-
Sand (M)	35	Log-normal	$\mu = ...$, $\sigma = ...$	0.12/0.15	4.66/49.8
Sand (M-F)	51	Log-normal	$\mu = ...$, $\sigma = ...$	0.08/0.12	6.65/68.67
Sand (F)	168	Log-normal	$\mu = ...$, $\sigma = ...$	0.05/0.07	4.23/199.24
Silt	82	Log-normal	$\mu = ...$, $\sigma = ...$	0.10/0.10	54.26/104.14
(Organic) Clay	2	Deterministic		-	-

3.4 Internal friction angle (φ)

The peak internal friction angle is a defining parameter in the Houlsby & Byrne method since it is used to determine the end-bearing capacity factors (N_q, N_γ) and the interface friction angle (δ). For each identified sand layer the friction angle variation will be determined based on the outcomes of the correlation with CPT data. Weibull, Gamma, Normal and Log-normal distributions were fitted. The Weibull distribution performed very well for scenarios in which the data had a clear upper bound while the (log-)normal distribution performed best in other cases. Variation in distribution type is therefore allowed.
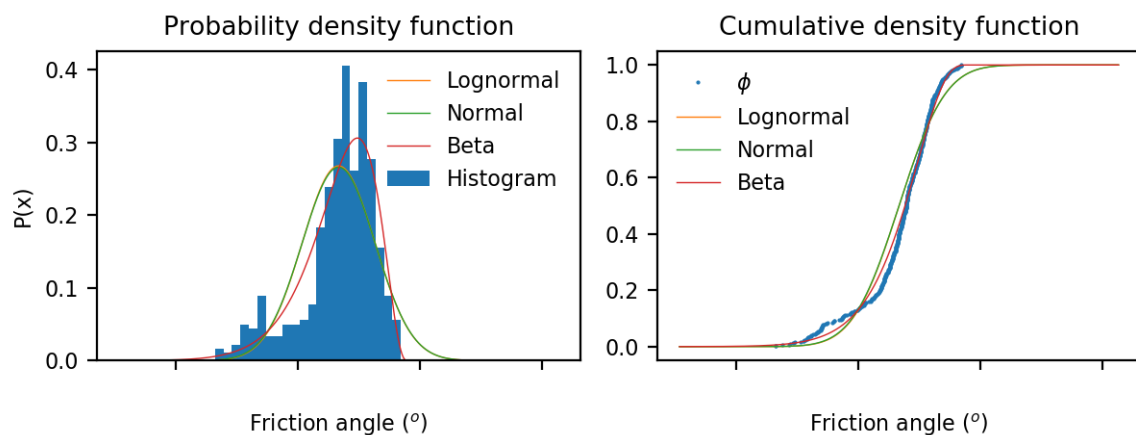

Figure 4.27: Friction angle distribution of one identified physically homogeneous sand layer

4.6. Evaluation

One of the main reasons for discussion of applying reliability-based design in geotechnical engineering is the uncertainty in parameter estimates. In this Section the impact of specific assumptions is discussed as well as the integration of the parametric uncertainties in the reliability-based design framework.

1. Impact of model decisions

Several modelling decisions which were made during the quantification of parametric uncertainties require some remarks:

1.1 Trade-offs in assessment of weak stationarity

In Section 4.3 the objective assessment of weak stationarity is discussed. The only study which is available to do this was performed by Phoon et al. in 2003. However, several disadvantages come with this approach. Firstly critical values have not been determined for all autocorrelation models. Secondly it is only possible to assess weak stationarity with respect to 5% reliability.

Another aspect which creates difficulties is the presence of relatively thin soil layers. Since the variation profile of such a unit is small it is difficult to assess weak stationarity in an objective manner. Ignoring the presence of these layers would result in unconservative design. Therefore a trade-off between weak stationarity and practicality should always be made in these cases. Layer identification has been selected as the first and foremost important aspect with respect to design in this research.

It was observed in the output data that in some cases the scale of fluctuation estimated is small. This results in more fluctuations at closer distance. However, based on visual inspection this did not result in any significant unrealistic soil profiles and simulation was deemed successful. Errors like these can always be expected since the high dependency of the quality of the variation data after detrending.

1.2 Assessment for parameters with little data

There is not sufficient data available to quantify the variability of all soil parameters. There is literature available which provides standard variability values for soil parameters (e.g. Phoon and Kulhawy, 1999). However, the ranges presented are so large that they would result in unrealistic design estimates. Therefore it was chosen to determine representative deterministic values for the undrained shear strength (s_u), adhesion factor (α) and for the soil unit weight (γ_s) and permeability (k) of some soil types.

2. Integration in reliability-based design framework

Before an installation design computation (Chapter 2) is performed to assess whether installation is feasible (Chapter 3) a design profile should be made which is representative for the location of installation. Figure 4.28 shows how all the elements discussed in this Chapter are used to define such a soil profile.
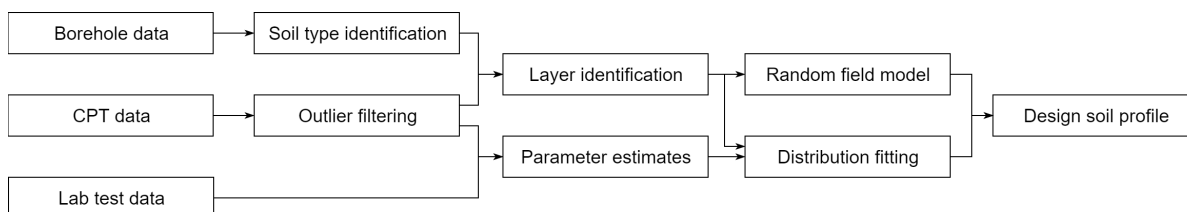

Figure 4.28: Flowchart on retrieving a design profile which is used in direct reliability analysis

In short the processed cone penetration test data and borehole data is used for identification of physically homogeneous soil units. Afterwards a vertical random field model is constructed for simulation of the cone resistance variation in these units. Continuous probability density functions were quantified for the other soil parameters and attributed to each layer. The random field model for cone resistance (q_t) forms the design profile together with the continuous probability density functions for soil unit weight (γ_s), friction angle (ϕ) and permeability (k). If a variability description proves to be infeasible a representative value is used.

<div align="right">

5

</div>

Model uncertainties

Uncertainty originates from parameter estimates as well as the mismatch between model outcomes and reality. In this Chapter an attempt is made to decrease or quantify model uncertainties where possible.

5.1. Overview

Geotechnical models are often simple to use while they describe complex soil-structure interaction (Phoon and Kulhawy, 2005). This applies to the design models discussed in Chapter 2 as well. Developing such simple models implies the need of two types of simplifications. The first is the necessity of incorporating empiricism (Phoon and Kulhawy, 2005). The second is the simplification of physical phenomena (Knut and Bjerager, 1992). Two paths are available for dealing with model uncertainty. The first is better representing physical phenomena or in other words: improving the model. The second is quantifying model uncertainty itself.

1. Representation of physical phenomena
There are several model elements which require a better description of the physical phenomena they are representing. First of all the incorporation of stress enhancement in layered soils is not discussed in the original design method proposed by Houlsby and Byrne (2005b). Furthermore the underpressure patterns in both the CPT-based design method and the Houlsby & Byrne method cannot cope with the presence of layers with different permeabilities. In addition to that the (linear) underpressure profiles and their effect on resistances do not represent realistic scenarios (Senders and Randolph, 2009). This is expected to cause problems during application in subsoils with layers of different permeability. Additionally there are no guidelines for selecting the value of the two empirical coefficients in the CPT-based design method (k_p & k_f). Finally empirical critical suction formulations are believed to mismatch with the actual suction which is possible to apply (Panagoulias et al., 2017). There is no clear understanding of the effects of physical phenomena like soil arching, plug loosening and internal erosion on the maximum suction which can be applied. In Section 5.3 some of these elements are discussed and design methods are adapted where possible.

2. Quantifying model uncertainty
It is important that we understand the reliability of the model when a design computation is made (Knut and Bjerager, 1992). There are two methods to incorporate model uncertainty in a reliability analysis. One can try to quantify the variation of empirical model parameters and treat them as random variables. Difficulty with this is that these empirical model parameters are often correlated to soil parameters as well as each other. It is more common to quantify uncertainty of the entire model in a stochastic manner (Knut and Bjerager, 1992). In this approach a model factor is determined based on the results of a design computation and corresponding tests. The model factor for each test is simply equal to the measured value divided by the test value. This method has been used for several studies on soil-structure interaction (Tang and Phoon, 2017; Burlon et al., 2014; Dithinde et al., 2011; Phoon and Kulhawy, 2005). A robust stochastic analysis on model uncertainty requires three elements: large scale tests, representative databases and high-quality tests (Phoon and Kulhawy, 2005). Insufficient installation data of suction bucket jackets is available. Therefore it will be attempted to quantify the uncertainty of the predicted installation resistance based on monopile self-weight penetration data (Section 5.2).

5.2. Stochastic model uncertainty factor

The outcomes of a direct reliability analysis do not reflect actual failure probabilities if one does not consider the impact of model uncertainty (Lacasse and Nadim, 1994). Stochastic assessments determine model factors based on a limited amount of measurements (Burlon et al., 2014; Dithinde et al., 2011; Phoon and Kulhawy, 2005). On average approximately thirty values are used while an absolute minimum of five has been used in the past by Knut and Bjerager (1992). Unfortunately this number of comparable test cases is not available for suction bucket (jacket) installation. Nevertheless, in this Section an attempt will be made to estimate model uncertainty based on the self-weight penetration data of large diameter monopiles. There are sufficient measurements of this process.

1. Monopile self-weight penetration
Apart from the start phase the installation process of monopiles and suction bucket jackets is fundamentally different. Nevertheless the soil-structure interaction during self-weight penetration is (almost) identical. Both concepts consist of large circular steel profiles. While D/t ratios differ, they are relatively large for the large diameter monopiles considered in this analysis (D/t > 90). Besides the similarities in geometry the installation design methods of suction bucket jackets are based on open-ended pile design as well (Andersen et al., 2008; Houlsby and Byrne, 2005b). A better estimate could be given by using suction bucket installation data without a doubt. However, monopile self-weight penetration provides a proper alternative due to the availability of over 120 measurements.

Two measurements are performed during self-weight penetration of a monopile: the submerged weight of and on the pile and the penetration depth. During installation design of suction bucket jackets the self-weight penetration depth is the primary interest. However, the model factor (I) will be determined for the penetration resistance (R) at self-weight penetration depth (d_{swp}). This makes it easier to integrate into the design computation (Burlon et al., 2014). The model factor will be computed with Equation 5.1.

$$I = \frac{R(d_{swp})}{V} \quad \text{with:} \quad V = \text{submerged weight}, \quad R = \text{design resistance} \tag{5.1}$$

2. Model estimates
The soil parameters for each of the monopile locations has been determined identically to the procedure stated in Chapter 4. Because this computation only considers model uncertainties the mean value of each soil property is used (Knut and Bjerager, 1992). This means that the model factors computed present the range of deviations from reality excluding parameter uncertainty. The CPT-based design computation is performed with the most probable values for both the shaft and end-bearing factor (Section 2.3 and DNV, 1992). Figure 5.1 presents the measured and computed self-weight penetration for all cases using both models.
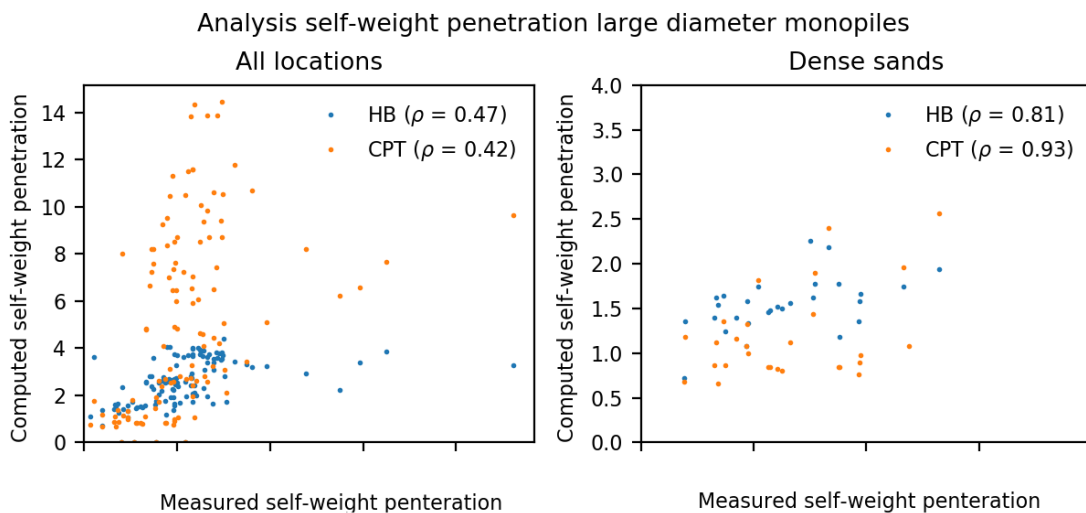

Figure 5.1: Computed versus measured self-weight penetration values of large diameter monopiles

It is noticeable that the CPT-based design method largely overestimates the self-weight penetration at many locations. This is attributed to the fact that the subsoil at these locations consists of clay or loose sand layers. Senders and Randolph (2009) already expected that the CPT-based method does not perform well in these conditions. Model uncertainty is best estimated for a consistent dataset. To avoid a bias in the model factor only locations with relatively dense sands will be used in this research (Knut and Bjerager, 1992). Two filter criteria were used: a soil behavior type index (I_c) lower than 2.05 and a relative density index (R_D) above 0.65 (Robertson and Cabal, 2010; Look, 2007). This resulted in a data series consisting of only cases where dense sand is present along the penetration depth. The predictions for these locations are significantly better. In total twenty-five locations remain (Figure 5.1) which is considered to be a decent amount of input for determining the model factor (Tang and Phoon, 2017; Dithinde et al., 2011; Phoon and Kulhawy, 2005).

3. Probability density function of the model factor

Model errors are commonly assumed to be log-normally distributed, while normal and Beta distributions could be possible as well (Phoon and Kulhawy, 2005; Knut and Bjerager, 1992). Since there is no interest in extreme tail probabilities (≈ 0.001) the fit can be performed with little data. Both goodness of fit tests are successful for the fit through both model factor datasets (Table 5.1). Finally the empirical distribution of the model factor is uni-modal. There is no gap between the model factors computed (Burlon et al., 2014). The mean model factors of the CPT-based and Houlsby & Byrne model are respectively 0.88 and 0.8. This shows that for these cases the model tends to slightly underestimate the resistance present in reality.
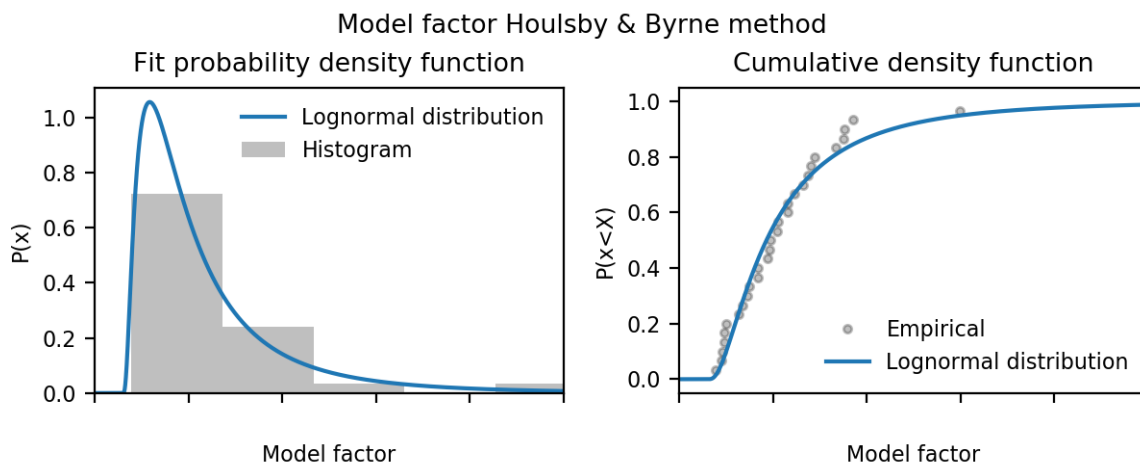
(a) Houlsby & Byrne method
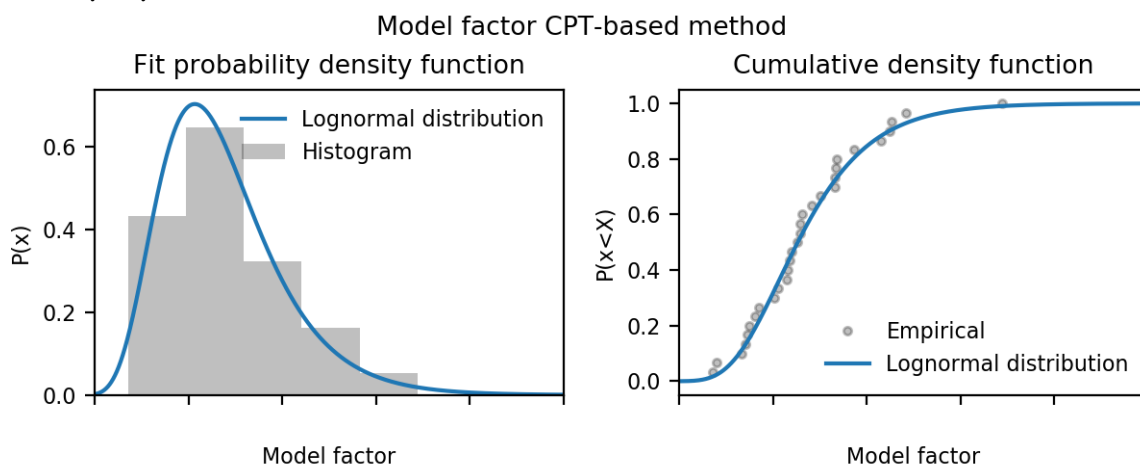
(b) CPT-based method

Figure 5.2: Model factors for both installation design models applied on monopile self-weight penetration in dense sands

4. Representative stochastic model uncertainty factor

A probability density function is a proven way of representing model uncertainties. Nevertheless it is often practical to use representative stochastic model uncertainty factors (Burlon et al., 2014; Knut and Bjerager, 1992). In this case the 95 % reliability interval of the model factor is computed using Equation 5.2. Because a log-normal distribution is used the mean and standard deviation need to be corrected (Equation 5.3). T_{n-1} represents the use of including statistical model uncertainty by drawing a value from the Student-t distribution ($T_{n-1} = 2.402$). Table 5.1 presents the 95 % confidence interval of model factors for both models.

$$I = \exp\left(\mu_{I,\ln} + T_{n-1}\sigma_{I,\ln}\sqrt{1 + \frac{1}{n}}\right) \tag{5.2}$$

$$\mu_{I,\ln} = \ln\mu_I - \frac{1}{2}\ln\left[\left(\frac{\sigma_I}{\mu_I}\right)^2 + 1\right] \quad , \quad \sigma_{I,\ln} = \left\{\ln\left[\left(\frac{\sigma_I}{\mu_I}\right)^2 + 1\right]\right\}^{0.5} \tag{5.3}$$

Table 5.1: Results goodness of fit tests for fitting of log-normal distribution through model factors

Model	μ	σ	N	Distribution	χ^2	χ_c^2	KS	KS_c	$I_{0.025}$	$I_{0.975}$
CPT-based	1.23	0.56	25	Log-normal	3.32	47.40	0.08	0.15	0.46	2.76
Houlsby & Byrne	0.87	0.89	25	Log-normal	0.20	46.19	0.10	0.15	0.15	5.00

Figure 5.3 presents the difference between the use of a 95 % reliability interval based on conventional theory and using the stochastic model uncertainty factor for the CPT-based design method (Alm and Hamre, 2001). One can see that for all locations (except one) the measured resistance lies between the confidence interval of the stochastic model uncertainty factor. Estimating the range of possibilities has become significantly more realistic using Equation 5.2. In Section 5.3 an improved estimation method for the end-bearing coefficient (k_p) is proposed which improves the accuracy of the model significantly while even reducing the 95% reliability interval up to 30%. The upper bound estimates by the stochastic model factor are significantly higher. This has to do with the shape of the log-normal distribution which has a wide tail.
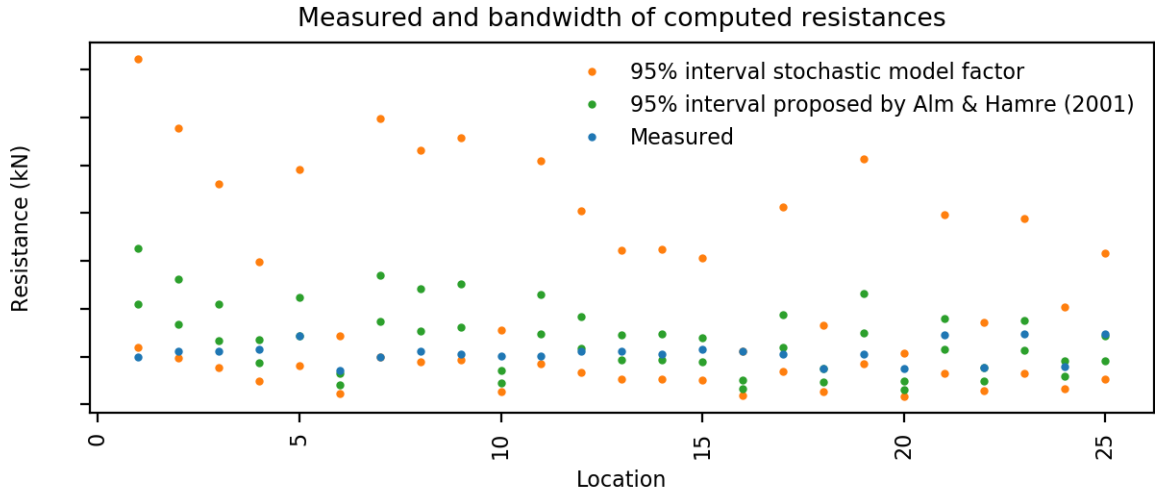

Figure 5.3: Difference in reliability interval between the stochastic model factor and conventional methods (CPT-based design)

5.3. Model assessment

The installation design models were closely examined and in this Section adaptations are proposed to increase the representation of physical phenomena. Where possible the impact of these adaptations on the stochastic model uncertainty factor will be assessed.

1. Houlsby & Byrne method

Elements of the Houlsby & Byrne model which require assessment are the bearing capacity factors (N_c, N_q and N_γ) and the incorporation of the seepage analysis into the design method.

1.1 Incorporating the seepage model

Figure 5.4 shows the influence of incorporating the results of the FE seepage model (Section 2.4) in the Houlsby & Byrne method. The original linear suction profile based on factor a is an oversimplification for layered soils as presented in Figure 5.4. By directly incorporating the results of the seepage analysis the representation of physical phenomena in the Houlsby & Byrne method is improved. Both underpressures and effective stresses are now able to vary non-linearly over depth. If the underpressure exceeds the effective stress level, zero effective stress will be applied (Figure 5.4).
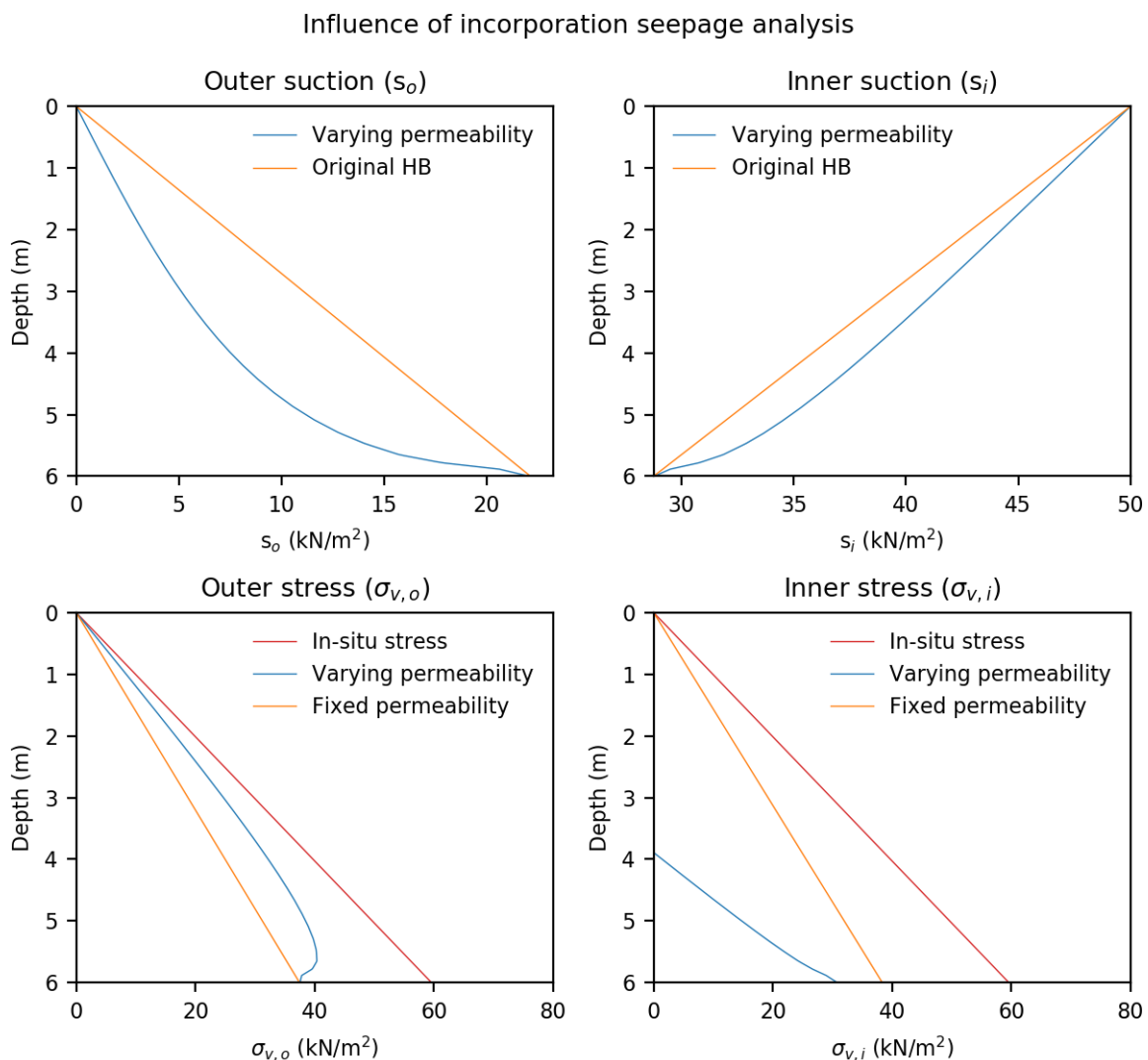

Figure 5.4: Influence of incorporation seepage analysis in the vertical effective stress assessment Houlsby & Byrne method

1.2 Bearing capacity factors

The Houlsby & Byrne method is based on the original strip bearing capacity method developed by Prandtl. Terzaghi adapted it to the now commonly used Equation 5.4. Later the bearing capacity factors (N_q, N_c and N_γ) were determined for shallow and deep foundations by Meyerhof (1951) (Verruijt, 2012).

$$q = cN_c + \sigma'_v N_q + \gamma_s \frac{B}{2} N_\gamma \tag{5.4}$$

The bearing capacity factor (N_q), which determines the influence of the overburden pressure, correlates with the internal friction angle (ϕ). Equation 5.5 presents the commonly used expression for shallow foundations in non-cohesive soils (Meyerhof, 1951). N_q is used to determine the last bearing capacity factor (N_γ) as well (Equation 5.6). The internal friction angle in (pure) cohesive soils is zero. Therefore the bearing capacity factors N_q and N_γ reduce to respectively one and zero in cohesive soils. The bearing capacity factor for cohesion (N_c) is only used in cohesive soils and set equal to nine (Houlsby and Byrne, 2005a).

$$N_q = \tan^2\left(\frac{\pi}{4} + \frac{\phi}{2}\right) \exp^{\pi \tan(\phi)} \quad \text{(non-cohesive soils)} \quad , \quad N_q = 1 \quad \text{(cohesive soils)} \tag{5.5}$$

$$N_\gamma = 1.5(N_q - 1)\cot(\phi) \quad \text{(non-cohesive soils)} \quad , \quad N_\gamma = 0 \quad \text{(cohesive soils)} \tag{5.6}$$

$$N_c = 0 \quad \text{(non-cohesive soils)} \quad , \quad N_c = 9 \quad \text{(cohesive soils)} \tag{5.7}$$

It is probable that significant model uncertainty is caused by the estimates of the bearing capacity factors presented above. Finite element models should be used to provide better estimates. This is not possible within the scope of this study. Therefore the model factor presented in Section 5.2 incorporates the uncertainties caused by the incorporation of the bearing capacity factors.

2. CPT-based method

Model uncertainty in CPT-based design is believed to originate from the determination of the empirical coefficients and the simplified underpressure profile in the prediction of the inner- and outer shaft resistance.

2.1 Empirical coefficients

Ranges for both empirical coefficients in the CPT-based design formulation are given by several authors (Section 2.3). Most named are the values proposed by DNV (1992). Andersen et al. (2008) found ranges of tip resistances widely ranging for dense sands (k_p = 0.05-0.6). The values for the empirical factor on shaft resistance (k_f) proposed by Senders and Randolph (2009) originate from a formulation of Lehane et al. (2007). However, the empirical coefficient in the formulation was modified in such a way that it (again) corresponds to the values proposed by DNV (1992). Concluding one might say that current literature presents little guidelines for selecting the empirical coefficient based on site specific data. This is not desirable since only using the most probable values is likely to result in large model uncertainty (Figure 5.2a & Section 6.4).

An improved estimate of the end-bearing coefficient (k_p) would be very valuable. A calibrated coefficient (k_p) was determined for all twenty-five filtered locations presented in Figure 5.1. This calibration was performed with a constant (and most probable) empirical shaft resistance coefficient (k_f) of 0.001 (DNV, 1992). This is because large variations of k_p due to changes in k_f are not expected during self-weight penetration (Andersen et al., 2008). Calibration resulted in a series which correlates well with high relative densities (R_D > 0.65) (Look, 2007). The formulation proposed by Jamiolkowski et al. (2003) is used to estimate relative densities at the tip of the bucket. This is not ideal since the relative density estimates are expected to contain inaccuracies (Section 4.2).

Figure 5.5 shows the proposed relations between the empirical end-bearing coefficient (k_p) and the estimated relative density (R_D) for three different values of the empirical shaft friction coefficient (k_f). It is observable the range of values possible for k_p are very similar to the range proposed by Andersen et al. (2008). However, with these adaptations it is possible to estimate the variation of the end-bearing coefficient over depth. The error of estimate of k_p is normally distributed with a zero mean and standard deviation of 0.1.
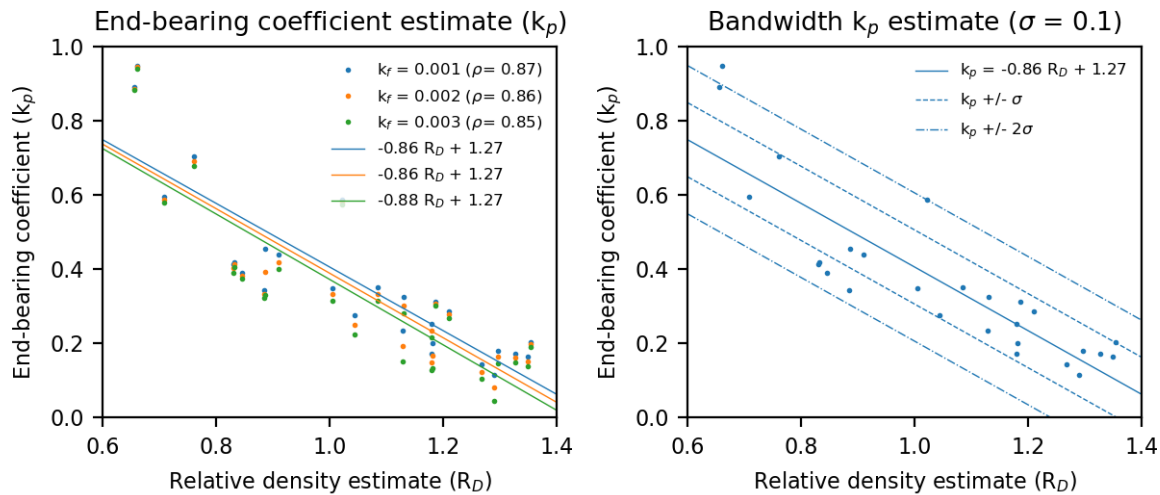
$$k_p = 1.27 - 0.86R_D \tag{5.8}$$

Figure 5.5: Fitted relation end-bearing coefficient with corresponding standard deviation of error

The model uncertainty decreases when Equation 5.8 is implemented in the design method. Similar to Section 5.2 the model factors are computed and a distribution is fitted (Figure 5.6). The probability density function of the model factor shifts from a log-normal to a normal distribution. The mean value of the model factor is equal to 1.01. Also the 95% reliability interval of the stochastic model uncertainty factor reduces by approximately 30 %. It must be mentioned that this analysis is based on the assumption that self-weight penetration of monopiles and suction-bucket jackets is comparable. The range in end-bearing factors (k_p) seems to suggest that this assumption is correct, but of course caution should be exercised.
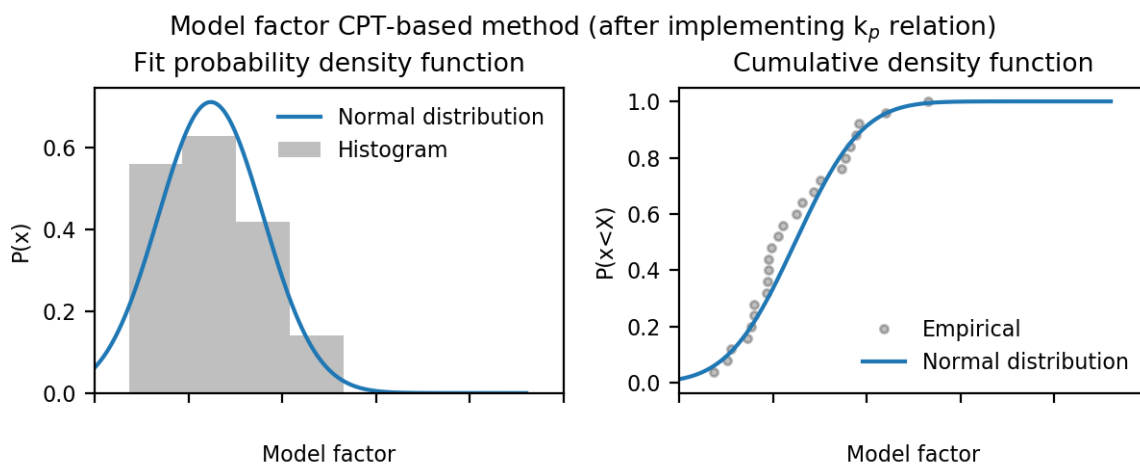

Figure 5.6: Model factor distribution after implementing relationship between relative density (R_D) and end-bearing coefficient (k_p)

2.2 Influence of underpressure

The assumptions regarding the influence of suction proposed in the original paper by Senders and Randolph (2009) comply with the installation data considered in that paper. Nevertheless, the incorporation of two physical phenomena lacks similarities with the processes occurring during installation. The first simplification is the assumption that the influence of the suction on the water pressures near the outside of the skirt is equal to zero. Viewing the results of the seepage analyses presented in Section 2.4 it can be stated that this assumption does not hold. Furthermore it is assumed that the inner total inner skirt resistance reduces linearly between zero and critical suction (Figure 5.7). This is not only physically incorrect but also not applicable in layered soils since the formulation of the suction limit is not yet possible in an accurate way.

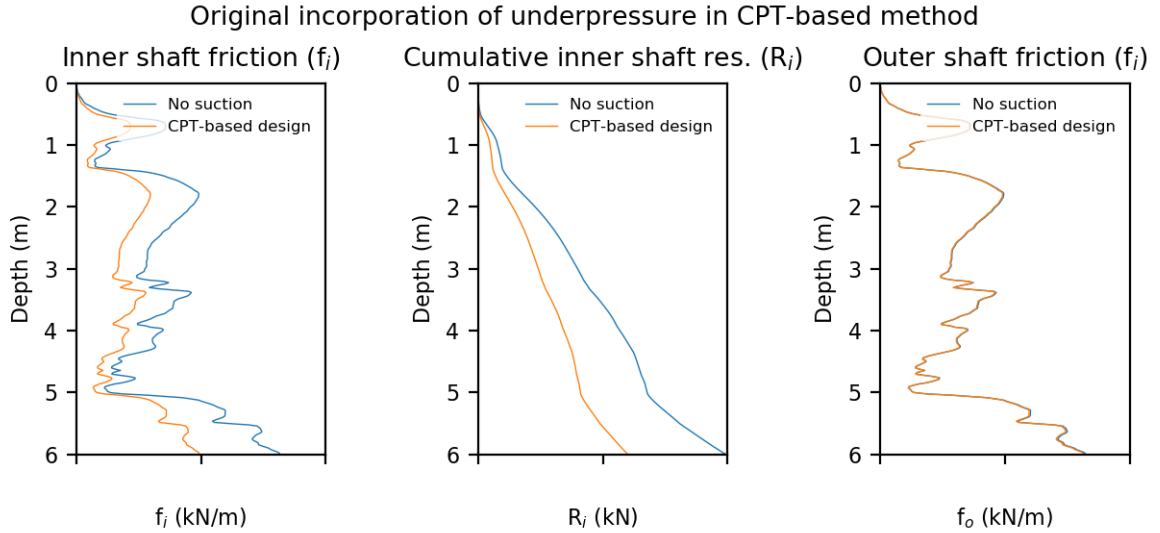## Original incorporation of underpressure in CPT-based method

Figure 5.7: Example of influence of underpressure on the skirt friction in the original CPT-based model

One can see that the wall friction is reduced by an equal factor over the entire depth in the current computational model and that the outer skirt friction is not affected by suction. However, when one compares this profile to the resulting effective stresses from the seepage analysis some peculiarities are spotted (Figure 5.4). First one can see that the effective stress in the top of the inner soil plug becomes zero. This would result in (approximately) zero frictional forces. This is not the case in the current CPT-based method. Furthermore the resistance reduction should not be equal over depth and suction affects the outer resistance.

The seepage analysis results in the normalized seepage profile in- and outside the bucket skirt (a_i & a_o). Considering the above implementation of the seepage analysis in the CPT-based analysis is required. The reduction in local skirt friction is determined to be proportional to the reduction in effective stresses (Equation 5.9). In Figure 5.8 the result of the adaptation is presented for a case scenario.

$$R_{i,s}(d) = \int_0^d f_i(z) \left(\frac{\sigma'_{vi}(z) - a_i(z)s}{\sigma'_{vi}(z)} \right) dz \quad , \quad R_{o,s}(d) = \int_0^d f_o(z) \left(\frac{\sigma'_{vo}(z) - a_o(z)s}{\sigma'_{vo}(z)} \right) dz \tag{5.9}$$

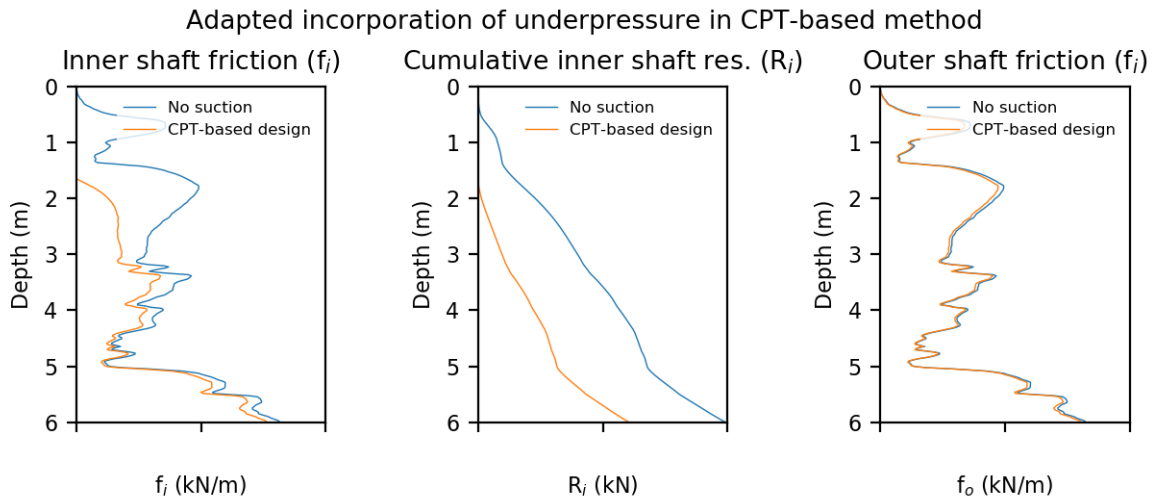## Adapted incorporation of underpressure in CPT-based method

Figure 5.8: Example of incorporation of underpressures in the adapted CPT-based model

2.3 Representative tip resistance

The cone resistance profile is highly variable over depth. In current design methods no remarks are given and therefore the instantaneous cone resistance is applied (Senders, 2008; Andersen et al., 2008). This does not create any problems in the computation of inner- and outer skirt resistance because they consist of the contribution of small frictional forces over the length of the skirt. However, using the instantaneous cone resistance for the end-bearing capacity computation is not realistic. This is for two reasons:

1. Suction profiles are generated which show similar variation to the cone resistance. Varying underpressure at this speed is both unrealistic and not feasible and common in practice.

2. Narrow peaks of high cone resistance can result in high computed required suction values which give the perception of failure while the actual end-bearing capacity is expected to be lower.

Originally averaging of the cone resistance has been applied to compensate for the difference between size of the cone in the cone penetration test and the (closed-ended) pile installed (Xu et al., 2008). Later open-ended pile formulations were developed when (especially the offshore) market for these piles grew. Three methods were developed: Fugro-05 (Kolk et al., 2005), ICP-05 (Jardine et al., Jardine et al.) and NGI-05 (Clausen et al., 2005). In these methods two averaging methods were used for computing a representative average cone resistance value:

1. Use the average cone resistance between 1.5 times the diameter above and below the pile tip.

2. Use the Dutch method which is an weighted value of arithmetic averages (of which some are computed with a minimum path rule) between eight times the diameter above the pile tip and four times below.

Suction buckets have small length over diameter ratios (L/D <1). Therefore making use of the diameter is not possible. The diameter of the cone used in a cone penetration test does not differ much from the wall thickness. The Dutch method was originally developed for closed ended longer piles. Since suction buckets beneath jackets are relatively shallow the averaging would occur over a too large extent. It was decided to use the normal averaging method in this research. In Figure 5.9 it is visible that the averaging technique eliminates the very small fluctuations in the suction profile while still allowing for fluctuations in total resistance. This is a slight improvement with respect to using the instantaneous resistance.
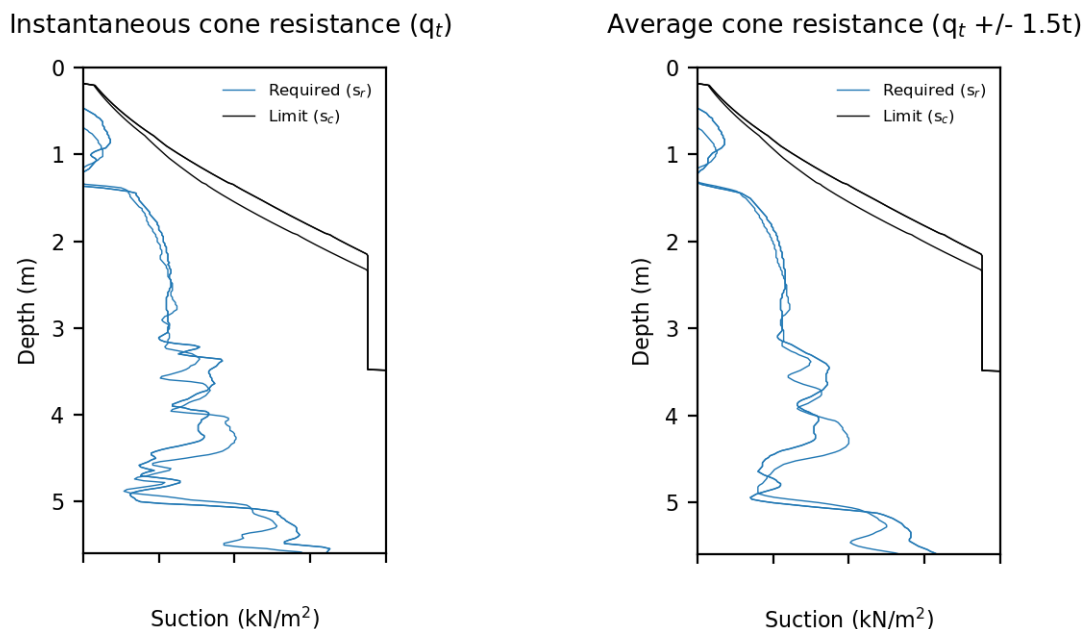

Figure 5.9: Influence of cone resistance averaging on design output of the CPT-based model

3. Critical suction
The critical suction is a much debated topic in research on suction buckets (Panagoulias et al., 2017). Three limitations (soil, pumps and structural) will be combined to develop a critical suction profile in this research.

3.1 Soil plug heave
Soil plug heave can be caused by displacement of the soil by the skirt as well as excessive applied suction. Soil heave due to displacements is taken into account by accounting for a so called free space during design. Tran et al. (2007) recommended approximately 5-6 percent which is implemented in practice as well. Soil heave due to displacements decreases when the diameter of the bucket increases. Predicting the exact value of soil heave in non-cohesive soils is not possible at this moment (Section 2.5).

Heave of an entire cohesive and impermeable soil plug can occur when the applied underpressure on the soil plug area (A_p) is larger than the submerged weight (W') and inner skirt resistance combined (Equation 5.10) (Randolph and Gourvenec, 2011).

$$A_p s_c > R_i + W \tag{5.10}$$

3.2 Reverse-end bearing
When the difference between outside and inside vertical effective stresses becomes too large local plastic failure can occur (Houlsby and Byrne, 2005b). This is plausible for suction-bucket foundations because the inner effective stresses will be reduced at deeper penetration depths. Local penetration failure causes soil flow into the caisson without any further penetration. The limit suction can be computed by equalizing the outer ($\sigma_{v,o}$) to the inner effective stress ($\sigma_{v,i}$) while adding a factor accounting for bearing capacity against uplift (reference is made to Houlsby and Byrne, 2005b; 2005a). In the original paper it was mentioned that this value is approximately equal to the critical gradient limit. This will be more governing than reverse end-bearing since permeability fluctuations have a large influence. Elaboration is given in Paragraph 3.5.

3.3 Liquefaction
Increased pore pressures can result in reduced effective stresses (up to zero). Local suction limits are reached when the soil close to the tip of the inner soil plug liquefies (Senders and Randolph, 2009). Estimating the suction level at which liquefaction occurs is relatively easy. The calculation requires two inputs: the effective stress ($\sigma_{v,i}$) and the normalized suction effect (a_i). The normalized suction effect is the result from the seepage study described in Section 2.4. The local underpressure required for liquefaction is equal to the local effective stress. The critical amount of suction under the lid is then simply found with Equation 5.11. During model tests it was found that the soil at the skirt tip is constrained by the soil around it. In these tests it was observed that the soil limit can be better approached by the exit gradient at the seabed inside the bucket skirt. This phenomenon is discussed in Paragraph 3.5 of this Section.

$$s_c = \frac{\sigma_{v,i}(h)}{a_i(h)} \tag{5.11}$$

3.4 Soil plug loosening
The Houlsby and Byrne method (2005b) already allows for incorporation of larger plug permeability during suction-assisted installation. Experiments performed by Tran et al. (2007) not only suggest this phenomenon but also show that the increase permeability of the plug is larger at higher penetration depths (Harireche et al., 2014). The main cause of these changes in permeability is attributed to the occurrence of soil heave. Due to soil heave the volume of the soil increases and therefore more voids are created. This causes the permeability of a sandy inner soil plug to increase by approximately 3 to 3.5 times (Erbrich and Tjelta, 1999). Harireche et al. (2014) proposed Equation 5.12 to account for varying soil plug permeabilities over penetration depth. Values of 1.3 for initial permeability ($k_{r,0}$) and 3.0 for the increase of plug permeability per meter of relative penetration depth (H/D) (α_k). Little extra research has been performed on the variation of these parameters. However, for caissons with a depth to diameter ratio of approximately 0.5 the results of Equation 5.12 correspond to earlier studies (Houlsby and Byrne, 2005b; Erbrich and Tjelta, 1999).

$$k_r = \alpha_k \frac{H}{D} + k_{r,0} \tag{5.12}$$

3.5 Exit gradient

In earlier model tests it was observed that liquefaction at the pile tip does not necessarily govern suction failure in the soil. This is due to the fact that the soil at the pile is constrained by the material around it (Senders and Randolph, 2009). The exit gradient at the seabed inside the caisson was used for developing the current empirical formulas for suction limits in homogeneous sandy soils. Both the exit gradient and critical exit gradient can be determined. As a result the critical suction limit is determined according to Equation 5.13. Figure 5.10 shows that the estimate based on the axisymmetric model described in Section 2.4 corresponds to the empirical result of Feld (2001). This phenomena will be used to determine the soil suction limit since it provides stricter limits than the liquefaction criterion.

$$i = \frac{p}{\gamma_w s} \quad , \quad i_c = \frac{\gamma'_s}{\gamma_w} \quad , \quad s_c = s\gamma'_s \tag{5.13}$$
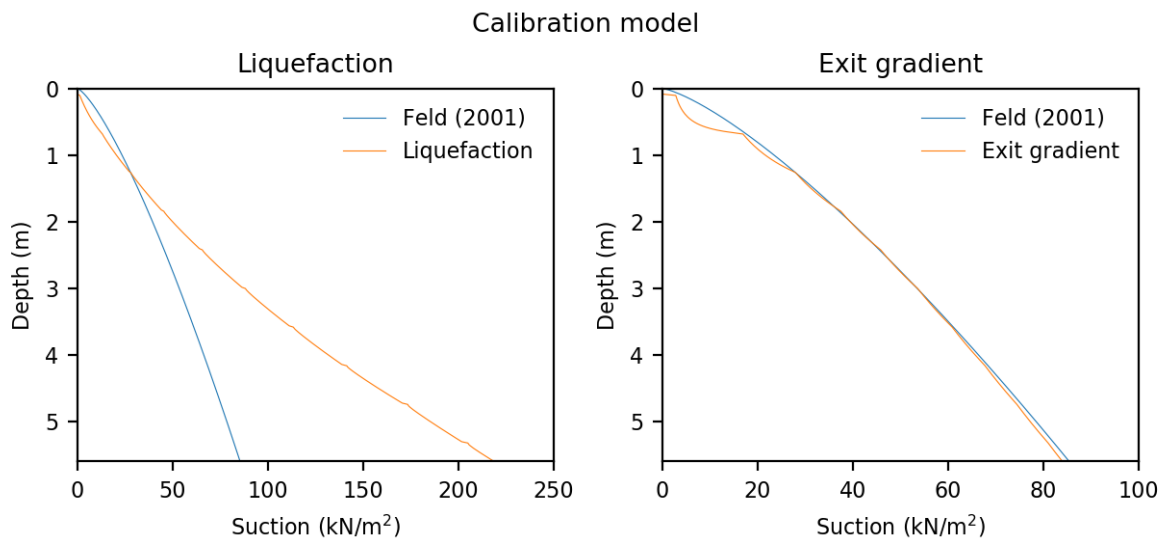

Figure 5.10: Calibration of axisymmetric finite element model output to empirical critical suction formulations based on the exit gradient

In reality subsoils consisting of layers with varying parameters will be present. This makes the current method inaccurate for two main reasons:

- Soil plug loosening will cause an increase of the permeability inside the plug. As a consequence pressure gradients change and therefore the soil suction limit will change.

- Permeability varies between layers. This will have an effect on the pressure gradients throughout penetration. As a consequence the critical suction computed by Equation 5.13 changes.

Figure 5.11 shows the effect of incorporating the inner plug loosening formula of Harireche et al. (2014) on the suction limit based on the exit gradient. It is visible that the limit suction increases significantly. This is deemed plausible since previous research already showed that the original empirical formulations are expected to be too conservative.

Incorporating the effect of varying permeability and soil weights results in a wide range of limit profiles (Figure 5.11). It must be remembered that the exit gradient is not a failure mechanism in itself (Chapter 3). However, it can contribute to the failure mechanisms of piping, inner erosion, plug heave and excessive loosening. To which extent which failure mechanism occurs is unknown at this point. A start is probably made at inner erosion, loosening and plug heave. If the critical gradient is exceeded over a long length of the skirt piping is expected to occur. Regardless of the failure mechanism the exit gradient is a conservative choice.
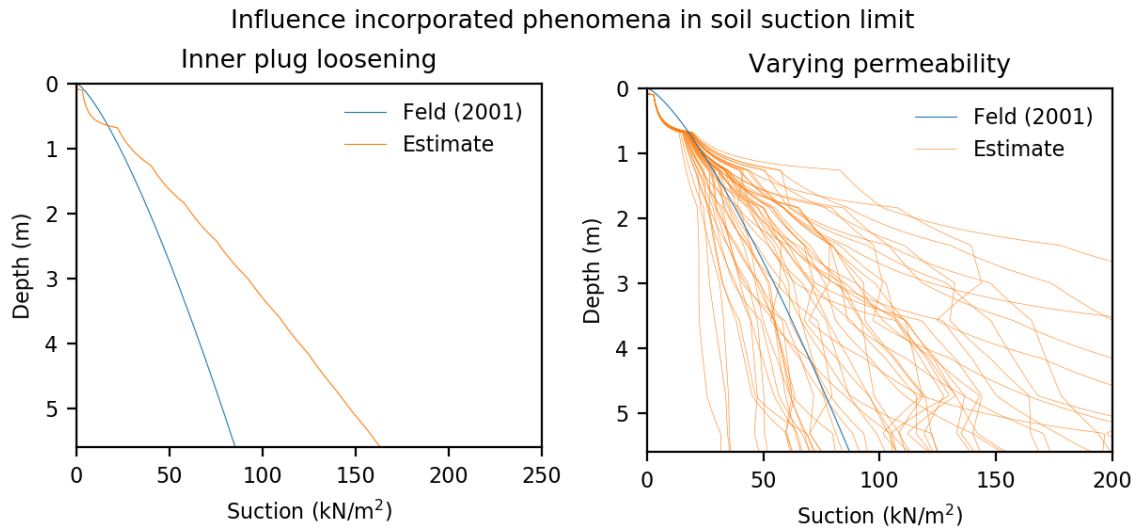
Figure 5.11: Effect of inner plug loosening and permeability variation on the exit gradient soil suction limit outcome

This method of computing critical suction limits is deemed the most appropriate. The liquefaction limit will overestimate the critical suction limit and ignore failure mechanisms as heave and piping. Furthermore it depends very much on the (enhanced) vertical stress. In Chapter 6 it will be discussed that the computation of this stress is very sensitive to the parameter estimates done in Chapter 4. Since the method based on the exit gradient is independent of stress enhancement it provides a more objective criterion and will be used in this research.

3.6 Cavitation and buckling limits
It is expected that cavitation and buckling criteria could provide strict limits to the applicable suction at locations with shallow water depths (Ibsen and Thilsted, 2010). Section 2.5 discussed the computation of cavitation limits. Buckling limits (over depth) need to be retrieved from a separate study on this structural failure mechanism. It falls outside the scope of this research to develop a separate formulation for buckling.

The actual critical suction profile will consist of a combination of the three limitations. The minimal value of the buckling, cavitation and soil limit for each penetration depth is the actual governing mechanism.

5.4. Evaluation

The geotechnical installation design methods presented in Chapter 2 form a good basis but require adaptation. This is especially the case for layered soils. The adaptations as well as the incorporation of the remaining model uncertainty in the reliability-based design framework are discussed in this Section.

1. Model adaptations

The following adaptations to the installation model will be implemented based on the preceding analysis:

1.1 Houlsby & Byrne method

The only adaptation made to the Houlsby & Byrne method is the integration of the normalized underpressure FE model (Section 2.4) into the effective stress profile. This results in more realistic estimates of the effect of underpressure on the effective stresses in subsoils with layers of varying permeability.

1.2 CPT-based method

The empirical parameter estimation for the CPT-based design method is changed for this research. Instead of using the most probable values for both coefficients in sand the end-bearing coefficient (k_p) is determined using Equation 5.8. The influence of suction on inner- and outer skirt resistance is taken into account according to Equation 5.9.

1.3 Critical suction

Critical suction will not be formulated according to the empirical equations discussed in Section 2.5 anymore. Instead of this different estimates of critical suction over depth will be combined. For non-cohesive soils this will be the minimum of three elements over depth: the exit gradient, cavitation and buckling limit.

1.4 Computational implications

Both the CPT-based model and Houlsby & Byrne model described in Chapter 2 could be solved in one go for homogeneous soils. This is because both the profile of underpressure and stress enhancement can be solved analytically. Directly solving the problem for the suction profile has become impossible. This is due to the implementation of the coupling with the seepage model. This has to do with the fact that the resistance (reduction) is coupled with the amount of suction applied. The suction required has to be solved iteratively (Figure 5.12).
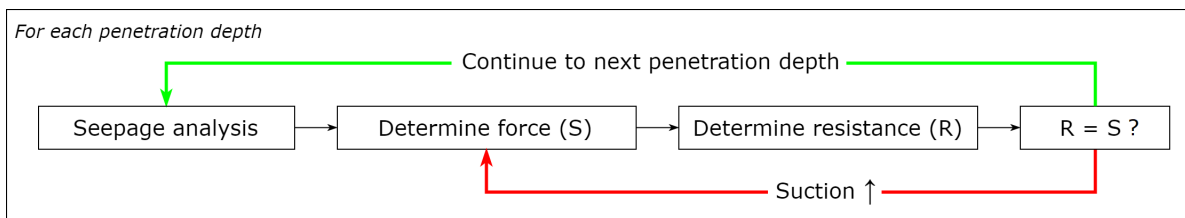

Figure 5.12: Iterative procedure required for solving adapted CPT-based and Houlsby & Byrne penetration study models

2. Integration in reliability-based design framework

It is tempting to simulate both model and parametric uncertainty at the same time to get a full assessment of installation reliability. Unfortunately this could lead to a wrong perception of the feasibility level. The stochastic model uncertainty factors are based on design computations for which the mean value of each parameter is used. As a consequence the model uncertainty factor is only valid for this scenario.

Due to the coupling of model and parametric uncertainty it is unwise to integrate model uncertainties simultaneous with parametric uncertainties. The mean design case should be used to simulate the effects of model uncertainty while the original model can be used to simulate the effects of parametric uncertainty. Although this might sound like an accuracy loss it has benefits as well. It allows for examination of the influence of single elements (e.g. model factors, parameter estimates) on overall uncertainty (Chapter 6). Lastly it should be mentioned that it is possible to incorporate the uncertainty of the end-bearing empirical factor as a random variable.

6

Quantitative reliability analysis

The climax of the reliability based design process is the quantitative (or direct) reliability analysis. Quantified uncertainties are integrated in the design computations to analyze the feasibility of installation, probability of events and model sensitivity.

6.1. Overview

In this Section the principles of a direct reliability analysis will be introduced and applied to suction bucket jacket installation design.

1. Introduction

Design problems can often be simplified to a comparison between a possible load (S) and possible resistance (R). Failure occurs when the load on a system exceeds the resistance of the system. In reliability analyses this principle is represented by a limit state function (Equation 6.1). If the limit state value (Z) is below zero the system fails for the implemented design conditions. If the limit state value is above zero the design is considered feasible for those conditions (Jonkman et al., 2017). Application of this principle on suction bucket jacket design is relatively straightforward. For example one could see the required suction (s_r) as a load (S) and the critical suction (s_c) as a resistance (R). If the required suction exceeds the critical suction the limit state is below zero and installation is expected to fail (Panagoulias et al., 2017).

$$Z = R - S \qquad (6.1)$$

Conventional design calculations use (conservative) parameter estimates which lead to an analysis of the limit state with two deterministic elements. A direct reliability analysis takes uncertainties into account. For a simple problem one can express the load (S) and resistance (R) as distributed values in similar units. When one plots the probability density function of these values the distributions can overlap. Failure occurs where the load overlaps the resistance. The probability of failure is then computed as the surface underneath the overlapping area (Figure 6.1). This is can be done by direct integration (Lacasse and Nadim, 2007).
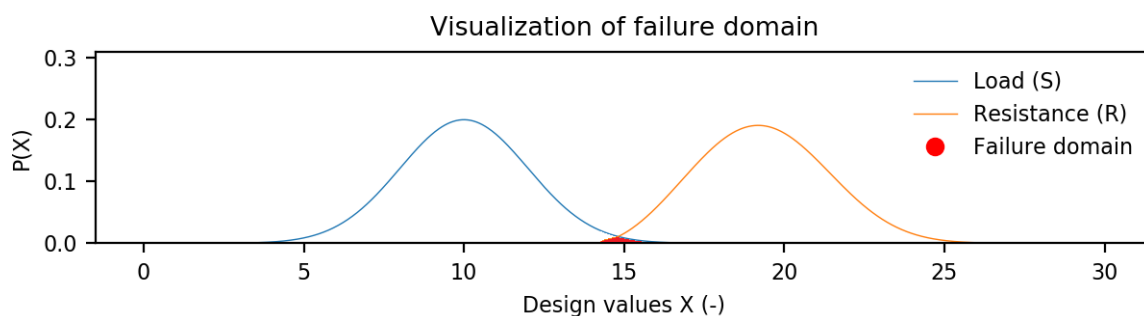

Figure 6.1: Visualization of the failure domain for a one-dimensional distributed load and resistance

67

A target probability value is required to assess the feasibility of installation. Its value is often based on the amount and type of damage if failure occurs. No permanent damage or life loss due to failed geotechnical installation of suction bucket jackets is expected. The target failure probability is set to 10^{-2} (ISO, 2015). Quantifying a target failure probability is also possible based on economic impacts but this falls outside the scope of this research (Vrijling, 2001).

2. Simulation methods

Suction bucket jacket design can be considered a multi-dimensional problem. It has many different parametric uncertainties. Therefore more complex simulation methods than depicted in Figure 6.1 are required.

A level III analysis is the most extensive option. Parameters are randomly generated according to their previously determined variability (Chapter 4). The most common method is the Monte-Carlo analysis. Possible design conditions are generated in thousands of simulations (N_t). For each of these simulations the limit state value (Z) is assessed. The probability of failure is then simply computed as the sum of simulations with a failed limit state (N_f, Z<0) divided by the total amount of simulations (N_t). This method provides the most accurate description of the failure probability if sufficient simulations are performed. It can handle multi-dimensional problems well due to the simple simulation of parametric uncertainties. The drawback is the computational time due to the amount of simulations required (Phoon, 2008; Lacasse and Nadim, 2007).

A level II method tries to approach the failure domain of a level III analysis. The most common method is the First Order Reliability Method (FORM). Methods like these are very fast in approaching the solution of the reliability analysis due to the linearization of the limit state (Jonkman et al., 2017). Drawbacks are the inability to cope with problems which have many dimensions (e.g. different parameters). Application of these methods in geotechnical engineering seldom occur (Christian, 2004). Finally, level I methods provide a semi-deterministic alternative. Safety factors from existing design standards are applied on either individual parameters or on total design outcomes of a deterministic computation. The limit state is simply checked by comparing the two single values corresponding to the load and resistance. This is by far the fastest method but does not provide any information on the origins of failure.

3. Suction bucket jacket installation

In Chapter 3 it was already discussed that specific failure probabilities for each possible event or failure mechanism will be hard to examine. This is due to the inability of the current geotechnical installation design methods to capture the physical behavior of mechanisms like soil plug heave, excessive loosening or inner erosion. Nevertheless two important design computations are performed: self-weight and suction-assisted penetration. Also the application of the contingency measures ballasting and backfilling is examined.

Two assessments require two limit states. The limit state for self-weight penetration requires a minimum penetration depth ($d_{swp,r}$). This threshold is set to 0.5 meter. If the computed self-weight penetration is below 0.5 meters, ballast needs to be applied. The amount of ballast required is therefore conditional to whether insufficient self-weight penetration occurs. The limit state is presented in Equation 6.2.

$$Z = d_{swp} - d_{swp,r} \qquad \text{with:} \qquad d_{swp,r} = 0.5m \tag{6.2}$$

Formulation of the limit state for suction-assisted penetration is more complicated. At first sight one would use the required suction (s_r) minus the critical suction (s_c). However, these absolute values give no insight in the proximity of failure of the entire system but only at each individual depth. Hence, instead of using suction values in (kN/m^2) the suction pressures are normalized with respect to the critical suction (Equation 6.3). A higher required suction than critical suction still has a limit state function value below zero as a consequence. This change does not affect the functioning of the limit state in the quantitative reliability analysis.

$$Z = 1 - \frac{s_r}{s_c} \tag{6.3}$$

Suction bucket jacket installation design is multi-dimensional and contains numerical procedures. The multi-dimensionality of the problem requires a level III approach. Due to the application of the finite element seepage model one installation design computation takes several seconds. An attempt will be made to reduce the amount of simulations. A Markov Chain Monte Carlo analysis with subset simulation is implemented and elaboration is given in Section 6.2.

6.2. (Markov Chain) Monte Carlo simulation

This Section presents background in both methods used to perform the direct reliability analyses in this research. It starts with a short elaboration on the regular Monte Carlo analysis after which optimization using Markov Chains and subsets is discussed.

1. Monte Carlo simulation (MCS)

It is difficult to compute the failure probability for a multi-dimensional problem with fast simulation methods or direct integration (Jonkman et al., 2017). The only practical solution is performing a level III analysis. Monte Carlo simulation has been applied on different problems in geotechnical engineering in the past (e.g. Stuyts et al., 2017; Griffiths et al., 2009; Fenton and Griffiths, 2005). A Monte Carlo simulation is based on many simulations (N_t). Each parameter is randomly sampled from its variability descriptor for each simulation. The installation design computation is performed with each parameter set. The limit state values are determined and stored. The amount of simulations for which the limit state is below zero is counted (N_f). The failure probability and expected coefficient of variation can then be computed using Equation 6.4.

$$P_f = \frac{N_f}{N_t} \quad \text{with:} \quad \text{COV} = \sqrt{\frac{1 - P_f}{N P_f}} \tag{6.4}$$
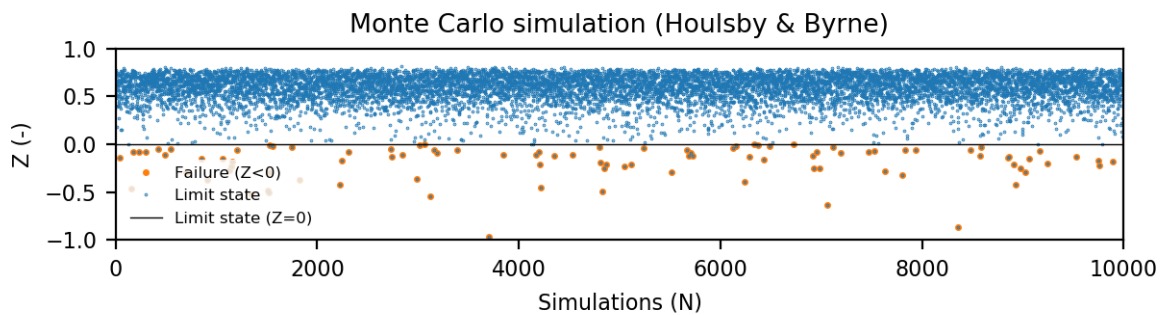

Figure 6.2: Results of simulations during a regular Monte Carlo simulation on one location with the Houlsby & Byrne method

It is expected that suction bucket jacket installation (in the case study wind farm) has a small probability of failure. Using little simulations in a Monte Carlo simulation can therefore lead to a wrong estimate of the probability of failure. Based on several trial runs it was examined that at least 10000 simulations are required for a probability of failure with a coefficient of variation of approximately one percent (Figure 6.3). Computational time will be extensive since numerical methods (the seepage analyses) are used in each simulation. Conventional methods of optimization (e.g. importance sampling) are only applicable for problems with limited dimensions and simple failure regions (Au and Beck, 2001). This research attempts to use the Markov Chain Monte Carlo method with subset simulation. This is recommended as an ideal method for estimating small failure probabilities in multi-dimensional problems (Phoon, 2008).
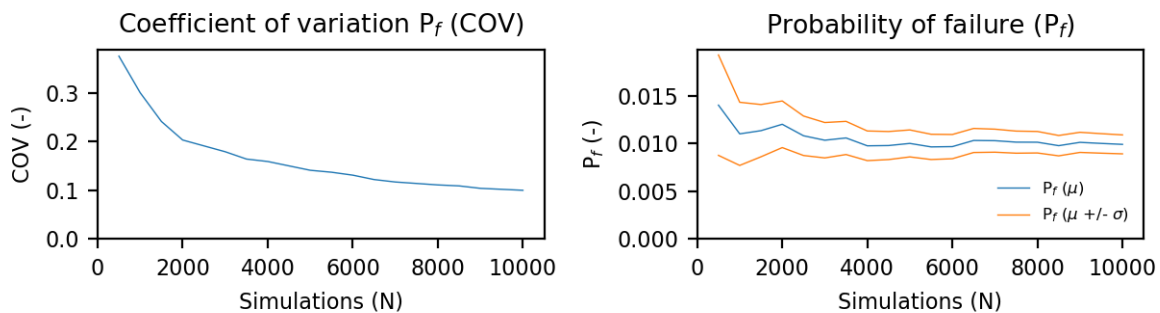

Figure 6.3: Influence of the amount of simulations on the reliability of the Monte Carlo analysis on one suction bucket installation computation

2. Subset simulation

Subset simulation has first been introduced by Au and Beck in 2001. In this method the failure probability is computed as the product of conditional probabilities of intermediate failure events (Au and Beck, 2001).

The entire procedure starts with an initial Monte Carlo analysis with N_s simulations (Figure 6.4). The empirical cumulative density function of the limit state values (Z) of all simulations is computed. The limit state value corresponding to a cutoff probability (p_0) is determined. This limit state value is the first intermediate limit state ($Z_{t,1}$) (Figure 6.4). The probability of obtaining a limit state value below $Z_{t,1}$ is therefore p_0. All parameters sets (θ_1) from simulations which resulted in limit states lower than this intermediate limit state ($Z < Z_{t,1}$) are saved as seeds for future simulation in so called Markov Chains. The amount of seeds (N_c) is equal to the product of the cutoff probability (p_0) and the amount of simulations (N_s).
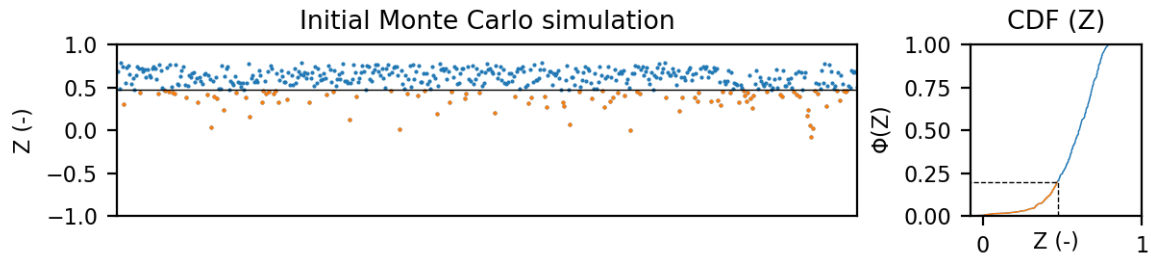

Figure 6.4: Initial Monte Carlo analysis (left) and selection of first intermediate limit state (right)

At this point the first subset simulation can start at each seed parameter set (θ_1). Each of these seeds serves as the first link in the Markov Chain. New links (e.g. parameter sets) in the chain will be simulated from the previous link using the Modified Metropolis algorithm. This algorithm provides a method of sampling from the previous state. This increases the probability of generating a state which is below the intermediate limit state. In paragraph 3 the Modified Metropolis algorithm is explained and optimized. A similar amount of simulations (N_s) is performed evenly distributed over all the Markov Chains. A new intermediate state ($Z_{t,2}$) can be selected using the empirical cumulative density function of N_s limit state values (Z) and the cut-off probability (p_0). Figure 6.5 shows the output given by two subsequent subset simulations. It is possible to see the intermediate limit states ($Z_{t,n}$) progressing towards zero.
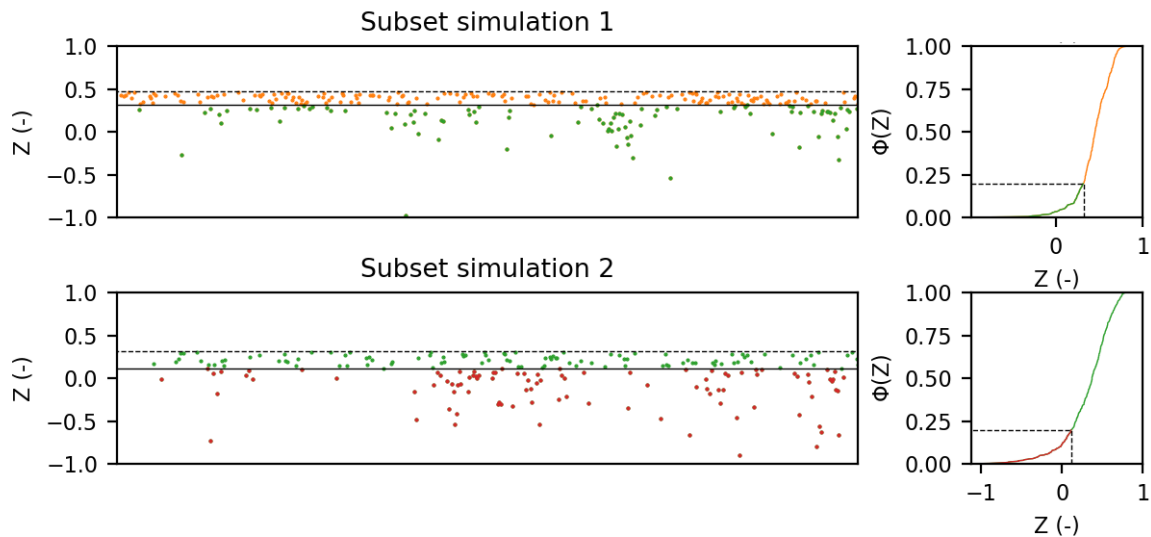
Figure 6.5: Subset simulations (left) and selection of intermediate limit states (right)

The last subset simulation is completed if the resulting intermediate threshold ($Z_{t,n}$) is below zero. This last subset has a limit state value of zero and the last conditional failure probability is determined similar as in a Monte Carlo simulation ($P_{f,n} = N_{f,n}/N_s$). Knowing the amount of subsets (n) and the last conditional failure probability ($P_{f,n}$) the total failure probability can be computed using Equation 6.5.

Figure 6.6: Final subset simulation (left) with the definitive limit state ($Z_{t,n}=0$) (right)

$$P_f = P(Z_{t,1}) \prod_{i=1}^{n-1} P(Z_{t,i+1}|P_i) \tag{6.5}$$

The accuracy of the subset simulation depends on the ability of the algorithm to generate a representative set of scenarios within the parameter space. The choices of three different model elements determine the accuracy of the Markov Chain Monte Carlo analysis:
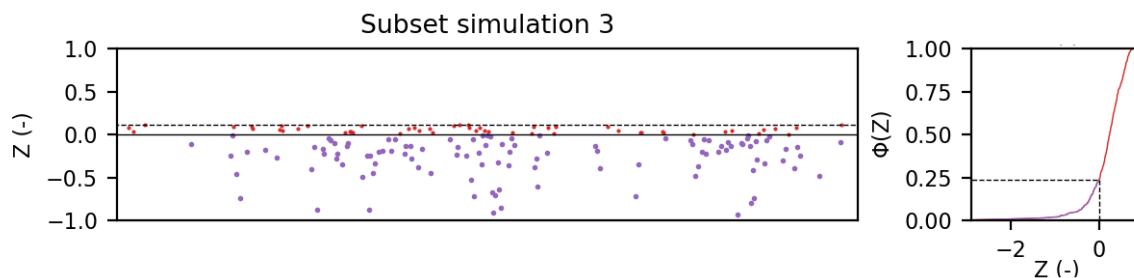
1. *The cutoff probability value (p_0):*
   The larger the cutoff probabilityis, the more Markov Chains are generated. As a consequence the probability that part of the parameter space is missed becomes lower. Selecting a high cutoff probability causes slower convergence. This is due to the fact that there will be fewer links in the Markov Chains.

2. *The amount of simulations (per subset) (N_s):*
   The larger the amount of simulations per subset the more scenarios will be generated during the initial Monte Carlo analysis. Therefore more of the parameter space will be populated. A disadvantage of a high number of simulations is the increased computational time.

3. *The type and shape of the sampling distribution in the Modified Metropolis algorithm:*
   The Modified Metropolis algorithm requires a proposal distribution as an input. The choice of type and shape of this distribution determines the efficiency of the sampling. If chosen wrong the parameter sets within a Markov Chains can be too correlated. This causes less of the parameter space to be populated and could lead to an offset in the computed failure probability. Elaboration on this topic is presented in Paragraph 3.

Phoon (2008) presents a small sensitivity analysis on selecting the proper cutoff probability (p_0) and amount of simulations per subset (N_s) for a simple problem. Generally speaking the more simulations and the higher the cutoff probability is, the more accurate the failure probability is. In Section 6.3 the accuracy and efficiency of the application of the MCMC algorithm on suction bucket jacket installation is discussed.

3. Modified Metropolis algorithm (MMH)
During simulation of the subsets new parameters are generated using the Modified Metropolis algorithm. The parameter set corresponding to the most recent link in the Markov Chain (θ_{i-1}) serves as a starting point. Then the original distribution and a sampling distribution are used to set-up a new (candidate) state of parameters (θ_i). If the candidate state (θ_i) results in a limit state value lower than the intermediate limit state ($Z_{t,i}$) the candidate state parameter set is accepted as the next link in the Markov Chain (Au and Beck, 2003). Below an example is given for the application of the MMH algorithm on sampling a new friction angle (ϕ):

1. The parameter set corresponding to the last link in the Markov Chain (θ_{i-1}) is selected.

2. For each parameter a candidate parameter is generated based on the original value and the addition of a random sample (ζ_i) (e.g. for the friction angle in Equation 6.6).

$$\phi_i = \phi_{i-1} + \zeta_i \tag{6.6}$$

The random sample (ζ_i) is retrieved by randomly picking a number from a proposal probability density function (p_j^*) positioned on the original value (ϕ_{i-1}). The proposal distribution is often normally distributed (original Metropolis algorithm) but can be asymetric as well (Modified Metropolis Algorithm).

3. The proposed value for the candidate state (θ_i) is accepted based on the outcome of the calculation of the acceptance ratio (Equation 6.7). The first term of the acceptance ratio represents the ratio of probabilities from the original probability density function (P). The second term represents the conditional probabilities for the proposal distributions (p_j^*) located around each state.

$$r_a = \frac{P(\phi_i)}{P(\phi_{i-1})} \cdot \frac{p_j^*(\phi_{i-1}|\phi_i)}{p_j^*(\phi_i|\phi_{i-1})} \tag{6.7}$$

4. A random number (z) is simulated from a uniform distribution between 0 and 1.

5. If the random number (z) is lower than the acceptance ratio the candidate state (θ_i) is accepted. Otherwise the original state value (θ_{i-1}) is used (Equation 6.8 & 6.9).

$$\text{if:} \quad z < r_a \quad : \quad \theta_i = \theta_i \tag{6.8}$$

$$\text{if:} \quad z > r_a \quad : \quad \theta_i = \theta_{i-1} \tag{6.9}$$

4. Optimizing the proposal distribution for MMH sampling
As stated in paragraph 2 the selection of the proposal distribution (p_j^*) is essential for proper functioning of the MCMC simulation. Selecting the type and shape of the proposal distribution can be a tedious job. If the spread of the proposal distribution is too low the values generated by the MMH algorithm will be too correlated. Vice versa the percentage of accepted candidate states becomes too low if the sampling distribution is too wide. An ideal sampling distribution shows little correlation and a decent percentage of accepted values.

The effectiveness of sampling by different types and shapes of proposal distributions are evaluated in this research. This is done by performing 10000 MMH simulations for each probability density function used in the analysis. After the simulation two methods are used to assess the effectiveness of each proposal distribution. Firstly the acceptance rate is computed for the simulated series. Secondly the empirical autocorrelation model is plotted. The corresponding scale of fluctuation (δ) for a fit of the single exponential function is determined too (Table 4.1). The proposal distributions are then optimized for an acceptance ratio of 50 % and a low scale of fluctuation (δ). Figure 6.7 shows the selection of a normal distribution with a standard deviation of five as proposal distribution for sampling of the internal friction angle in one layer.
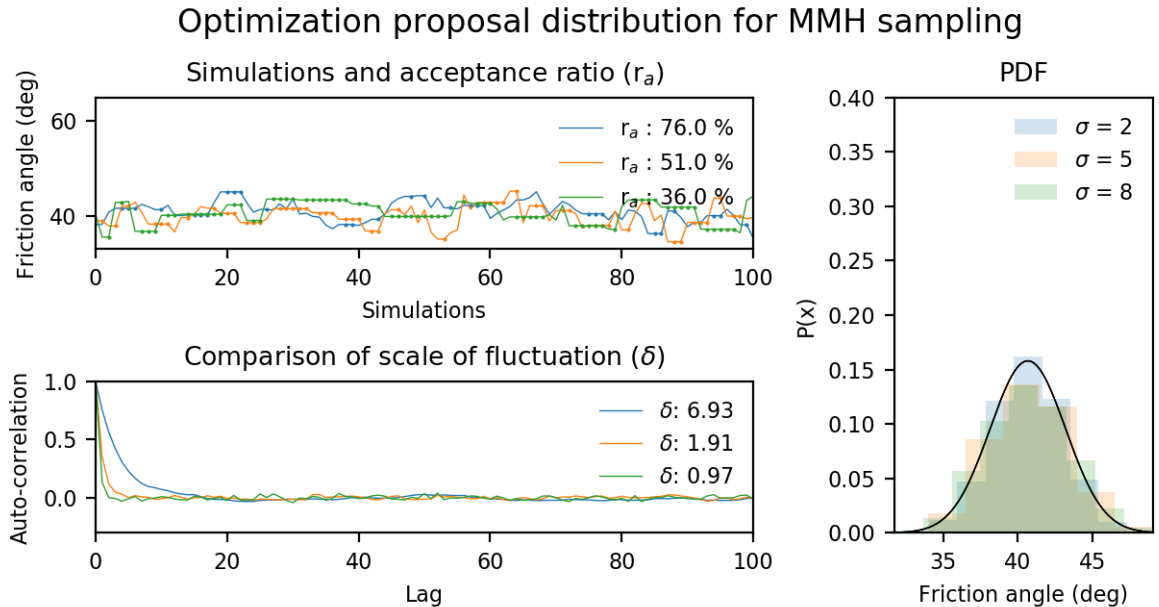

Figure 6.7: Example of optimization of the proposal distribution for the friction angle distribution in one layer

6.3. Case study example

This Section is dedicated to showing a full quantitative reliability analysis for an example suction bucket jacket location by incorporating all earlier work. This analysis contains all aspects required for understanding the findings during this research.

1. Case study

The example wind farm dataset described in Chapter 4 is used to develop a case study for this research. The case study will be performed at one anonymous location but its characteristics reflect reality.

1.1 Location and geometric parameters

The design will be made for a suction bucket jacket with three buckets and a self-weight of over XXX tons. Although the bucket skirt length (L) is equal to X meters the target penetration depth is limited to X.X meters. This is mainly due to the application of a filter layer with a thickness of X meter (+/- X m).

(a) Overview of example location

(b) Bathymetric survey

Figure 6.8: Example location top view with site investigation campaign elements and bathymetry

Four downhole seabed cone penetration tests were performed at the example location. Two are located in the vicinity of the same bucket (Figure 6.8a). Samples were made using a borehole close to the centerline of the jacket. Samples were retrieved up to a depth of approximately 6 meters. No triaxial tests were performed at this location. Hardly any difference in seabed level is present. The maximum observed difference is approximately X centimeters. The suction bucket jackets will be placed in a water depth of approximately XX meters with respect to low astronomical tide (LAT). This water depth will be governing for cavitation.

1.2 Design soil profile

The borehole log shows similarities to the soil behavior type index. The soil mainly consists of fine to medium sized dense sands over the skirt length of the buckets. At lower depths these sands become very silty. At depths of around 3 meters small silt layers/lenses are identified. Even a small clay layer (0.1 to 0.2 meters) is identified at the location of Leg 1. This clay layer is not expected to provide a full seal around the bucket.

The entire procedure described in Chapter 4 has been applied to develop the design soil profiles of all four CPT locations. Soil units where identified, matched and a vertical random field model was created for each location. Probability density functions for permeability, friction angle and soil unit weight are attributed to each identified layer. The clay layer which should be present at leg 1 (according to the geophysical survey) is not observed in the data at hand and therefore not present in this analysis.

1.3 Reduced qualitative reliability analysis
It is not possible to use the full fault and event tree for the quantitative reliability analysis because of two reasons. First of all some of the events cannot occur due to the site conditions. Second of all some design methods lack the accuracy for implementation in a direct reliability analysis.

Several observations can still be made regarding the example location. Boulders were not observed during geophysical survey campaigns. Besides that no gravel or organic soils are present near the bucket locations. Therefore preferential flow is not expected. Seabed scour is not likely to occur since a filter layer is applied before the start of installation. The presence of only one very small clay layer eliminates the probability of occurrence of soil plug lift as well. Although there could be a risk of punch through after penetration of the filter layer the jacket needs to stay attached to the installation vessel during the first meters of installation.

The determination of the soil suction limit is performed according to the simplified procedure based on the exit gradient described in Section 5.3. As mentioned in Chapter 5 it is expected that cavitation and buckling will possibly provide stricter limits than the soil conditions (Ibsen and Thilsted, 2010). It is therefore essential to incorporate both phenomena in the analysis if a realistic failure probability needs to be obtained. All of the above leads to the reduced fault tree displayed in Figure 6.9.
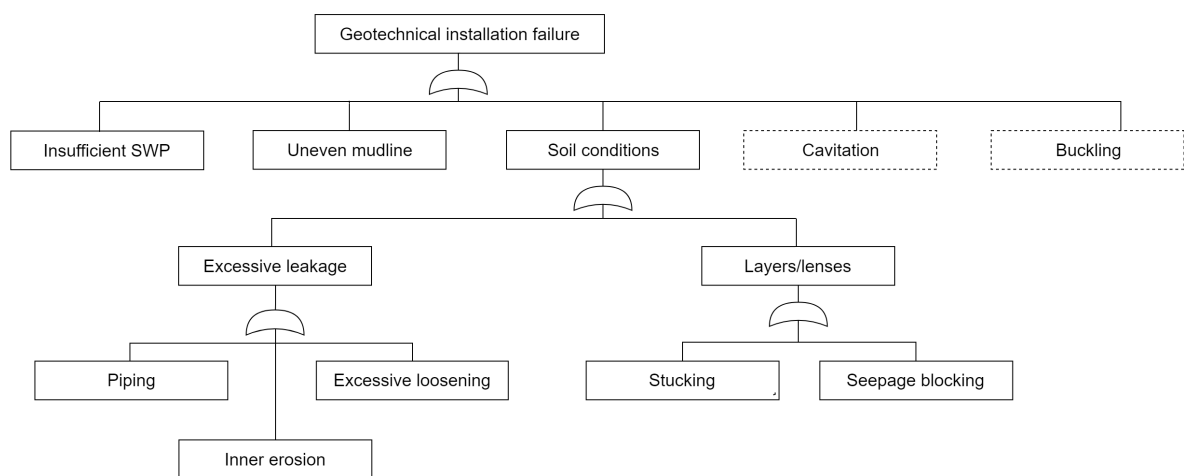

Figure 6.9: Reduced fault tree for reliability analysis at the example location

Most of the events in the event tree consider lifting operations. These fall outside of the scope of this research. Some other effects (e.g cyclic pumping, jetting and jacking) do not have proper design methods which can describe them. Only two elements of the event tree will be considered in this analysis. The first is the application of ballast at insufficient self-weight penetration. The second is the application of back-filling after refusal below target depth. When either of them occurs the size of the contingency measure can be quantified. This can provide insight on the required material on board during installation.

2. Deterministic computation
A deterministic computation will be performed before starting any direct reliability analysis. The original cone resistance profiles are used in this analysis. Expected values with a probability of exceedance of 0.5 are used for each of the other parameters.

2.1 Applied and critical suction
Limit suction is computed according to the methods described in Section 2.5. The exit gradient provides the strictest limit for all three legs. Structural limitations are the second ones governing. Cavitation does not seem to play a dominant role at this location. It is believed that current formulations for the soil suction limit are too conservative since several phenomena are not included (Section 2.5 & 5.3).

Applied suction profiles are available for all three buckets. The applied suction never exceeds the limit suction in the deterministic analysis. In the coming two sections the theoretical minimal required suction is computed. Caution must be exercised while comparing the minimum required suction to the applied suction in practice. Since installation was completed without any problems it is expected that higher underpressures were applied than strictly necessary.

2.2 Houlsby & Byrne method

Figure 6.10 shows the result of the output computation using only expected values. Computed required suction is systematically below the applied suction. This is especially the case for leg 2. The profiles for leg 1 and leg 3 tend to move towards the line of measured suction for larger penetration depths. The self-weight penetration is almost half a meter off with respect to the measured data. This is significant when one considers the target depth of X.X meter. An overestimate of self-weight penetration is unconservative.

Figure 6.10: Results of deterministic installation design computation at the example location using the Houlsby & Byrne method

2.3 CPT-based design

Figure 6.11 shows the deterministic result of the CPT-based method. It is visible that the self-weight penetration estimates show little error. Furthermore one can see that the required suction profile varies significantly over depth. This is due to the direct influence of the cone resistance profile (q_t) on the end-bearing capacity. Although variation is present the average required suction seems to correspond to the applied one.
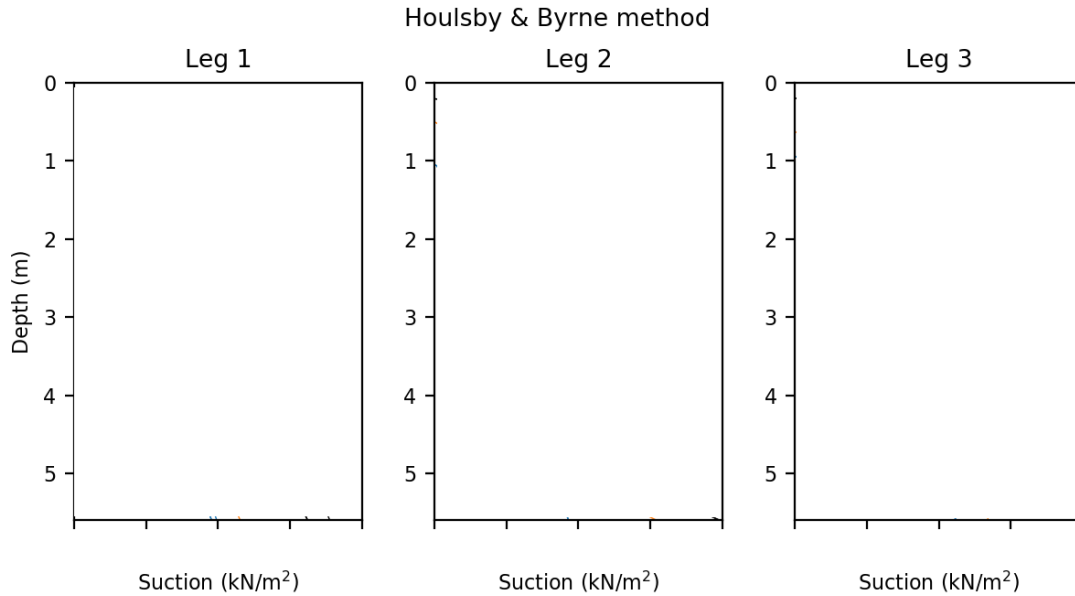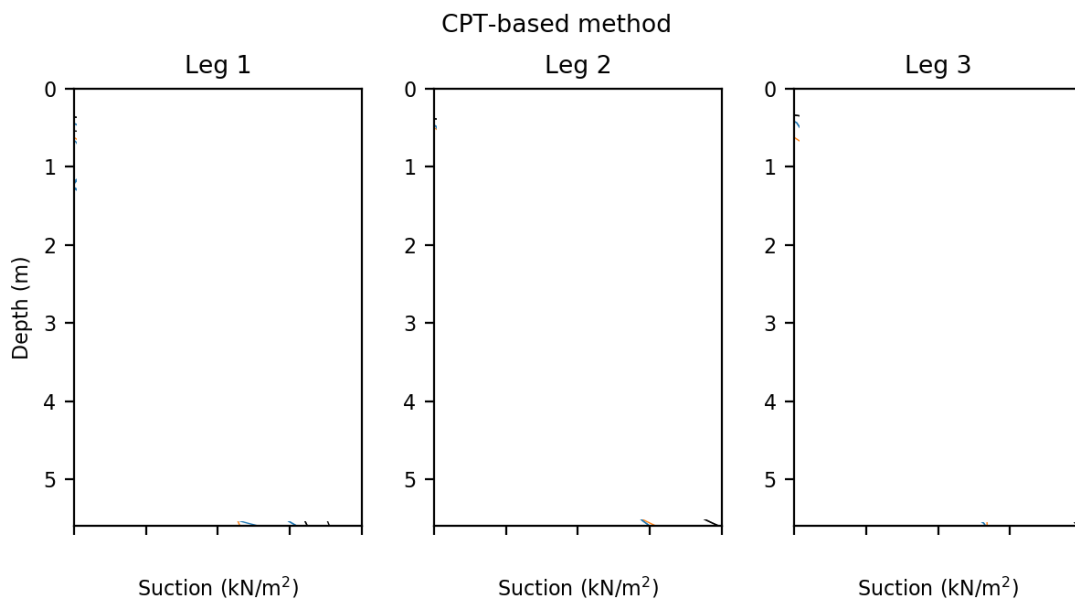

Figure 6.11: Results of deterministic installation design computation at the example location using the CPT-based method

3. Direct reliability analysis

Initially a Monte-Carlo analysis (N = 10000) is performed for all locations. These results are used to perform three analyses. First the possible variation in required suction profiles is assessed. Secondly the probability of different failure mechanisms is assessed and the fault tree is evaluated. Finally it is investigated whether it is possible to apply contingency measures in some of the failure scenarios.

3.1 Required underpressure

For each penetration depth an empirical cumulative density function was made of all underpressure values simulated. The 95% reliability interval can be extracted from this distribution. Several peculiarities can be spotted when one examines the outcome of this analysis for the Houlsby & Byrne method. First one can see that the method does not perform well at shallow depths. The measured self-weight penetration cannot be estimated by the Houlsby & Byrne method. Furthermore it is visible that the measured underpressure only starts to fall inside the reliability interval after penetration depths of approximately three meter.

Figure 6.12: Median suction profiles including their 95% reliability interval computed with the Houlsby & Byrne method

The CPT-based method provides better reliability intervals than the Houlsby & Byrne method. It is visible that the applied suction falls inside this reliability interval throughout the entire installation. It accurately estimates self-weight penetration although it has a very low lower bound. Figure 6.13 also presents a suction correction applied to the reliability interval. The suction correction is applied to make sure that underpressure is never reduced when below the critical suction. It is also gives a more reliable image since fast fluctuations corresponding to a cone resistance profile are not feasible and expected in practice.
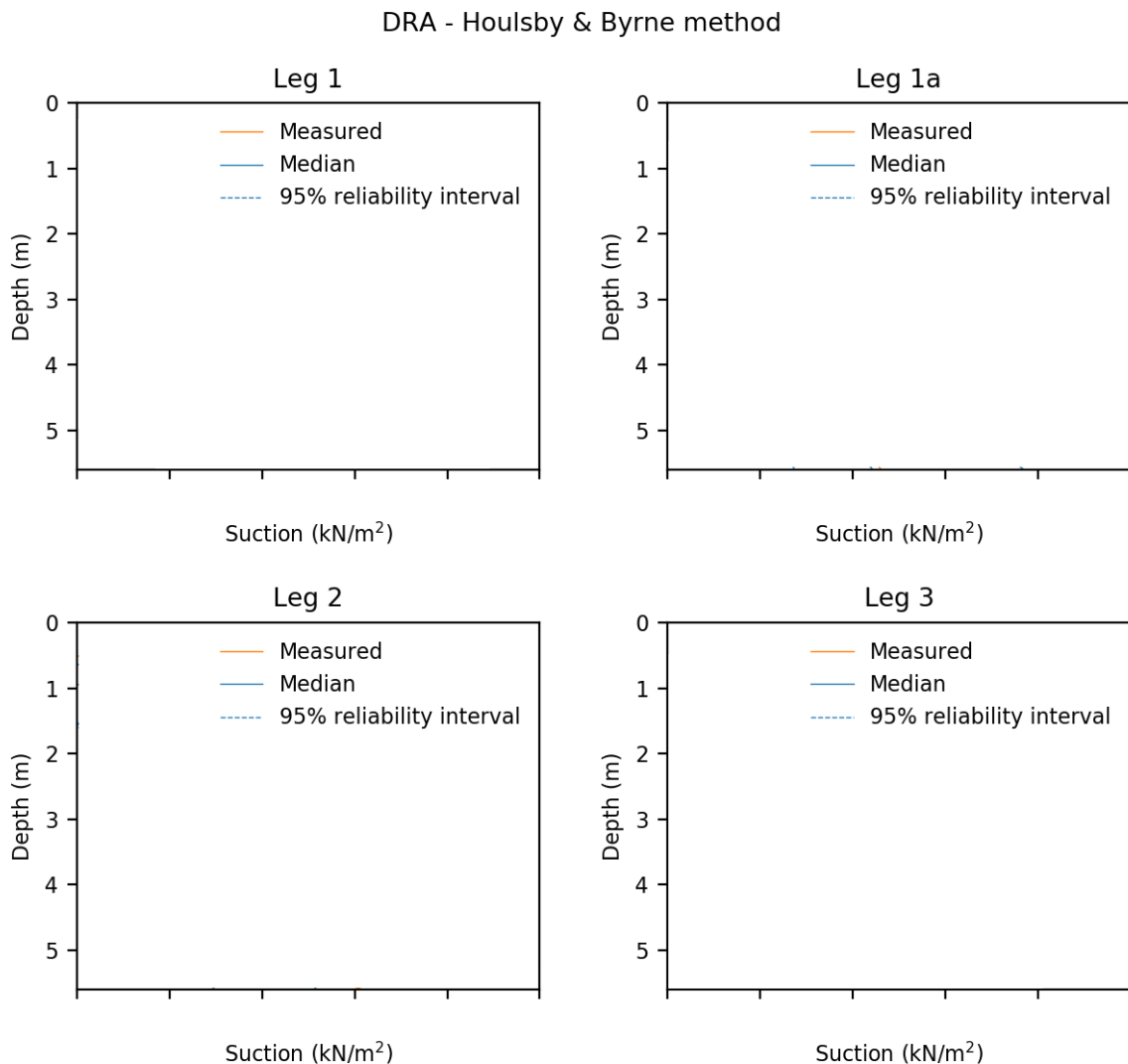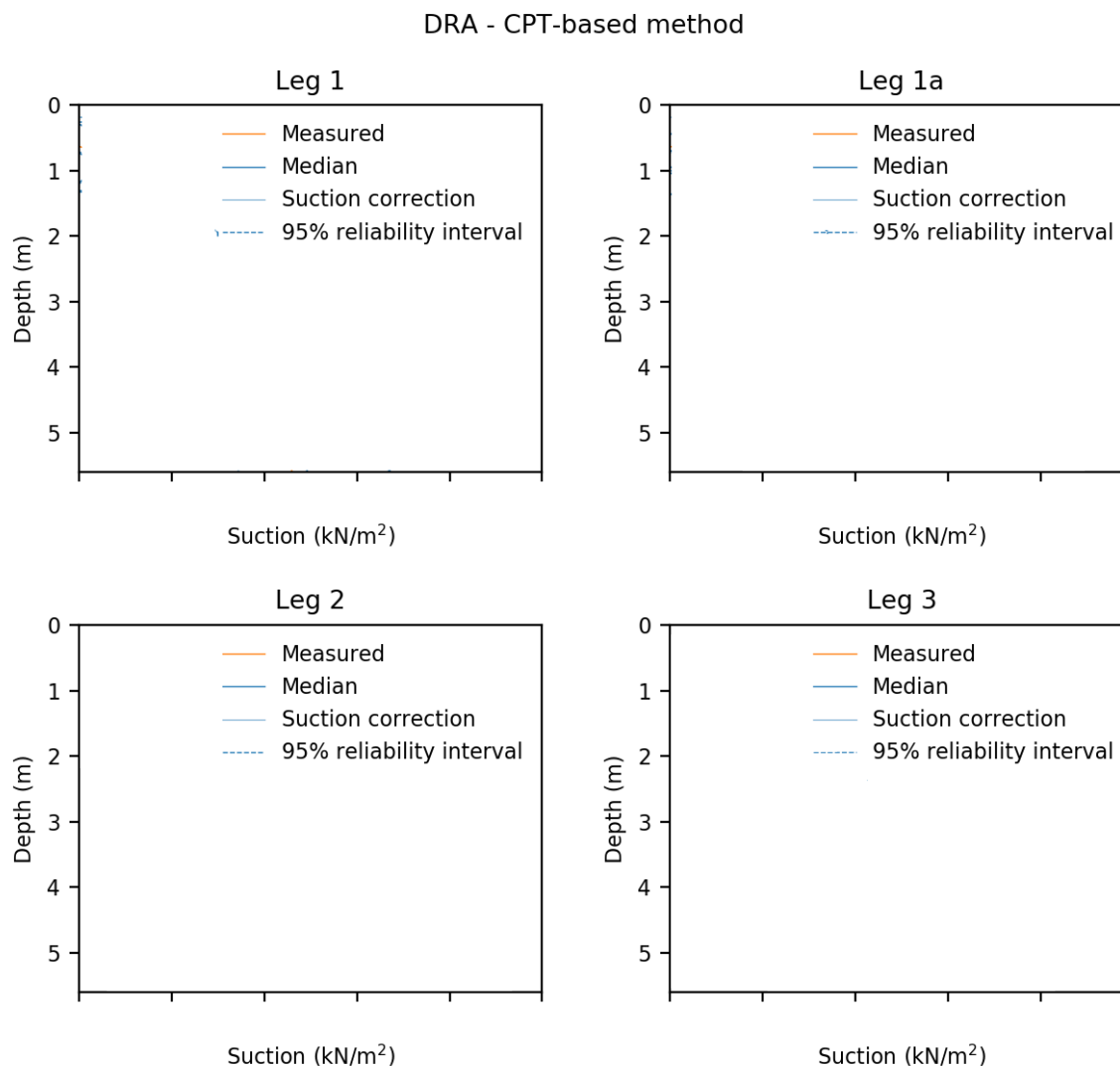
Figure 6.13: Median suction profiles including their 95% reliability interval computed with the CPT-based method

It is visible that both the required suction profiles for all four legs correspond to each other for both of the models used. This implies that large influences due to soil profile differences are not expected. It also shows that exceeding tilt requirements during installation or at target penetration depth is not plausible. Since no coupled installation analysis of all buckets is performed this requirement is not further investigated.

3.2 Insufficient self-weight penetration
Table 6.1 shows that the Houlsby & Byrne method never fails for self-weight penetration. The outcome confirms the observation based on the 95% reliability intervals (Figure 6.12). The reason for this overestimation lies in the formulation of the end-bearing resistance. The vertical effective stress (σ'_v) plays a major role in the estimate of the end-bearing value (R_b). As a consequence of the small vertical effective stress at lower depths this resistance component will be small too.

$$R_b = (\sigma_v N_q + \gamma' \frac{t}{2} N_\gamma) \pi D t \tag{6.10}$$

While deterministic estimates of self-weight penetration performed with CPT-based design were accurate the probability of occurrence of insufficient penetration depths is high. The reason that the CPT-based method simulates more instances of insufficient self-weight penetration can be attributed to high cone resistances at lower depths. Random field modelling intensifies this effect since high cone resistances can be simulated at zero penetration. This is caused by two aspects:

1. The trendline of the first layer does not necessarily start at zero cone resistance.

2. The variation simulated is not dependent on location since using autocorrelation models eliminates this. This allows for simulating a high cone resistance value directly at the start of penetration.

Table 6.1: Probability of occurrence of insufficient self-weight penetration for both methods and all legs

Location	Leg 1	Leg 1a	Leg 2	Leg 3
Houlsby & Byrne	0	0	0	0
CPT-based	0.3063	0.7649	0.7184	0.5674

Later the possibility of applying ballast weights to enlarge the self-weight penetration depth will be assessed. This will greatly reduce the failure probabilities in CPT-based design. To improve the estimate of CPT-based design one can attempt random field modelling with a fixed trendline through the intersection of the axes.

3.3 Soil failure
Limitations due to the maximum exit gradient criterion are governing the installation feasibility assessment. Failure probabilities for both the CPT-based and the Houlsby & Byrne method are high. Especially the CPT-based design method computes many failure scenarios. This is due to the fact that peaks can be present in the required suction profile due to the generation of high end-bearing resistance based on peaks in the cone resistance profile. In research it is doubted that soil limitations provide such strict limits and it is believed that these are too conservative. In design practice these limitations are not even taken into account.

Table 6.2: Probability of occurrence of soil failure for both methods and all legs

Location	Leg 1	Leg 1a	Leg 2	Leg 3
Houlsby & Byrne	0.2434	0.2882	0.2748	0.1636
CPT-based	0.3952	0.5414	0.4940	0.542

3.4 Buckling
Buckling is one of the most dominant failure mechanisms. In practice two buckling scenarios are defined: a flow and partial flow scenario. Partial flow scenarios are only present when a low permeable layer is present above a high permeable layer. Section 6.4 will show that these scenarios will be governing for high required underpressures. Since detailed structural studies are not part of the scope of this research it was infeasible to make a distinction between both scenarios for this analysis.

Table 6.3: Probability of occurrence of buckling for both methods and all legs

Location	Scenario	Leg 1	Leg 1a	Leg 2	Leg 3
Houlsby & Byrne	Flow	0.2046	0.1574	0.3466	0.1028
	Partial flow	0.0100	0.0030	0.0538	0.0004
CPT-based	Flow	0.0854	0.3670	0.3144	0.3758
	Partial flow	0.0	0.0002	0.0	0.0

3.5 Cavitation
Cavitation limits never govern installation. Table 6.4 presents the failure probability due to the mechanism of cavitation. These scenarios will always be preceded by buckling failure and are therefore non existent.

Table 6.4: Probability of occurrence of cavitation for both methods and all legs

Location	Leg 1	Leg 1a	Leg 2	Leg 3
Houlsby & Byrne	0.0034	0.0006	0.0330	0
CPT-based	0	0.0001	0	0

3.6 Application of ballast

Ballast weights can be applied in blocks of 200 tons up to 600 tons. All simulations of the direct reliability analysis are checked on whether their self-weight penetration is insufficient (d_{swp} <0.5 m). If this is the case the amount of ballast required to penetrate the suction bucket jacket up to the minimum depth is checked. If the ballast required exceeds 600 tons the installation is deemed unsuccessful. Figure 6.14 shows the output of the computation for one bucket location. In practice it will be attempted to start pumping first. If a stable underpressure is reached successfully there is no need to apply ballast.
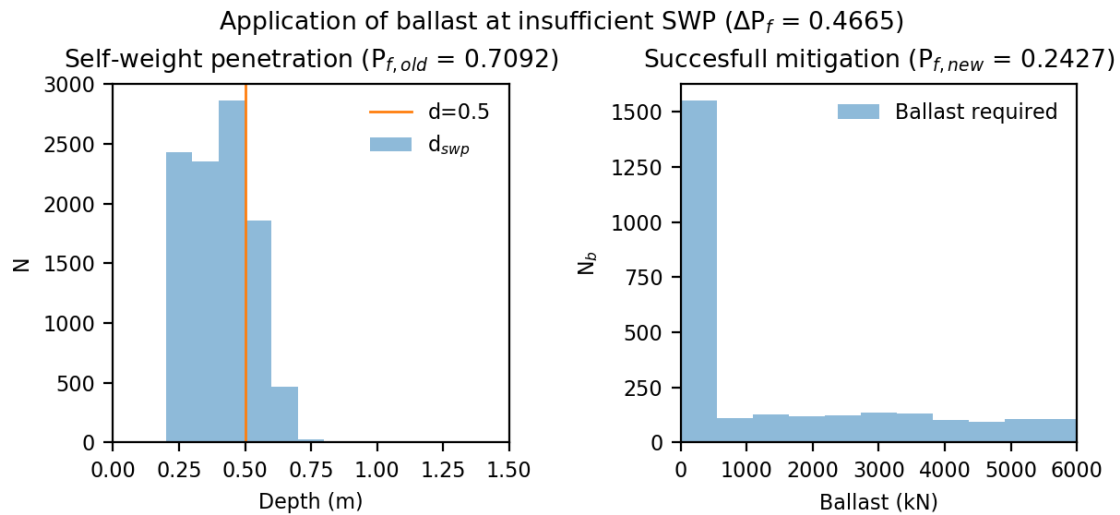
Figure 6.14: Ballast application for leg 1 of the case study example when applying the CPT-based design method

3.7 Application of backfill material

Backfill material can be used to fill empty spaces left. These empty spaces can occur due to two reasons. The first is seabed differences which cause empty spaces at some of the buckets. The second is refusal between target but before final penetration depth. All scenarios were analyzed to check whether backfilling could be a succesfull contingency. Figure 6.15 shows the result of this analysis. The volume of backfill material required does not include the amount which can be required to fill the empty spaces inside the filter layer.

Figure 6.15: Application of the analysis on backfill material at failure between target and maximum penetration depth

4. Conclusion

All probabilities need to be combined to quantitatively assess feasibility of suction bucket (jacket) installation:

4.1 Individual buckets

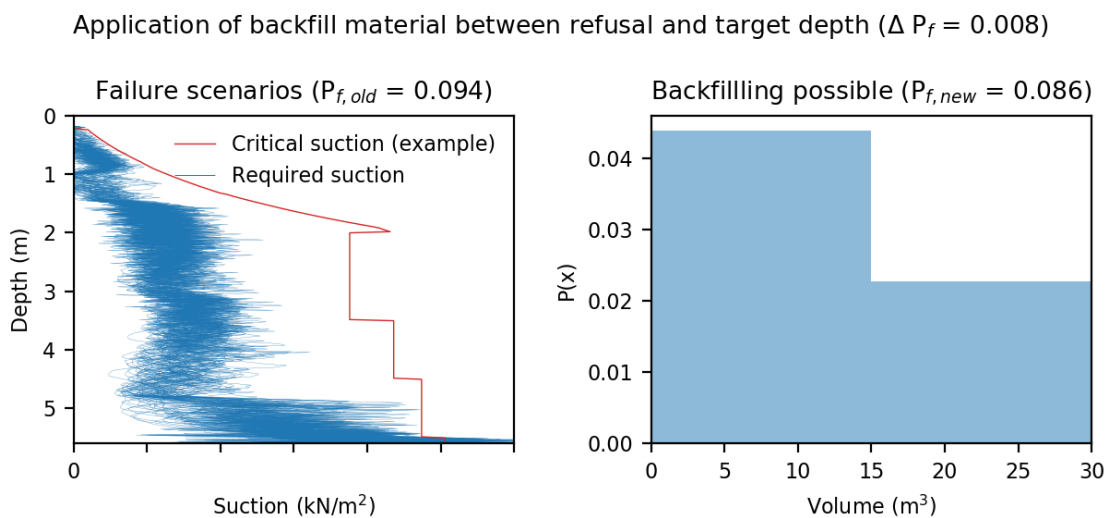Table 6.5 shows all computed failure probabilities including the effect of mitigation measures. If one examines these outcomes closely it can be seen that the sum of probabilities is unequal to the total probability. The reason for this is the fact that the failure region of some mechanisms overlap. For example, buckling limits are already exceeded if cavitation occurs. Therefore the probabilities do not simply add up.

Table 6.5: Combination of all probabilities for all design methods, legs, failure mechanisms and contingency measures

	Houlsby & Byrne				CPT-based method			
	Leg 1	*Leg 1a*	*Leg 2*	*Leg 3*	*Leg 1*	*Leg 1a*	*Leg 2*	*Leg 3*
Self-weight penetration	0	0	0	0	0.3063	0.7649	0.7184	0.5674
Ballast	0	0	0	0	-0.2642	-0.5503	-0.5478	-0.4665
Soil failure	0.2434	0.2882	0.2748	0.1636	0.3952	0.3670	0.4940	0.5420
Buckling	0.2046	0.1574	0.3466	0.1028	0.0854	0.5414	0.3144	0.3758
Cavitation	0.0034	0.0006	0.0330	0	0	0.0002	0	0
Backfilling	-0.0064	-0.0018	-0.0022	0	-0.0032	-0.0044	-0.006	-0.0002
$\mathbf{P}_{f,swp}$:	0	0	0	0	0.0421	0.2146	0.1706	0.1009
$\mathbf{P}_{f,suc}$:	0.3674	0.3822	0.4676	0.2436	0.4294	0.6596	0.5898	0.6634

Two aspects influence the outcome of the quantitative reliability analysis and as a consequence the computed failure probability is not exact. Firstly it is expected that there is much model uncertainty embedded in both the penetration study methods and critical suction computation. Secondly not all failure mechanisms and contingencies can be quantified using existing design methods. These aspects have a large impact on the outcome failure probability (Section 3.4).

4.2 Jacket configuration

Individual bucket installation has been assessed in this research due to insufficient knowledge on horizontal variability. This computation gives insight in the failure mechanisms of individual buckets. However, it is insufficient for an objective quantitative assessment of feasibility of installation of the jacket configuration.

A system reliability analysis is normally suitable for combining multiple individual limit states. Probabilities of failure can easily be computed if the elements are mutually exclusive or completely dependent (Jonkman et al., 2017). In these cases the elementary bounds of the failure probability lie between the maximum individual probability of failure and the sum of all failure probabilities. Unfortunately neither of these scenarios is the case for suction bucket jacket installation. The probability of failure of the jacket will lie between the elementary bounds. Methods are available which can compute narrower bounds of the failure probability of systems based on individual normally distributed limit states (Ditlevsen and Madsen, 1996).

Such a system reliability approach is problematic for suction bucket jacket installation. In each simulation during the quantitative reliability analysis the limit state value is analyzed over the entire depth. As a result the value is selected at a depth where the limit state is the closest to failure. The limit state equation was normalized with the critical suction values to perform this analysis (Section 6.1). As a consequence the limit state values from different simulations can be generated at different depths and cannot simply be compared.

If one wants to use a system reliability approach the total installation therefore needs to be abandoned for an assessment of a single failure mechanism at a single penetration depth. Figure 6.16 shows the normally distributed (non normalized) limit state values for buckling computed with the CPT-based method close to target penetration depth. Between each set of limit states the correlation coefficient can be determined. In the case of Figure 6.16 the correlation coefficients are: $\rho_{1,2} = 0.0016$, $\rho_{1,3} = 0.0173$ and $\rho_{2,3} = 0.0015$. Besides the correlation coefficient the reliability index (β), a measure for proximity to failure, is required.

$$\rho_{i,j} = \frac{\text{COV}(Z_i, Z_j)}{\sigma(Z_i)\sigma(Z_j)} \qquad , \qquad \beta_i = \frac{0 - \mu(Z_i)}{\sigma(Z_i)} \tag{6.11}$$
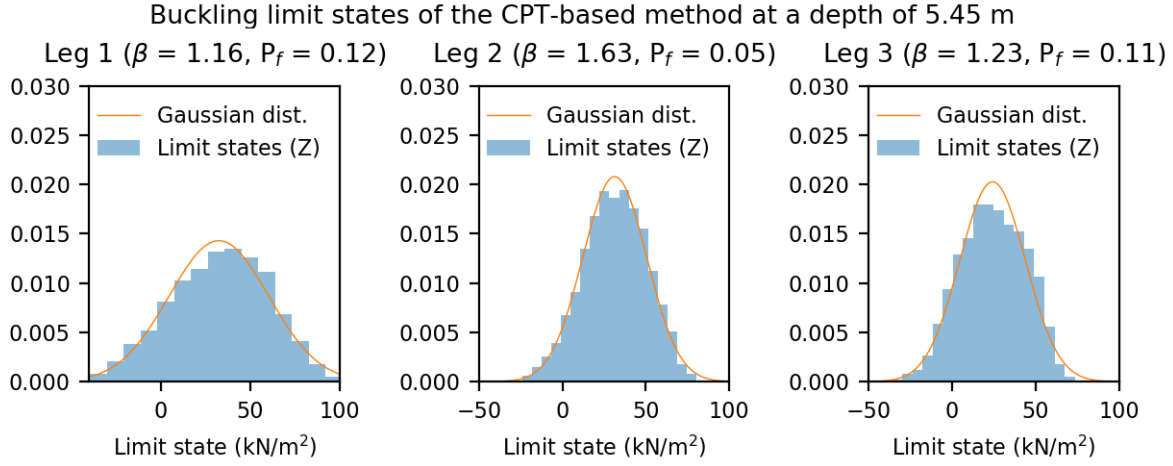
Figure 6.16: Distribution of limit state values simulated near target penetration depth for all buckets with failure mechanism of buckling

Figure 6.17 shows Venn diagrams displaying the principles of Ditlevsen bounds. It starts with the failure probability of one bucket ($P_{f,1}$). Afterwards the limit state domain of a second bucket is added ($P_{f,2}$). Using the correlation coefficient ($\rho_{1,2}$) the overlap between both failure domains can be computed ($P_{f,1\cap2}$). This is subtracted from the sum to obtain the total failure probability. If another bucket is added ($P_{f,3}$) overlap can occur between its domain and that of bucket one, two or even both. By subtracting the largest individual overlapping area (in this case: $P_{f,2\cap3}$) the error of ignoring the overlapping area of all three domains is minimized. The minmium and maximum values can be found if all three combinations of this analysis are performed (Jonkman et al., 2017).

(a) Failure probability leg 1   (b) Combination of leg 1 and 2   (c) Ditlevsen bound for leg 1, 2 and 3
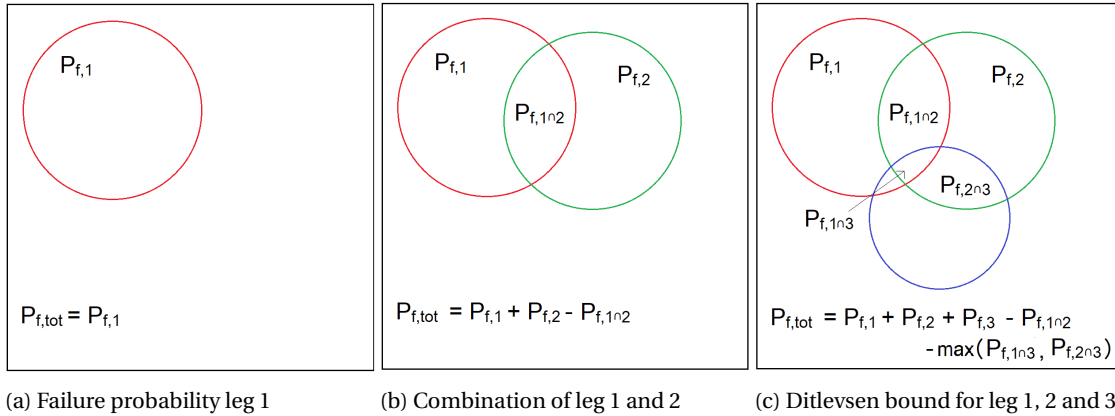
Figure 6.17: Venn diagram of system reliability principles used for the development of the Ditlevsen bounds

Computing the overlapping areas between each of the failure domains can be done with Equation 6.12 and 6.13. The elementary bounds of the failure probability due to buckling at a depth of ≈ 5.5 meters lie between 0.1226 and 0.2828. By application of the Ditlevsen bounds method these are narrowed down to 0.2319 and 0.2637. This is a significant decrease of uncertainty although the upper bound hardly decreases.

$$\max(\Phi(-\beta_1)\Phi(-\beta_2^*), \Phi(-\beta_1^*)\Phi(-\beta_2)) \leq P(F_1 \cap F_2) \leq \Phi(-\beta_1)\Phi(-\beta_2^*) + \Phi(-\beta_1^*)\Phi(-\beta_2) \tag{6.12}$$

$$\beta_1* = \frac{\beta_1 - \rho_{1,2}\beta_2}{\sqrt{1 - \rho_{1,2}^2)}} \quad , \quad \beta_2* = \frac{\beta_2 - \rho_{1,2}\beta_1}{\sqrt{1 - \rho_{1,2}^2)}} \tag{6.13}$$

It is plausible that probability bounds of individual failure mechanisms at separate depths can be computed for the entire jacket configuration. Unfortunately this does not give proper insight in installation feasibility as a whole. Since failure can occur at any depth it does not make sense to perform this computation for separate depths.

6.4. Sensitivity studies

A quantitative reliability analysis can provide more insights than just the failure probability and reliability intervals of the design output. In this Section the origin of uncertainties are examined via several sensitivity analyses. These analyses can lead to findings regarding model applicability as well as insight in the governing parameters of installation design. Three aspects are analyzed:

1. Background of failure scenarios computed in the direct reliability analysis.

2. Sensitivity of the design output to parameter estimation and variability.

3. Efficiency and application of the Markov Chain Monte Carlo simulation method.

1. Background failure scenarios

For each location all the design profiles at failure scenarios (Z<0) were plotted in a histogram with respect to the probability density function they are sampled from. Again the Houlsby & Byrne as well as the CPT-based method are examined.

1.1 Houlsby & Byrne method

Figure 6.18 shows the results of one of these analyses for the Houlsby & Byrne method. It is visible that failure is likely to be caused by low permeability layers. This failure mechanism is called seepage blocking (Chapter 3). If this is combined with high friction angles and higher permeabilities in lower layers the soil resistance is increased even further and failure is more likely. These phenomena are visible in Figure 6.18.
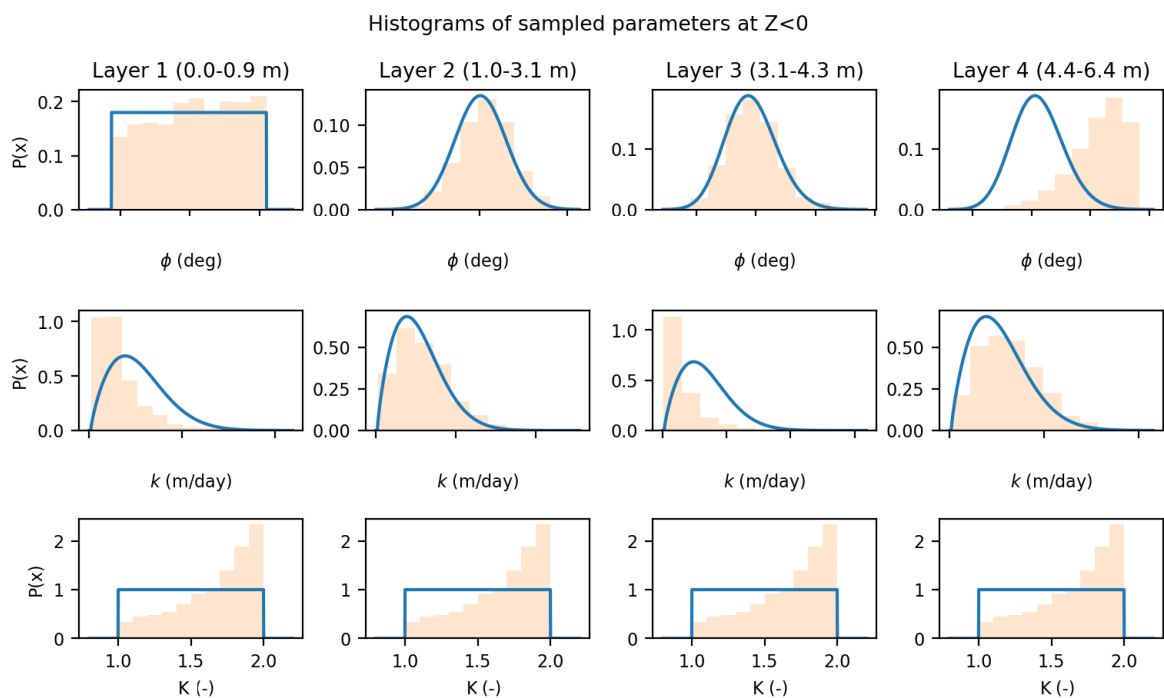
Figure 6.18: Parameter values observed in different layers during failure scenarios of the Houlsby & Byrne method

The soil unit weight variation is of little importance for the output of the Houlsby & Byrne computation. Contrary to the soil unit weight a proper estimate of the stress ratio is essential in non-cohesive soils. Many failure scenarios are located between stress ratios of 1.5 to 2.

These results can be used to improve the setup of future site investigations. Failure is most likely to occur at higher penetration depths. Therefore knowledge of permeability as well as the friction angle at intermediate depths is important. The stress ratio (K) seems to be the most important parameter to estimate correctly. This is very difficult in sandy soils (Section 4.2). This makes the impact of the uncertainty on installation design with the Houlsby & Byrne method large.

1.2 CPT-based method

Figure 6.19 shows the sensitivity of the CPT-based method to the variation of the internal friction angle and the permeability of different layers. Again low permeability layers over layers with a high friction angle are governing the failure domain. The friction angle remains important when enhanced stresses are used to compute the resistance reduction due to applied underpressures. If stress enhancement is ignored both the stress ratio as well as the friction angle become unnecessary for application of the CPT-based method. However, it was noticed that this leads to lesser correspondence to measured underpressures.
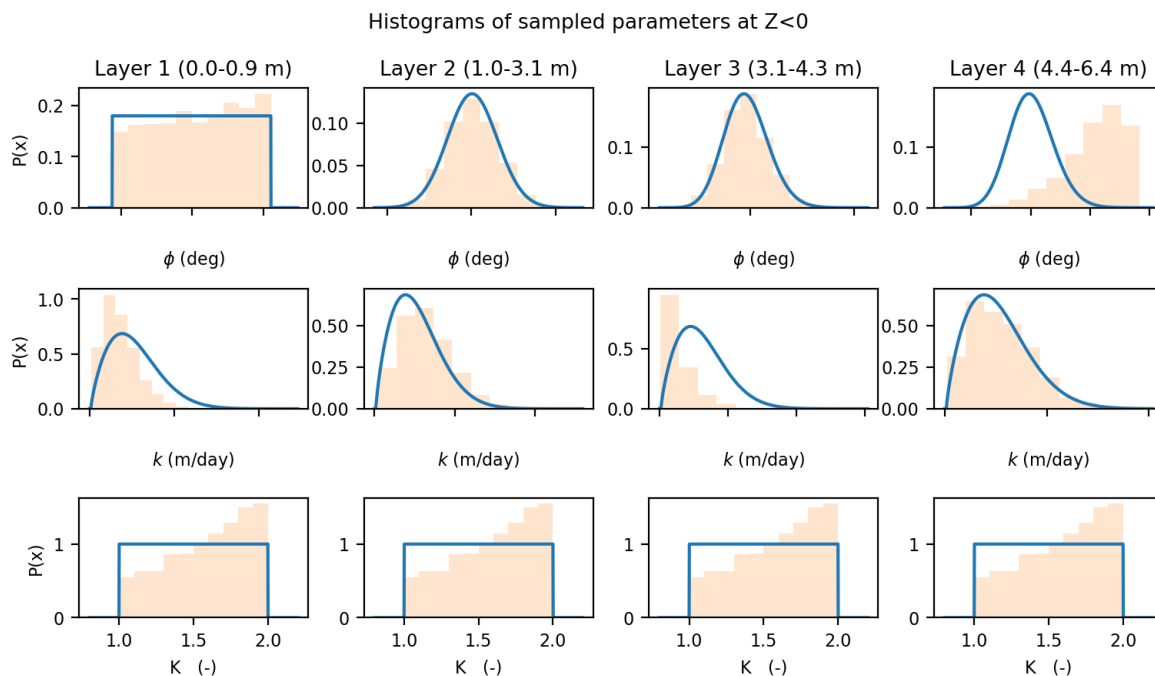
Histograms of sampled parameters at Z<0

Figure 6.19: Parameter values observed in different layers during failure scenarios of the CPT-based method

1.3 Soil suction limit

The results of the quantitative reliability analysis show relatively large failure probabilities of exceeding the soil suction limit. Especially the application of the CPT-based method results in high failure probabilities (Table 6.5). A sensitivity analysis was performed on the background of all soil failure scenarios to investigate the origin of these high failure probabilities. Figure 6.20 shows all failures scenarios of the CPT-based method for leg 1 of the case study example. It is visible that some parameter combinations cause very low soil suction limits over depth. Two reasons are believed to contribute to this:

1. Failure always occurs for low permeabilities simulated in the top layer. This is logical when one examines the background of the soil suction limit in Equation 6.14. If higher pumping speeds need to be applied to create sufficient underpressure while the permeability of a layer is low, the change of head increases. The change of hydraulic head in the top layer is the criterion used for the suction limit profile. Therefore these situations cause low soil suction limits.

$$q = k\frac{dh}{ds} \quad , \text{if } q \uparrow \text{ and } k \downarrow \text{ then } \frac{dh}{ds} \uparrow \tag{6.14}$$

2. The cone resistance values simulated in the top layers can be high due to a large mean cone resistance in layer two and three. As a result the end-bearing resistance significantly increases. As a consequence the required suction and therefore the failure probability increases.

In practice soil suction limits are not incorporated in the design assessment. Only buckling and cavitation limits are included. It is expected that this has to do with the unreliability of the soil suction limit formulation. In Section 5.3 it was adressed that incorporating plug loosening should improve the current approach. However, due to the wide range of profiles after applying permeability variation the method still seems unusable.
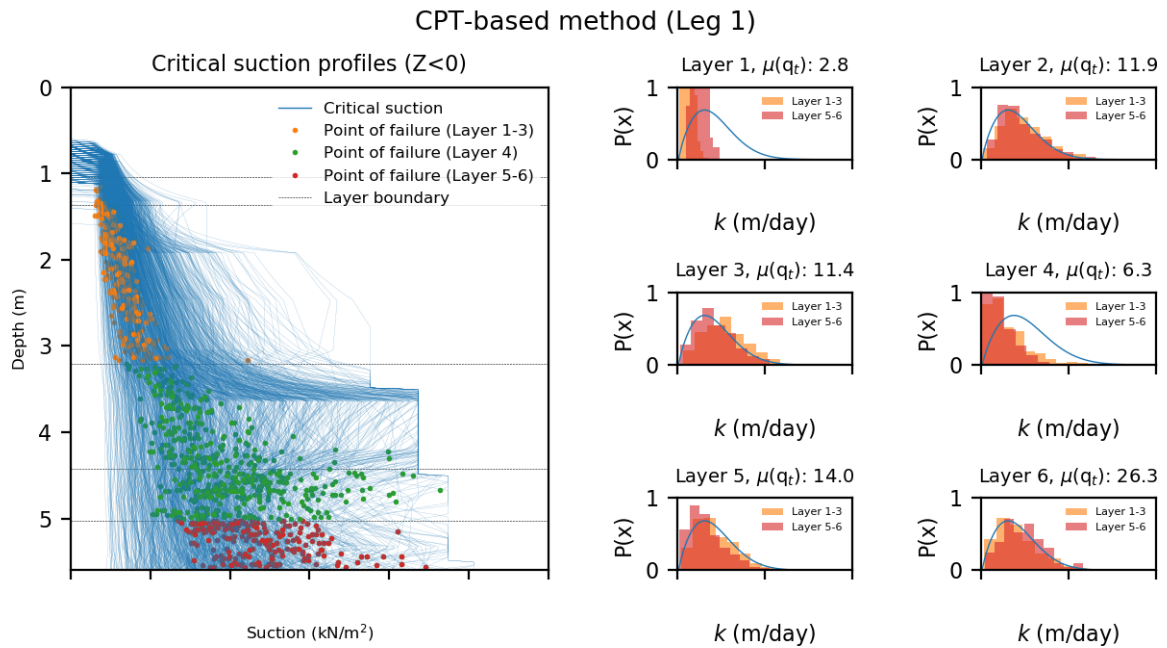
Figure 6.20: Critical suction failure scenarios, points of failure and histograms if soil limitations are governing for CPT-based design

It is believed that the profiles with low soil suction limits in Figure 6.20 are unrealistic for multiple reasons. Firstly there is the fact that the exit gradient is not a failure mechanism on its own. Before the failure mechanism of excessive leakage occurs either piping, much inner erosion or excessive loosening has to occur. Theoretically the exceedance of the exit gradient only indicates the start of inner erosion. Therefore it is believed that much resilience is left and the current approach is much too conservative for proper application.

2. Sensitivity of design output to parameter variability
The influence of variability on the design output was examined for four parameters: permeability (k), internal friction angle (ϕ), stress ratio (K) and the end-bearing empirical coefficient (k_p). Please note that the soil suction limit can differ between the liquefaction and exit gradient limit throughout these analyses.

2.1 Influence of permeability variation (k)
Incorporation of a seepage analysis is required for proper functioning of the models in layered soils. In current practice the seepage analysis is performed only once, with fixed permeabilities. In this analysis the effect of varying permeability is examined. If this is proves to be negligible it would have two consequences. First the elimination of variability estimates can be achieved. Secondly the finite element model only has to be executed once per direct reliability analysis. This would drastically reduce runtime.
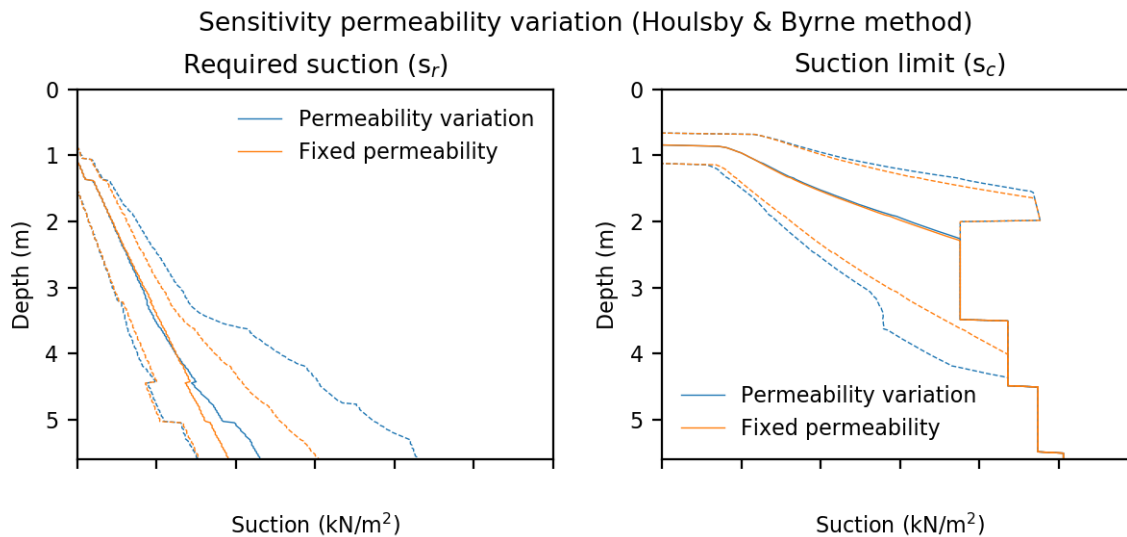
Figure 6.21: Influence of permeability variation on the output of the Houlsby & Byrne method applied on leg 1 of the example location

Large influence on the Houlsby & Byrne method can be observed in Figure 6.21. This is mainly due to the effect of suction on the inner skirt resistance. Paragraph 1 already showed the high influence of the stress ratio and friction angle. If these are combined with low permeabilities required suction becomes high. These scenarios cannot occur when fixed permeabilities are applied. Hence failure mechanisms like stucking or seepage blocking will never be simulated and can therefore not be taken into account.
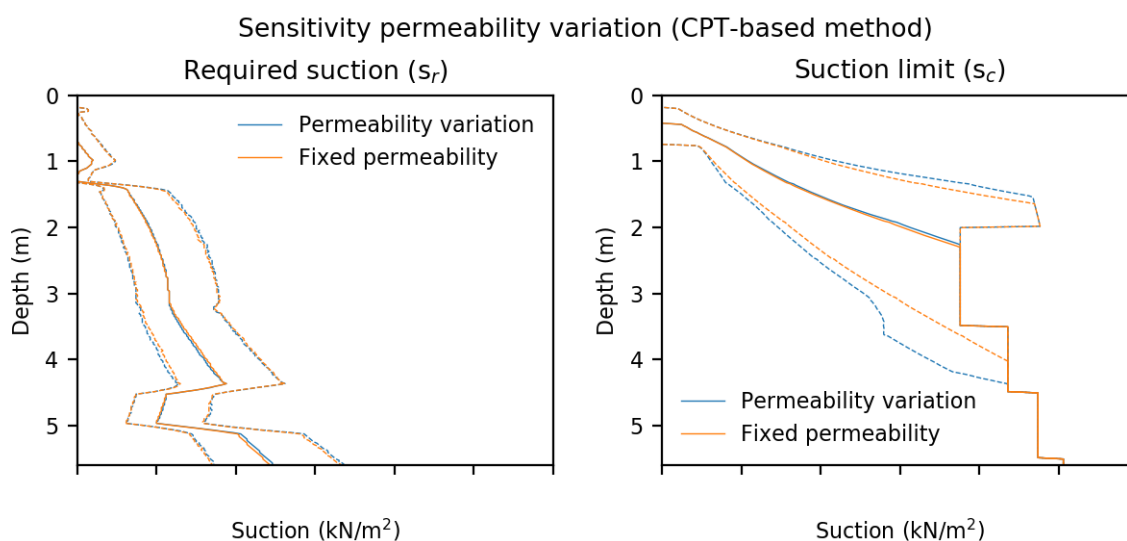

Figure 6.22: Influence of permeability variation on output of the CPT-based design method applied on leg 1 of the example location

The CPT-based profiles are not affected that much by permeability variation (Figure 6.22). This is due to the fact that the contribution of skirt friction to the total resistance is relatively low with respect to that of the end-bearing capacity. Nevertheless permeability variation remains essential for estimating failure scenarios like stucking and seepage blocking. Especially when different soil types are present (e.g. gravel or clay) incorporating possible permeability variation can provide essential information on installation feasibility.

Figure 6.21 and 6.22 show the influence of permeability variation on the liquefaction limit as well. Especially the lower limit increases due to the fact that the influence of underpressure does not vary anymore. Permeability variation has a significant influence on the suction limit when one computes this based on the exit gradient (Figure 6.20). This is expected since permeability and unit weight serve as the only input for this computation. Elaboration on these effects was presented in Paragraph 1 of this Section.

2.2 Influence of internal friction angle variability (ϕ)
Figure 6.23 shows the median and 95 % reliability interval of the required suction for a direct reliability analysis with expected friction angles and quantified distributions described in Section 4.5. It is noticeable that the influence on the outcome of the Houlsby & Byrne method is small. Effects on critical suction are minimal too. This implies that most of the variation in the Houlsby & Byrne method can be attributed to the estimate of the stress ratio (K). This is discussed in the paragraph 2.3.
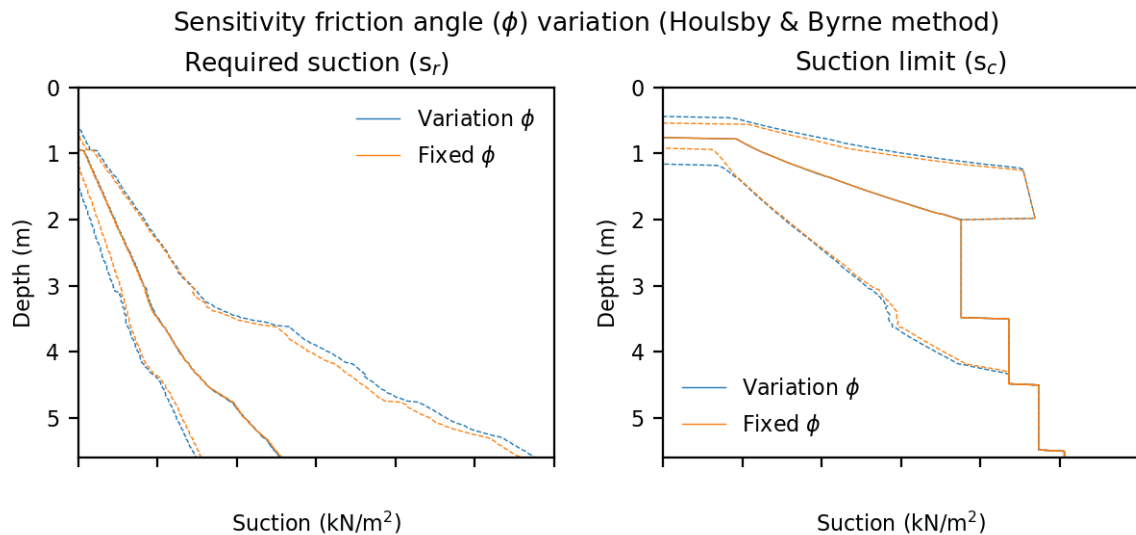
Figure 6.23: Sensitivity of the Houlsby & Byrne method to the variability of the internal friction angle (ϕ)

The influence of variability of the internal friction angle on the CPT-based method is minimal. When enhanced stresses are used to estimate the skirt friction and end-bearing resistance reduction they do serve as an input. However, variability of the stress ratio (K) is even more important in these cases. If stress enhancement is not incorporated the internal friction angle is irrelevant in the CPT-based method.

The friction angles are estimated based on the correlation with the cone resistance profiles and estimated relative density in this research. It is expected that triaxial tests nearby the installation location could improve the accuracy of the esimate. These type of site investigations are unrealistic for each and every location since associated costs will be high. The CPT-based method requires less parameters which seems beneficial for cost efficient design.

2.3 Effect of stress ratio (K) estimate and variability

The stress ratio estimate is of major influence on the output of the Houlsby & Byrne method. Almost all failure scenarios are caused by a high stress ratio estimate. Approximately 1000 scenarios with low ($K < 1.1$) and high ($K > 1.9$) stress ratios can be extracted from the output of one Monte-Carlo analysis. Figure 6.24 shows the median suction profiles for these groups. The exit gradient suction limit is not affected by the stress ratio. Therefore the liquefaction limit is incorporated as the soil suction limit in this analysis.
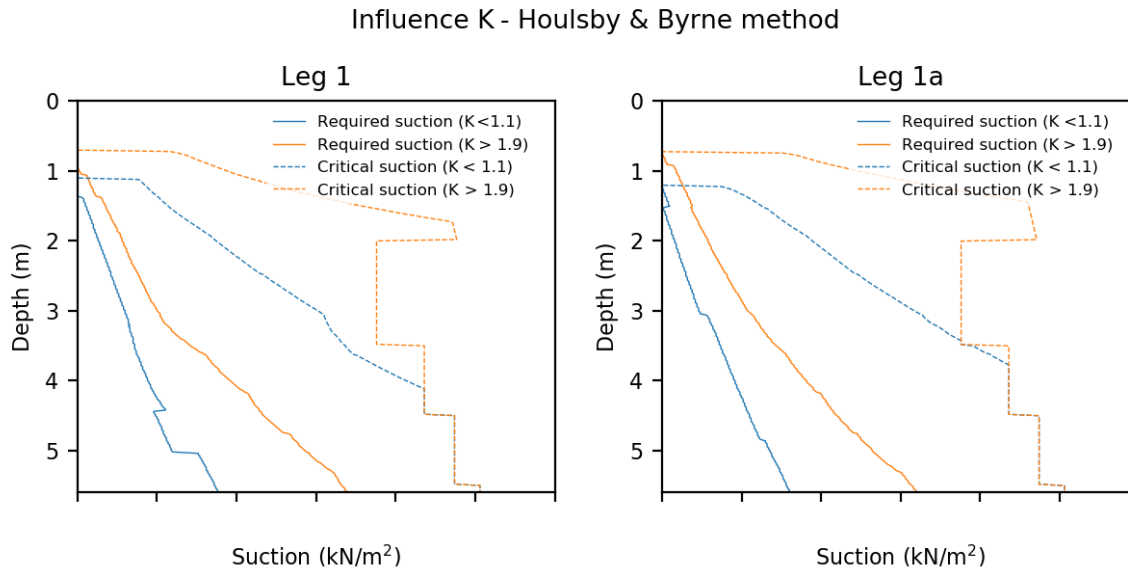

Figure 6.24: Sensitivity of the Houlsby & Byrne method to the stress ratio (K); median profiles for low and high estimates

Figure 6.24 shows that both the liquefaction suction limit as well as the required suction profile significantly increases for a higher stress ratio. The origin of this phenomenon lies in the formulation of stress enhancement. A higher stress ratio results in large enhanced inner stresses. This has two consequences. Firstly the liquefaction limit increases. Secondly the inner friction greatly increases. As a consequence the contribution of the inner skirt resistance becomes unrealistically high. This is especially the case for high stress ratios ($K>1.5$) and at deeper penetration depths.

A solution for unrealistic design outputs could be to use a different estimate for the computation of enhanced stresses and skirt friction. If a lower value is used for stress enhancement and a higher value is used for skirt friction compuation the problem is partially solved. However, for the case study locations this method results in insuffcient resistance and therefore an underestimation of the required suction (Figure 6.25).
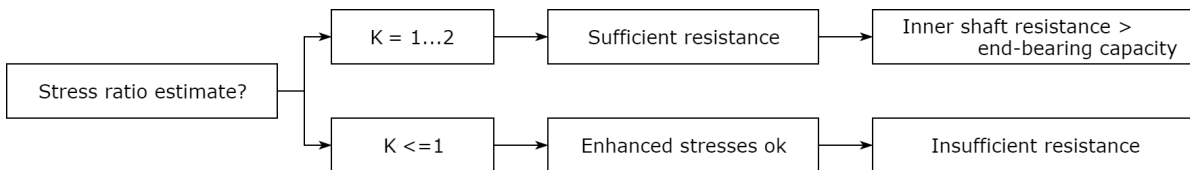

Figure 6.25: Problem with stress ratio estimate on the output of the Houlsby & Byrne method

The impact of the stress ratio estimate on the Houlsby & Byrne method (and especially on stress enhancement) is very large. When one also considers the fact that estimating this parameter in non-cohesive soils is hardly feasible the Houlsby & Byrne method seems not sufficient for application.

2.4 Effect of site specific estimate of the end-bearing empirical coefficient
The site specific estimate of the end-bearing empirical coefficient (k_p) used in CPT-based design seemed to improve the results. Previously only highest expected and most probable values were used to compute the best estimate and upper bound of the resistance profile. Figure 6.26 shows a comparison between the use of the conventional recommended values (k_p = 0.3 & 0.6) and the adapted estimate based on estimated relative density (R_D).
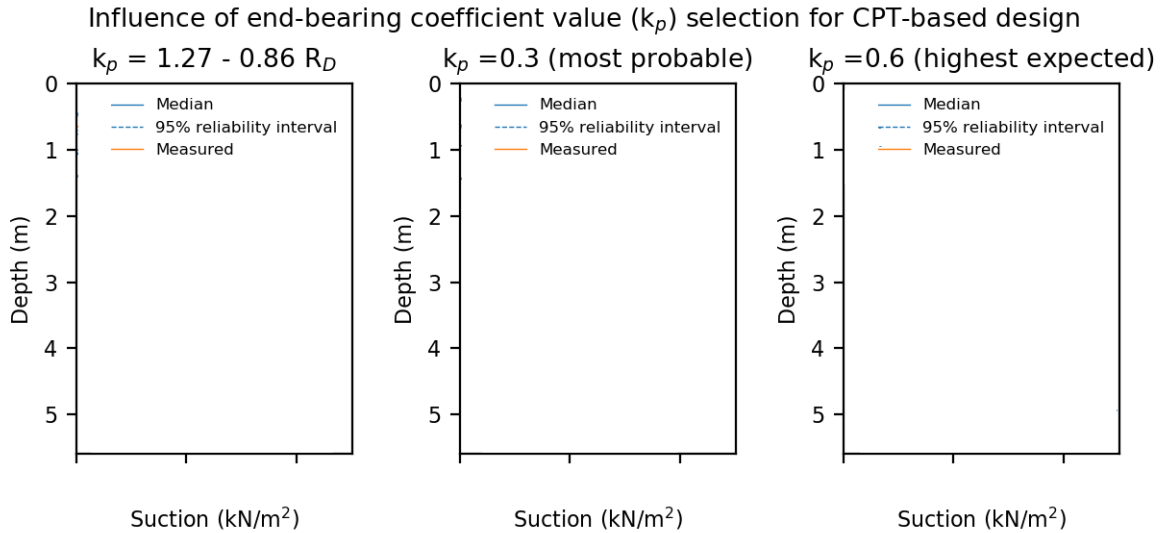
Figure 6.26: Improvement in accuracy by implementing the estimation formula for the end-bearing coefficient based on relative density

Figure 6.26 shows that the estimate of the required suction using the most probable value of the end-bearing empirical coefficient (k_p = 0.3) is inaccurate. The computed resistance is very low compared to the resistance encountered in reality. As a consequence the required suction profile is low as well. The profile corresponding to the highest expected value (k_p = 0.6) performs significantly better. However, at higher penetration depths (d>4.8) the upper bound of the reliability interval becomes very high. As a consequence the failure probability increases significantly. The results after application of the new estimation method perform best. The reliability interval corresponds well to the applied underpressures.

Using the Jamiolkowski estimation method of relative density introduces transformation uncertainties (Section 4.2). Furthermore, there seems no physical basis for application of similar empirical coefficients during self-weight and suction-assisted penetration. Therefore discussion regarding the estimation formula for the end-bearing coefficient remains (Chapter 7). Nevertheless, a consequent application of a site specific estimation approach of the empirical parameters can result in improved design accuracy (Figure 6.26).

3. Application of MCMC simulation

The application of Markov Chain Monte Carlo did not result in a significant improvement with respect to the Monte Carlo method. In this Section elaboration on this verdict is presented.

3.1 Simulations performed

The accuracy of Markov Chain Monte Carlo simulation was examined for leg 1 of the case study location. Sampling distributions were optimized for all soil parameters in all layers according to the procedure described in Section 6.2. Previously the required installation profiles could be compared to all components of the critical suction profile to determine the individual probability of each failure mechanism (e.g. buckling, cavitation, soil). However, since the limit state determines the behavior of the convergence of the MCMC method only one failure mechanism can be analyzed per simulation. Due to the unknown behavior of each limit state and the multi-dimensionality of the problem a cut-off probability of 0.5 is used. Simulations were performed for both penetration study method with respectively 1000, 500 and 200 computations per subset.

3.2 Integration of random fields

No examples of integrated random field models in MCMC simulations were found in existing literature. The input of a random field simulation is a vector of random numbers from a standard Gaussian distribution (μ=0, σ=1). The Modified Metropolis Hastings algorithm was simply applied on each of these random numbers. Figure 6.27 shows the result of one analysis of convergence towards high resistances while using this methodology. One can see that the resistance increased to over 2.4 times with respect to the original resistance over 25 simulations. Therefore integration of the random fields seems successful.
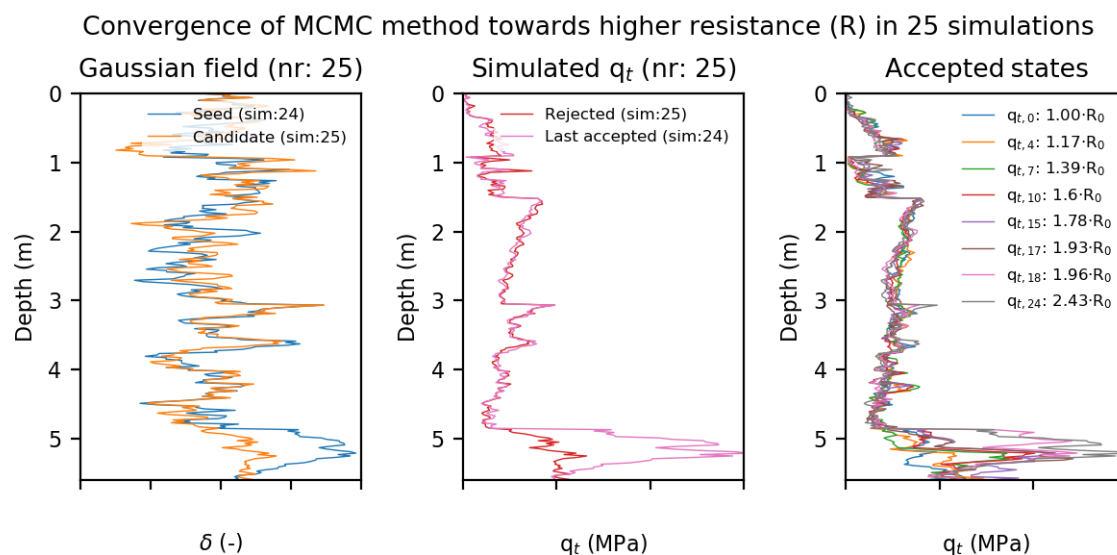
Figure 6.27: Assessment of convergence of the random field model in a Markov Chain Monte Carlo simulation for increasing resistance

3.3 Conclusion

Unfortunately the Markov Chain Monte Carlo method with subset simulation did not result in similar results as the Monte Carlo analysis. Three disadvantages were observed which lead to the conclusion that Markov Chain Monte Carlo simulation might not be an optimization with respect to a regular Monte Carlo analysis.

- Integration of the random field model remains difficult due to the many random numbers required as an input. This has slow convergence as a consequence.

- The method is not accurate when subsets of 1000 simulations are used. More simulations per subset could be a solution. However, using more would render the use of this method useless since it hardly decreases simulations with respect to regular Monte Carlo simulation in this case.

- Since the failure state differs per failure mechanisms and influences the behavior of the analysis the Markov Chain Monte Carlo should be executed once for each failure mechanism. This increases the amount of simulations with respect to regular Monte Carlo simulation.

<div align="right">

7

</div>

Findings, discussion & recommendations

This research aimed to contribute to two different developments: the installation design methods of suction bucket jackets and the application of reliability-based design methods in offshore geotechnical engineering. Findings, discussion and recommendations regarding both topics are presented in this Chapter.

7.1. Research conclusion

A full reliability-based analysis was performed to determine the impact of geotechnical uncertainties on installation design of suction bucket jackets for offshore wind.

Two geotechnical installation design methods are suitable for application in this study: the Houlsby & Byrne and the CPT-based method. Both original methods cannot cope well with layered soils of varying permeability. Two improvements are required to eliminate this model error. An axisymmetric finite element model which computes non-linear underpressure development needs to be integrated into both methods to allow for permeability variation. Secondly a relation between the layer characteristics and the empirical coefficients in CPT-based design is required. In this research one estimation method for the end-bearing coefficient in denser sands was developed based on monopile installation data. These two adaptations improve the representation of physical phenomena and therefore reduce the impact of model uncertainty.

An objective description of parameter variability is required before the impact of parametric uncertainties can be assessed. A survey dataset from practice results in challenges which are seldom addressed by current literature. Four tools are available for layer identification: Robertson classification, the statistical moving window method, Bartlett profiling and borehole logs. A combination is required for an optimal result. Vertical random field modelling of the cone resistance variability is possible provided that a trade-off is made between prerequisites and practicality. Probability density functions verified with goodness of fit tests provide an objective description of parameter variability, provided that sufficient data is available.

A quantitative reliability analysis on a case study in non-cohesive soils provided insight in model sensitivity to different parameters. Reliability intervals of simulated required suction profiles can be used to set an objective lower and upper bound during design. The Houlsby & Byrne method proved to be very sensitive to the estimate of the ratio of horizontal over vertical stresses (K). This estimate has a contradictory influence on the accuracy of computation of the skirt friction and enhanced vertical effective stresses. Furthermore, it is very hard to estimate in non-cohesive soils. The adapted CPT-based method performed significantly better.

Quantifying the probability of failure of an entire jacket configuration remains infeasible. The survey data and methods available do not allow for proper modelling of horizontal soil variability. Furthermore, application of a system reliability approach is infeasible due to the continuous installation process. As a consequence only feasibility of individual buckets on the jacket can be assessed. Even in these outcomes much epistemic uncertainty remains. This is due to the fact that not all failure mechanisms and effects of contingency measures can be quantified accurately by the current design methods.

The impact of geotechnical uncertainties on installation design of suction bucket jackets is significant. Application of reliability-based design methods leads to improved understanding of model sensitivity to different parameter estimates and the dominant failure mechanisms during installation.

7.2. Findings and discussion on suction bucket jacket installation design

Different suction bucket jacket installation design methods were evaluated, adapted and applied in this research. Findings regarding penetration study and critical suction methods are discussed in this Section.

1. Houlsby & Byrne method
The performance of the Houlsby & Byrne method is unsatisfactory. It fails to properly quantify an installation profile as a consequence of model behavior and parameter estimates.

1.1 Overestimation self-weight penetration depth
Self-weight penetration is overestimated by the Houlsby & Byrne method. Accuracy was assesssed by comparing the installation design results to the self-weight penetration data of suction bucket jackets and large diameter monopiles. Even the lowest values observed in the output of the quantitative reliability analysis are below the measured self-weight penetration depths. The underestimation of the end-bearing resistance by the current formulation is believed to be the cause. In Equation 7.1 it is visible that the vertical effective stress (σ_v') has a large influence on the end-bearing resistance (R_b). At small depths (so during self-weight penetration) the effective stress value will be small. As a consequence the estimated self-weight penetration will be high.

$$R_b = (\sigma_v' N_q + \gamma' \frac{t}{2} N_\gamma)(\pi D t) \tag{7.1}$$

1.2 Contradictory influence of the stress ratio estimate
The results of the Houlsby & Byrne method are sensitive to the ratio of horizontal over vertical stresses. Besides being a major component in the computation of skirt friction it serves as an input parameter for computing the inner and outer enhanced stresses by frictional forces further up the skirt. A large stress ratio is required for a sufficient estimate of the skirt friction and a low ratio is required for proper stress enhancement. Additionally a proper parameter estimation method for the stress ratio in sandy soils is absent. As a result the uncertainty of the model is enhanced by the uncertainty of the parameter estimate itself.
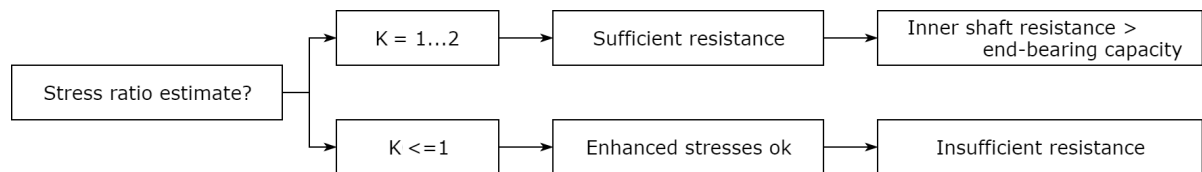

Figure 7.1: Contradictory behavior of the Houlsby & Byrne method for different stress ratio (K) estimates

1.3 Parameter sensitivity of the stress enhancement formulation
The stress enhancement formulation proposed by Houlsby and Byrne (2005b) shows varying accuracy for different parameter combinations. Especially at high angles of internal friction (ϕ) and stress ratios (K) the estimate of inner enhanced stress is too high. As a result the inner skirt friction becomes the dominant resistance force in these cases. This is counterintuitive since inner friction should be mostly reduced by the applied underpressure. Caution is required while selecting the parameters used for stress enhancement.

Using inner enhanced stresses to assess suction limits based on liquefaction can be unrealistic for soil profiles with a high stress ratio. Overestimation of stress enhancement can result in unconservative liquefaction limits. Estimating a reliable liquefaction limit based on enhanced stresses is therefore difficult too.

1.4 Using the peak angle of internal friction
When the bucket progresses into the soil it is expected that large strains are generated in sandy soils next to the skirt. The current method uses the peak friction angle which is the maximum friction angle on the stress strain curve. If the strain exceeds the value corresponding to the peak friction angle the value of the friction angle decreases in denser sands. As a result it is expected that the peak friction angles used as input are too conservative. Effects like these are important for open-ended pile design in sands and could therefore be relevant for suction bucket installation. Since the Houlsby & Byrne method underperformed the progression of the peak friction angle during penetration was not further investigated.

2. CPT-based method

Two adaptations to the original CPT-based method are proposed in this research. These make the method applicable in layered soils of varying permeability. However, discussion regarding empirical parameter estimation and the influence of fluctuations in the cone resistance profile is possible.

2.1 Improved incorporation underpressure in subsoils with layers of varying permeability

Implementation of the axisymmetric finite element seepage model guarantees application of the CPT-based method in soils of layered permeability. The original method assumed the effect of underpressure on the outside of the skirt as non-existent. This is incorrect. Furthermore, the in-place resistance was reduced with a factor based on the empirical soil suction limit. This is not advisable since large model uncertainty is present in the formulations of this limit.

The adaptation proposed in this research eliminates both drawbacks of the original method. The end-bearing resistance and skirt friction (both inside and outside) are reduced at a similar rate as the reduction of effective stresses near the skirt. If one makes use of enhanced stresses the internal friction angle (ϕ) and stress ratio (K) need to be estimated. This is not the case for in-situ stresses. The CPT-based method becomes applicable in subsoils of varying permeability and the dependence on the empirical soil suction limit is eliminated as a consequence of these adaptations.

2.2 Specific estimate of the end-bearing empirical coefficient (k_p) in dense sands

Only most probable and upper bound values for the empirical coefficients are available at this moment. This has a large effect on the accuracy of CPT-based design. An empirical estimation formula for determining the end-bearing coefficient was determined based on large diameter monopile installation data (Equation 7.2). Using the relation between the end-bearing coefficient and the relative density estimate leads to improved results of installation design in (dense) sands ($R_D > 0.65$). Although design methods of monopile and suction bucket (jacket) self-weight penetration are based on similar principles the difference in their geometry might affect the accuracy of this relation.

$$k_p = 1.27 - 0.86 R_D \tag{7.2}$$

Equation 7.2 was developed with relative density estimates computed with a relation developed by Jamiolkowski et al. (2003). Some of the relative density estimates are above one which is physically impossible (Equation 7.3). It is known that the Jamiolkowski formula can provide overestimates in some conditions. Although Equation 7.2 results in improved design results caution should be exercised while applying it in different conditions or with different relative density estimation methods. Additionally it can be stated that the Jamiolkowksi equation requires the cone resistance as an input. Therefore direct integration in the design method should be possible as well.

$$R_D = \frac{e_{max} - e}{e_{max} - e_{min}} \tag{7.3}$$

A final remark should be made regarding the value of the empirical coefficients during self-weight and suction-assisted penetration. In the current method the coefficients are similar throughout both phases. Main reason for this is the fact that the in-place resistance is reduced by the effect of applied underpressures. However, the similarity remains peculiar due to the fact that the physical processes occurring in both phases are fundamentally different.

2.3 Influence of fluctuations in the cone resistance profile

The value of the cone resistance has a high impact on the total resistance via the computation of the end-bearing capacity. The required suction profile can vary significantly if the cone resistance shows large variation. Application of the required suction profile computed with CPT-based design is not feasible in practice. This is due to the inabillity to instantly vary the applied underpressures with the pumps available. A more continuous profile is expected.

The conventional CPT-based method uses instantaneous cone resistance values for computing the end-bearing capacity. This can result in the computation of unrealistic failure scenarios in the case of presence of small peaks in the cone resistance profile. Applying a cone resistance averaging technique similar to the ones in pile design results in a slightly smoothened profile. As a result some design errors can be eliminated. However, the effect and accuracy of replacing the pile diameter from existing cone resistance averaging methods for pile design by the wall thickness of a suction bucket is unknown.

3. Critical suction
Soil limitations are the most uncertain aspect of the three phenomena which form a combined critical suction profile. Existing empirical formulations cannot be used in soils of varying permeability.

3.1 Liquefaction at the inner skirt tip
An attempt was made to estimate the limit suction based on the criterion provided by liquefaction at the inner skirt tip. While this is an easy and fast way to compute soil suction limits it is heavily dependent on parameter estimates. If enhanced stresses are used the stress ratio estimate is of high importance for the output of the computation. If in-situ stresses are used this soil suction limit is believed to be too conservative. Furthermore, research already showed that surrounding soils might prevent failure during local liquefaction and that the exit gradient is governing.

3.2 Critical exit gradient at the inner seabed level
Computing soil suction limits based on exit gradients of the underpressure close to the inside of the skirt forms the basis of all empirical formulations at the moment of writing. In this research a similar method is used. However, it is extended with the incorporation of varying permeability in the subsoil and the phenomenon of soil plug loosening. The new approach leads to increased failure probabilities when compared to the liquefaction limit. A large advantage of this method is that it only requires a permeability and soil unit weight estimate.

The critical exit gradient is no failure mechanism in itself. If it occurs at the top of the soil plug inner erosion and deposition under the lid is believed to take place. This will not cause immediate failure since limited loosening and soil heave is taken into account during design. Installation becomes problematic if piping, soil heave or excessive erosion occurs. It is expected that failure does not occur immediately after exceeding the critical gradient. Therefore the current design method is expected to be too conservative.

3.3 Impact of model uncertainty on feasibility assessment
The values for the suction limit and therefore the uncertainty of its computational results have a significant influence on the failure probability of installation. They define the resistance component of the limit state equation. A proper feasibility assessment is hindered by the current methods of quantifying critical suction. The model uncertainty is high and the current methodology does not incorporate all phenomena.

4. Shortcomings of the design methods
There are not sufficient accurate design methods available to quantify the probability of occurrence of all events and failure mechanisms. As a consequence there are missing links in the entire analysis.

3.1 Failure mechanisms
A reduced fault tree was used since there are no proper design methods for some phenomena. Interactions with the filter layer are not well understood. Basic formulas exist for computation of reverse end-bearing, soil plug heave and lift. However, practical application in layered soils and verification lacks. Quantifying the probability of preferential flow or the interaction of seepage patterns is difficult. This is due to the fact that horizontal variability cannot be modelled accurately. Uncertainty of the failure probability outcome increases by not taking into account these phenomena.

3.2 Events and contingency measures
Although the need and extent of ballasting and backfilling can be quantified the absolute effect of many contingency measures remains unknown. The reduction of resistance by contingencies like cyclic pumping and jetting cannot be quantified with current design methods. This makes the effect of these measures hard to determine. As a consequence the outcome failure probability is expected to be too conservative.

3.3 Suction bucket jacket configuration
Current research hardly considers installation of a suction bucket jacket configuration. An extra installation requirement in addition to target penetration depth is introduced: excessive tilt. After installation design the profiles of required suction should be compared to examine whether pumping speeds should be individually adjusted. Since individual pumps are used in practice the pumping speeds can be varied quite easily.

Failure caused by an uneven seabed as well as due to subsoil differences is introduced. If one bucket fails to install the entire installation fails. Interaction of developed seepage patterns can occur when buckets are closely positioned to each other.

7.3. Findings and discussion on reliability-based design methods

Applying statistical methods on an actual survey dataset of an offshore wind farm resulted in findings and discussion regarding their applicability. In this Section these are presented in chronological order of application in the reliability-based design framework throughout this research.

1. Median bandwidth filtering

Outliers need to be filtered from the cone resistance profile to avoid negative influences on the required suction profile. The median bandwidth filtering method can be applied on the cone resistance and shaft friction profile. It is required that the original method is adapted to only filter out local minima and maxima. Otherwise it can result in errors between layers which show a large natural variation in cone resistance or shaft friction. Successful automatic filtering on 203 cone penetration tests was achieved with this method.

2. Layer identification

A combination of multiple identification methods is advised for thorough layer identification at a cone penetration test location. It was observed that neither of the methods used in this research is flawless.

The Robertson soil behavior type index (I_c) provides a method to identify thin soil layers and can differentiate best in the top layers. A disadvantage is that differences in trendlines cannot be detected. Methods using a statistical moving window can provide an objective assessment of soil units before a vertical random field model is constructed. Individual assessment of the sampling window width per soil profile is required to achieve optimal accuracy. Unfortunately no objective identification thresholds are available for these techniques. Finally the geological history and soil type based on a borehole log can serve as a verification method, provided that the borehole log is positioned close to the cone penetration test location.

In all cases these identification methods provide point estimates of the layer thicknesses. Lateral variation of layer thickness can be observed from geophysical data. An accurate assessment of this variation is required for quantifying mechanisms like preferential flow which require 3D modelling. This is impossible with the current one-dimensional identification methods.

3. Vertical random field modelling

Random field modelling of the cone resistance profile is applied on (ideal) datasets in academic studies on reliability-based design in geotechnical engineering. Using a survey dataset of an offshore wind farm gave insight in several aspects worth mentioning.

3.1 Combining empirical autocorrelation models

Several empirical autocorrelation functions from the same soil unit and corresponding cone resistance sections can be used to fit a theoretical autocorrelation model. Literature did not provide any guidelines for this process in situations where layer geometry differs or tests are positioned further away from each other.

Several matching criteria were introduced to assess whether the empirical autocorrelation function of different cone resistance sections can be combined. The criteria used in this research are the result of several different attempts. The units should have a similar soil behavior type index ($\Delta I_c < 5\%$) and belong to the same geological deposit. Furthermore, it is required that the depth ranges of both units overlap and their trendline shows similar behavior. Opportunities for further narrowing or optimization of these criteria exist. Nevertheless, these criteria result in an applicable model for the data used in this research.

3.2 Trade-off between statistical criteria and applicability technique

A trade-off between the strict prerequisites (physical homogeneity and weak stationarity) and applicability in practice is required. Current research hardly examines both criteria. Discussion on applicability of this technique is avoided by not addressing the statistical background.

Difficulties occur when random field modelling is used for installation design purposes. Fitting an autocorrelation model describing variation with separation distance is, for instance, hard for thinner soil layers. This is due to the fact that the extracted variation profile is short. The assessment of weak stationarity increases in difficulty for thinner soil units as well. It was observed that using the strict prerequisites prevents application of random field modelling for installation design purposes. Trade-offs should be made by the modeller while constructing a vertical random field model of the cone resistance.

3.3 Unrealistic simulated values in top layers

Conventional application of this technique can simulate unrealistic cone resistance values in the top layers of the subsoil. This influences the accuracy of self-weight penetration in CPT-based design. Two reasons are believed to be the cause:

Firstly there is the fact that simulated variation profiles do not depend on location. As a consequence high end-bearing capacities can be generated at zero depth. This seems unrealistic and is an aspect which is advised to take into account. One could condition the model to provide a zero cone resistance at the top. Another option is to not use a random field model for the design of self-weight penetration depth at all.

Secondly there is an implementation aspect if the values of the trendline are low. To avoid the generation of negative cone resistances the simulated Gaussian process is transformed to a log-normal process. Problems arise when the mean value of the trendline becomes low or even negative. It is advised to condition the trendline to one if this occurs. This avoids transformation problems.

4. Impact of the jacket configuration

Both the continuous process of installation as well as the jacket configuration of the foundation provides challenges regarding the application of reliability-based design methods.

4.1 Horizontal random field modelling

Modelling of horizontal variability is required if the probability of failure mechanisms like preferential flow needs to be quantified. If coupled installation of all buckets needs to be analyzed it is beneficial too. Horizontal random field modelling of the cone resistance was attempted with the survey data available. Literature shows the scale of fluctuation is largely influenced by cone resistance values at little separation distance. Values of the cone resistance variation at similar depths but at different locations were hardly correlated in the survey data used in this research. As a result the scale of fluctuation was too small to properly simulate horizontal variability of the cone resistance.

While it is evident that there was correspondence between the profiles a credible scale of fluctuation could not be obtained. Similar results were observed during a literature study on horizontal random field modelling. While the one study finds large horizontal scale of fluctuations the other finds very small ones. Values can even show large differences inside one dataset of one study. Of course differences in horizontal variability per site could be possible. Considering the above, suspicion rises that successful application of horizontal random field modelling could be a coincidence in some cases. This method is therefore assessed as unsuitable for application in practice.

4.2 System reliability for installation of a jacket configuration

Horizontal variability cannot be quantified based on the survey dataset available. Therefore installation feasibility was assessed per individual bucket. A system reliability approach can be used to analyze the reliability of a system consisting of multiple elements. However, one aspect of suction bucket installation design prevents application of this approach. Normally a system reliability approach compares elements with a single limit state. However, the limit state resulting from individual bucket installation is the governing value of many limit state values over the penetration depth.

The limit state approach described above hinders application of system reliability principles. Combined probabilities of failure due to one failure mechanism at one specific penetration depth can be computed using a method called Ditlevsen bounds. Although this method takes correlation between locations into account it does not give any insight in the overall feasibility of successful installation of the entire jacket configuration.

7.4. Recommendations for future research

The previous conclusions, findings and discussion result in several recommendations for future academic research on both suction bucket jacket installation design as well as reliability-based design methods.

1. Suction bucket jacket geotechnical installation design

The three main topics of advised future research are the empirical coefficients in CPT-based design, quantifying other installation design phenomena and investigation of interactions with the filter layer.

1.1 Further investigation on estimation methods for empirical coefficients in CPT-based design

This research showed that improving the estimation of empirical parameters used in CPT-based design is possible and can lead to more accurate results. Nevertheless research on two aspects is required:

Empirical parameter estimation methods need to be further developed based on existing data. In this research an estimation method for the empirical end-bearing coefficient in denser sands was developed. This equation depends on the relative density estimate by Jamiolkowski et al. (2003). Since some of the estimates are unrealistic this design method requires improvement. Self-weight penetration of both monopiles and suction bucket jackets is continuously measured in the field. This is valuable data which can be used to analyze potential parameter estimation methods.

The fundamental principles behind suction bucket installation need to be examined to define consistent and physically representative empirical parameter estimation methods. Similar shaft friction (k_s) and end-bearing (k_p) coefficients are used during self-weight and suction-assisted penetration. This is peculiar because the processes around the penetrating skirt tip are fundamentally different. Furthermore it should be investigated whether it is feasible using relative density for the estimation of layer specific empirical parameters. Directly estimating the end-bearing and shaft friction should be possible too since the cone resistance depends on density characteristics. Research on physical processes occuring during installation can help understanding these phenomena.

1.2 Quantify installation design phenomena

Estimating required suction can be performed reasonably well with the current method. However, a proper feasibility assessment requires good estimates of the limitations. While buckling and cavitation studies can be performed the limits for the subsoil can hardly be described. Research is required regarding phenomena governing the soil installation limits. Future research should try to aim to develop a reasonable method which is generally applicable throughout different soil conditions. Developing such a method would increase the possibility of a more accurate failure probability assessment. As a consequence the application of suction bucket (jacket) technology in non-standard conditions becomes more feasible.

1.3 Investigate interactions with the filter layer

Before penetration in the subsoil occurs the suction bucket (jacket) needs to penetrate through the filter layer of the scour protection. This is one of the four system components in installation design but hardly incorporated in current design methods. Interaction of the bucket skirts with the filter layer throughout installation is not properly understood. Observations in the field and previous or future laboratory tests could result in a simplified method to take these interactions into account. A start can be made by quantifying the contribution of the rocks in the filter layer to resistance elements like skirt friction or end-bearing capacity.

2. Reliability-based design in offshore geotechnical engineering

Reliability-based design is underdeveloped in offshore geotechnical engineering. Size of datasets forces researchers and engineers to be creative and develop usable methods. The following is recommended:

2.1 Increase fundamental research on soil parameter estimation and variability

In this research proper variability of all parameters in all soil types could not be quantified based on the survey data available. Standard variability descriptors of parameters can be obtained. However, literature presents such a wide range that the output of the direct reliability analysis would render useless. The soil parameter estimate is fundamental for successful evolution as well as application of design methods. Proper research on parameter estimation and its variability is essential for future applications of reliability-based design in offshore geotechnical engineering.

2.2 Assess the applicability of (horizontal) random field modelling
This research examined the application of random field modelling of the cone resistance variation using a survey dataset from practice. Vertical random field modelling was possible after the application of several criteria. However, constructing a model in horizontal direction proved to be impossible.

Large differences in horizontal scales of fluctuation were observed in both literature as well as in the dataset used in this research. In the discussion it was already seriously doubted whether a theoretical autocorrelation can be fitted reliably through little and widely scattered data points. An objective assessment of the physical background of the cone penetration test in combination with the purpose of horizontal random field modelling is required. This should lead to an advice on whether modelling soil parameters using a horizontal random field model results in a realistic output.

7.5. Recommendations for practice

This research was performed in collaboration with a major contractor and concerns offshore geotechnical installation. As a consequence the findings and discussion result in several recommendations for practice.

1. Suction bucket jacket geotechnical installation design
Outcomes of this research can be used to steer towards a more efficient suction bucket jacket installation design process. Three main recommendations are presented in here:

1.1 Use the output of the quantitative reliability analysis to improve site investigation
The analysis of output of the quantitative reliability analysis showed that CPT-based design is preferential over the Houlsby & Byrne method. It was also found that permeability estimates are an essential parameter to compute suction profiles over depth. Potential failure mechanisms can be overlooked when single values of permeability are used. Knowledge on governing parameters on installation design can aid setting the scope of site investigation campaigns. Based on this study it is advised to perform the bulk of the particle size distribution tests in the upper soil layers. This can give insight in permeability of these layers and therefore insight in the probability of occurrence of the dominant failure mechanism: seepage blocking.

1.2 Steer towards CPT-based design approach
In general an offshore cone penetration test is cheaper and faster to perform than extensive laboratory tests. It also provides more site-specific data which is essential for accurate installation design of suction bucket jackets. In recent years the cone penetration test played an ever more important role during site investigation campaigns. It is advised to steer towards application of the CPT-based design method since it provides a more accurate and location specific design results than the Houlsby & Byrne method. Investing in data and research which can aid the estimation of the empirical parameters (Section 7.4) is therefore also a relevant recommendation for practice.

1.3 Invest in gathering more relevant data on geotechnical installation
This research showed that simple installation data of offshore support structures can have a large impact. Gathering the self-weight penetration data of large diameter monopiles helped in developing a site-specific assessment approach of an empirical coefficient in CPT-based design. It is advised to continue or even expand these measurements. Measuring phenomena like soil heave inside suction buckets and pumping volumes during installation can result in valuable data. This could aid the development of practical design methods for soil heave, filter layer interactions and phenomena contributing to excessive leakage (e.g. loosening, piping). All of this helps reducing the uncertainty embedded in current installation design methods.

2. Reliability-based design in offshore geotechnical engineering

Many challenges remain regarding the research on reliability-based design methods in offshore geotechnical engineering, let alone regarding application in practice. Several initial steps can be taken to cope with geotechnical uncertainties in an objective manner in practice.

2.1 Improve data storage and automation throughout execution of a project

Current methods of storing and processing soil data are unpractical and do not aid in dealing with uncertainties in an objective manner. This has to be improved if (on the long term) reliability analyses are to be performed on a more regular basis. Consistent raw data files of site investigation and survey campaigns greatly help the efficiency of data processing and therefore the analysis of parametric uncertainties. More insight can be gained in parameter variability in certain regions/geological deposits when data is stored in a consistent manner. This could provide a basis for a more general assessment of feasibility of installation of support structures in nearby areas.

2.2 Gradually introduce methods and tools to realize maximum efficiency

Applying a full reliability-based design analysis each time an offshore foundation is installed will not be feasible in the nearby future. Nevertheless, the analysis performed in this research contains many individual components which can already make a difference in understanding and dealing with uncertainties. If one wants to work towards a more objective and reliability-based design approach it is advised to gradually introduce elements into existing projects.

Ideas of starting points can be small or large in the amount of effort they take. Small steps like expanding the layer identification method with the methods presented in this research or visualizing the output of the Robertson graph in a second order sense can already help. One could also work on fitting probability density functions to soil parameter estimates within individual projects (e.g. friction angle, permeability). These can than be used to select the characteristic design parameters on a statistical basis (e.g. a 95% reliability interval). Another option is to perform a quantitative reliability analysis on the location which is expected to be governing for a project. This can aid in defining the feasibility of the entire project.

2.3 Investigate possible application on other topics

Application of reliability-based design is of course not limited to suction bucket jacket installation. Actually, suction bucket penetration is a relatively complex geotechnical process which requires uncommon parameter estimates like permeability and design methods with a large model uncertainty. Furthermore, as mentioned in Section 7.3 it is difficult to estimate overall failure probabilities for installation of a multi-footed structure. A concept with more available installation data or a lower model uncertainty is by definition more suitable for an assessment with reliability-based techniques. In such cases more accurate failure probability estimates can be expected.

Bibliography

[1] Alm, T. and Hamre, L. (2001). Soil model for pile driveability predictions based on CPT interpretations. In *Proceedings of the 15th International Conference on Soil Mechanics and Geotechnical Engineering*, pages 1297–1302, Istanbul, Turkey. Balkema.

[2] Andersen, K. H., Jostad, H. P., and Dyvik, R. (2008). Penetration Resistance of Offshore Skirted Foundations and Anchors in Dense Sand. *Journal of Geotechnical and Geoenvironmental Engineering*, 134(1):106–116.

[3] Andersen, K. H. and Schjetne, K. (2013). Database of Friction Angles of Sand and Consolidation Characteristics of Sand, Silt, and Clay. *Journal of Geotechnical and Geoenvironmental Engineering*, 139(7):1140–1155.

[4] Asgarpour, M. (2016). Assembly, transportation, installation and commissioning of offshore wind farms. In Chong, N. and Ran, L., editors, *Offshore wind farms: Technologies, Design and Operation*, chapter 17, pages 527–541. Woodhead Publishing.

[5] Au, S. K. and Beck, J. L. (2001). Estimation of small failure probabilities in high dimensions by subset simulation. *Probabilistic Engineering Mechanics*, 16(4):263–277.

[6] Au, S. K. and Beck, J. L. (2003). Subset Simulation and its Application to Seismic Risk Based on Dynamic Analysis. *Journal of Engineering Mechanics*, 129(8):901–917.

[7] Bailey, H., Senior, B., Simmons, D., Rusin, J., Picken, G., and Thompson, P. M. (2010). Assessing underwater noise levels during pile-driving at an offshore windfarm and its potential effects on marine mammals. *Marine Pollution Bulletin*, 60(6):888–897.

[8] Baldi, G. (1986). Interpretation of CPT's and CPTU's: 2nd part: Drained Penetration of Sands. In *Proceedings of the 4th International Geotechnical Seminar on Field Instrumentation and In-Situ Measurements*, pages 143–156, Singapore. Nanyang Technological Institute.

[9] Bilgili, M., Yasar, A., and Simsek, E. (2011). Offshore wind power development in Europe and its comparison with onshore counterpart. *Renewable and Sustainable Energy Reviews*, 15(2):905–915.

[10] Biot, M. A. (1962). Mechanics of Deformation and Acoustic Propagation in Porous Media. *Journal of Applied Physics*, 33(4):1482–1498.

[11] Bolton, M. D. (1986). The Strength and Dilatancy of Sands. *Géotechnique*, 36(1):65–78.

[12] Breton, S. P. and Moe, G. (2009). Status, plans and technologies for offshore wind turbines in Europe and North America. *Renewable Energy*, 34(3):646–654.

[13] Burlon, S., Frank, R., Baguelin, F., Habert, J., and Legrand, S. (2014). Model factor for the bearing capacity of piles from pressuremeter test results – Eurocode 7 approach. *Géotechnique*, 64(7):513–525.

[14] Byrne, B. W. and Houlsby, G. T. (2003). Foundations for offshore wind turbines. *Philosophical Transactions of the Royal Society of London A: Mathematical, Physical and Engineering Sciences*, 361(1813):2909–2930.

[15] Carrier III, W. D. (2003). Goodbye, Hazen; Hello, Kozeny-Carman. *Journal of Geotechnical and Geoenvironmental Engineering*, 129(11):1054–1056.

[16] Chapuis, R. (2004). Predicting the saturated hydraulic conductivity of sand and gravel using effective diameter and void ratio. *Canadian Geotechnical Journal*, 41(5):787–795.

[17] Christian, J. T. (2004). Geotechnical Engineering: How Well Do We Know What We Are Doing? *Journal of Geotechnical and Geoenvironmental Engineering*, 130(10):985–1003.

[18] Christian, J. T., Ladd, C. C., and Baecher, G. B. (1994). Reliability Applied to Slope Stability Analysis. *Journal of Geotechnical Engineering*, 120(12):2180–2207.

[19] Clausen, C. J. F., Aas, P. M., and Karlsrud, K. (2005). Bearing Capacity of Driven Piles in Sand, the NGI approach. In *Proceedings of the 1st International Symposium on Frontiers in Offshore Geotechnics*, pages 677–681, Perth. Taylor and Francis.

[20] Dekking, F. M., Kraaikamp, C., Lopuhaä, H. P., and Meester, L. E. (2005). *A Modern Introduction to Probability and Statistics: Understanding Why and How*. Springer-Verlag, Delft, 5th edition.

[21] Dithinde, M., Phoon, K.-K., De Wet, M., and Retief, J. V. (2011). Characterization of Model Uncertainty in the Static Pile Design Formula. *Journal of Geotechnical and Geoenvironmental Engineering*, 137(1):70–85.

[22] Ditlevsen, O. and Madsen, H. O. (1996). *Structural reliability methods*. Wiley, New York, 178th edition.

[23] DNV (1992). Foundations - Classification Notes No. 30.4. Technical report, Det Norske Veritas.

[24] DNVGL (2017a). Recommended Practice - DNVGL-RP-C212. Offshore soil mechanics and geotechnical engineering. Technical Report August, DNVGL.

[25] DNVGL (2017b). Recommended Practice - DNVGL-RP-E303. Design and installation of plate anchors in clay. Technical Report April, DNVGL.

[26] Doherty, P. and Gavin, K. (2010). Statistical review of CPT data and implications for pile design. In Robertson, P. K. and Mayne, P. W., editors, *Proceedings of the 2nd international Symposium on Cone Penetration Testing*, volume 3, Huntington Beach.

[27] Doherty, P. and Gavin, K. (2011). The Shaft Capacity of Displacement Piles in Clay: A State of the Art Review. *Geotechnical and Geological Engineering*, 29(4):389–410.

[28] Dong Energy (2014). Installation of suction bucket jacket (photograph).

[29] Erbrich, C. and Tjelta, T. (1999). Installation of Bucket Foundations and Suction Caissons in Sand - Geotechnical Performance. In *Offshore Technology Conference*, Houston, Texas. Offshore Technology Conference.

[30] European Commision (2014). A policy framework for climate and energy in the period from 2020 to 2030. Technical report, European Commission, Brussels.

[31] European Wind Energy Association (2013). Deep water: the next step for offshore wind energy. Technical report, European Wind Energy Association, Brussels, Belgium.

[32] Feld, T. (2001). *Suction Buckets: a new innovation foundation concept, applied to offshore wind turbines*. Doctoral thesis, Aalborg University.

[33] Fenton, G. A. (1999). Random Field Modeling of CPT Data. *Journal of Geotechnical and Geoenvironmental Engineering*, 125(6):486–498.

[34] Fenton, G. A. and Griffiths, D. V. (2003). Bearing-capacity prediction of spatially random c – phi soils. *Canadian Geotechnical Journal*, 40(1):54–65.

[35] Fenton, G. A. and Griffiths, D. V. (2005). Three-Dimensional Probabilistic Foundation Settlement. *Journal of Geotechnical and Geoenvironmental Engineering*, 131(2):232–239.

[36] Firouzianbandpey, S., Griffiths, D. V., Ibsen, L. B., and Andersen, L. V. (2014). Spatial correlation length of normalized cone data in sand: case study in the north of Denmark. *Canadian Geotechnical Journal*, 51(8):844–857.

[37] Foglia, A. and Ibsen, L. B. (2014). Bucket foundations : a literature review. Technical report, Aalborg University.

[38] Gavin, K. (2018). Use of CPT for the design of shallow and deep foundations on sand. In Hicks, M., Pisano, F., and Peuchen, J., editors, *Cone Penetration Testing 2018: Proceedings of the 4th International Symposium on Cone Penetration Testing*, pages 45–61, Delft. CRC Press.

[39] Griffiths, D. V., Huang, J., and Fenton, G. A. (2009). Influence of Spatial Variability on Slope Reliability Using 2-D Random Fields. *Journal of Geotechnical and Geoenvironmental Engineering*, 135(10):1367–1378.

[40] Harder, H. and von Bloh, G. (1988). Determination of representative CPT-parameters. In *Proceedings of International Conference: Penetration testing in the UK*, pages 237–240, Birmingham. Thomas Telford.

[41] Harireche, O., Mehravar, M., and Alani, A. M. (2014). Soil conditions and bounds to suction during the installation of caisson foundations in sand. *Ocean Engineering*, 88(1):164–173.

[42] Houlsby, G. T. and Byrne, B. W. (2005a). Design procedures for installation of suction caissons in clay and other materials. *Proceedings of the Institution of Civil Engineers*, 158(3):75–82.

[43] Houlsby, G. T. and Byrne, B. W. (2005b). Design procedures for installation of suction caissons in sand. *Proceedings of the Institution of Civil Engineers*, 158(3):135–144.

[44] Ibsen, L. B., Liingaard, M., and Nielsen, S. A. (2005). Bucket Foundation, a status. In *Proceedings Copenhagen Offshore Wind Conference*, Copenhagen.

[45] Ibsen, L. B. and Thilsted, C. L. (2010). Numerical study of piping limits for suction installation of offshore skirted foundations an anchors in layered sand. In Gouvernec, S. and White, D., editors, *Proceedings of the 2nd International Symposium on Frontiers in Offshore Geotechnics*, pages 421–426, Perth. Taylor and Francis.

[46] ISO (2015). General principles on reliability for structures. Technical report, International Standard Organisation, Geneva.

[47] Jaky, J. (1944). The coefficient of earth pressure at rest. In Hungarian (A nyugalmi nyomas tenyezoje). *Journal for Society of Hungarian Architects and Engineers (Magyar Mernok es Epitesz-Egylet Kozlonye)*, pages 355–358.

[48] Jamiolkowski, M., Lo Presti, D. C. F., and Manassero, M. (2003). Evaluation of relative density and shear strength of sands from CPT and DMT. *Soil Behaviour and Soft Ground Construction*, pages 201–238.

[49] Jardine, F. M., Chow, F. C., Overy, R. F., and Standing, J. R. (2005). *ICP Design Methods for Driven Piles in Sands and Clays*. Thomas Telford, London, United Kingdom.

[50] Jonkman, S. N., Steenbergen, R. D. J. M., Morales-Napolés, O., Vrouwenvelder, A. C. W. M., and Vrijling, J. K. (2017). *Probabilistic Design: Risk and Reliability Analysis in Civil Engineering*. Delft University of Technology, Delft, 4th edition.

[51] Knut, R. O. and Bjerager, P. (1992). Model Uncertainty Representation in Geotechnical Reliability Analysis. *Journal of Geotechnical Engineering*, 118(3):363–376.

[52] Kolk, H. J., Baaijens, A. E., and Senders, M. (2005). Design criteria for pipe piles in silica sands. In *Procedings of the 1st international Symposium on Frontiers in Offshore Geotechnics*, pages 711–716, Perth. Taylor and Francis.

[53] Lacasse, S. and Nadim, F. (1994). Reliability Issues and Future Challenges in Geotechnical Engineering for Offshore Structures. In *7th International Conference on the Behaviour of Offshore Structures*, pages 9–38, Cambridge. MIT Press.

[54] Lacasse, S. and Nadim, F. (2007). Probabilistic Geotechnical Analyses for Offshore Facilities. *Georisk*, 1(1):21–42.

[55] Leanwind (2017). Driving cost reductions in offshore wind. Technical report, WindEurope.

[56] Leblanc, C. (2009). *Design of Offshore Wind Turbine Support Structures: Selected topics in the field of geotechnical engineering*. Doctoral thesis, Aalborg University.

[57] Lehane, B. M., Jardine, R. J., Bond, A. J., and Frank, R. (1993). Mechanisms of Shaft Friction in Sand from Instrumented Pile Tests. *Journal of Geotechnical Engineering*, 119(1):19–35.

[58] Lehane, B. M., Schneider, J. A., and Xu, X. (2005). The UWA-05 method for prediction of axial capacity of driven piles in sand. In *Frontiers in Offshore Geotechnics*, pages 683–689, London. Taylor and Francis.

[59] Lehane, B. M., Schneider, J. A., and Xu, X. (2007). Development of the UWA-05 Design Method for Open and Closed Ended Driven Piles in Siliceous Sand. In Camp, W., Castelli, R., Laefer, D. F., and Paikowsky, S., editors, *Contemporary Issues in Deep Foundations*, pages 683–689, Denver. American Society of Civil Engineers.

[60] Lesny, K. and Richwien, W. (2011). Design, construction and installation of support structures for offshore wind energy systems. In Sørensen, J. D. and Sørensen, J. N., editors, *Wind Energy Systems*, chapter 16, pages 479–518. Woodhead Publishing, 1st edition.

[61] Lillifors, H. W. (1967). On the Kolmogorov-Smirnov test for normality with mean and variance unknown. *Journal of the American Statistical Association*, 62(318):399–402.

[62] Lloret-Cabot, M., Fenton, G. A., and Hicks, M. A. (2014). On the estimation of scale of fluctuation in geostatistics. *Georisk: Assessment and Management of Risk for Engineered Systems and Geohazards*, 8(2):129–140.

[63] Look, B. G. (2007). *Handbook of Geotechnical Investigation and Design Tables*. Taylor and Francis Group, London, 13th edition.

[64] Lozano-Minguez, E., Kolios, A. J., and Brennan, F. P. (2011). Multi-criteria assessment of offshore wind turbine support structures. *Renewable Energy*, 36(11):2831–2837.

[65] Lunne, T., Robertson, P. K., and Powell, J. J. (1997). *Cone Penetration Testing in Geotechnical Practice*. Taylor and Francis, London, 1st edition.

[66] Malhotra, S. (2011). Selection, Design and Construction of Offshore Wind Turbine Fundations. In Al-Bahadly, I., editor, *Wind Turbines*, chapter 10, pages 231–263. InTechOpen.

[67] Massey, F. J. (1951). The Kolmogorov-Smirnov Test for Goodness of Fit. *Journal of the American Statistical Association*, 46(253):68–78.

[68] Mayne, P. W. (2014). Interpretation of geotechnical parameters from seismic piezocone tests. In Robertson, P. K. and Cabal, K. I., editors, *3rd International Symposium on Cone Penetration Testing, CPT14*, pages 47–73, Las Vegas. Gregg Drilling and Testing.

[69] Mayne, P. W. and Kulhawy, F. H. (1982). K0 - OCR Relationships in soil. *Journal of the Geotechnical Engineering Division*, 108(6):851–872.

[70] Mayne, P. W. and Peuchen, J. (2018). Evaluation of CPTU cone factor for undrained strength of clays. In Hicks, M. A., Pisano, F., and Peuchen, J., editors, *Cone Penetration Testing 2018: Proceedings of the 4th International Symposium on Cone Penetration Testing*, pages 423–429, Delft. CRC Press.

[71] Meyerhof, G. (1951). The Ultimate Bearing Capacity of Foundations. *Géotechnique*, 2(4):301–332.

[72] Nadim, F. (2015). Accounting for Uncertainty and Variability in Geotechnical Characterization of Offshore Sites. In Schweckendiek, T., van Tol, A., Pereboom, D., and Cools, P. M. C. B. M., editors, *Geotechnical Safety and Risk V*, pages 13–35. IOS Press, 1st edition.

[73] Negro, V., López-Gutiérrez, J. S., Esteban, M. D., and Matutano, C. (2014). Uncertainties in the design of support structures and foundations for offshore wind turbines. *Renewable Energy*, 63:125–132.

[74] Odong, J. (2007). Evaluation of Empirical Formulae for Determination of Hydraulic Conductivity Based on Grain-Size Analysis. *Journal of American Science*, 3(3):54–60.

[75] Panagoulias, S., van Dijk, B. F. J., Drummen, T., Askarinejad, A., and Pisano, F. (2017). Critical Suction Pressure During Installation of Suction Caissons in Sand. In *Offshore Site Investigation and Geotechnics: 'Smarter Solutions for Future Offshore Developments'*, volume 8, pages 570–577, Londen. Society of Underwater Technology.

[76] Panayides, S., Powell, T. A., and Schrøder, K. (2017). Penetration Resistance of Suction Caissons in Layered Soils - a Case Study. In *Offshore Site Investigation and Geotechnics: 'Smarter Solutions for Future Offshore Developments'*, volume 8, pages 562–569, Londen. Society of Underwater Technology.

[77] Phoon, K.-K. (2008). *Reliability-based design in geotechnical engineering: Computations and Applications.* Taylor and Francis, London, 1st edition.

[78] Phoon, K.-K., Asce, M., Quek, S.-T., and An, P. (2003). Identification of Statistically Homogeneous Soil Layers Using Modified Bartlett Statistics. *Journal of Geotechnical and Geoenvironmental Engineeringl,* 129(7):649–659.

[79] Phoon, K.-K. and Kulhawy, F. H. (1999). Characterization of geotechnical variability. *Canadian Geotechnical Journal*, 36(4):612–624.

[80] Phoon, K.-K. and Kulhawy, F. H. (2005). Characterisation of model uncertainties for laterally loaded rigid drilled shafts. *Géotechnique*, 55(1):45–54.

[81] Phoon, K.-K., Quek, S.-T., and An, P. (2004). Geostatistical analysis of cone penetration test (CPT) sounding using the modified Bartlett test. *Canadian Geotechnical Journal*, 41(2):356–365.

[82] Prendergast, L. J., Reale, C., and Gavin, K. (2018). Probabilistic examination of the change in eigenfrequencies of an offshore wind turbine under progressive scour incorporating soil spatial variability. *Marine Structures*, 57(1):87–104.

[83] Rackwitz, R. (2000). Reviewing probabilistic soils modelling. *Computers and Geotechnics*, 26(3):199–223.

[84] Randolph, M. F., Cassidy, M., Gourvenec, S., and Erbrich, C. (2005). Challenges of Offshore Geotechnical Engineering. *Ground Engineering*, 38(9):32–33.

[85] Randolph, M. F. and Gourvenec, S. (2011). *Offshore geotechnical engineering.* Spon Press, London, 1st edition.

[86] Randolph, M. F. and Murphy, B. S. (1985). Shaft Capacity of Driven Piles in Clay. In *Offshore Technology Conference*, Houston. Offshore Technology Conference.

[87] Randolph, M. F., O'Neill, M. P., Stewart, D. P., and Erbrich, C. (1998). Performance of Suction Anchors in Fine-Grained Calcareous Soils. In *Offshore Technology Conference*, Houston. Offshore Technology Conference.

[88] Robertson, P. K. (1989). Soil classification using the cone penetration test. *Canadian Geotechnical Journal*, 27(1):151–158.

[89] Robertson, P. K. (2009). Interpretation of cone penetration tests — a unified approach. *Canadian Geotechnical Journal*, 46(11):1337–1355.

[90] Robertson, P. K. (2010). Estimating in-situ soil permeability from CPT & CPTu. In Robertson, P. K. and Mayne, P. W., editors, *Proceedings of the 2nd International Symposium on Cone Penetration Testing*, pages 734–74, Huntington Beach.

[91] Robertson, P. K. (2016). Cone penetration test (CPT)-based soil behaviour type (SBT) classification system — an update. *Canadian Geotechnical Journal*, 53(12):1910–1927.

[92] Robertson, P. K. and Cabal, K. L. (2010). Estimating soil unit weight from CPT. In Robertson, P. and Mayne, P., editors, *Proceedings of the 2nd International Symposium on Cone Penetration Testing (CPT'10)*, Huntington Beach, California, USA. California State Polytechnic University.

[93] Robertson, P. K. and Cabal, K. L. (2015). *Guide to Cone Penetration Testing for Geotechnical Engineering.* Gregg Drilling and Testing, 6th edition.

[94] Rodrigues, S., Restrepo, C., Kontos, E., Teixeira Pinto, R., and Bauer, P. (2015). Trends of offshore wind projects. *Renewable and Sustainable Energy Reviews*, 49:1114–1135.

[95] Rusaas, P., Giske, S. R., Aas-Jakobsen, A., Barret, G., Christiansen, P. E., and Baerheim, M. (1995). Design, Operation Planning and Experience from the Marine Operations for the Europipe Jacket with Bucket Foundations. In *Offshore Technology Conference*, pages 885–895.

[96] Saue, M., Aas, P. M., Anders, K. H., and Solhjell, E. (2017). Installation of Suction Anchors in Layered Soils. In *Offshore Site Investigation and Geotechnics: 'Smarter Solutions for Future Offshore Developments'*, pages 507–515, Londen. Society of Underwater Technology.

[97] Senders, M. (2008). *Suction caissons in sand as tripod foundations for offshore wind turbines.* Doctoral thesis, University of Western Australia.

[98] Senders, M. and Randolph, M. F. (2009). CPT-Based Method for the Installation of Suction Caissons in Sand. *Journal of Geotechnical and Geoenvironmental Engineering*, 135(1):14–25.

[99] Senpere, D. and Auvergne, G. A. (1982). Suction Anchor Piles - A Proven Alternative to Driving or Drilling. In *Offshore Technology Conference*, volume 14, pages 483–487, Houston. Offshore Technology Conference.

[100] Streif, H. (2004). Sedimentary record of Pleistocene and Holocene marine inundations along the North Sea coast of Lower Saxony, Germany. *Quaternary International*, 112(1):3–28.

[101] Sturm, H. (2017). Design Aspects of Suction Caissons for Offshore Wind Turbine Foundations. In Yunsup, S., editor, *International Conference on Soil Mechanics and Geotechnical Engineering*, volume 19, pages 45–63, Seoul, South Korea. ISSMGE Technical Committee TC 209.

[102] Stuyts, B., Ellerey, G. D., Davidson, J., and Torres, I. (2017). A Methodology for the Probabilistic Assessment of Pile Refusal due to Boulder Encounter. In *Offshore Site Investigation and Geotechnics: 'Smarter Solutions for Future Offshore Developments'*, volume 8, pages 688–694, Londen. Society of Underwater Technology.

[103] Tang, C. and Phoon, K.-K. (2017). Model Uncertainty of Eurocode 7 Approach for Bearing Capacity of Circular Footings on Dense Sand. *International Journal of Geomechanics*, 17(3):1–9.

[104] Tjelta, T.-I. (1994). Geotechnical Aspects of Bucket Foundations Replacing Piles for the Europipe 16/11-E jacket. In *Offshore Technology Conference*, volume 26, pages 73–82, Houston. Offshore Technology Conference.

[105] Tjelta, T.-I. (2014). Installation of Suction Caissons for Offshore Wind, presentation at the Danish Geotechnical Society Seminar.

[106] Tjelta, T.-I. (2015). The suction foundation technology. In Meyer, V., editor, *Proceedings of the 3rd International Symposium on Frontiers in Offshore Geotechnics*, pages 85–93, Oslo. CRC Press.

[107] Topham, E. and McMillan, D. (2017). Sustainable decommissioning of an offshore wind farm. *Renewable Energy*, 102:470–480.

[108] Tran, M. N., Randolph, M. F., and Airey, D. W. (2007). Installation of Suction Caissons in Sand with Silt Layers. *Journal of Geotechnical and Geoenvironmental Engineering*, 133(10):1183–1191.

[109] UNFCC (2015). Paris agreement.

[110] Universal Foundation (2018). Case Study: Horns Rev 2.

[111] Uzielli, M., Lacasse, S., Nadim, F., and Phoon, K.-K. (2006). Soil variability analysis for geotechnical practice. In *International Workshop on Characterisation and Engineering Properties of Natural Soils*, volume 3, pages 1653–1752. Taylor and Francis.

[112] Uzielli, M., Simonini, P., and Cola, S. (2008). Statistical identification of homogeneous soil units for Venice lagoon soils. In Huang, A. B. and Mayne, P. W., editors, *Geotechnical and Geophysical Site Characterization: Proceedings of the 3rd International Conference on Site Characterization*, pages 1209–1216, Taiwan. CRC Press.

[113] Uzielli, M., Vannucchi, G., and Phoon, K.-K. (2005). Random field characterisation of stress-normalised cone penetration testing parameters. *Géotechnique*, 55(1):3–20.

[114] Verruijt, A. (2012). *Soil mechanics.* Delft University of Technology, Delft, 1st edition.

[115] Vrijling, J. K. (2001). Probabilistic Design of Water Defense Systems in the Netherlands. *Reliability Engineering & System Safety*, 74(3):337–344.

[116] Vrijling, J. K. and van Gelder, P. H. A. J. M. (2002). *Probabilistic Design in Hydraulic Engineering.* Delft University of Technology, Delft, 1st edition.

[117] Wang, X., Zeng, X., Li, J., Yang, X., and Wang, H. (2018). A review on recent advancements of substructures for offshore wind turbines. *Energy Conversion and Management*, 158:103–119.

[118] Weston, D. (2014). Suction Bucket Foundation at Borkum Riffgrund 1 (photograph).

[119] Whitehouse, R. J. S., Harris, J. M., Sutherland, J., and Rees, J. (2011). The nature of scour development and scour protection at offshore windfarm foundations. *Marine Pollution Bulletin*, 62(1):73–88.

[120] Wickremesinghe, D. S. (1989). *Statistical characterization of soil profiles using in situ tests.* Doctoral thesis, University of British Columbia.

[121] Wittrup, S. (2016). Nyt havmøllefundament skal stå sin prøve i gigantisk havmøllepark (photograph).

[122] Wong, S. Y. (2004). *Stochastic Characterization and Reliability of Saturated Soils.* Doctoral thesis, University of Manchester.

[123] Xu, X., Schneider, J. A., and Lehane, B. M. (2008). Cone penetration test (CPT) methods for end-bearing assessment of open- and closed-ended driven piles in siliceous sand. *Canadian Geotechnical Journal*, 45(8):1130–1141.

[124] Zaaijer, M. (2003). Comparison of monopile , tripod , suction bucket and gravity based design for a 6 MW turbine. In *Offshore Wind Energy in Mediterranean and Other European Seas*, Naples. Delft University of Technology.

A
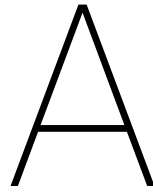
Case study wind farm

This Appendix gives a brief overview of the site conditions and location of the case study wind farm. It is only published in the report presented to GeoSea (DEME group) since some data given is confidential.

B

Background on applied methods

A full reliability-based analysis requires the application of many individual methods regarding filtering, identification and simulation. As a consequence many small individual decisions and considerations were made of which not all could be described extensive in the main body of this report. This Appendix is intended to provide insight in the following topics:

1. **Median bandwidth filtering of the cone penetration test results, page 112:**
   The original method had differences in dealing with boundaries between soil units. Therefore adaptations were required which are described here.

2. **Optimize window width for statistical layer identification, page 113:**
   The sensitivity of both statistical layer identification methods depends heavily on the width of the sampling window. Background is given in this Appendix.

3. **Objective assessment of weak stationarity of soil units, page 114:**
   The only method available for objective assessment of weak stationarity was applied. Difficulties were observed for several cases and therefore this approach has not been used. Here it is stated why.

4. **Sharp fluctuations of simulated cone resistance profiles, page 115:**
   The simulated cone resistance profiles show sharper fluctuations than the original ones. The cause of this phenomenon is explained in this Section.

5. **Transformation cone resistance from normally to lognormally distributed, page 116:**
   Performing a transformation of the cone resistance distribution requires adaptations to the trendline. The procedure applied in this research is described here.

6. **High upper bounds in lognormal model factor distributions, page 117:**
   It was observed that the upper bound of the stochastic model uncertainty reliability interval was very high. This is due to the distribution chosen. More elaborate information is given in this Appendix.

1. Median bandwidth filtering of CPT results

The median bandwidth computes the median of subsequent segments in the cone resistance profiles. After the median has been computed it computes a representative standard deviation based on the standard deviation of its own (σ(n)) and either the preceding or following segment (σ(n-1) or σ(n+1)). Equation B.1 is used for this procedure. Bandwidths of approximately 20 centimeters with 25 measurement points are used since they functioned best on the dataset under consideration in this research.

$$\sigma_r(n) = \min\left(\sqrt{\sigma^2(n-1) + \sigma^2(n)} \quad , \quad \sqrt{\sigma^2(n) + \sigma^2(n+1)} \right) \tag{B.1}$$

The upper and lower bound of the bandwidth of each segment is found by adding or subtracting two times the representative standard deviation. The value of two is present in current literature and worked best (for both shaft and cone resistance) in the 203 cone penetration test results obtained (Wickremesinghe, 1989).

However, application of this method is not without filtering errors. This has a simple reason. Bandwidths of neighboring segments need to overlap significantly to be able to capture large variations in the cone resistance profile. If a median value of a band changes significantly the profile shifts. If this occurs it could be that it falls outside the bandwidths of both segments. This is not a measurement error and should therefore not be filtered out. Figure B.1 shows examples of such errors.

The decision was made to apply another filtering rule. Only local minima and maxima of the profiles should be allowed to be filtered out of the profile. As a result the shifting profile between two segments will not be touched by the algorithm. Figure B.1 shows a good example of the proper functionality of this addition to the median bandwidth filtering method.
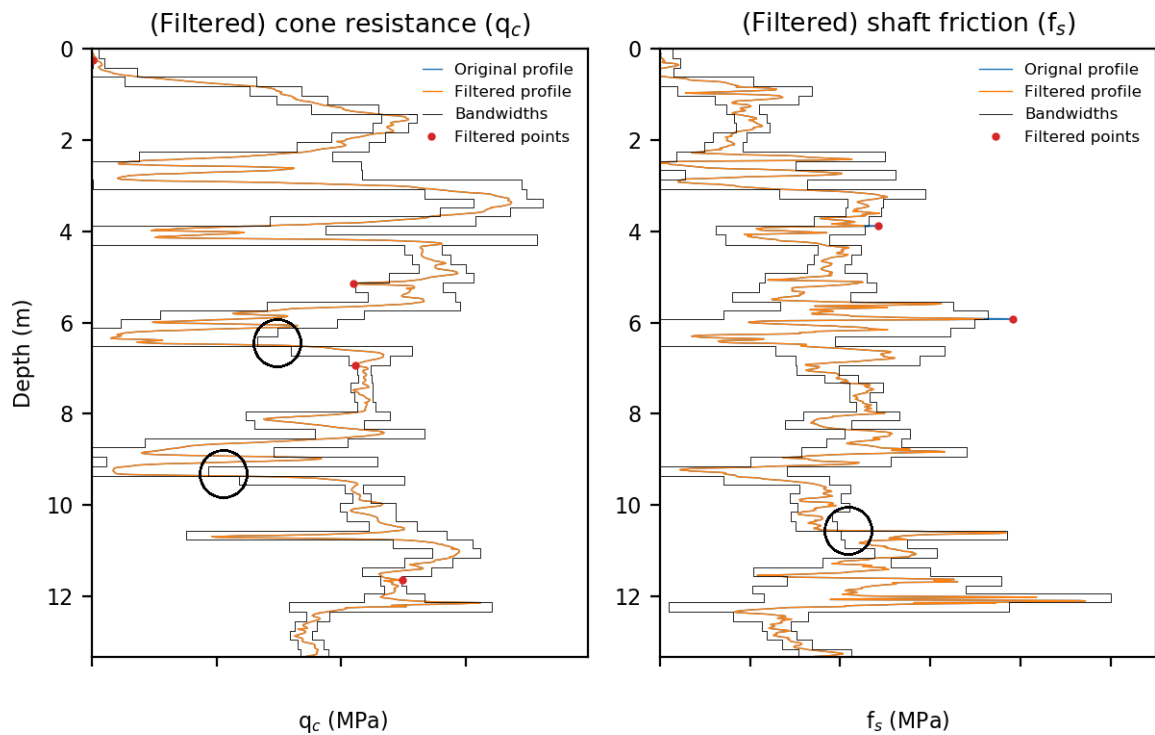

Figure B.1: Example of necessity of adaptation of the median bandwidth filtering approach

This approach successfully filtered out all measurement errors from all 203 cone resistance profiles. Of course these could have been spotted by hand. However, this procedure optimizes the process based on objective criteria.

2. Optimizing the statistical layer identification methods

Two methods make use of a moving window over the cone resistance profile to identify layer bounds based on changes of statistical properties: the statistical moving window method and Bartlett profiling. There are two difficulties regarding the application of both methods:

1. The profile values cannot be compared to thresholds to objectively apply the methods and identify layer boundaries. Proposed thresholds based on specific test data are presented in literature but no generic method can be applied.

2. The bandwidth of the moving window differs per study in which the methods are applied. No fixed and recommended window width is available.

A bandwidth of 1.5 meter is applied in one study on the statistical moving window method (Uzielli et al., 2006). This is combined with an identification threshold of a coefficient of variation of 0.1. Figure B.2 shows that this set up results in a profile which is not distinct. This is due to the fact that the coefficient of variation of the profile is relatively large in general. Using a window width of only 10% of the original does result in relatively distinct peaks which roughly correspond to the Robertson identification bounds. Please do note that the original method was intended to identify physically homogeneous soil units and not layer boundaries. Although this sounds similar there is a slight difference between the two.
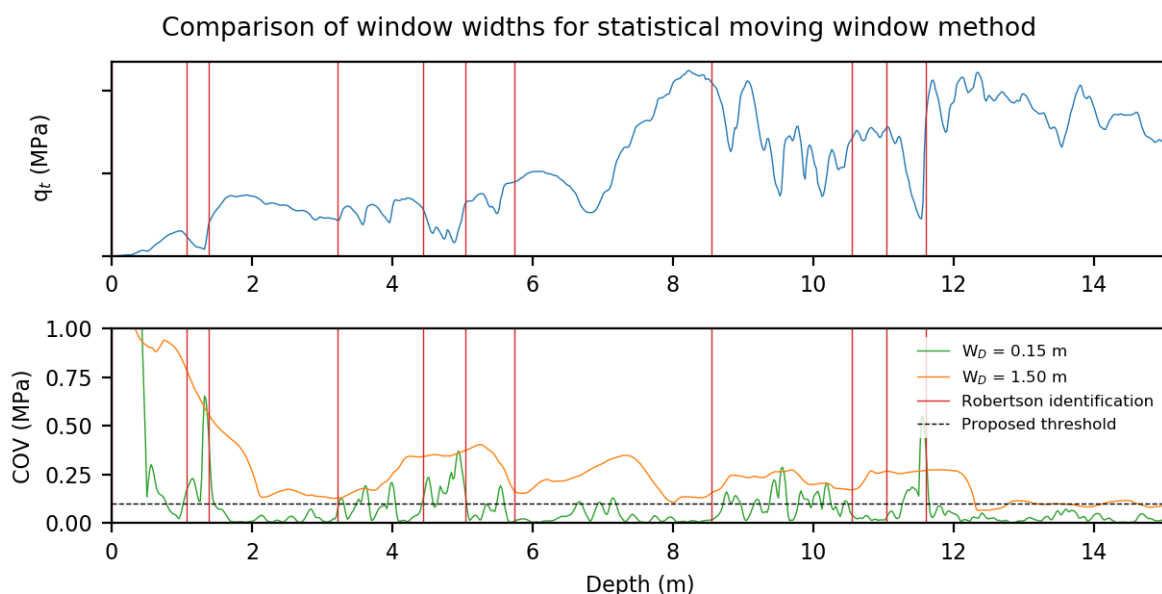

Figure B.2: Difference between proposed and indivdiually adjusted window width for the statistical moving window method

The same behaviour can be observed when applying the Bartlett profiling method of layer identification. In literature window widths of approximately one meter are advised in combination with an identification threshold of a Bartlett value of 200. Figure B.3 shows that these parameters do not deliver proper results. Slightly reducing the bandwidth does allow for identification of bounds similar to the soil behaviour type index (for example at d = 3 and 4.5 m). Decreasing the moving window width results not only in more distinctive peaks, but more peaks in general. Not all distinct peaks can be attributed to a layer bound. Therefore this method cannot be applied independently. Apart from this aspect a proper identification threshold was not found during application.

Statistical identification of layers based on characteristics of a moving window over the cone resistance is not a method which can be applied individually. Nevertheless, it can help assisting the identification based on the soil behavior type index. They could be relevant in a scenario in which the soil type stays similar but the cone resistance profile shifts in trend line. Identification of two layers could be required for random field modelling in such cases.
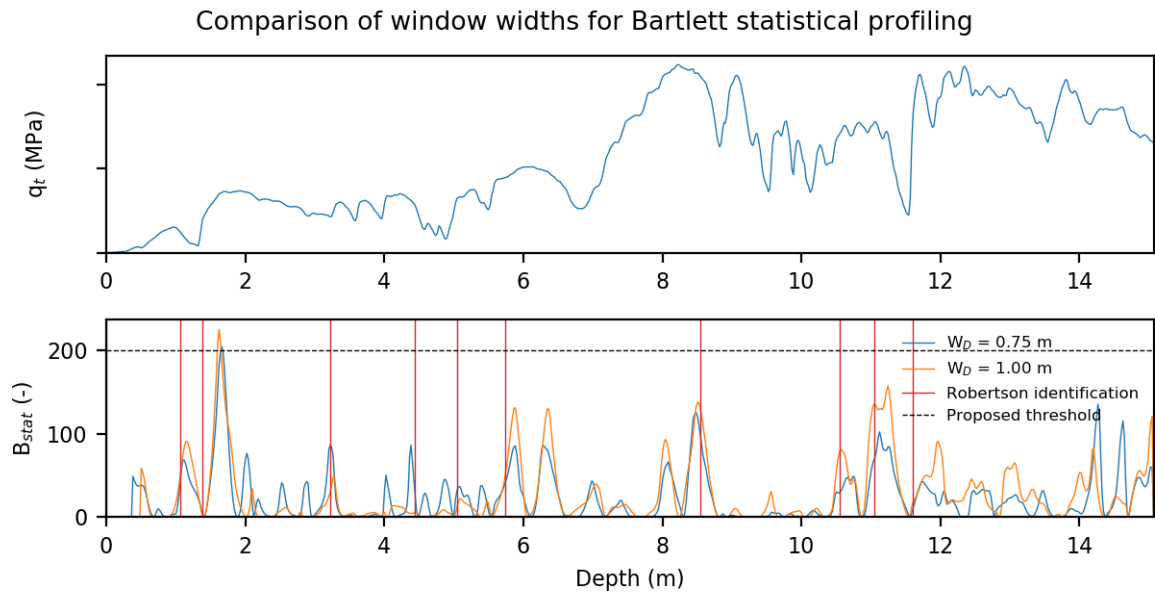
Figure B.3: Differences between proposed and individually adjusted window width for Bartlett profiling

3. Objective assessment of weak stationarity of soil units
 The only objective manner of assessing whether the detrended cone resistance is weakly stationary is proposed by Phoon et al. (2004; 2003). Again Bartlett statistical profiling is used (Section 4.3). However, this time it is applied on the detrended variation profile. Critical values for which the hypothesis of weak stationarity could be rejected can be computed. First of all the empirical autocorrelation structure of the data assessed should be computed. Secondly one needs to compute the scale of fluctuation (δ) corresponding to the best fitting theoretical autocorrelation model. Reference is made to Section 4.4 for more information on this topic.
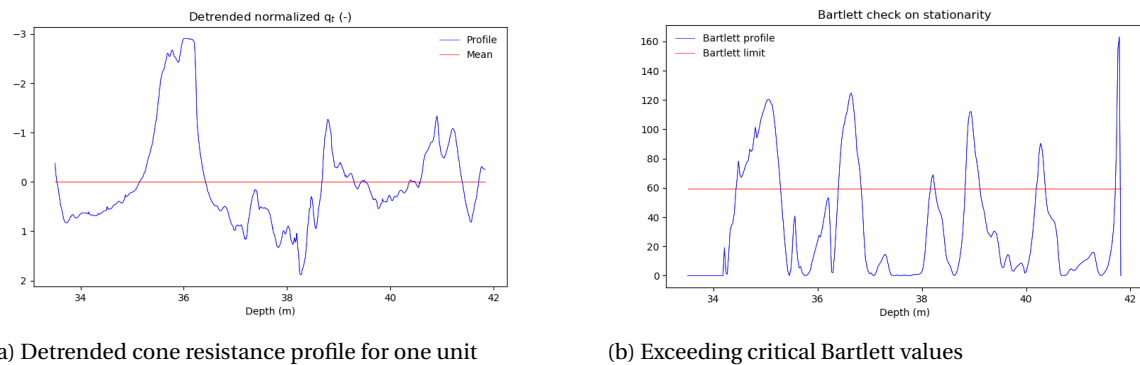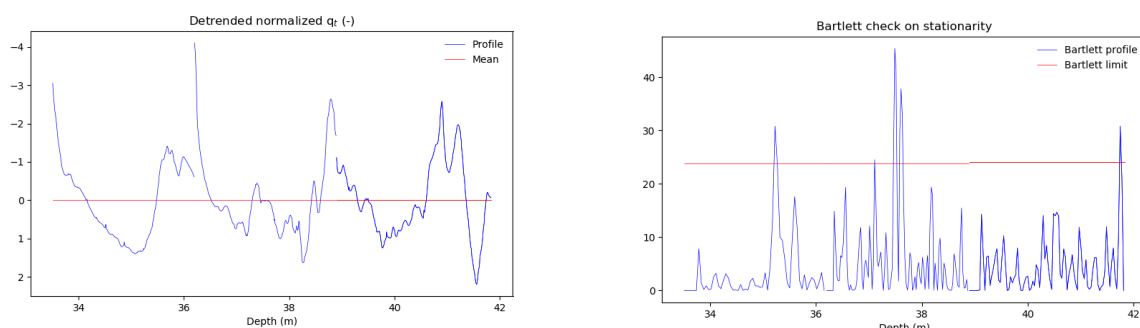

(a) Detrended cone resistance profile for one unit

(b) Exceeding critical Bartlett values

Figure B.4: Soil unit which does not pass the Bartlett test on weak stationarity

Using the scale of fluctuation (δ) the sampling distance of the data series can be determined. There are several criteria regarding the sampling distance. The number of sampling points (N) within one scale of fluctuation (δ) should be between 5 and 50. The sampling length (total length divided by scale of fluctuation, $1/\delta$) must be between the same bounds. Finally the bandwidth of the moving window must be either 1 (for N<50) or 2 (for N>50) times the scale of fluctuation (δ). Phoon et al. (2003) proposes critical values per theoretical autocorrelation model based on these sampling parameters (Table B.1).

Table B.1: Critical Bartlett values for theoretical autocorrelation models and normalized sampling lengths (I_2) (Phoon et al., 2003)

Theoretical autocorrelation model	Norm. sampl. length (I_2)	Rejection level of test value (B_{crit})
Single exponential	1	$(0.23k+0.71) \ln(I_1) +0.91k+0.23$
	2	$(0.36k+0.66)\ln(I_1)+1.31k-1.77$
Binary noise	1	$(0.30k+0.29) \ln(I_1) +1.15k-0.52$
Cosine exponential	1	$(0.28k+0.43) \ln(I_1) +1.29k-0.40$
Second-order Markov	1	$(0.42k-0.07) \ln(I_1) +2.04k-3.32$
Squared exponential	1	$(0.73k-0.98) \ln(I_1) +2.35k-2.45$

Subsequently these were used to assess stationarity. When the Bartlett test value stays below these critical values the hypothesis does not have to be rejected. This test is based on a 5% reliability. This means the layer can be assumed to be weakly stationary. If the Bartlett test value exceeds the critical value the layer should be subdivided into two sub-layers for which the stationarity should be checked again. Exceedance of the critical value could occur (e.g. when small silt or gravel layers are present, Figure B.5). Individual judgement should be applied every time the data is assessed to avoid splitting the soil unit in too much layers.

(a) Detrended cone resistance profile for sub-divided unit

(b) Improved Bartlett profile for sub-divided unit

Figure B.5: Result of division of soil unit to improve stationarity of the soil units

4. Sharper fluctuations of the simulated cone resistance profile

Figure 4.20 in Section 4.4 shows a simulated profile and original profile of the vertical fluctuation in the cone resistance. In some instances it was observed that lower frequency fluctuations are generated by the random field model. This can be caused by two aspects:

1. A smaller scale of fluctuation than for the original cone resistance profile can be the consequence of the averaging of empirical auto-correlation models. As a consequence the correlation based on separation distance is lower and smaller fluctuations are generated. Thinner soil units are expected to enhance this phenomenon.

2. High simulation frequency over depth causes high frequency noise. In this study the original sampling frequency of the cone resistance profile is used for simulation. This implies that approximately 125 random numbers per meter are required for simulation. In essence this increases the probability of small fluctuations.

First of all the small scale fluctuations do not pose problems for application of the CPT-based design method. Especially when cone resistance averaging is applied the small scale fluctuations will average out and be non-existent in the resistance computation. Higher scale of fluctuations and less small scale fluctuations were observed when a lower sampling frequency is used on the cone penetration test results. However, it was decided not to pursue this approach because retrieved data would be ignored.

5. Transformation of the cone resistance from normal to log-normally distributed

Figure B.6 shows the importance of transformation from a Gaussian process to a log-normal one. When the cone resistance at low depths is taken as normally distributed non-realistic negative cone resistances can be simulated. This is physically impossible and should be prevented at all times. Therefore the data should be transformed to a non-negative bounded-normal, log-normal or Beta distribution. Since the transformation to log-normal distributed cone resistances is the easiest this was selected.
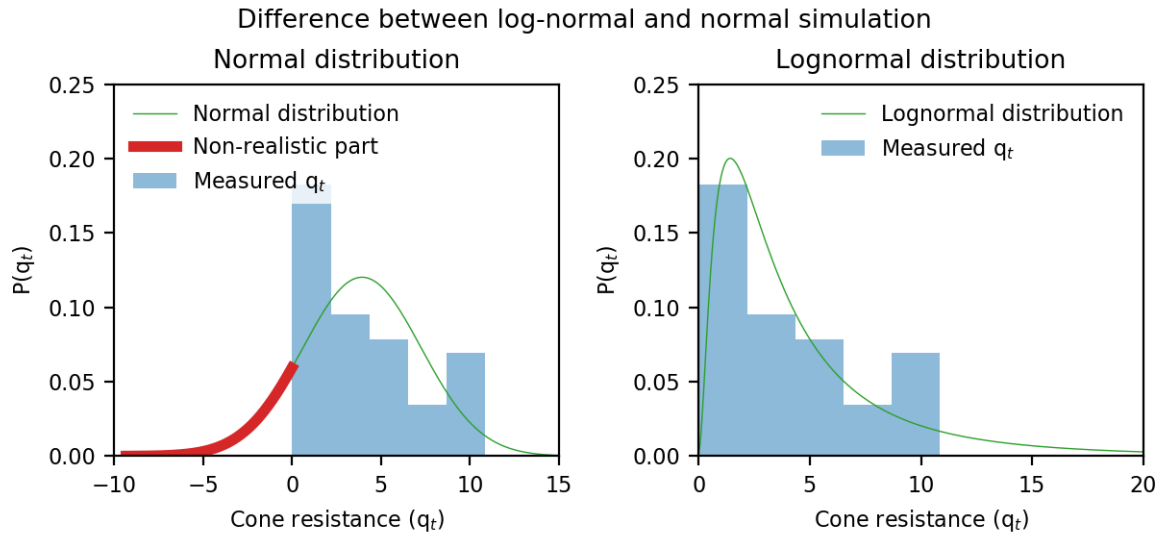

Figure B.6: Visualization of transformation from normal to lognormally distributed cone resistances in the top layer of one profile

While this transformation looks easy on the basis of Figure B.6 and the procedure described in Section 4.4 there is one catch. The trendline (and therefore the mean value) of the process is not constant. When the trend of the cone resistance is upwards low (or even negative) values can be observed for a fitted trendline. This creates errors in the transformation to a non-negative distribution (Figure B.7a). It was decided to set the trendline to one whenever it is below one. This allows for generation of a random field at all times (Figure B.7b).
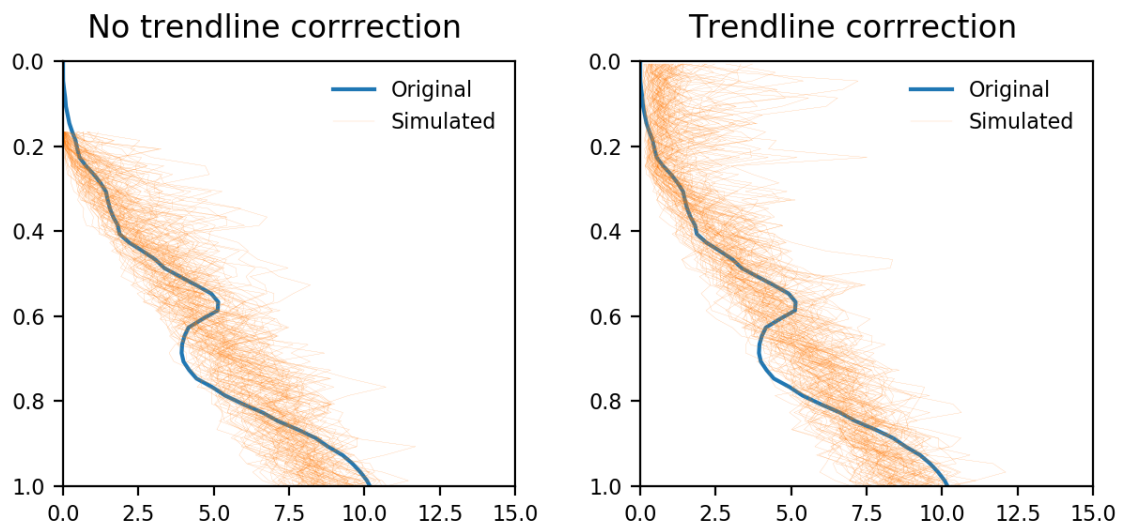
(a) Distances between cone penetration tests   (b) Cone resistance profiles

Figure B.7: Differences observed when correction for trendline values below one is applied

6. High upper bounds in lognormal model factor distributions

A model factor can be fitted through all installation design results as well. For an in-depth description of the model factor reference is made to Section 5.2. Figure B.8 shows the resulting bandwidths when a normal 95% stochastic model uncertainty factor is applied. It is visible that the lower bound is sufficient in only half of the situations. This is no basis for design.
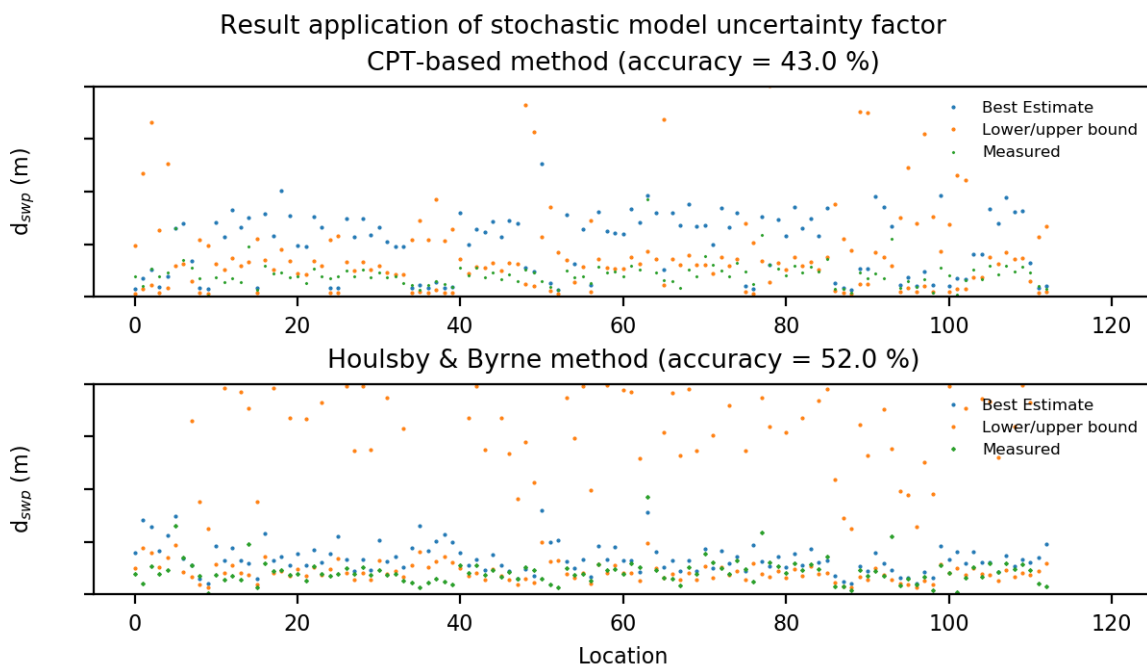

Figure B.8: Model factors fitted through all monopile self-weight penetration data

It is obvious that the accuracy of the bandwidths can be improved when the model itself is improved. Figure B.9 shows how the effectiveness of the model factor estimates improves when one adapts one of the end-bearing empirical coefficients for CPT-based design. It also shows that if one does not take the reliability interval but applies a reliability threshold for the lower bound the accuracy of the estimate can be improved. Defining the lower bound stochastic model factor at a probability of exceedance of 0.99 results in a correct lower bound for self-weight penetration in 96% of the times.
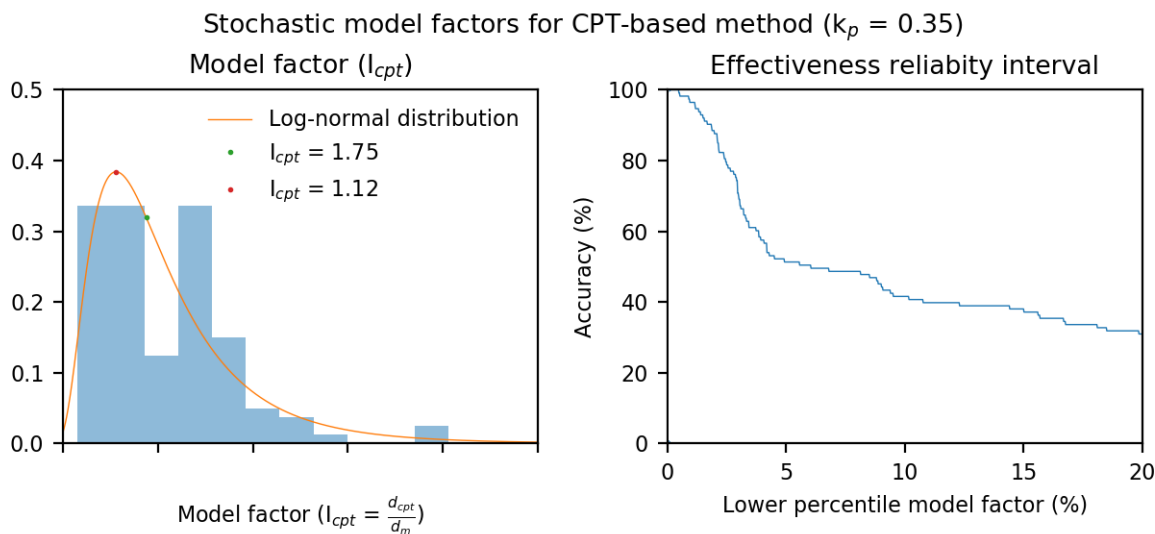

Figure B.9: Improve empirical coefficients and effect of using lower threshold instead of reliability interval